Immunotherapeutic Opportunities in Oesophageal Adenocarcinoma

Richard PT Evans

Institute of Immunology and Immunotherapy

College of Medical and Dental Sciences

University of Birmingham

2024

A thesis submitted to The University of Birmingham for the degree of Doctor of Philosophy.

Acknowledgements

I feel immensely privileged to have been afforded the opportunity to complete this PhD. The body of work I have set forth in this thesis has been both a challenging and rewarding experience. My clinical work enables me to improve the lives of the individual patients that I am lucky enough to care for. Whereas this wonderful journey into scientific research will hopefully enable me to benefit the lives of others beyond my day to day interactions. I would like to thank my supervisor Professor Paul Moss OBE for his inspiration and motivation throughout my time in his lab. His unsurpassable enthusiasm for research has been truly infectious and helped me to find my path into discovery science. The Moss Group which has been established and maintained for many years by Professor Moss has an immense amount of knowledge and expertise which has supported me throughout my PhD. In particular I would like to thank Dr Hayden Pearce and Dr Wayne Croft who have been exceptionally helpful during the design, development and completion of my PhD.

I would also like to thank my supervisor Mr Ewen Griffiths without whom I would never have discovered such a fantastic opportunity. Mr Griffiths has ensured not only that I had the support of the Upper GI department at the Queen Elizabeth Hospital, all of whom have been incredibly helpful in their support of tissue acquisition but that I could rely on his vast expertise in the field of oesophageal cancer to help guide my research. I would like to thank the patient support groups at the Queen Elizabeth Hospital and Walsall Manor Hospital as well as the patients themselves. Without their overwhelmingly generous donations of samples and finance such work would not have been possible.

Finally I would like to thank my wife and children who have given me the time and support to complete my PhD without which none of this would have been possible.

Abstract

Integration of immunotherapy into the treatment pathways for many solid cancers has led to important improvements in survival outcomes. Until recently there was no evidence to confirm that immunotherapy could improve survival over and above current gold standards in treatment for patients with potentially curative oesophageal cancer. Checkmate 577 has demonstrated that adjuvant PD-1 inhibition improves disease free survival for patients who have undergone neoadjuvant chemoradiotherapy and oesophagectomy. Oesophageal adenocarcinoma (OAC) is potentially susceptible to immunotherapy however little is known about the tumour microenvironment (TME). This thesis explores the immunophenotypic landscape of oesophageal adenocarcinoma to identify new mechanisms for immunotherapy.

A combination of proteomic and transcriptomic studies have identified that the OAC TME is dominated by immune and stromal populations. T cells are the majority immune population, and a range of effector and regulatory subsets were identified. OAC is broadly immunogenic and CD39+ T cells, generally regarded as correlates of a tumour-specific cytotoxic cellular response, are observed in both CD4+ and CD8+ T cell subsets. T cells within the TME often express an exhausted phenotype with high levels of checkpoint expression (PD-1, Tigit, TIM-3, LAG-3). A highly proliferative population of T cells has been identified that exhibit features of tumour specificity but in addition feature similar rates of checkpoint expression. Neoadjuvant chemotherapy decreases immunosuppressive Tregs and can potentially decrease exhaustion in effector phenotypes.

These findings have significant implications in the development of novel immunotherapy which is already starting to show promise in improving survival for this challenging cancer.

Table of Contents

Table of Figures

List of Abbreviations

ADCC- Antibody dependent cellular cytotoxicity
AF700- Alexa fluor 700
AJCC- American Joint Committee on Cancer
APC- Antigen presenting cell
APC (flow)- Allophycocyanin
APC-Cy7- Allophycocyanin-cyanin 7
CAFs- Cancer associated fibroblasts
CCR- Chemokine receptor
CD- Cluster of differentiation
CTLA-4- Cytotoxic T-lymphocyte antigen 4
CXCR- CXC chemokine receptor
DC- Dendritic cell
DMSO- Dimethyl Sulphoxide
DNA- Deoxyribonucleic acid
ER- Endoplasmic reticulum
FCS- Foetal calf serum
FITC- Fluorescein isothiocyanate
FLOT- Fluorouracil, Leucovorin, Oxaliplatin, Docetaxel (perioperative chemotherapy regimen)
FSC- Forward scatter
HLA- Human leukocyte antigen
ICI- Immune checkpoint inhibitors
IFN- Interferon
IHC-Immunohistochemistry
Il- Interleukin
ITIM- Immunoreceptor tyrosine based inhibitory motif
IQR- Interquartile range
LAG-3- Lymphocyte activation gene 3
MDSC- Myeloid derived suppressor cell
mRNA- Messenger ribonucleic acid

NACT- Neoadjuvant chemotherapy
NICE- National Institute for Health and Care Excellence
NK- Natural killer
NKT- Natural killer T cell
OAC- Oesophageal adenocarcinoma

OCCAMS- Oesophageal cancer clinical and molecular stratification consortium

PBMC- Peripheral blood mononuclear cells

PBS- Phosphate buffered saline

PD-1- Programmed cell death 1

PD-L1/2- Programmed cell death ligand ½

PE- R-phycoerythrin

PE-Cy5- R-phycoerythrin cyanine 5

PE-Cy7- R-phycoerythrin cyanine 7

PerCPCy5.5- Peridinin chlorophyll protein complex-cyanine 5.5

PET- Positron Emission Tomography

QEHB- Queen Elizabeth Hospital Birmingham

SCC- Squamous cell cancer

SSC- Side scatter

TAP- Transporter associated with antigen processing

T_{CM}- Central memory T cell

TCR- T cell receptor

T_{EM}- Effector memory T cell

TEMRA- Effector memory T cell CD45RA positive

TIGIT- T cell receptor with Ig and ITIM domains

TIL- Tumour infiltrating lymphocytes

TIM-3 T cell membrane protein 3

TLR- Toll like receptor

TME- Tumour microenvironment

TNF- Tumour necrosis factor

TNM- Tumour, Nodes Metastasis staging

Treg- T Regulatory cell

TRM- Tissue resident memory

UHB- University Hospitals Birmingham

Chapter 1: Introduction

The Immune System

The immune system has undergone evolutionary development to protect the body against both external pathogenic threats but it is also integral in maintaining internal homeostasis. Self-regulation of cell turnover is crucial in preventing dysregulated proliferation of host cells. The immune system in turn aims to control and prevent excessive inflammation and malignant change[1]. Identification and recognition of stimuli that evoke an immune response are identified as immunogens which enables a cascade of reactions coordinating an immune response. Immunity has evolved to provide immediate unspecified responses to antigen in the form of the innate immune system that are particularly evident at the site of communication between the outside world and the body. Sustained and specific immune responses are driven by the adaptive immune system. Initially adaptive responses may take days or weeks to develop; however, it provides a mechanism for immune memory and prior or repeated exposure ensures that the adaptive immune system can provide a more vigorous and rapid response to a known threat[2]. Communication and integration of the innate and adaptive immune system aims to provide a complete mechanism for managing immunogenic threats. The immune system maintains homeostasis by determining self from non-self to ensure that excessive responses do not cause auto destruction. Autoimmune disease is increasingly common and represents a misalignment of the host immune system to self and non-self. Failure of threat recognition from self or non-self is a key mechanism for disease initiation and progression. A number of mechanisms for cancer development have been identified however the failure of the immune system to moderate and manage uncontrolled cellular proliferation is a potential for therapeutic modulation and intervention. This body of work

aims to focus on the role of the adaptive immune and seeks to identify maladaptive immune biology in the pathogenesis of oesophageal cancer. Identification of such maladaptive processes may provide opportunities for the development of immunotherapy.

Innate Immune System

The innate immune system provides a mechanism for primary identification of an external pathogen. Pathogens express several signature molecules known as pathogen-associated molecular patterns (PAMPs) which are recognised by evolutionary conserved germline encoded host sensor pathogen recognition receptors (PRRs) such as Toll like receptors (TLRs) expressed on innate immune cells[3]. The innate immune system has both key cellular and acellular components that provide a complex immediate response to pathogens. Phagocytic cells such as macrophages and neutrophils which patrol the body and ingest pathogens. Identification of a pathogen by innate immune cells stimulates additional cellular recruitment and inflammation such as dendritic cells which aim to coordinate and recruit the innate and adaptive system through antigen presentation. Mast cells, eosinophils and basophils provide an important contribution by releasing inflammatory mediators such as histamine, cytokines and proteolytic enzymes. Complement activation by antigen-antibody reactions, exposure to polysaccharide and gram negative bacteria as well as mannose binding lectin pathway all provide an acellular mechanism for pathogenic cell death. The innate immune system provides a preformed initial response that may not be able to provide a response of sufficient specificity or magnitude to end the pathogenic insult.

Adaptive Immune System

The adaptive immune system provides an extended safety mechanism for the management of pathogens that are not initially eliminated by the innate immune system. Activation of the

adaptive immune system however may take days to upscale to a specific threat. The strengths of the adaptive immune system rely on the significant diversity of pathogen recognition and long term antigen memory. Lymphocyte development of antigen specific receptors are determined by the process of random rearrangement and splicing together of multiple DNA segments that code for the antigen-binding areas of the receptors. Gene rearrangement occurs early in cell development prior to antigen exposure leads to the production of a repertoire of over 10^8 T-cell receptors and 10^{10}antibody specificities, 10^9 adequate to cover the range of pathogens likely to be encountered in life.

Lymphocyte memory evolves from naïve lymphocytes clonally expanding after antigen recognition. Memory cells persist after eradication of infection and facilitate more rapid transition of naïve to effector phenotypes after re-infection. Subsequent antigen exposure will stimulate a more specific and selective immune response increasingly capable of dealing with reinfection. The two main types of lymphocyte are T and B cells which originate from the same lymphoid progenitor to provide single antigen specific cells which can differentiate in specific lymphocyte subsets to coordinate an adaptive response.

B cells

B cells mature in the bone marrow and produce cell specific antibodies. Immunoglobulin that is pre bound to its parent B cell aims to identify and bind antigen. High affinity antigen-immunoglobulin interaction stimulates a series of reactions that enables B cell proliferation and differentiation. B cells have the potential to differentiate to antibody producing plasma cells or memory B cells. Maturation and memory of activated B cells continues in secondary lymphoid structures where migrating B cells may terminally differentiate into memory B cells (germinal centre independent memory B cells) or alternatively activated B cells undergo

rapid proliferation to form the germinal centre. B cells exposed to the germinal centre may undergo clonal expansion of antigen-specific B cells which is accompanied by B cell receptor (BCR) diversification through somatic hypermutation. B cells exiting germinal centres provide memory B cells (germinal centre dependent memory B cells) or long lived plasma cells[4]. Plasma cell secreted antibodies may aim to neutralise the function of the pathogen, enable opsonisation to facilitate phagocytosis or provide the first step to the complement cascade and development of the membrane attack complex.

T cells

T cells are defined by their T cell receptor (TCR) associated co-receptors CD8 and CD4. Cytotoxic CD8 T cells recognise and kill abnormal host cells such as virally infected cells or tumour cells through major histocompatibility complex (MHC). CD4 T helper cells activate other cells during the adaptive immune response through cytokine and chemokine release. Like B cells, T cells are initially made in the bone marrow however in contrast to B cells T cells migrate to the thymus for further maturation. Maturation in the thymus enables an expansive expression of a wide array of self-antigens in the thymus is essential for the negative selection of self-reactive T cells and the establishment of central tolerance[5].

TCR Gene Rearrangement within the Thymus

Thymocytes initially undergo positive selection in the cortex of the thymus. Cortical thymic epithelial cells enable differentiation of conventional αβ T cells which arise from random gene rearrangement of V,D and J segments encoded by the recombination activating genes RAG1 and RAG2[6]. Variability in gene rearrangement provides a total diversity of population estimated at 10^{18} αβ combinations. T cell progenitors induce TCRβ expression, which is

sufficient to provide the signals required for the expression of the coreceptors CD4 and CD8, as well as TCRα gene rearrangement, without any ligand engagement[7]. Cortical T cell selection and acquisition of MHC restriction through downregulation of CD4 or CD8 occurs as result of MHC peptide affinity[7]. TCR expression is associated with CD3 which is expressed by all T cells is a prerequisite of TCR upregulation and signalling[8]. The development of γδ T cells arises from double negative thymocytes, as the rearrangement of the TCRγ and δ chains occurs in the double negative stages[9]. γδTCR self-oligomerizes, like the pre-TCR, and initiates intracellular signaling pathways that affirms on going γδ status[10].

Central Tolerance

Recognition of self is crucial to preventing autoimmune damage. Central tolerance is identified as the process of T cell selection during thymocyte differentiation that eliminates T cells that react to self. Double positive CD4 and CD8 T cells that fail to recognise MHC die as a result of neglect. Positive selection occurs within the T cell population when TCR have a low affinity for MHC. T cells subsequently mature into single positive CD4 or CD8 T cells. TCR with a high affinity for MHC may undergo clonal deletion, clonal diversion , receptor editing or anergy. Epithelial cells of the thymic cortex (cTECs) are required for positive selection of thymocytes, whereas medullary thymic epithelial cells (mTECs) and DC are more important for Treg differentiation and clonal deletion. TCR engagement of low-affinity self-peptide MHC ligands presented by cTECs transduces a signal that promotes survival and differentiation. TCR engagement with high-affinity self-peptide–MHC results in expression of Nur77 and Bim and apoptotic cell death.

Peripheral Tolerance

Central tolerance provides the mainstay of preventing autoimmunity however on going peripheral condition and development of further tolerance is required. Not all self-antigens are expressed within the thymus therefore mechanisms for peripheral tolerance are required. Anergy and peripheral deletion enable on going immunoediting. Activated T cells in response to a TCR signal and a costimulatory signal mediated by CD28 ligation, and will then secret cytokines such as IL-2. Further stimulation is required otherwise anergy ensues leading to long-term hyporesponsiveness which is characterised by an active repression of TCR signalling and IL-2 expression. Peripheral deletion may occur through differing apoptotic mechanisms through both Fas and Bim mediated pathways.

Antigen Processing and Presentation

Antigen presentation to initiate T cell responses occurs via major histocompatibility complex (MHC). MHC class I are found on nearly all nucleated cells and display peptides from endogenously synthesised proteins to CD8 T cells whereas MHC class II are found on antigen presenting cells such as dendritic cells, macrophages and B cell which present antigenic peptides to CD4 T cells. Expression of MHC is closely controlled by cytokine expression including interferon gamma which increases MHC expression. MHC are also identified as Human Leukocyte Antigens (HLA) which are highly polymorphic exhibiting the greatest polymorphism within the human genome with multiple variants of each gene. MHC I incorporate HLA-A, B and C whereas MHC II include HLA-DR, DP and DQ.

Antigen presentation is dependent on the source of the antigen. Endogenous antigens such as tumour associated or tumour specific proteins, viruses or intracellular bacteria are upregulated on MHC I. Exogenous proteins are taken up by APCs and subsequently presented via MHC II to CD4 T cells. Endogenous proteins are processed in the proteasome which comprises of a complex of proteases that break peptides down to 8-11 amino acids

which can be moved to the endoplasmic reticulum by transporters associated with antigen processing (TAP 1&2). A new MHC I molecule formed in the endoplasmic reticulum is linked to TAP transporters by Tapasin from which peptide transfer can occur[11]. Once peptide is bound to from the MHC complex the TAP transporter dissociates allowing the MHC I molecule to be upregulated on the cell surface.

MHC II form in the endoplasmic reticulum with and invariant chain (li) which can subsequently migrate through the golgi apparatus. Progressive cleaving of the invariant chain leads to the formation of class II invariant chain peptide (CLIP). CLIP prevents premature loading of peptide until the molecule is in the late endosomal compartment where HLA-DM can cleave CLIP from the molecule and in turn facilitate loading of exogenous peptide. MHC II is then moved to the cell surface to enable presentation to CD4 T cells.

Antigen Presenting Cells and Co-stimulation

Recognition of cognate antigenic peptides presented at MHC complexes by TCR CD4 and. CD8 T cells induce activation even in naïve populations. The level to which a T cell is activated and the subsequent efficacy, proliferation and differentiation can be modulated by both stimulatory and inhibitory co-receptors. Co-signalling ligands and scouter-receptors have been identified on nearly all cell types but have been shown to be most prolific and significant on APCs as the primary drivers of T cell activation and differentiation in secondary lymphoid structures[12]. Co-signalling molecules are members of the tumour necrosis factor receptor superfamily (TNFRSF) and the immunoglobulin superfamily (IgSF). TNFRSF receptors contain one or more extracellular cysteine-rich domains (CRDs), whereas their ligands contain a conserved extracellular TNF homology domain (THD)[13]. The IgSF includes several co-signalling families of which the CD28 and B7 families are perhaps the

most well-described families of IgSF receptors. The significant heterogeneity of TNFRSF and IgSF enables co-stimulation across cell types in both a stimulatory and inhibitory capacity.

Activation of naïve T cells from a quiescent arise as the result of TCR-CD3 signalling. CD28 has been identified as the predominant co-stimulatory receptor which can enable proliferation and differentiation. Progeny T cells do not then require further co-stimulation when exposed to antigen alone facilitating and expedited T cell response.

T cell Memory and Activation

In response to stimulus activated T cells proliferate and adopt functional roles for the clearance of antigen. After eradication of the stimulus around 95%of T cells apoptose leaving a remaining population of cells with a specific memory phenotype. Memory is broadly defined by phenotype from which four subsets of memory T cell can be identified, naïve T cells, central memory T cells, effector memory T cells and T effector memory RA positive cells (Tnaive, $T_{CM,}$ $T_{EM,}$ TEMRA). Naïve T cells can differentiate into either T_{CM} or T_{EM} following activation. TEMRA populations are common in CD8 T cells but relatively uncommon in CD4 populations. Identification of memory subsets is possible as a result of their chemokine expression CCR7 and expression of CD45RA(Tnaive CCR7+CD45RA+, T_{CM} CCR7+CD45RA-, T_{EM} CCR7-CD45RA-, TEMRA CCR7-CD45RA+) [14].

CCR7 enables Tnaive and T_{CM} to circulate through tissue and secondary lymphoid structures to identify antigen. CCR7 ligands CCR19 and CCR21 facilitate migration and activation. T_{CM} on recognition of antigen have the ability to differentiate into an effector phenotype however lack immediate effector function. T_{EM} downregulate CCR7 become increasingly cytolytic but lose their proliferative capacity. They express integrins and chemokine receptors such as CXCR3 necessary for localization to inflamed tissues including tumour. Transcription factors

promote the development and function of Tem and Tcm cells, and T-bet, Blimp1, ID2, and STAT4 expression is associated with Tem cells, while Eomes, TCF1, BCL-6, ID3, and STAT3 expression is associated with cm cells[15]. TEMRA cells overall as the terminally differentiated effector cells supported by low Interleukin-2 and high interferon gamma secretion, high cytotoxicity, low proliferative capacity and high sensitivity to apoptosis. However TEMRA populations which are CD57- do demonstrate high proliferative capacity and differentiation plasticity[16].

Activation in addition to antigen stimulation may result due to local cytokine, chemokine and inflammatory products of cell death. T cell subsets respond to different stimuli to provide a coordinated comprehensive response. Upon activation T cells upregulate specific cell surface markers. CD69 has been recognised as an early marker of activation and increasingly in combination with other cell surface markers such as CD103 may also identify tissue residency populations. CD25 and CD38 have also been recognised as markers of activation. CD38 is an ADP ribosyl hydrolase expressed at differing levels on haemopoietic cells and is also expressed in a subset of thymocytes and antigen activated T cells. Nuclear proteins such as Ki-67 have also been identified as key markers of activation.

Helper CD4 Response

Naïve CD4 T cells have the potential to differentiate into a number of distinct lineages as a result of exposure to a specific antigen. CD4 and TCR interaction with exogenous proteins from MHC II complex on APCS induces downstream signalling that enables proliferation and differentiation. CD4 differentiation is further affected by the concentration of antigen within the microenvironment, the concentration and variety of cytokines and the type of APC and subsequent co-stimulation.

CD4 T cell lineage nomenclature was initially determined dependent on when they were discovered (Th1,Th2), thereafter they were defined by their function and cytokine production. Th1 cells are crucial in the elimination of intracellular pathogens including viruses and some bacteria. Il-12 from monocytes, macrophages and DCs stimulates Th1 differentiation via upregulation of T-box transcription (T-bet) and STAT-4 within naïve T helper populations. IFN-γ within the microenvironment stimulates NK cells to produce Il-12. Th1 cells subsequently produce IFN-γ, Il-2 and lymphotoxin A (Lfa). Il-2 can promote differentiation of CD8 T cells to a cytotoxic profile and facilitate Treg *survival and activation*[17]. Th2 cells predominantly respond to extracellular pathogens such as parasites and helminths and differentiate as a result of GATA-3 and STAT-6. Il-4 secretion from Th2 provides a positive feedback loop for *naïve CD4 cells*[18]. It also causes B-cell class switching and production of IgE and downregulation of IFN-γ. Th2 production of Il-5 enable recruitment and activation of eosinophils which is known to contribute to allergy in correlation with Il-9.

Th17 cells produce evolve from naïve CD4 cells in Il-6, Il-21, TGF-β rich environment are stimulated by STAT-3 to transcription factor retinoic acid receptor-related orphan receptor gamma-T (RORγt) mediated production of IL-17, Il-21, Il-22, Il-26 and CCL20[19]. Th17 cells are able to respond to extracellular bacteria and fungi as Il-17 enable production of pro-inflammatory cytokines such as TNF- α, Il-1, Il-6 cause chemotaxis of inflammatory cells. Il-21 in addition to activating T cells activates NK cells and drives differentiation of B cells into memory cells and plasmocytes. Mature Treg can develop centrally in the thymus or can differentiate from naïve CD4 in the periphery. The provide a mechanism for immunotolerance and prevention of autoimmune destruction as a result of Il-10, TGF-β and IL-35. The role of Tregs in malignancy varies however their immunosuppressant qualities have overall been associated with reducing the immune response to tumour and in turn enable

tumour progression[20]. Follicular T helper cells are found in follicular lymphoid tissues and enable priming of B cells. CXCR5 expressing T follicular cells develop in Il-6 and Il-21 rich environment and require ICOS co-stimulation for development[21].

Cytotoxic T cell Responses

CD8 T cells are the primary mechanism for eliminating intracellular pathogens such as viruses and bacteria and also the primary mechanism for anti-tumour immunity[22]. There are three key pathways by which CD8 T cells eliminate malignant or infected host cells. Cytotoxic T cells recognise antigen via MHC I interactions and induce apoptosis through the introduction of granzymes. Similar to that of NK cells CD8 T cells produce perforins which polymerise to provide access through the cell membrane of the target cell to deliver cytotoxic granules containing granzymes which are serine protease which cleave intracellular protein leading to cell destruction. CD8 T cells when activated produce large volumes of IFN-γ, TNF-α *and* TNF-β which have anti- tumour and anti-infected cell properties. IFN-γ specifically can induce upregulation of MHC I to enable T cell recognition. This is particularly important in malignancy where tumours have been identified to actively downregulate MHC I to facilitate immune evasion. CD8 and to a lesser degree CD4 cell may express Fas ligand which can bind to Fas on the targeted cell. FasL/Fas interaction at the cell surface causes the cell to trimerise inducing a signalling cascade that activates a caspase cascade resulting in apoptosis.

NK cells

NK cells are a key part of the innate immune system but share common attributes with the adaptive immune system such as CD8 T cells. NK cells originate from a common lymphoid progenitor and mature in the bone marrow through a process of inhibitory receptor

engagement with MHC I molecules. Unlike T cells, NK cell receptor are germline encoded, providing wide variation in NK cell receptors. Further maturation occurs in the periphery via homeostatic proliferation or antigen-driven proliferation. Evidence suggests that in addition to direct cytolytic effects against tumours NK cells may divert CD4 profiles to a Th1 phenotype which has been associated with improved anti-tumour immunity[23]. Healthy cells express limited if any NK cell activating receptors and conversely express high levels of MHC I which interact killer immunoglobulin-like (KIR) family inhibitory receptors preventing NK induced apoptosis. Virally infected or tumour cells often downregulate MHC I but upregulate NK cell activating receptors such as NKG2D, Ly49 and NKp46 enabling NK mediated tumour destruction[24,25]. NK cells also play a significant role in antibody-mediated cancer therapies by utilizing the Fcγ receptor to carry out antibody-dependent cellular cytotoxicity[26]. In the context of tumour immunology NK cells similar to other tumour targeting cells within the immune environment may become ineffective. A tumour driven chronic suppressive immune microenvironment and persistence of tumour can favour tumour progression via immune-editing[25]. The inability of NK cells to control tumour may also arise as they have insufficient anti-tumour activity as they are focused to different functions such as regulation of mucosal immunity. Cancer associated fibroblast (CAFs) can inhibit NK cell activity by downregulating DNAM-1, NKp30 and NKp44. Tumour associated macrophages (TAMs) have also been identified to reduce NK degranulation and IFN-γ production.

NK cells are defined by their expression of CD56 but absence of CD3. They can be further subdivided based on the relative expression of CD56 and CD16. $CD56^{dim}16+$ and $CD56^{bright}16-$ are the two predominant types of NK cells. $CD56^{dim}16+$ account for 90% of circulating NK cells and express high levels of high levels of KIRs, the maturation marker CD57, and mediates natural and antibody-dependent cellular cytotoxicity, exhibiting high levels of perforin and enhanced killing. $CD56^{bright}16-$ predominate in tissue and secondary lymphoid

structures upregulating NKG2A, have limited perforin production and express high levels of inflammatory cytokines such as TNF-α, GM-CSF and IFN-γ[27]. Circulating CD56^{bright}16- express CD62L, CCR7, CXCR4, and CXCR3 that allow their preferential recruitment to secondary lymphoid organs, tumour, and inflamed tissues conversely CD56^{bright}16- NK cells CD62L but express other adhesion molecules, including the α integrin subunit CD49a, CD69 and CD103.

Checkpoint opportunities

Checkpoint inhibition is increasingly being used across cancer types to provide a new strategy against invasive malignancy. This thesis will focus on expression of checkpoint within the context of oesophageal adenocarcinoma. Initial studies of TILs in the TME have looked at broad phenotypes such as CD4, CD8, Treg (FoxP3, CD25) and the impact they may have on patient outcome. Increasingly sequencing techniques have been used to survey the transcriptome of oesophageal cancer to fully appraise the maximal extents of checkpoint expression and in turn help contextualise the benefits of looking at individual checkpoint markers in isolation. Bulk-RNA seq has been to identify expression of gene targets for immune therapy – PD-L1, LAG3, TIM3, TIGIT, ICOS, CCR2, CCR5, CXCR4, and CSF1R in patients with OAC. They have reported that high levels of co-expression of immune regulatory targets in OAC patients may limit the efficacy of checkpoint monotherapy.

PD1-PDL1/2 Axis

Programmes cell death-1 (PD-1) transmembrane protein also known as CD279 is an inhibitor of both adaptive and innate immune responses, and is expressed on activated T, NK and B lymphocytes, macrophages, dendritic cells and monocytes. Upregulation of PD-1 occurs in response to Transcription factors such as nuclear factor of activated T cells (NFAT), NOTCH, Forkhead box protein (FOX) O1 and interferon (IFN) regulatory factor 9

(IRF9). PD-1 is upregulated in the presence of chronic antigen exposure and as a result is found in high frequency in the TME and chronic infection. It plays a crucial role in maintaining balance between tumour recognition and breakdown and inadvertent tissue destruction. PD-1 binds to PD-Ligand 1 and PD-Ligand 2 (PDL1-/2) which are expressed by tumour macrophages, some activated T cells and B cells, DCs and some epithelial cells, particularly under inflammatory conditions. In addition, PD-L1 is expressed by tumour cells as an adaptive immune mechanism to escape anti-tumour responses[28,29]. PD-L1 is upregulated in response to downregulation of PTEN which may lead to the activation of PI3K/AKT pathway and facilitate the expression of PD-L1. PD-1 signalling due to PD1-PDL1/2 interaction invokes T-cell exhaustion, a reversible inhibition of T-cell activation and proliferation. Blockade of the PD-1 axis has been shown to have a significant anti-tumour effect[30–35].

TIGIT

T-cell Ig and ITIM domain (TIGIT) has been identified as co-inhibitory receptor expressed by regulatory T cells (Tregs), activated T cells, and natural killer (NK) cells[36–38]. TIGIT is a transmembrane glycoprotein receptor with an Ig-like V-type domain and an ITIM in its cytoplasmic domain. TIGIT binds to one of two ligands on APCs, CD155 and CD112 which prevents maturation and enables a tolerogenic phenotype. The balance of immunoregulation is well demonstrated by the Ig superfamily receptors. DNAX accessory molecules such as DNAM-1 and CD226 have a low affinity for CD155 and CD112 expressed on naïve and effector cells providing a co-stimulatory interaction. Co-stimulatory and co-inhibitory competition (TIGIT/CD226-CD155/CD112) control T cell function potentially impacting tumour activity and providing a mechanism for immunomodulation. TIGIT engagement has been shown to inhibit T cells not only indirectly via induction of tolerogenic DCs but also by

impeding CD226 dimerisation on T cells themselves, thus directly avoiding the delivery of costimulatory signals further highlighting opportunities for immunotherapy.

LAG-3

Lymphocyte activation gene-3 (LAG3, CD223) is an immunosuppressive checkpoint molecule expressed on activated and exhausted CD4 and CD8 T cells as well as Tregs. The LAG3/MHC II complex on CD4+ cells negatively modulates T-cell activity and enhances antigen self-tolerance when displayed on CD8+ cells. Conversely, LAG3 binding to MHC II on Treg cells advances the suppressive effect on T-lymphocytes, enforcing the negative immune regulation effect of LAG3. LAG3 expression has been shown to increase in the context of chronic antigen exposure as demonstrated in solid tumours leading to T cell exhaustion. LAG3 inhibition has been suggested as potential target of immunotherapy in solid tumours including oesophageal cancer.

TIM-3

T cell immunoglobulin and mucin domain-containing protein 3 (TIM3), is a member of the TIM family of immunoregulatory proteins and a type 1 trans membrane protein. It was originally identified on IFNγ producing $CD4^+$ and $CD8^+$ T cells however further investigation has shown it is also expressed on Treg, myeloid, NK and mast cells. In its ligand-unbound form, TIM-3 interacts with HLA-B-associated transcript 3 (BAT3) and maintains T cell activation by tyrosine kinase LCK recruitment. TIM-3 binds galectin 9 which can be bound to the surface of tumour cells and can also be secreted by tumour cells, APCs. Galectin 9 has two carbohydrate recognition domains and can promote the oligomerization of TIM3, thus potentially facilitating the formation of other TIM3–ligand complexes such as carcinoembryonic antigen-related cell adhesion molecule 1 (CEACAM1)–TIM3. TIM-3

galectin 9/CEACAM1, binding subsequently leads to the release of BAT3 and allows recruitment of the tyrosine kinase FYN. This results in the disruption of immune synapse formation and in phosphatase recruitment. Ultimately, the cell becomes anergic or undergoes apoptosis, which is mediated by intracellular calcium release. Immunotherapy directed inhibition of TIM-3 ensures on going TIM-3-BAT3 interaction maintaining cell functionality.

Epidemiology of Oesophageal Cancer

Oeosphageal cancer is defined by Cancer Research UK (CRUK) as "a cancer of unmet need" due to its dismal prognosis that has not has not changed significantly over the past two decades. It is the seventh most common cancer globally accounting for the sixth most common cause of cancer mortality[39]. In 2018 an estimated 572 000 new cases of oesophageal cancer worldwide were diagnosed in 2018 of which 85 000 were OACs (Age Standardised Incidence Rate (ASR) 0.9 per 100 000, both sexes combined) and 482 000 OSCCs (ASR 5.3). The estimated number of deaths attributable to oesophageal cancer was 508,000. It is important to recognise that within the limits of epidemiological studies both incidence and mortality rates for oesophageal cancer continue to decrease which is likely to be the result of rising living standards and healthcare provision in low and middle income countries (LMICs). Outside Western countries improvement in survival outcomes have also been attributed to screening programs and increased health education in endemic areas. Between 1990 and 2017, age-standardised incidence decreased by 22·0%, mortality decreased by 29·0%, and disability adjusted life years (DALYs) decreased by 33·4% globally[40]. However, as a result of population growth and ageing, the total number of new cases increased by 52·3%, from 310 000 to 473 000; the number of deaths increased by 40·0%, from 311 000 to 436 000; and total DALYs increased by 27·4%, from 7·68 million to 9·78 million[*]. In 2017,

age-standardised incidence was 2·7 times higher, mortality 2·9 times higher, and DALYs 3·0 times higher in males than in females[40]

There are two main subtypes of oesophageal cancer: oesophageal squamous cell carcinoma (OSCC) and adenocarcinoma (OAC). OSCC accounts for 85% of newly diagnosed oesophageal cancers. Cases are predominantly concentrated in Asia where around 400,000 cases of SCC are diagnosed annually[41]. Sub-Saharan Africa has been identified to have the highest SCC incidence rates globally. Incidence rates ranged from 11.1 per 100 000 in Eastern Africa (ASR >16 in Mongolia, Malawi and Kenya) to 1.0 per 100 000 in Northern Africa, Northern America and the Caribbean and Central America[37]. OAC exhibits a different distribution in incidence and prevalence as compared to SCC. OAC is more commonly identified in affluent Western populations with less than 10 countries globally having higher OAC ASRs than OSCC. The UK and the Netherlands exhibits the highest global incidence of OAC with reported rates of 4.4 new cases per 100 000 annually[41]. OAC has been shown to a greater degree to disproportionately affect men as compared to OSCC. The current trajectory of oesophageal cancer in the UK predicts that by 2030 1 in 120 men will die from oesophageal cancer.

Oesophageal Squamous Cell Carcinoma

Smoking has been identified as a major risk factor for OSCC. Smoking remains a significant risk factor in ex-smokers and a volume dependent relationship has also been identified with smoking with a pack year greater than 30 showing an increased risk of developing OSCC[42]. Increased alcohol consumption has also been identified to confer an increased risk of OSCC[43,44]. Modifiable dietary factors can significantly alter OSCC risk. A high intake of fruit and vegetables has been demonstrated to reduce the risk of OSCC[45]. This is likely to be due to the increased folate, vitamin C and fibre. Conversely Beta-carotene, vitamin E, vitamin D

and selenium have not shown reduced ESCC incidence or mortality[46–48]. Repeated thermal injury in the form of consumption of excessively hot beverages has been shown to increase OSCC risk. Viral infections have not definitively been shown to be a risk factor however is a potential risk with HPV which requires further investigation[49–51].

Mutations in genes that regulate the cell cycle and cell differentiation have also been linked to the transition of normal squamous cell mucosa through dysplastic changes to invasive carcinoma. Comprehensive genomic analysis, which was conducted using whole-genome sequencing, whole-exome sequencing, and array comparative genomic hybridization, has revealed that more than 83% of ESCCs contained a somatic mutation in *TP53*[52]. Mutations in genes that control the cell cycle (*CDKN2A*, *RB1*, *NFE2L2*, *CHEK1*, and *CHEK2*), or experience differentiation (*NOTCH1* and *NOTCH3*), have been found in 2–10% of OSCCs[52–54]. Epigenetic alterations in DNA methylation and histone modification have also been identified in the development of OSCC however as yet this has provided limited translational opportunity[55].

Oesophageal Adenocarcinoma

Gastro oesophageal reflux (GORD) has been identified as the major risk factor for OAC. Reflux of acidic gastric contents into the lower oesophagus causes recurrent tissue damage, chronic inflammation and dysplastic remodeling known as Barrett's oesophagus. Increasing central obesity in Western populations increases the incidence of GORD and in turn OAC. Obesity is itself a risk factor for malignancy which is only partly explained by increasing rates of GORD[56]. GORD is significantly more common with increasing age, smoking and NSAID use whereas new data suggests symptoms of reflux are equivocal between sexes[40,57]. There remains contrasting evidence as to whether medical and surgical treatment of reflux reduces the risk of developing OAC[58–60]. OAC exhibits significant male predominance in

incidence which ranges from around 6:1 in Europe but as high as 7.6:1 in North America[61]. Smoking and increasing age are associated with an overall increased risk of OAC. NSAIDs and statins are associated with a reduced risk of OAC, the Add-Aspirin trial specifically looking at the potential overall survival benefits of aspirin in oesophageal, gastric, breast, colon, rectum and prostate is on going[62–64].

Barrett's oesophagus (BO) is a complex genetically predisposed premalignant condition that affects up to 2% of the population in western countries and denotes a pathophysiological pathway of normal oesophagus progressing into metaplasia, dysplasia and subsequent invasive adenocarcinoma carcinoma[65]. The metaplastic transition of squamous to columnar epithelium in response to chronic stress and inflammation as the result of refluxing gastric acid and bile. The risk of Barrett's progressing to invasive carcinoma is low at around 0.3-0.6% of BO patients can be expected to progress to OAC in one year. Surveillance and active treatment of low and high grade dysplasia potentially limits this this progression[66]. The origin of BO is widely believed to originate from the stomach however single cell sequencing data from BO shows significant transcriptomic similarities between BO and oesophageal significant transcriptomic similarities between BO and oesophageal submucosal[67–69]. The expression of stem cell associated gene OLFM4 in both BO and submucosal glands may suggest that both cellular populations originate from the same progenitor cell. Further transcriptomic studies may subsequently delineate the origins of BO and subsequent transition of BO to OAC.

Normal oesophageal tissue is susceptible to significant genomic stress which subsequently leads to multiple passenger mutations that may not necessarily progress to pathological change[70]. It is key therefore to identify potential driver mutations that will subsequently lead to the development of OAC. OAC displays marked chromosomal instability and thus may be classified as a C-type neoplasm, which may be driven mainly by structural variation rather

than mutations[71]. A mean of 4.4 driver mutations, derived more commonly from mutations rather than copy number alterations, are required to enable tumour development[72]. Genomic and transcriptomic analysis has identified indicators of poor prognosis including acquired *TP53, SMAD4, ARID1A* and GATA4 mutations. OAC exhibits significant intra-tumour heterogeneity demonstrating continued malignant evolution that can potentiate progression, drug resistance and overall poor outcomes[73]. Furthermore this inherent clonality may drive resistance against precision oncology because amplification of certain potentially targetable genes such as *ERBB2* (encoding HER2), may be present in the primary tumour but absent in circulating tumour cells and metastases[74].

Presentation, Investigation and Treatment of OAC

Screening of asymptomatic patients for oesophageal cancer is not currently feasible due to the low prevalence of OAC. Surveillance for OAC within Barrett's cohorts may be used but benefits are limited[75]. Novel screening techniques to identify Barrett's are being developed including the Cytosponge which enables immunohistochemical assessment of oesophageal mucosa for Trefoil factor 3. After a diagnosis of OAC is made the patient undergoes clinical staging in order to assess if surgery is an appropriate treatment.

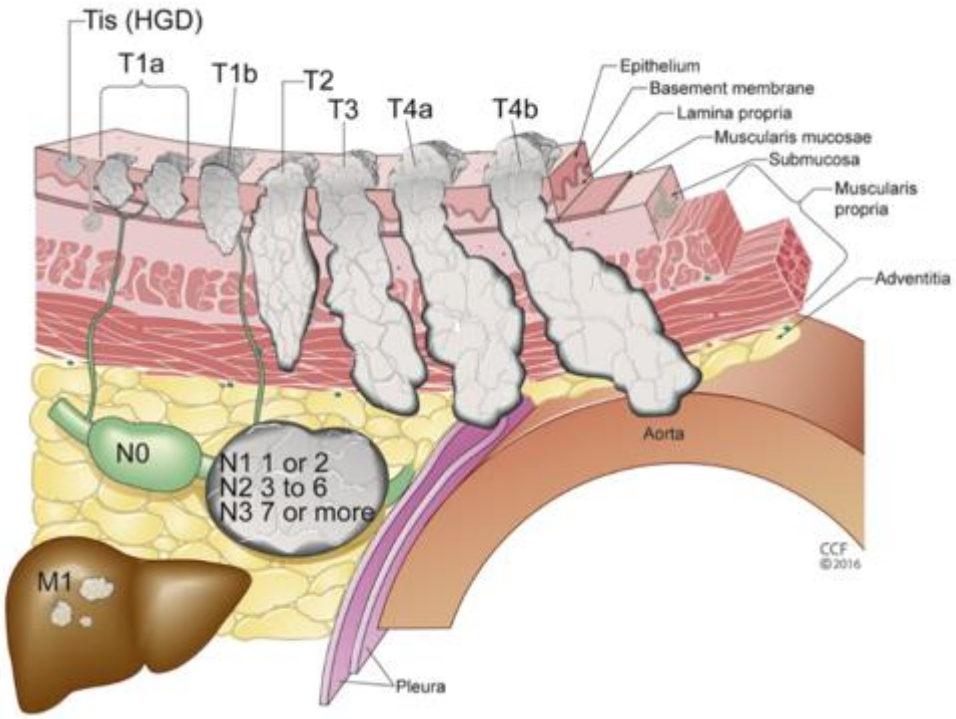

Figure 3 - TNM Staging of Oesophageal Cancer[76]

The treatment of choice for early invasive disease without nodal metastasis is endoscopic resection whereas the gold standard for locally advanced oesophageal cancer includes peri-operative or neoadjuvant oncological treatment followed by oesophagectomy. The specific regimen of neoadjuvant treatment varies depending on histological subtype and may be inclusive of radiotherapy as well as chemotherapy. In the UK immunotherapy is not currently used in the neoadjuvant setting.

Evidence shows that neoadjuvant treatment improves overall survival in oeosphageal cancer but is associated with moderate morbidity and occasional mortality[77]. The choice of first line neoadjuvant chemotherapy regimen has been updated since the publication of the FLOT4 trial in 2019[78]. The FLOT trial compared fluorouracil, leucovorin, oxaliplatin and docetaxel (FLOT) to ECF/ECX. Patients receiving FLOT had an increased median overall survival of

15 months and an increased estimated 2-year, 3-year, and 5-year survival rates of 9%. Median survival was 35 months in the ECF/ECX group and 50 months in the FLOT group. Controversy remains as to the gold standard of neoadjuvant treatment.
Adjuvant treatment in oesophageal cancer is often dependent on the initial choice of neoadjuvant treatment and typically comments at 10-12 weeks after surgery.

Surgery

Oesophagectomy is associated with significant morbidity and mortality but remains the mainstay of curative treatment for locally advanced disease. Surgery facilitates en-bloc removal of the tumour and associated lymphatics in order to completely remove the primary cancer and local sites of potentially lymphatic spread. A minimum standard of 15 lymph nodes should be removed for pathological assessment.

Immunotherapy and Monoclonal Antibody Therapy

Due to cost and efficacy, there is limited use of immunotherapy approved by NICE for oesophageal cancer. KEYNOTE, CheckMate and ATTRACTION trials have all significantly contributed to the evidence base for the clinical role of immunotherapy in oeosphageal cancer. Currently the most influential trial within the curative treatment pathway is the CheckMate 577 trial which evaluated adjuvant Nivolumab in resected (R0) oesophageal tumours after the administration of CROSS based chemoradiotherapy and showed a median disease-free survival of 22.4 months compared t*o* 11.0 months for placebo[79]. Subsequently adjuvant Nivolumab has been adopted into the NICE guidance for patients with completely resected oesophageal cancer who have residual disease after previous neoadjuvant chemoradiotherapy.

Initial success seen for potential curative patients as seen in Checkmate 577 has not been replicated in subsequent trials. Keynote 585 introduced PD-1 inhibitor pembrolizumab to peri-operative chemotherapy in patients undergoing resection[80]. Most patients received a peri-operative fluorouracil based regimen with a small proportion receiving FLOT. Despite a significant improvement in the rate of complete pathological response this did not translate to an improvement in event-free survival. Preliminary results of Matterhorn were reported at the European Society of Medical Oncology meeting 2023, the trial evaluated the impact of the addition of PD-L1 inhibitor durvalumab to peri-operative FLOT[81]. Initial results have shown a significant improvement in the rate of complete pathological response however survival data is still awaited.

A single arm phase 2 feasibility trial, The PERFECT trial evaluated the addition of neoadjuvant PD-L1 inhibitor atezolizumab to CROSS based chemoradiotherapy[82]. A subsequent propensity matched analysis of patients from a high volume centre who had not been part of the trial was undertaken demonstrating no improvement in pCR or survival. The use of PD-1/PD-L1 inhibition remains unclear and further trials stratifying patients dependent on CPS/TPS scores will likely follow. The use of combination immunotherapy/monoclonal antibody therapy will potentially show greater promise. Evidence within the metastatic setting has been more forthcoming, Keynote 811 evaluated the benefit of adding pembrolizumab to chemotherapy and trastuzumab in Her2 positive metastatic gastric/GEJ cancer demonstrating improved progression free survival with the addition of PD-1 inhibition[83]. A phase 1b trial of Nivolumab with or without LAG-3 inhibitor relatlimab in addition to NACRT for oesophageal and junctional cancers has finished recruiting and is due to complete in 2022[84].

As previously stated the most immunotherapy research has been conducted in the palliative setting and pembrolizumab was approved for the treatment of patients with chemotherapy-

refractory PD-L1–positive gastric/GEJ cancer [85]. NICE however does not recommend the use of checkpoint inhibitors in metastatic oesophageal cancer. Current NICE guidance has been heavily influenced by the results of Keynote-061, comparing pembrolizumab to paclitaxel for patients with advanced disease which did not demonstrate a survival advantage. The use of combination therapy for first line palliative chemotherapy is currently being investigated[86]. Neoadjuvant monoclonal antibody therapy for oesophageal cancer has been evaluated in the ST03 trial in which VEGF inhibitor bevacizumab was given in addition to peri-operative ECX for resectable gastric, oesophagogastric junction, or lower oesophageal adenocarcinoma[87]. The addition of a VEGF inhibitor prior to performing an oesophagectomy led to a significant increase in anastomotic complication rates and as such the trial was concluded early. Further monoclonal therapies are under investigation with trial undergoing in epidermal growth factor inhibitors (eGFR).

Hypothesis

The aim of the thesis is to provide a comprehensive understanding of the immune landscape in oesophageal adenocarcinoma. Active comparison of circulating and tumour infiltrating immune profiles will seek to provide an oesophageal specific understanding of the tumour microenvironment from which bespoke therapies can be developed. Oesophageal adenocarcinoma is a tumour with a high mutational burden and as such has been seen as a potentially susceptible tumour for immunotherapy. Advances in survival associated with the administration of immunotherapy in other cancers such as melanoma, lung and renal led to mirrored clinical immunotherapy trials in oesophageal cancer. Sadly, expected survival improvements with immunotherapy have not been achieved in oesophageal cancer. There remains a significant lack of evidence of the immune contexture in oesophageal

adenocarcinoma and the thesis will aim to provide a greater foundation from which oesophageal specific therapies can be developed.

Aims

- Chapter 3 defines the immune landscape of oesophageal adenocarcinoma using flow cytometric analysis. A comparison of circulating and tissue infiltrating lymphocytes is a major focus of the research.
- Chapter 4 utilizes single cell transcriptomics to determine subsets of immune cells within the OAC microenvironment
- Chapter 5 extends the flow cytometric analysis to study the features of tissue resident populations
- Chapter 6 uses a multicolour flow cytometry panel to comprehensively phenotype T and NK cell populations with a focus on memory subsets in relation to chemotherapy response.
- Chapter 7 will aim to confirm the presence of potentially clinically relevant immune populations previously identified within the transcriptome of oesophageal adenocarcinoma analysis.

Chapter 2: Materials and Methods

Patients

Patients with oesophageal adenocarcinoma were recruited at University Hospitals Birmingham NHS Foundation Trust, Queen Elizabeth Hospital (Birmingham, UK) under appropriate ethical approval (HBRC 18-304). All patients were above the age of 18 and had full capacity to provide consent.

Patient blood samples for the purpose of PBMC isolation were taken pre-operatively by the anaesthetic team. Up to 20ml of blood was taken per patient. For patients undergoing staging laparoscopy and endoscopy, up to eight endoscopic biopsies were taken. The number of biopsies is limited by endoscopic access to the tumour and bleeding risk and was determined by the operating clinician. Endoscopic biopsies were stored dry in a cryovial on ice and transferred to the HBRC for anonymisation in accordance with UoB Human Biomaterials Resource Centre 15/NW/0079 at the end of the procedure. Post-anonymisation, tissue samples were placed in growth media.

For patients undergoing oesophagectomy, the resection specimen was delivered fresh to the histopathology department where it was dissected by a pathology staff member. Dependent on macroscopic assessment of the tumour, a sample of normal and tumour tissue was excised and placed in a sterile Falcon tube on ice. During the duration of the study it became apparent that normal tissue was no longer deemed necessary for ongoing investigation and as such normal tissue sampling was terminated. All samples were immediately transferred to the HBRC for anonymisation in accordance with UoB Human Biomaterials Resource Centre 15/NW/0079. Post anonymisation tissue samples were placed in growth media.

Culture Media Solutions

Wash media- RPMI 1640 (Gibco BRL), 100U/ml Penicillin (Gibco BRL), 100µg/ml Streptomycin (Gibco BRL).

MACS buffer (sterile filtered)- 1x PBS (University of Birmingham), 10% Foetal Calf Serum (SBS Biologics), 2mM EDTA (Sigma).

Growth Media- RPMI 1640 (Gibco BRL), 100U/ml Penicillin (Gibco BRL), 100µg/ml Streptomycin (Gibco BRL), 2mM Glutamine, 10% Foetal Calf Serum (SBS Biologics), 100µg/ml Primocin (InvivoGen).

Freezing Media- Foetal Calf Serum (SBS Biologics), 10% DMSO (Sigma).

Digestion Solution- DMEM media supplemented with 10% FCS, 1% Penicillin/Streptomycin (all Life Technologies), 100µg/ml Primocin (InvivoGen), 1X Gentle Collagenase/Hyaluronidase (STEMCELL™ Technologies), 125µg/ml Liberase TL (Roche) and 50U/ml Benzonase® (Sigma-Aldrich).

PBMC Isolation

Up to 20ml of blood was added to an equal volume of RPMI. The blood/RPMI mixture was then layered on 15ml Ficol in Falcon tubes and centrifuged at 1800 rpm for 30 minutes (brake off). The PBMC layer was removed and decanted into a fresh tube. RPMI was added up to a total volume of 40ml. A cell count was performed using a haemocytometer and a further centrifugation was performed for 10 minutes at 1500 rpm. Pelleted PBMC were stored with freezing media in cryovials at a concentration 5 - 10 million cells per ml.

Tumour Infiltrating Lymphocyte Isolation for Flow Cytometry

Biopsy/resection tissue was dissected into small fragments using a scalpel and placed in a well of a 6 well plate. Growth media was added until the tissue fragments were covered, and plates

were placed in an incubator overnight (16-22 hours). Tissue was mechanically disrupted and resulting cell suspension was aspirated and filtered through a 70μl filter into a 15ml Falcon tube to remove remaining tissue fragments. The cell suspension was then centrifuged at 1500 rpm for 10 minutes. Pelleted TIL were used fresh or cryopreserved with freezing media in cryovials at a concentration 1 - 1.5 million cells per ml.

Cryopreservation of Purified PBMC and TIL

Cell suspensions were pelleted at 1000 rpm for 10 minutes to remove platelets and resuspended in ice cold freezing media. Cells were frozen at -80°C in a Mr Frosty (Nalgene) containing isopropanol to allow cooling at a constant rate of 1°C per minute. Cells were transferred to liquid nitrogen (-180°C) after 24 hours.

Thawing of Cryopreserved PBMC and TIL

Cryopreserved cells were removed from liquid nitrogen and placed in a water bath set at 37°C. Once completely thawed cells were transferred to pre-warmed growth media and washed at 1600 rpm for 10 minutes before resuspension in an appropriate volume for further work.

Flow Cytometry – Beckman-Coulter Gallios

For Chapters 3 and 4, data acquisition was carried out on a Gallios 10-parameter flow cytometer using CytoSoftware (Beckman-Coulter). Further offline analysis was performed with Kaluza Analysis Software (Beckman-Coulter). To enable isolated fluorochrome analysis compensation was performed to account for spectral overlap. Anti-mouse IgG-CompBeads (BD) were used to individually stain each fluorochrome conjugated antibody. Auto-compensation in CytoSoftware was used to effectively compensate spectral overlap. Cells were gated using FSC-H versus FSC-A to identify single cells. Single lymphocytes were determined

by their FSC-A and SSC-A properties. Dead cells were gated out using propidium iodide (PI) and live T cells were identified within the PI- CD3+ gate. T cells were further defined as CD4+ T helper cells and CD8+ cytotoxic T cells. NK cells were identified as CD56+CD3- and further defined using relative CD56 and CD16 expression.

Lymphocyte Subset Identification by Cell Surface Staining – Beckman-Coulter Gallios

PBMC or TIL were resuspended in 100µl of MACS buffer at a final concentration of 0.5-1x10^7 cell/ml. Cells were surface stained with a panel of fluorophore conjugated antibodies (Figures 2-4) for 20 minutes at 4°C. Cells were washed once in MACS buffer and resuspended in 150µl for cytometric analysis. At least 50,000 lymphocytes were recorded based on size and granularity using the FSC-A versus SSC-A plot.

Flow Cytometry – BD FACSymphony A3

Flow cytometric analysis for chapters 6 and 7 was carried out using a BD FACSymphony machine with BD FACS DIVA acquisition Software (26-parameter flow cytometry). Further offline analysis was performed using FlowJo analysis software (BD-TreeStar). Compensation was performed to limit the impact of spectral overlap which was considerable given the number of fluorochromes used. Compensation Plus Beads (BD) were used to individually stain each fluorochrome conjugated antibody. Auto-compensation within FACS DIVA was used to compensate spectral overlap. Cells were gated using FSC-H versus FSC-A to identify single cells. Single lymphocytes were determined by their FSC-A and SSC-A properties. Dead cells were gated out using propidium iodide (PI). Antibody concentrations were titrated accordingly to limit spectral overlap.

Lymphocyte Subset Identification by Cell Surface Staining – BD FACSymphony

Cells were prepared for flow cytometric staining using sodium azide-free buffers. Cells were washed a further time in protein-free PBS. Cells were resuspended in the residual volume, and 1 µl of 1/10 diluted Fixable Viability Stain was added to each tube and vortexed immediately. Then 5µl of FcR block is added to the cell suspension and incubated for 10 minutes at room temperature protected. Without washing, cells were stained with a prepared antibody cocktail (Figures 5,6) in 50µl of Brilliant Stain Buffer per specimen. Cells were incubated for 30 minutes at 4°C. After incubation, cells were washed once in MACS buffer and resuspended in 150µl for cytometric analysis. At least 50,000 lymphocytes were recorded based on size and granularity using FSC versus SSC properties.

For cells requiring intracellular/intranuclear staining the further following steps were undertaken. Tru-Nuclear Transcription Factor Fix working solution was made by diluting one part 4x Fix Concentrate with three parts Fix Diluent. Tru-Nuclear was added to each specimen and incubated at room temperature for 45 minutes in the dark. Permeability buffer was then added to the cell suspension and tubes were centrifuged at 1800 rpm for 5 minutes. A further permeability buffer wash was performed before addition of the intracellular/intranuclear antibodies. Antibodies were incubated at 4°C for 30 minutes and subsequently washed with permeability buffer prior to resuspension in MACS buffer for flow cytometric acquisition.

Flow Cytometry Panels

A number of different flow cytometry panels were used in the thesis and are shown below in relation to each Chapter.

Flow cytometry panel used in Chapter 3 – Panel A (Figure 2)

Fixable viability	**BV510**
CD3	**FITC**
TIM-3	**PE**
CD25	**PE-DAZZLE**
CD8	**PerCpCy5.5**
CD127	**PE-Cy7**
TIGIT	**APC**
CD45	**AF700**
CD4	**APC-Cy7**
PD1	**BV421**

Flow cytometry panel used in Chapter 3 - Panel B (Figure 3)

Fixable viability	**BV510**
CD3	**FITC**
TCR va7.2	**PE**
CD19	**PE-DAZZLE**
CD16	**PerCpCy5.5**
CD56	**PE-Cy7**
ydTCR	**APC**
CD45	**AF700**
CD161	**APC-Cy7**
CD27	**BV421**

Flow cytometry panel used in Chapter 5 (Figure 4)

Fixable viability	**BV510**
CD3	**FITC**
GITR	**PE**
CD39	**PE-DAZZLE**
CD8	**PerCpCy5.5**
CD56	**PE-Cy7**
CD69	**APC**
CD45	**AF700**
CD4	**APC-Cy7**
CD103	**BV421**

Flow cytometry panel used in Chapter 6 (Figure 5)

Instrument / Configuration		BD FACSymphony™ A3	7 UV - 8 Violet - 6 Blue - 4 Yellow/Green - 3 Red	
Excitation Laser Line	Fluorescence Channel	Marker/Antibody	Clone	Cat. No.
UV 355 nm	BUV395	CD4	SK3	563550
	BUV496	CD8	SK1	741199
	BUV563	CD27	M-T271	741366
	BUV615	CD95	DX2	752346
	BUV661	ICOS	DX29	741664
	BUV737	CD38	HB7	612824
	BUV805	CD45	HI30	612891
Violet 405 nm	BV421	CD96	6F9	742794
	BV480	CD28	CD28.2	566110
	BV570-P	CD3	UCHT1	Biolegend
	BV605	BTLA	J168-540	743986
	BV650	CCR7	2-L1-A	566756
	BV711	TIGIT	741182	747839
	BV750	DNAM	DX11	747026
	BV786	CD45RA	HI100	563870
Blue 488nm	BB515	CD57	NK-1	565285
	BB630-P	CD127	HIL-7R-M21	custom
	BB660-P	LAG3	T47-530	custom
	BB700	PD1	EH12.1	566460
	BB755-P			
	BB790-P	CD69	FN50	Custom
Yellow / Green 561nm	PE	2B4	2-69	550816
	PE-CF594	KLRG1	14C2A07	Biolegend
	PE-Cy5	CD14/CD19	M5E2/HIB19	Biolegend/555414
	PE-Cy7	CD25	M-A251	557741
Red 640	AF647	CD160	BY55	562362
	R718	CD103	Ber-ACT8	752007
	FVS780	Viability		565388

Flow cytometry panel used in Chapter 7 (Figure 6)

Instrument / Configuration		BD FACSymphony™ A3	7 UV - 8 Violet - 6 Blue - 4 Yellow/Green - 3 Red	
Excitation Laser Line	Fluorescence Channel	Marker/Antibody	Clone	Cat. No.
UV 355 nm	BUV395	CD4	SK3	563550
	BUV496	CD8	SK1	741199
	BUV563	CD16	3G8	748851
	BUV615	CD94	HP-3D9	751525
	BUV661	TCRgd	11F2	750019
	BUV737	CD56	NCAM16.2	612766
	BUV805	CD45	HI30	612891
Violet 405 nm	BV421	GITR	V27-580	566423
	BV480	HLA-DR	G46-6	566113
	BV570-P	CD3	UCHT1	Biolegend
	BV605	CD161	DX12	747762
	BV650	CCR7	2-L1-A	566756
	BV711	Ki-67	B56	563755
	BV750	CD39	TU66	747079
	BV786	CD45RA	HI100	563870
Blue 488nm	AF488	HSP70	W27	Biolegend
	BB630-P	CD127	HIL-7R-M21	custom
	BB660-P	GrzB	GB11	custom
	PerCP-Cy5.5	GPR183	SA313E4	Biolegend
	BB755-P			
	BB790-P	CD69	FN50	Custom
Yellow / Green 561nm	PE	GrzA	CB9	Biolegend
	PE-CF594	FoxP3	259D/C7	562421
	PE-Cy5	CD14/CD19	M5E2/HIB19	Biolegend/555414
	PE-Cy7	CD25	M-A251	557741
Red 640	AF647	GrzK	G3H69	566655
	R718	CD103	Ber-ACT8	752007
	FVS780	Viability		565388

Data Handling and Statistical Analysis for Flow Cytometric Analyses

Statistical Analysis was performed using GraphPad Prism (GraphPad Software). To determine differences between groups a non-parametric Mann-Whitney Test was performed. A Wilcoxon signed rank test was used to determine differences between matched pairs. The null hypothesis was rejected when $p<0.05$. Multiple comparison data was analysed by Sidak's multiple comparison test. * indicated $p<0.05$, ** $p<0.01$, *** $p<0.001$, ****$p<0.0001$

Sample Processing for scRNA-seq

Tumour and macroscopically normal oesophageal tissue was collected in MACS® Tissue Storage Solution (Miltenyi Biotec) and cut into small fragments (<0.5mm^3) prior to placement in a gentleMACS™ C Tube (Miltenyi Biotec) containing 5ml pre-warmed Digestion solution. Dissociation of tissue fragments was achieved using a gentleMACS™ dissociator (Human Tumor Programme 1, 2 and 3) with incubation at 37°C for 30 minutes between each agitation. The single cell suspension was filtered through a 70µm filter and red blood cells were subsequently lysed. Cells were washed and resuspended in MACS buffer prior to immunostaining and FACS sorting. Single cell suspensions of digested tumour tissue were surface stained with anti-CD45 BV785 (2D1, Biolegend), anti-EpCAM APC (9C4, Biolegend) and anti-Podoplanin AF488 (NC-08, Biolegend) to allow for enrichment of immune cells, epithelial cells and fibroblasts, respectively. PI was added prior to sorting to exclude non-viable cells. Sorted cell populations were adjusted to 1 x 10^3/ml.

Samples with >85% cell viability were processed at the Genomics Birmingham Sequencing Facility (University of Birmingham, UK) for gene expression profiling using the 10X Genomics platform. Around 1.7 x 10^4 cells per sample were processed using the Chromium Controller (10X Genomics) for a recovery of 1 x 10^4 cells per sample, and library preparation was performed using the Chromium Single Cell 3′ Library & Gel Bead Kit v2 according to manufacturer's instructions. Library quantification and quality control was performed using

TapeStation (Agilent). Samples were sequenced on an Illumina NextSeq 500 (150 bps, paired-end) at a sequencing depth of >50,000 raw reads/cell.

Processing of scRNA-seq data

Bioinformatic processing and analysis was outsourced to the Moss Group Informatics lead Dr Wayne Croft and all of the methods below are as described for his work.

Raw sequencing read data were processed using Cell Ranger v5.0.1. Raw read bcl files were converted to fastq and aligned to the Human reference genome GRCh38 with cellranger mkfastq and cellranger count respectively, giving a matrix representing unique molecular identifiers (UMI's) per cell barcode per gene. The raw UMI matrices for each sample were processed using R v3.6.2 with the Seurat package v3.2.0. Matrices were filtered to remove cells with < 500 genes detected, > 3500 genes detected and cells with >10% of reads mapping to mitochondrial RNA. DoubletFinder was used to identify doublets and these were subsequently removed from further analysis.

Cell cycle score for each cell was calculated with Seurat CellCycleScoring function and the difference between G2M and S phase score quantified. For normalisation, Seurat SCTransform function was applied, regressing out percentage mitochondrial mapping and G2M-S phase cell cycle score difference. Data from all samples was then integrated using the IntegrateData function following Seurat SCTransfrom integration workflow on the top 8k most variable genes.

Unsupervised clustering and cell type annotation

All variably-expressed genes were used for dimensionality reduction, firstly by principal component analysis (PCA) and subsequently by uniform manifold projection (UMAP), selecting PCs 1:20 that explained the majority of the variance observed (assessed by elbow plots). A shared nearest-neighbour graph was constructed in PCA-space using PCs 1:20 with

Seurat FindNeighbors function. Clusters are identified within this graph using Seurat FindClusters function, optimising the modularity with the Louvain algorithm. The resolution parameter to control cluster granularity was automatically selected at 0.7 by iteratively increasing this parameter from 0.6 until the criteria of a minimum of 5 differentially expressed (FDR < 0.05 & min. 2-fold expression difference) cluster marker genes were no longer met. Cluster marker genes were identified with FindAllMarkers function using default parameters.

To annotate clusters with high-level cell type, canonical cell type marker gene expression level was assessed in combination with automated cell type annotation using SingleR v1.0.6. åon HPCA and Monaco reference sets. High level cell type markers used to inform annotation were CD3D (T cell), MS4A1 (B cell), IGKC (Plasmablast), EPCAM (Epithelial), MKI67 (Cycling), PECAM1 (Endothelial), DCN (Fibroblast), LYZ (Myeloid), TPSAB1 (Mast) Ambiguous cells that could not be clearly assigned to a high-level cell type were removed from further analysis. For finer grained analysis within high-level cell types, data were subset on the following groupings for independent analysis of each high level cell type: Lymphocyte T/NK (clusters T and NK), Lymphocyte B (B and Plasmablast), Stromal (Epithelial, Endothelial, Fibroblast, Myofibroblast), Myeloid, Mast and Cycling. Each subset was split back to the raw per-sample UMI matrix data and SCTransform integration procedure applied as previous. Dimensionality reduction, clustering and cell type annotations were then applied on these subsets as previously described. Clusters were annotated with phenotype and main gene discriminating from other clusters wherever possible. The T/NK group were subset further and re-clustered for the finer grained analysis of T and NK cells independently. The stromal grouping was also further subset for the independent analysis of Fibroblasts and Endothelial/Epithelial cells. At each iteration following subsetting and re-clustering, any cells that were carried over due to previous mis-clustering and hence assigned an incorrect cell type were removed from further analysis. Mis-

clustered cells were identified by assessing expression of a panel of high level cell type markers.

Cluster proportion comparisons

Samplewise proportions of each cluster were calculated and stratified by pre/post chemotherapy, Mandard score and tissue type. Wilcoxon rank sum test was applied to compare the distributions of cluster proportions observed.

Signature scoring

Cells were scored for signatures of interest using the Seurat AddModuleScore function. This score is calculated as the average expression of the gene module per single cell minus background expression from randomly selected control features with positive scores indicating that the gene module is expressed more highly than expected given the average population expression. T cell relevant signatures; naïve, cytotoxic, exhaustion, T regulatory cells, inhibitory checkpoints, stimulatory checkpoints and tissue resident memory cells were included. Fibroblast cells were scored for the gene sets CAF UP EAC progression, OAC UP and OAC DN. The distribution of signature scores from tumour sample data post and pre chemotherapy were compared using Wilcoxon rank sum test.

Differential expression

Genes differentially expressed in post vs pre chemotherapy and tumour vs adjacent normal sample data were identified using findMarkers with MAST option (test.use="MAST"), which uses a hurdle model tailored to scRNA-seq data. MAST is a two-part GLM that simultaneously models how many cells express the gene by logistic regression and the expression level by

Gaussian distribution. Differential expression testing is then done using the likelihood ratio test.

Gene set enrichments

Enrichment for Hallmark gene sets within clusters was assessed by gene set variation analysis using the R package GSVA.

Chapter 3: Phenotypic analysis of Lymphocytes in Peripheral Blood and Tumour in Oesophageal Adenocarcinoma

Introduction

The prognosis of oesophageal adenocarcinoma remains poor for most patients although there has been some improvement in survival with the advent of FLOT peri-operative chemotherapy[88]. Immunotherapy is a relatively new modality and the underlying mechanisms that mediate tumour regression to checkpoint inhibition are likely to vary for different tumours. Evidence specific to oesophageal adenocarcinoma predominantly uses immunohistochemical analysis of PD-1 and PD-L1 expression which, although beneficial in determining location of immune infiltrate, fails to define the detailed phenotypic and functional qualities of the immune infiltrate[89–91]. In order to understand potential opportunities for immunotherapy a wider understanding of the immune infiltrate is required. In addition, whilst neoadjuvant treatment has been shown to improve survival for locally advanced oesophageal cancer, little is known about the impact of neoadjuvant chemotherapy on the immune infiltrate of oesophageal cancer.

My work in this chapter undertakes a phenotypic analysis of the lymphocytic infiltrate in oesophageal adenocarcinoma. The immune infiltrate of chemotherapy-naïve and exposed patients is assessed with a particular focus on immunological features of lymphocytic 'exhaustion' and checkpoint expression. This analysis provides an overview of the immune landscape in oesophageal adenocarcinoma from which more detailed phenotypic assessments can be performed.

Methods

Blood and matched tumour samples were obtained from 30 patients with OAC.
Twenty patients had undergone treatment with neoadjuvant chemotherapy (NACT). The neoadjuvant treatment of choice during the study period was FLOT. Thirteen patients were identified to have responded to NACT (TRG 1-3) whereas seven patients failed to demonstrate a response (TRG4-5).

Peripheral blood lymphocytes and tumour infiltrating lymphocytes (TIL) were isolated and frozen prior to use. Samples were defrosted and stained with a panel of antibodies against 10 cell surface markers. Two flow cytometry panels (Figures 2,3) were completed for each matched pair were completed.

Results

Presence of CD4+ and CD8+ T Cells in Oesophageal Adenocarcinoma

Lymphocytes isolated from the peripheral blood and tumours of patients with OAC were stained with antibodies against a range of cell surface proteins and analysed by flow cytometry. Cells were gated initially to remove doublet cells before gating on live lymphocytes (CD45+ cells). T cells were classified based on their expression of CD3 and were subsequently defined based on their differential expression of CD4+ or CD8+ (n=30, Figure 7). No difference was seen in the proportion of CD4+ and CD8+ T cells in PBMC (p=0.15) or TIL (p=0.51) with a comparable CD4/C8 ratio in PBMC and TIL (p=0.062) (Figure 8.). Administration of neoadjuvant chemotherapy did not alter the proportion of CD4+ to CD8+ T cells in TIL (p=0.95). However, a 36% reduction in CD8+ T cells was seen in PBMC as compared to CD4+ T cells after treatment (p=0.012). CD4+ increased by 21% in PBMC of patients exposed to neoadjuvant chemotherapy (p=0.023, p=0.012, Figure 9).

I was also interested to assess how changes in the lymphoid pool correlated with the degree of pathological response to chemotherapy. Response to neoadjuvant chemotherapy was not associated with the proportion of CD4+ or CD8+ T cells in PBMC (p=0.65, p=0.77) and there was also no difference in the proportion of CD4+ or CD8+ T cells within TIL when comparing response to neoadjuvant chemotherapy (p=0.14, p=0.53).

These results demonstrate that T cells are the dominant T cell population in OAC. However, with the exception of circulating CD4+ T cells, exposure to, and subsequent response to, chemotherapy does not impact their proportion in OAC.

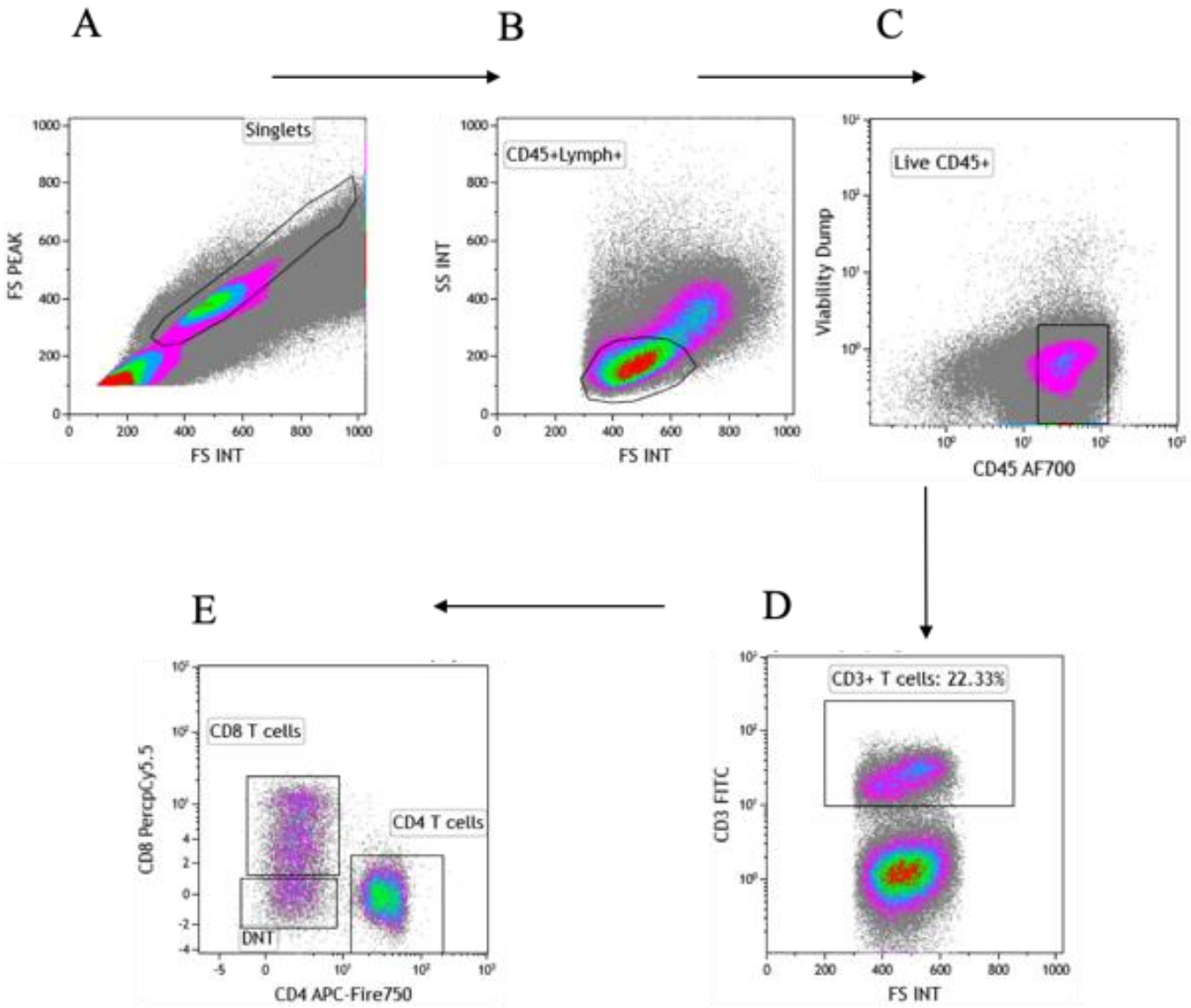

Figure 7. Gating strategies for the identification of CD4, CD8 and double negative T cells (DNT).
Cells were first gated to remove doublet cells (A), before gating on lymphocytes based on FSC-A and SSC-A properties (B). Lymphocytes were classified as being propidium iodide (PI) negative and CD45 positive cells C). T cells were identified from the CD45 positive population by the expression of CD3. CD4, CD8 and DNT cells were gated from the CD3 population (E). Plots shown are representative of TIL isolated from OAC tissue of a single individual.

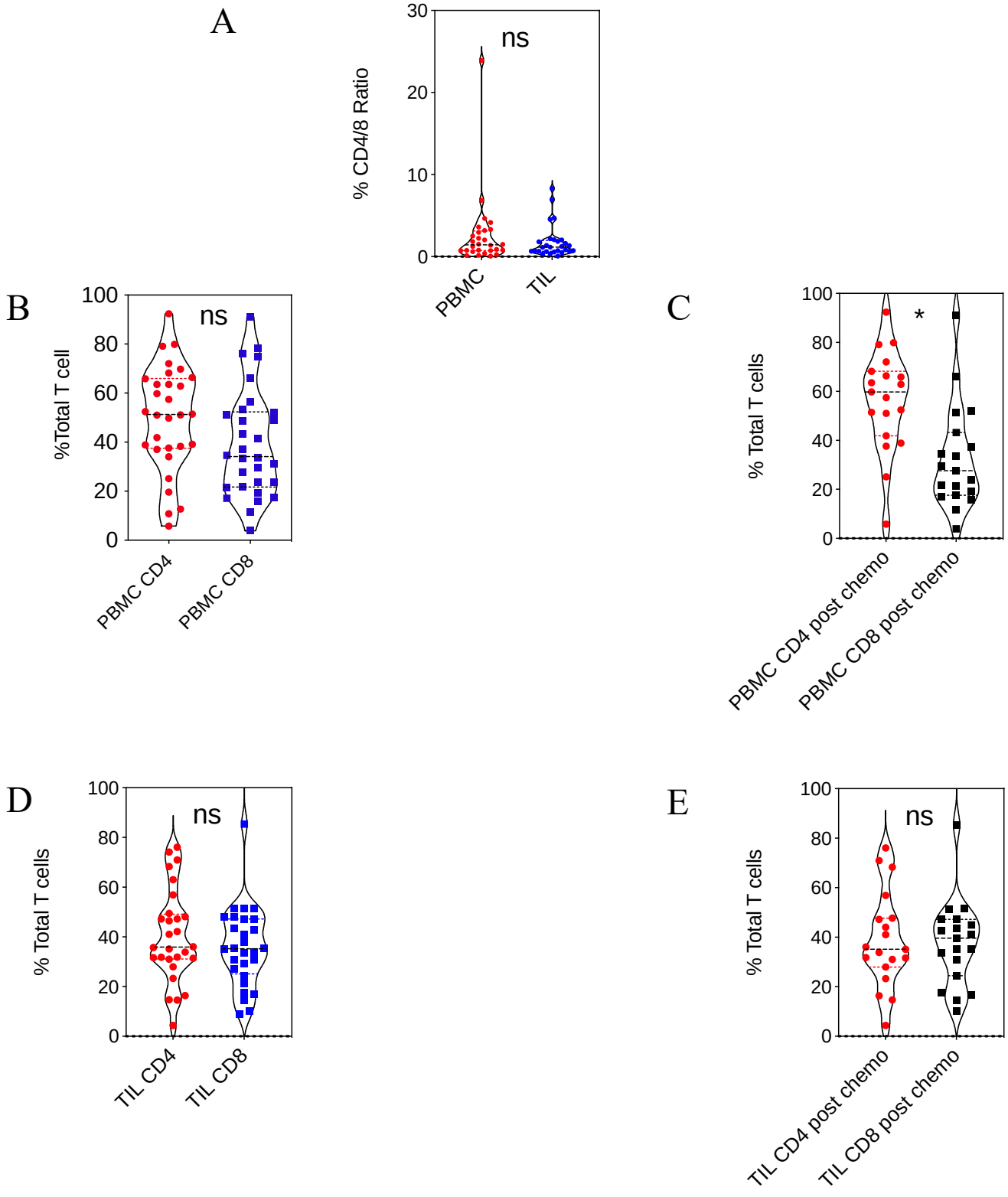

Figure 8. Proportion of CD4+ and CD8+ T cells in PBMC and TIL.
The proportion of CD4+ and CD8+ T cells in matched PBMC and TIL was calculated and expressed as a CD4:CD8 ratio (A). The proportion of CD4+ and CD8+ T cells in PBMC was determined as a proportion of total CD3+ (B), and was repeated for patients who had undergone neoadjuvant chemotherapy (C). The proportion of CD4+ and CD8+ in TIL was determined as a proportion of total CD3+ (D), and was repeated for patients who had undergone neoadjuvant chemotherapy (E). Each symbol represents an individual patient (n=30). Dashed horizontal lines indicate the median and dotted lines indicate the interquartile range. Data analysed by Wilcoxon matched-pairs signed rank test for matched samples(A,B,D), data analysed by Mann Whitney test for unpaired samples (C,E). * denotes $p<0.05$.

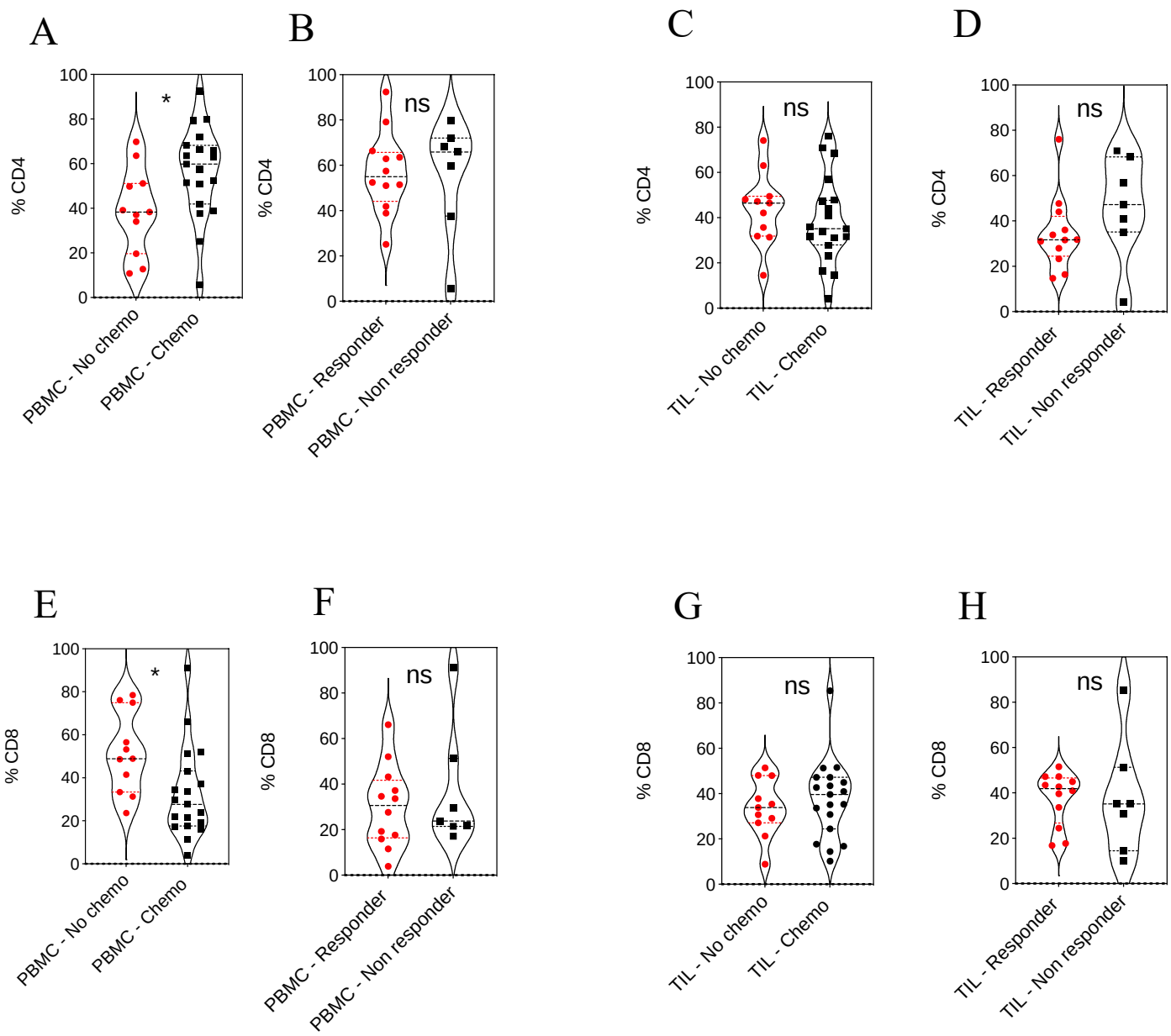

Figure 9. Differential impact of neoadjuvant chemotherapy on the proportion of CD4+ and CD8+ T cells in PBMC and TIL.
Differential proportion of CD4+ T cells in PBMC dependent on administration or absence of neoadjuvant chemotherapy (A) and subsequently dependent on response to chemotherapy (B). (responders defined as Mandard score 1-3, No chemo n=10, Chemo n=20). Differential proportion of CD4+ T cells in TIL dependent on administration or absence of neoadjuvant chemotherapy (C) and subsequently dependent on response to chemotherapy (D). Subsequent plots as provided for CD8+ T cell in PBMC and TIL dependent on exposure and response to chemotherapy (E-H, Responder n=13, non-responder n=7). Data analysed by Mann Whitney test, * denotes $p<0.05$.

Γδ, MAIT and CD161+ve T Cells in Oesophageal Adenocarcinoma

T cells were next classified dependent on their expression of γδ T cell receptor, TCRVα7.2 and CD161 in order to assess the potential importance of γδT cells, mucosal-associated invariant T cells (MAIT) or CD161+ T cells (n=30). MAIT cells are highly conserved in evolution and express a semi-invariant TCR which recognises derivatives from the riboflavin synthetic pathway expressed on MR1.

All three subtypes were detected in both PBMC and TIL (Figure 10). Only a small proportion of T cells were identified to be of the γδ lineage. The proportion of γδ in TIL was reduced by 42% as compared to PBMC (p=0.0067, Figure 11). However, there was no difference in the proportion of γδ T cells in PBMC or TIL when comparing patients who were treatment naive or had been given neoadjuvant chemotherapy (p=0.73, p=0.52). Equally, there was no difference in the proportion of γδ T cells in PBMC or TIL in those who did and those who did not respond to neoadjuvant chemotherapy (p=0.97, p=0.84).

MAIT cells increased threefold in OAC TIL and compared to PBMC (p=0.003, Figure 12). However there was no significant difference in the proportion of MAIT cells in PBMC or in TIL when comparing those who had and had not been given neoadjuvant chemotherapy (p=0.33, p=0.79). Equally there was no significant difference in the proportion of MAIT cells in PBMC or in TIL in those who did and those who did not respond to neoadjuvant chemotherapy (p=0.65, p=0.54).

CD161+ T cells were also increased threefold in OAC TIL when compared to PBMC (p=0.003, Figure 13). However, no difference was seen in the proportion of CD161+ T cells in PBMC or TIL when comparing patients who had and had not been given neoadjuvant chemotherapy (p=0.20, p=0.61). Equally there was no difference in the proportion of CD161+ T cells in PBMC or in TIL in those who did and those who did not respond to neoadjuvant chemotherapy (p=0.71, p=0.90).

These data show that γδ, MAIT and CD161+ T cells are identifiable in both the PBMC and TIL of patients with OAC. The proportion of γδ T cells is not influenced by environment or chemotherapy whilst the latter two populations are increased in TIL. However, their proportion at that site is not influenced by either chemotherapy or the response to this treatment.

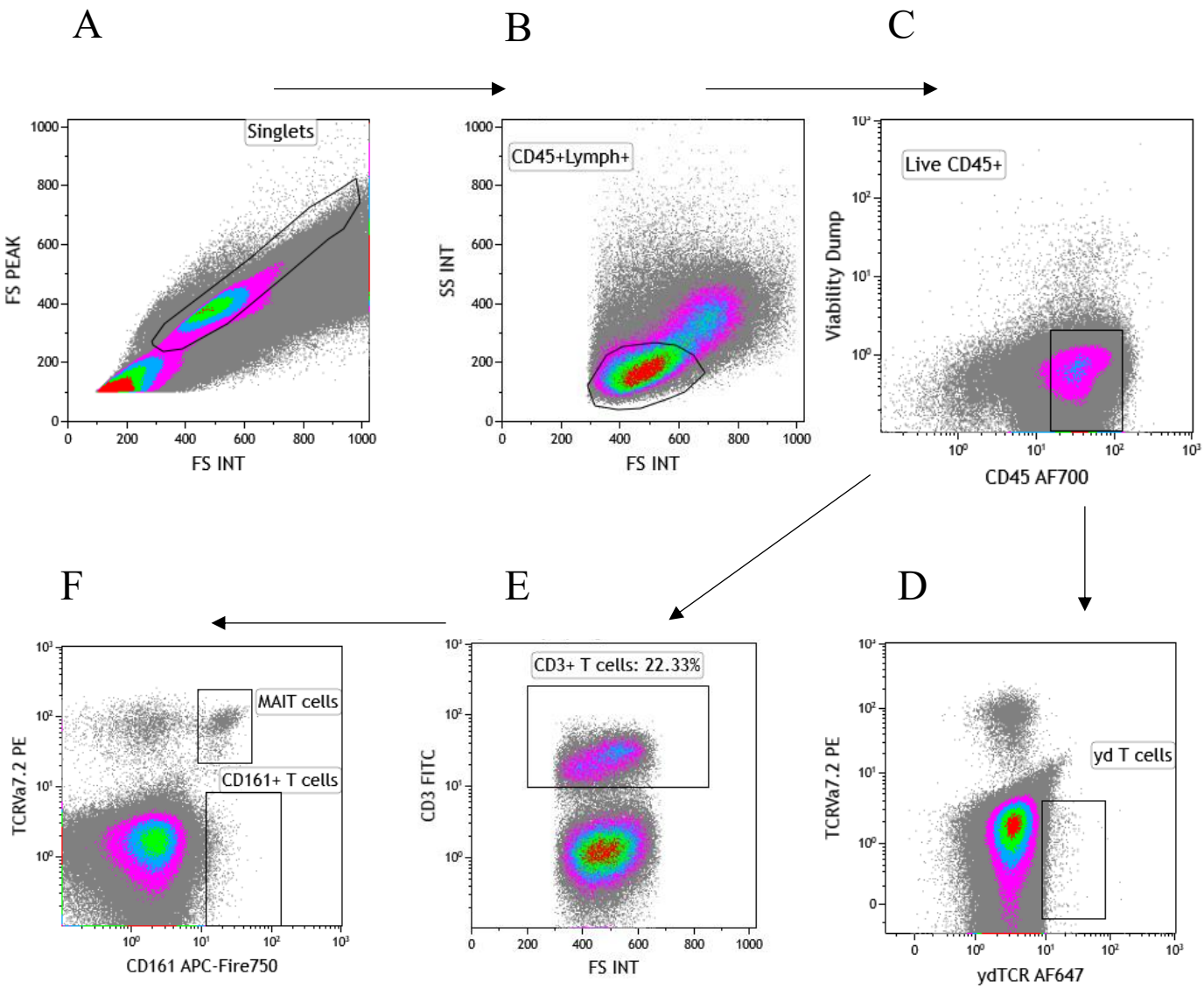

Figure 10. Gating strategies for the identification of γδ, CD161 and MAIT T cells
Cells were first gated to remove doublet cells (A), before gating on lymphocytes based on FSC-A and SSC-A properties (B). Lymphocytes were classified as being propidium iodide (PI) negative and CD45 positive cells (C). γδ T cells were identified as γδTCR+ lymphocytes (D). CD3+ T cells were isolated from lymphocytes (E). MAIT cells were defined as CD161 and T cell receptor alpha chain segment V alpha 7.2 (TCRVa7.2) positive whereas as CD161 T cells were negative for TCRVa7.2 (F)

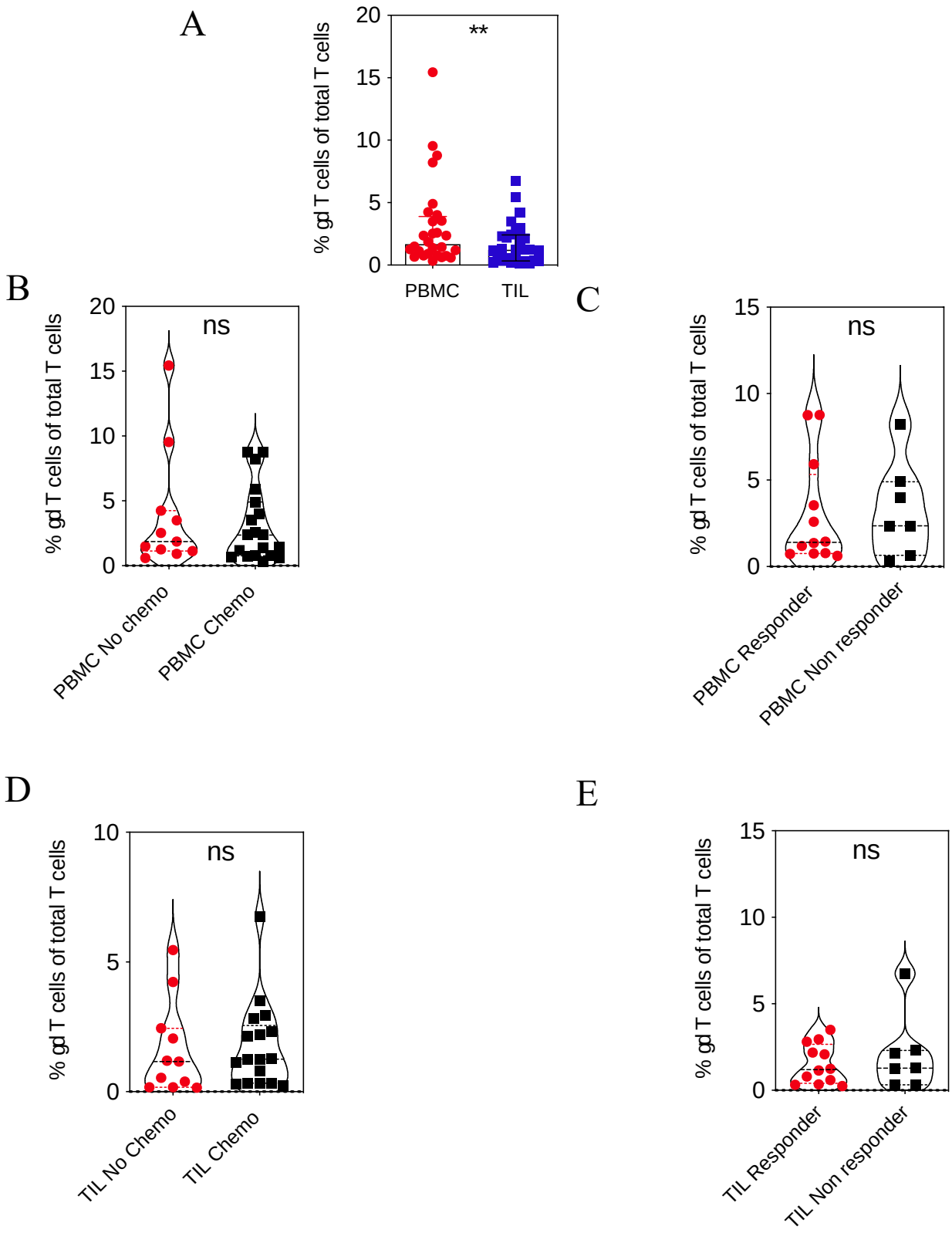

Figure 11. Proportion of yd T cells in PBMC and TIL.
The proportion of yd T cells in matched PBMC and TIL (n=30, A). Differential proportion of yd T cells in PBMC dependent on administration or absence of neoadjuvant chemotherapy (No chemo n=10, Chemo n=20, B) and subsequently dependent on response to chemotherapy (C, responders defined as Mandard score 1-3, Responder n=13, non-responder n=7). Differential proportion of yd T cells in TIL dependent on administration or absence of neoadjuvant chemotherapy (D) and subsequently dependent on response to chemotherapy (E). Each symbol represents an individual patient. Dashed horizontal lines indicate the median and dotted lines indicate the interquartile range. Data analysed by Wilcoxon matched-pairs signed rank test for matched samples(A), data analysed by Mann Whitney test for unpaired samples (B-E), ** denotes $p<0.01$.

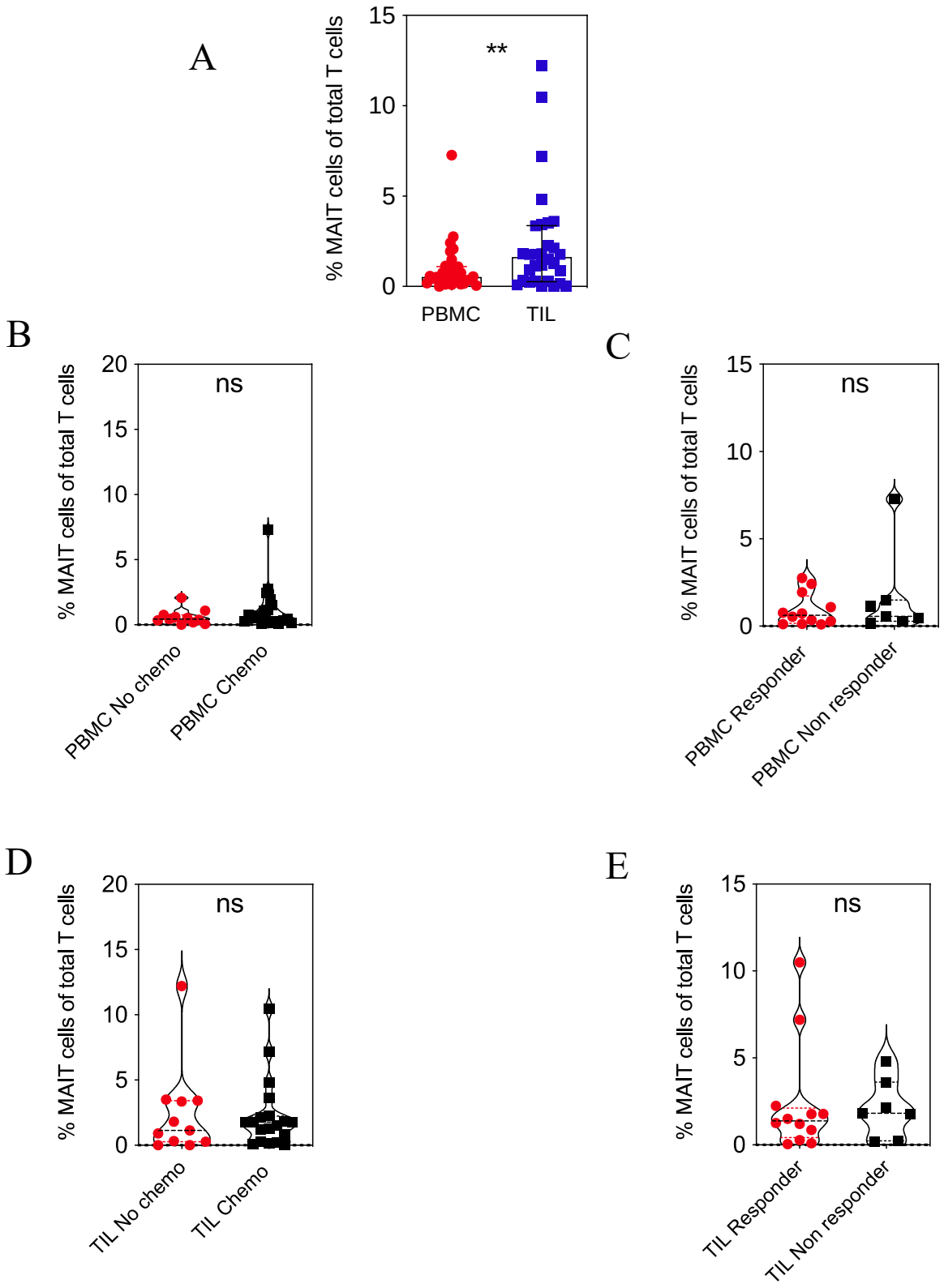

Figure 12. Proportion of Mucosal Invariant T cells (MAIT) in PBMC and TIL.
The proportion of MAIT cells in matched PBMC and TIL (n=30 A). Differential proportion of MAIT cells in PBMC dependent on administration or absence of neoadjuvant chemotherapy (chemo n=10, Chemo n=20, B) and subsequently dependent on response to chemotherapy (C, responders defined as Mandard score 1-3, responder n=13, non-responder n=7). Differential proportion of MAIT cells in TIL dependent on administration or absence of neoadjuvant chemotherapy (D) and subsequently dependent on response to chemotherapy (E). Each symbol represents an individual patient. Dashed horizontal lines indicate the median and Data analysed by Wilcoxon matched-pairs signed rank test for matched samples(A), data analysed by Mann Whitney test for unpaired samples (B-E), *** denotes p<0.001.

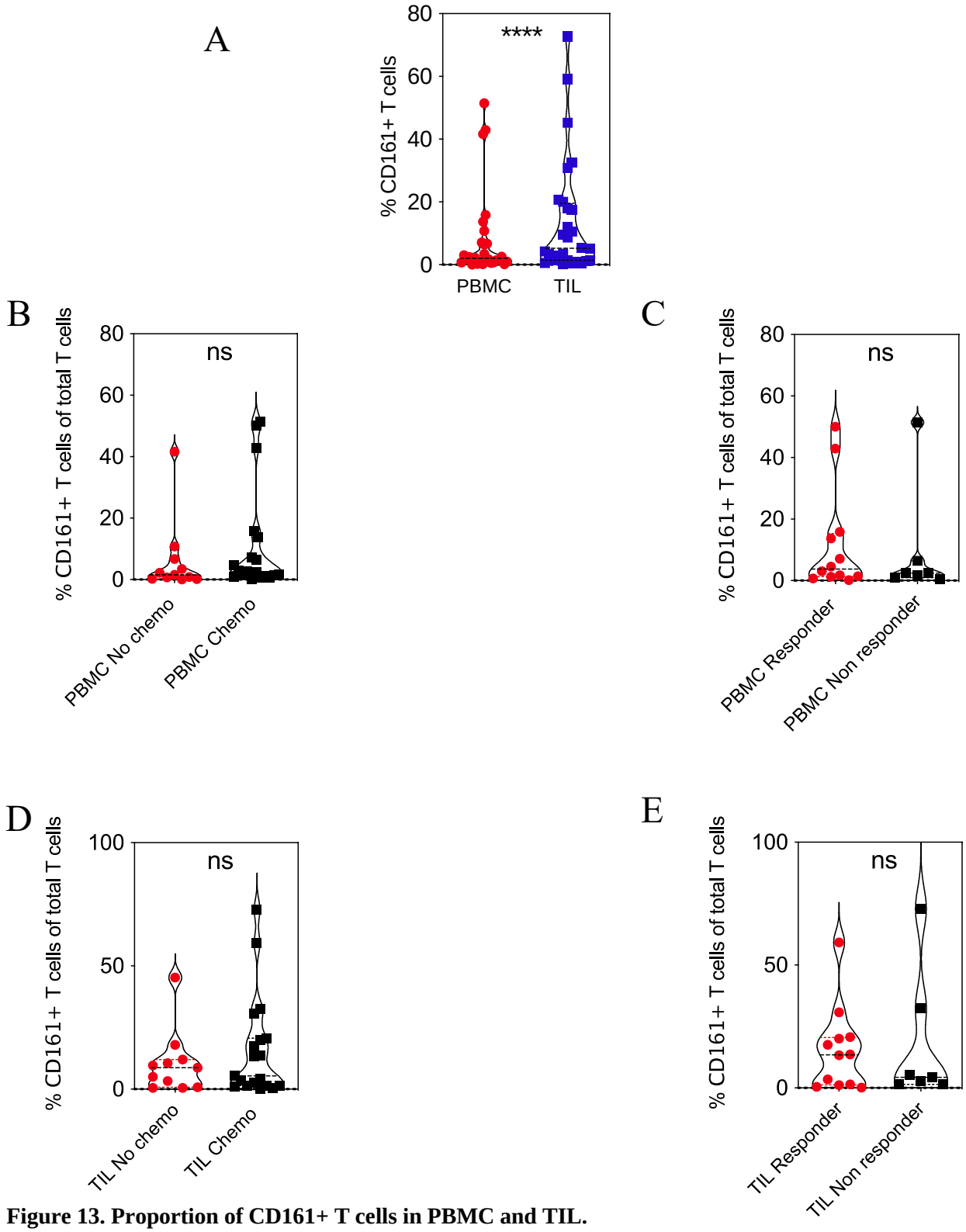

Figure 13. Proportion of CD161+ T cells in PBMC and TIL.
The proportion of CD161+T cells in matched PBMC and TIL (n=30A). Differential proportion of CD161+T cells in PBMC dependent on administration or absence of neoadjuvant chemotherapy (No chemo n=10, Chemo n=20, B) and subsequently dependent on response to chemotherapy (C, responders defined as Mandard score 1-3, responder n=13, non-responder n=7). Differential proportion of CD161+T cells in TIL dependent on administration or absence of neoadjuvant chemotherapy (D) and subsequently dependent on response to chemotherapy (E). Each symbol represents an individual patient. Dashed horizontal lines indicate the median and dotted lines indicate the interquartile range. Data analysed by Wilcoxon matched-pairs signed rank test for matched samples(A), data analysed by Mann Whitney test for unpaired samples (B-E), *** denotes p<0.001.

CD4+ T regulatory cells (Treg) are increased in Oesophageal Adenocarcinoma but their proportion is not related to neoadjuvant chemotherapy

T regulatory cells (Treg) are a dominant cell population in many tumours and were identified as a distinct population of CD4+ T cells based on the absence of CD127 expression and significant upregulation of CD25 (Figure 14). Tregs populations represented 13.6% of CD4+ T cells in tumour compared to 5.7% in blood and therefore were increased by a factor of 2.4 times in TIL as compared to PBMC ($p<0.0001$). There was no difference in their proportion in relation to prior treatment with neoadjuvant chemotherapy ($p=0.64$, $p=0.64$). Equally, no difference was seen in relation to response to neoadjuvant chemotherapy although a non-significant decrease was seen in the TIL populations of responder patients ($p=0.80$, $p=0.09$).

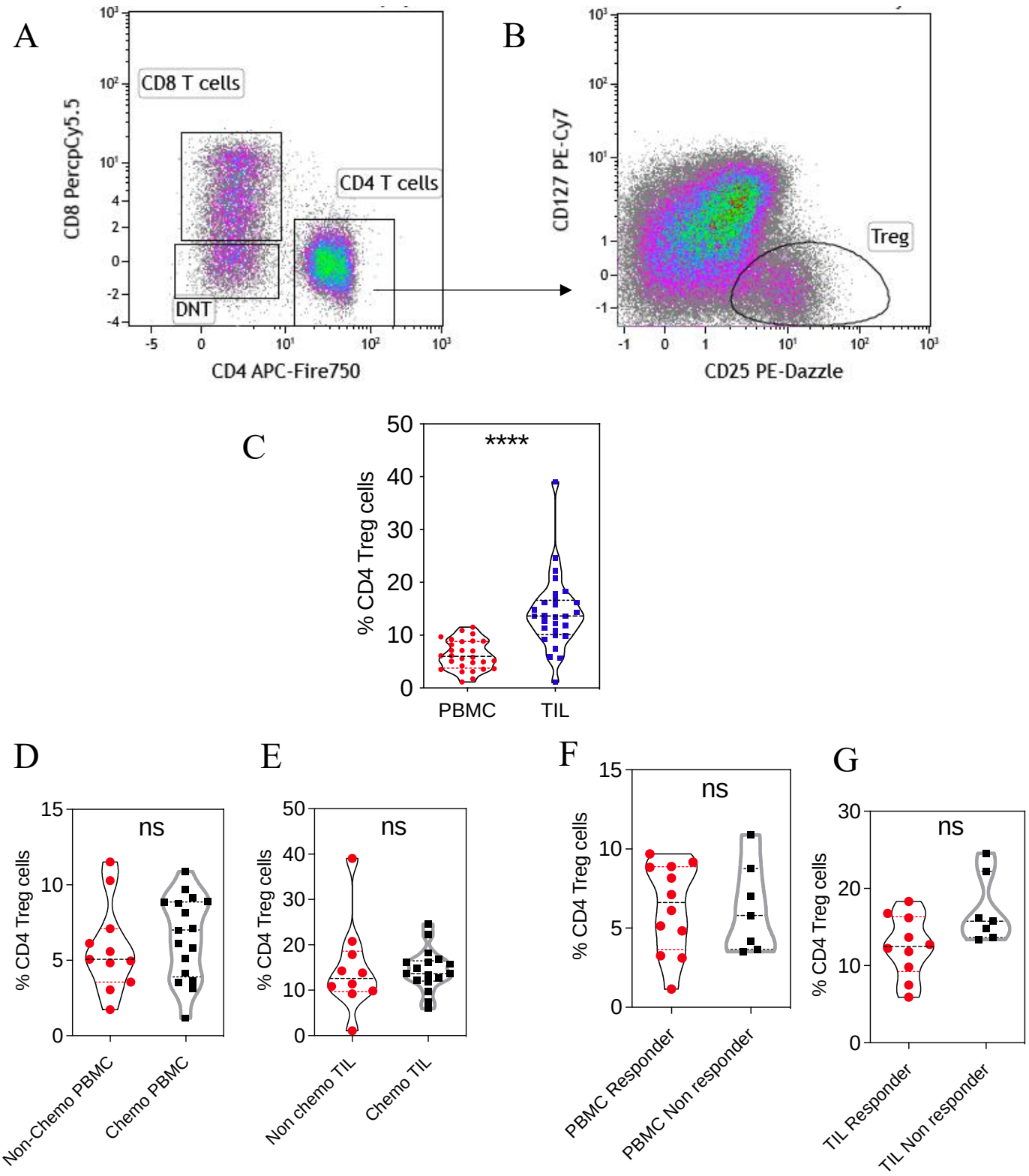

Figure 14. Tregs in matched PBMC and TIL.
Tregs were identified a proportion of CD4+ T cells (A) that were CD25 positive and CD127 negative(B). The proportion of Tregs in matched PBMC and TIL (n=30, C). Differential proportion of Tregs in PBMC dependent on administration or absence of neoadjuvant chemotherapy (No chemo n=10, Chemo n=20, D) and subsequently dependent on response to chemotherapy (E, responders defined as Mandard score 1-3, Responder n=13, non-responder n=7). Differential proportion of Tregs in TIL dependent on administration or absence of neoadjuvant chemotherapy (F) and subsequently dependent on response to chemotherapy (G). Each symbol represents an individual patient. Dashed horizontal lines indicate the median and dotted lines indicate the interquartile range. Data analysed by Wilcoxon matched-pairs signed rank test for matched samples(C), data analysed by Mann Whitney test for unpaired samples (D-G), * denotes $p<0.05$, **** denotes $p<0.0001$.

Expression of checkpoint proteins on CD8+ T cells

CD8+ T cells were next assessed for their expression of proteins associated with T cell checkpoints. In particular, antibodies against PD-1, TIGIT and Tim-3 were used to stain CD4+ and CD8+ T cells within the blood and TIL populations of OAC patients.

CD8+ TIL were seen to significantly upregulate expression of PD-1, TIGIT and TIM-3 compared to those within PBMC ($p<0.0001$, $p<0.0001$, $p<0.0001$, Figure 15). In particular, median expression of PD-1 increased from 27% in PBMC to 65% in TIL. Median expression of TIGIT increased from 27% to 48% and TIM-3 expression increased from 0.5% to 5.5%.

No difference was seen in the expression of PD-1 on CD8+ T cells in PBMC or TIL when comparing patients who had and had not been given neoadjuvant chemotherapy ($p=0.47$, $p=0.20$). Equally there was no difference in the expression of PD-1 on CD8+ T cells in PBMC or TIL in those who did and those who did not respond to neoadjuvant chemotherapy ($p=0.26$, $p=0.27$, Figure 16). No difference was observed in the expression of TIGIT on CD8+ T cells in PBMC or TIL in relation to chemotherapy treatment ($p=0.77$, $p=0.16$) or response to this modality ($p=0.30$, $p=0.71$, Figure 17). A similar pattern was present in relation to the expression of TIM-3 on CD8+ T cells in PBMC or TIL in relation to chemotherapy ($p=0.93$, $p=0.57$) or response ($p=0.48$, $p=0.92$ Figure 18). These results demonstrate that CD8+ TIL markedly upregulate a range of checkpoint proteins in patients with OAC. However, this is not influenced by chemotherapy or the response to treatment. These results may support the potential development of combined chemotherapy and immunotherapy regimens for multimodal OAC treatment.

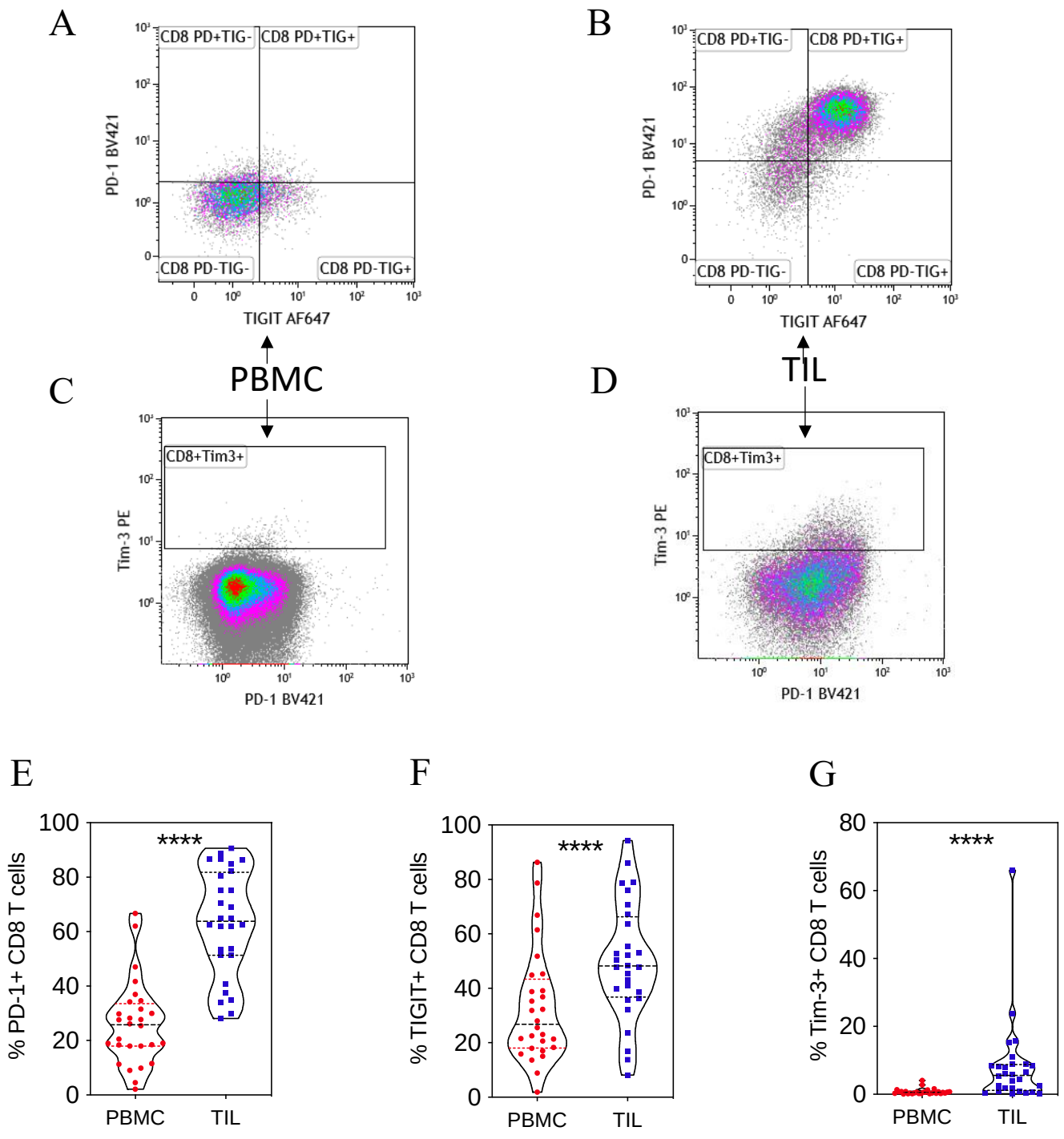

Figure 15. Checkpoint expression in matched PBMC and TIL CD8+ T cells.
Expression of PD-1, Tigit and Tim-3 was assessed on CD8+ T cells. Representative plots from matched PBMC (A,C) and TIL (B,D) are shown (n=30). Proportion of checkpoint positivity PD-1, Tigit and Tim-3 (E-G) for matched patient PBMC and TIL samples is shown. Each symbol represents an individual patient. Dashed horizontal lines indicate the median and dotted lines indicate the interquartile range. Data analysed by Wilcoxon matched-pairs signed rank test **** denotes p<0.0001.

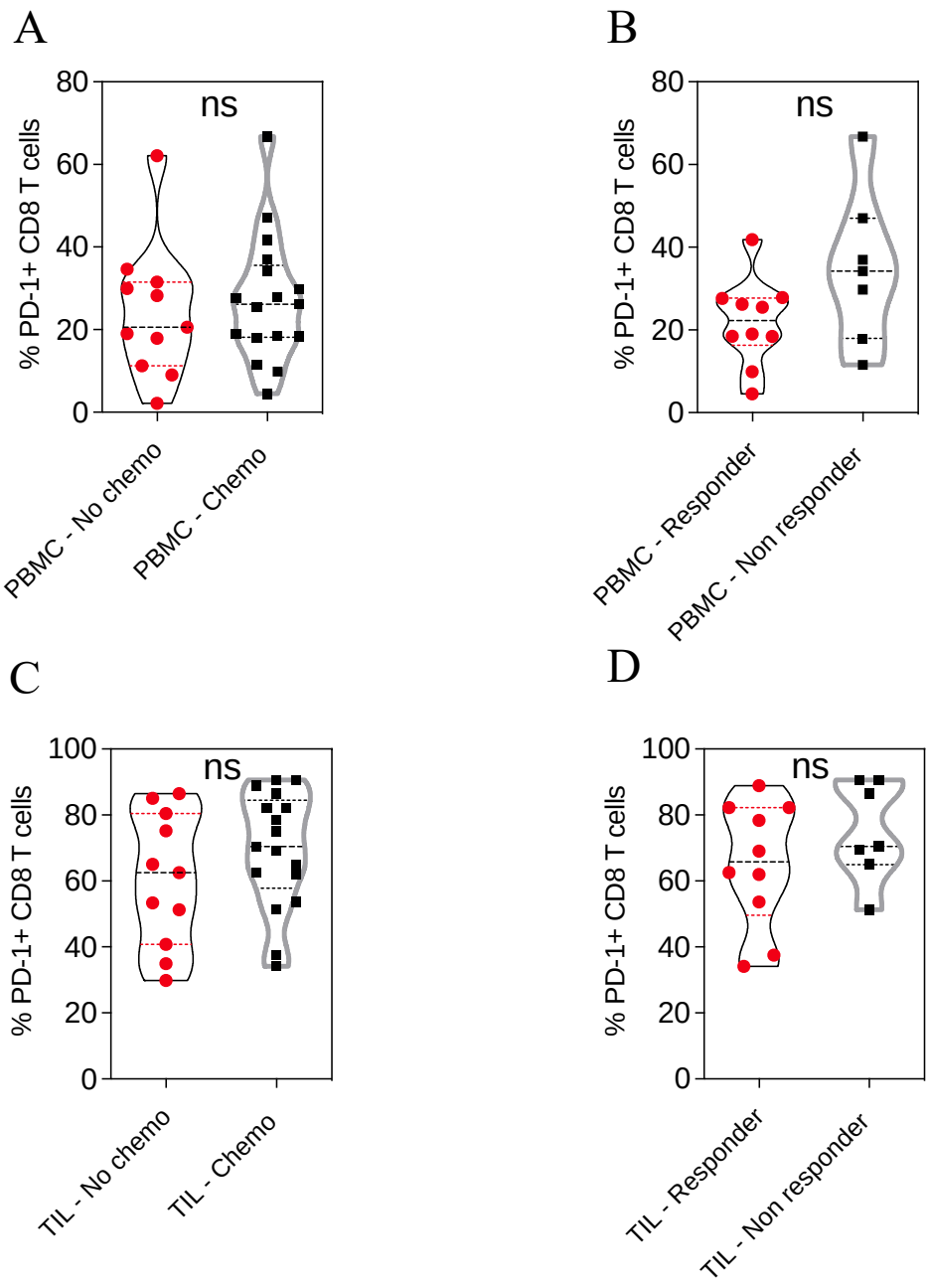

Figure 16. Impact of neoadjuvant chemotherapy on PD-1 expression in matched PBMC and TIL CD8+ T cells.
Expression of PD-1 was assessed on PBMC CD8+ T cells in patients who had and had not been administered neoadjuvant chemotherapy(No chemo n=10, Chemo n=20, A), subsequently this was assessed according to response to chemotherapy (B, responders defined as Mandard score 1-3, Responder n=13, non-responder n=7). Expression of PD-1 was also assessed on TIL CD8+ T cells in patients who had and had not been administered neoadjuvant chemotherapy(A), subsequently this was assessed according to response to chemotherapy (B, responders defined as Mandard score 1-3). Each symbol represents an individual patient. Dashed horizontal lines indicate the median and dotted lines indicate the interquartile range. Data analysed by Mann Whitney test.

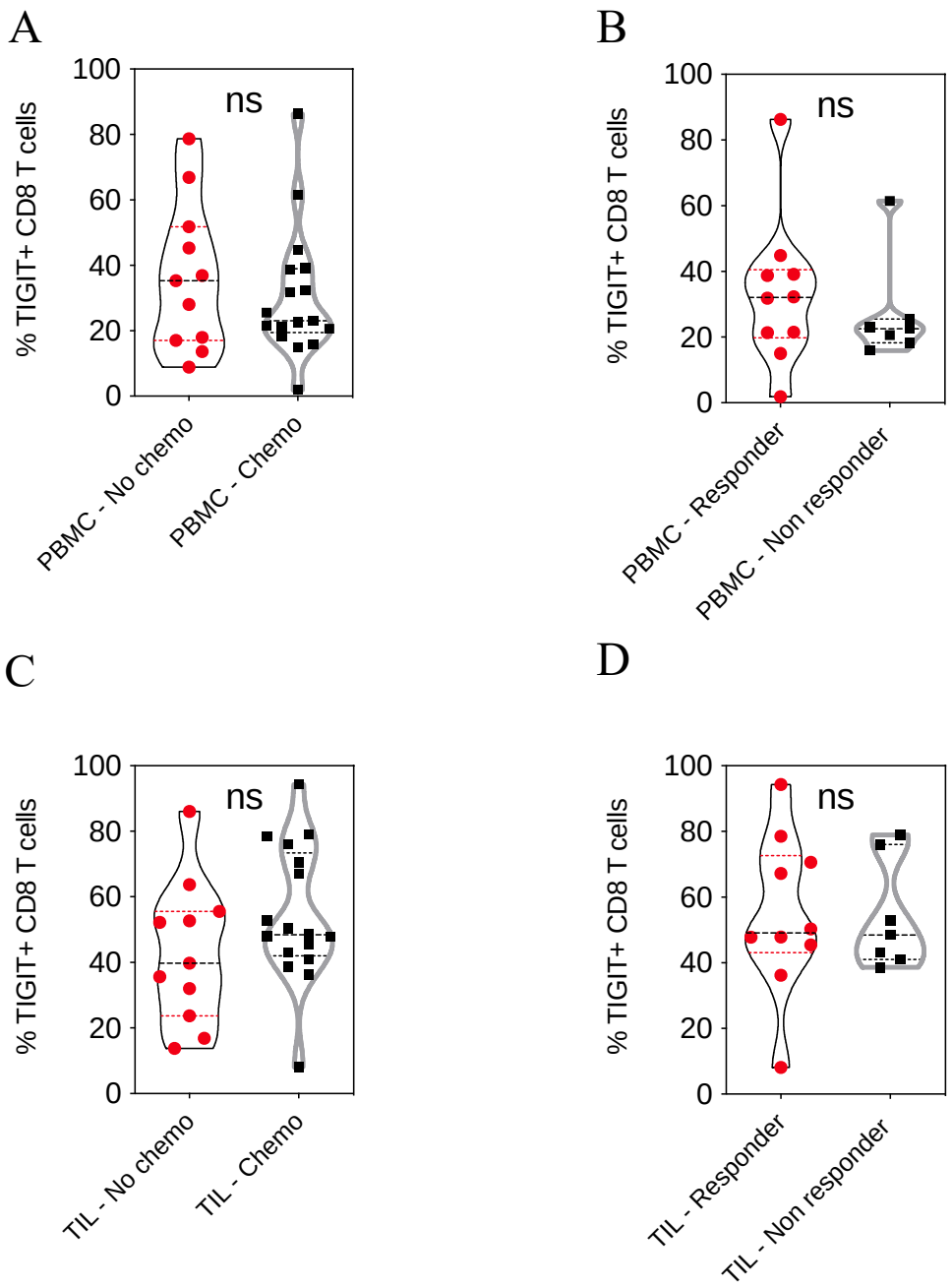

Figure 17. Impact of neoadjuvant chemotherapy on Tigit expression in matched PBMC and TIL CD8+ T cells.

Expression of Tigit was assessed on PBMC CD8+ T cells in patients who had and had not been administered neoadjuvant chemotherapy (No chemo n=10, Chemo n=20, A), subsequently this was assessed according to response to chemotherapy (B, responders defined as Mandard score 1-3, Responder n=13, non-responder n=7). Expression of Tigit was also assessed on TIL CD8+ T cells in patients who had and had not been administered neoadjuvant chemotherapy(A), subsequently this was assessed according to response to chemotherapy (B, responders defined as Mandard score 1-3). Each symbol represents an individual patient. Dashed horizontal lines indicate the median and dotted lines indicate the interquartile range. Data analysed by Mann Whitney test.

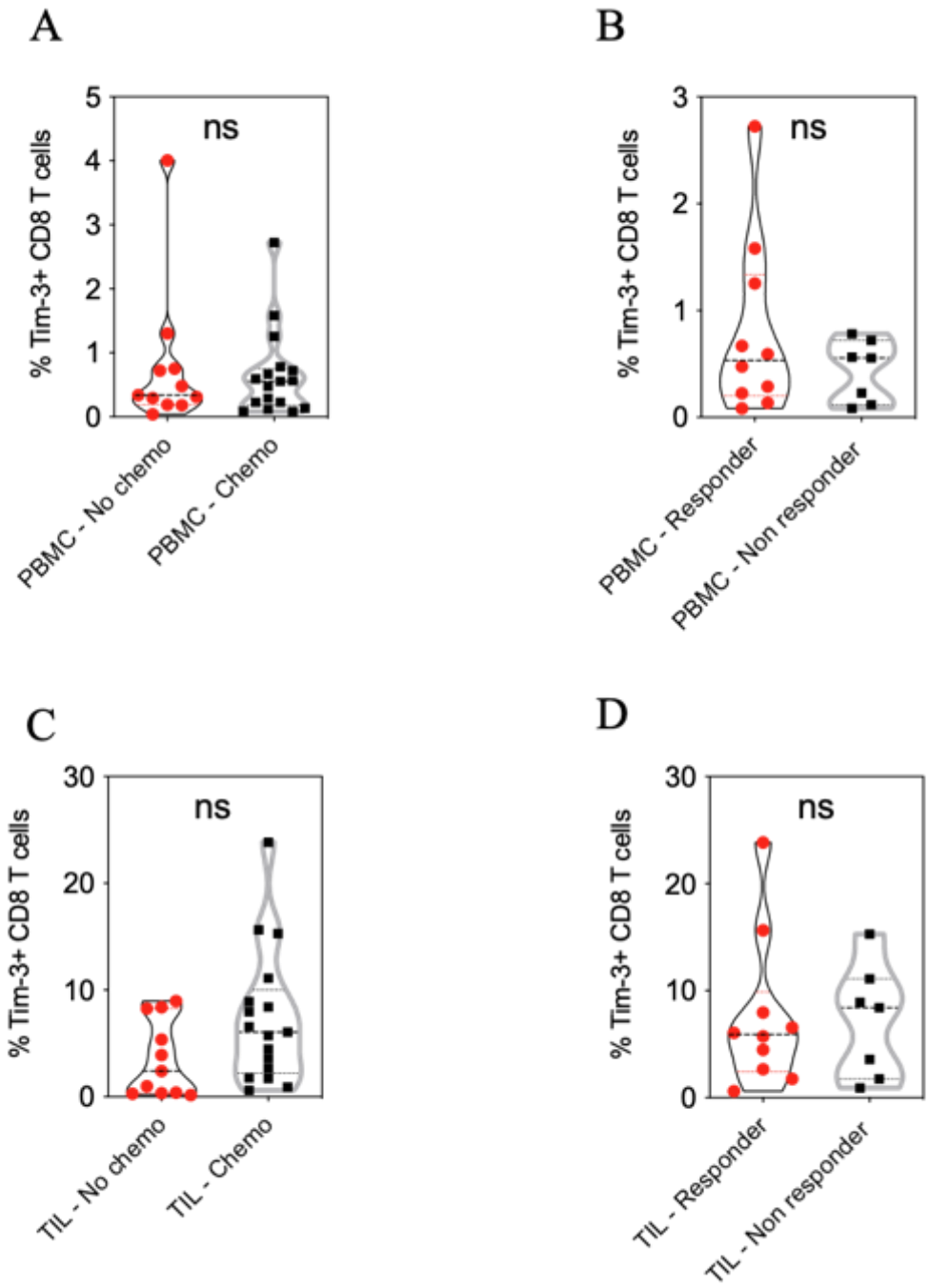

Figure 18. Impact of neoadjuvant chemotherapy on Tim-3 expression in matched PBMC and TIL CD8 T cells.

Expression of Tim-3 was assessed on PBMC CD8 T cells in patients who had and had not been administered neoadjuvant chemotherapy (No chemo n=10, Chemo n=20, A), A), subsequently this was assessed according to response to chemotherapy (B, responders defined as Mandard score 1-3, Responder n=13, non-responder n=7). Expression of Tim-3 was also assessed on TIL CD8 T cells in patients who had and had not been administered neoadjuvant chemotherapy(A), subsequently this was assessed according to response to chemotherapy (B, responders defined as Mandard score 1-3). Each symbol represents an individual patient. Dashed horizontal lines indicate the median and dotted lines indicate the interquartile range. Data analysed by Mann Whitney test.

Checkpoint Expression on CD4+ T cells

CD4+ T cells were next screened for their expression of checkpoint markers. CD4+ TIL were seen to significantly upregulate expression of PD-1, TIGIT and TIM-3 as compared to PBMC ($p<0.0001$, $p<0.0001$, $p<0.0001$, Figure 19). In particular, PD-1 increased three-fold with 71% of all CD4 T cells TIL expressing PD-1. TIGIT increased by over two-fold from 13% to 29% and TIM-3 expression was increased 5.5-fold from 1.2% to 6.8%.

No difference was seen in the expression of PD-1 in relation to chemotherapy ($p=0.90$, $p=0.44$) or response to chemotherapy ($p=0.08$, $p=0.34$, Figure 20). A similar pattern was seen in relation to expression of TIGIT (PBMC and TIGIT for chemotherapy; $p=0.73$, $p=0.37$) or response to treatment (PBMC and TIGIT; $p=0.84$, $p=0.97$). Finally, this profile was observed in relation to expression of Tim-3 for chemotherapy (PBMC and TIGIT for chemotherapy; $p=0.11$, $p=0.73$) or treatment response (PBMC and TIGIT; $p=0.34$, $p=0.26$).

As such, my findings demonstrate that CD4+ T cells markedly upregulate expression of checkpoint proteins within the tumour microenvironment but that this pattern is not influenced by either chemotherapy or the individual response to this treatment.

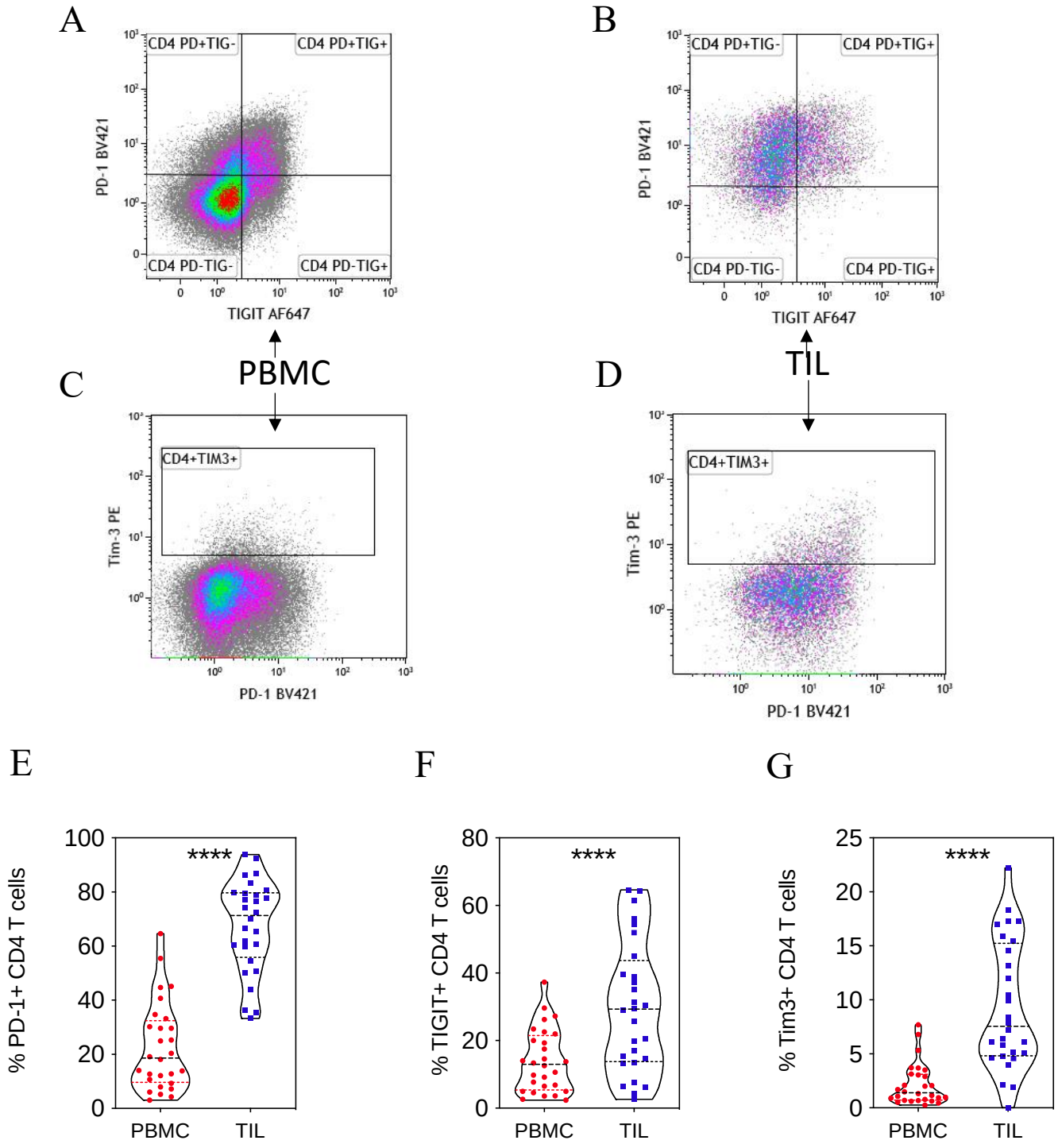

Figure 19. Checkpoint expression in matched PBMC and TIL CD4+ T cells.
Expression of PD-1, Tigit and Tim-3 was assessed on CD4+ T cells. Representative plots from matched PBMC (A,C) and TIL (B,D) are shown (n=30). Proportion of checkpoint positivity PD-1, Tigit and Tim-3 (E-G) for matched patient PBMC and TIL samples is shown. Each symbol represents an individual patient. Dashed horizontal lines indicate the median and dotted lines indicate the interquartile range. Data analysed by Wilcoxon matched-pairs signed rank test **** denotes p<0.0001.

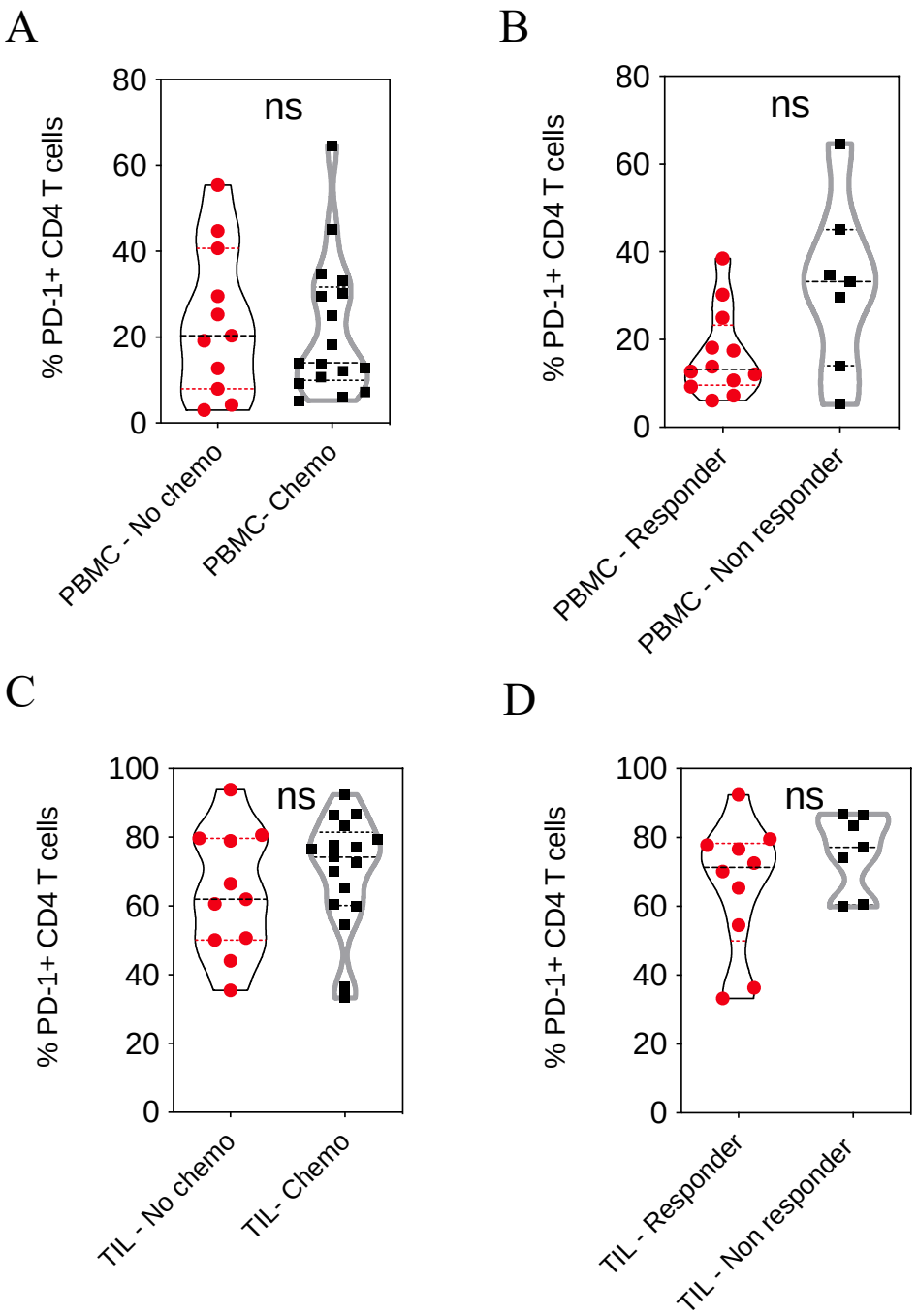

Figure 20. Impact of neoadjuvant chemotherapy on PD-1 expression in matched PBMC and TIL CD4+ T cells.

Expression of PD-1 was assessed on PBMC CD4+ T cells in patients who had and had not been administered neoadjuvant chemotherapy(No chemo n=10, Chemo n=20, A), subsequently this was assessed according to response to chemotherapy (B, responders defined as Mandard score 1-3, Responder n=13, non-responder n=7). Expression of PD-1 was also assessed on TIL CD4+ T cells in patients who had and had not been administered neoadjuvant chemotherapy(A), subsequently this was assessed according to response to chemotherapy (B, responders defined as Mandard score 1-3). Each symbol represents an individual patient. Dashed horizontal lines indicate the median and dotted lines indicate the interquartile range. Data analysed by Mann Whitney test.

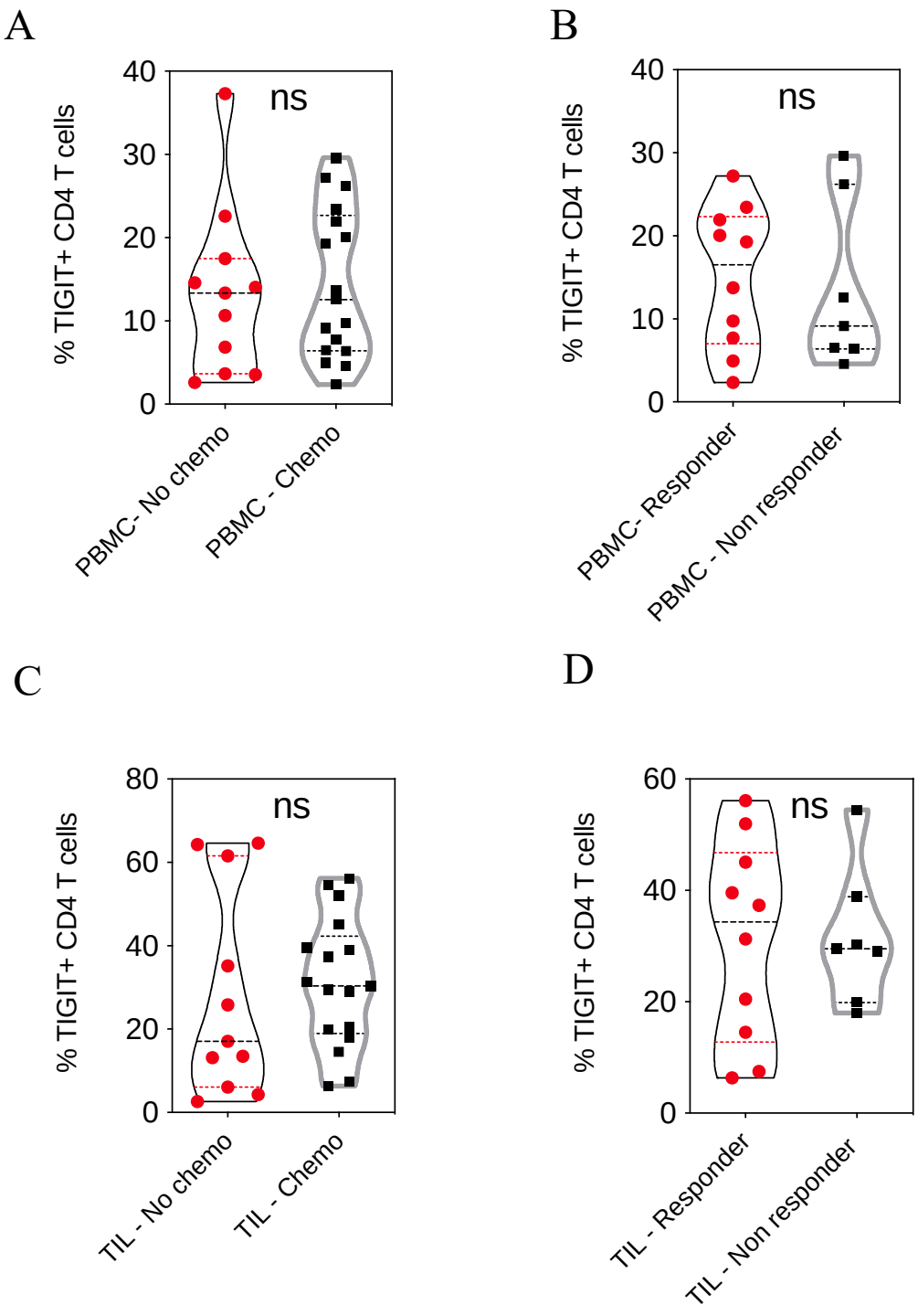

Figure 21. Impact of neoadjuvant chemotherapy on Tigit expression in matched PBMC and TIL CD4+ T cells.

Expression of Tigit was assessed on PBMC CD4+ T cells in patients who had and had not been administered neoadjuvant chemotherapy(No chemo n=10, Chemo n=20, A), subsequently this was assessed according to response to chemotherapy (B, responders defined as Mandard score 1-3 Responder n=13, non-responder n=7). Expression of Tigit was also assessed on TIL CD4+ T cells in patients who had and had not been administered neoadjuvant chemotherapy(A), subsequently this was assessed according to response to chemotherapy (B, responders defined as Mandard score 1-3). Each symbol represents an individual patient. Dashed horizontal lines indicate the median and dotted lines indicate the interquartile range. Data analysed by Mann Whitney test.

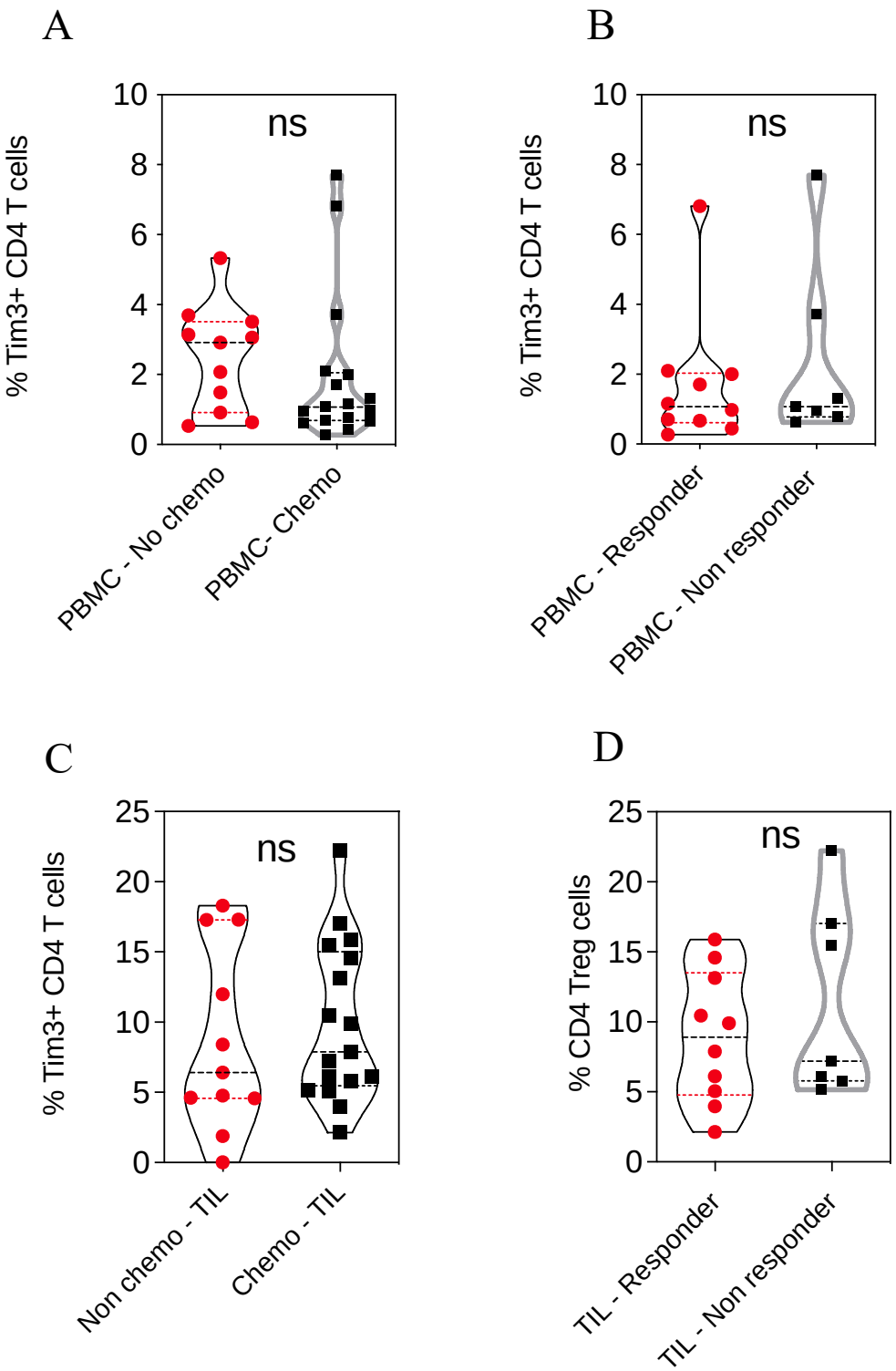

Figure 22. Impact of neoadjuvant chemotherapy on Tim-3 expression in matched PBMC and TIL CD4+ T cells.

Expression of Tim-3 was assessed on PBMC CD4+ T cells in patients who had and had not been administered neoadjuvant chemotherapy(No chemo n=10, Chemo n=20, A), subsequently this was assessed according to response to chemotherapy (B, responders defined as Mandard score 1-3). Expression of Tim-3 was also assessed on TIL CD4+ T cells in patients who had and had not been administered neoadjuvant chemotherapy (A), subsequently this was assessed according to response to chemotherapy (B, responders defined as Mandard score 1-3). Each symbol represents an individual patient. Dashed horizontal lines indicate the median and dotted lines indicate the interquartile range. Data analysed by Mann Whitney test.

Checkpoint Expression on T regulatory cells in patients with OAC

The expression of checkpoint markers was next assessed on T regulatory cells (Treg) in patients with OAC. T reg within TIL were seen to markedly upregulate the expression of PD-1, TIGIT and TIM-3 compared to that seen on PBMC ($p<0.0001$, $p<0.0001$, $p<0.0001$, Figure 23). In particular, PD-1 was increased seven fold with 40% of all Treg TIL expressing PD-1. TIGIT increased by over eight fold from 2.8% to 23% whilst TIM-3 expression was increased over seven fold from 1.9% to 14%.

Expression of PD1 on T reg was not influenced by prior chemotherapy (PBMC, TIL; $p>0.99$, $p>0.99$) or response ($p=0.59$, $p=0.63$, Figure 24) although a trend towards reduction was seen on cells within TIL in patients who responded well to chemotherapy. TIGIT expression on T reg within PBMC was not influenced by chemotherapy ($p=0.34$) but values were increased by 2.6 fold within the TIL of patients who had received chemotherapy ($p=0.02$, Figure 25). However TIGIT expression was not related to response to treatment ($p=0.55$, $p=0.64$).

No difference was seen in the expression of TIM-3 on T-reg in PBMC when comparing those who had and had not been given neoadjuvant chemotherapy ($p=0.61$) and equally there was no difference on T-reg TIL in patients who had received chemotherapy ($p=0.23$, Figure 26). I also saw no significant difference in the expression of TIM-3 on T-reg cells in PBMC or TIL in relation to response to neoadjuvant chemotherapy ($p=0.43$, $p=0.51$). As such, T-reg upregulate checkpoint proteins which would indicate a potential functional exhaustion phenotype. However, unlike CD4+ and CD8+ T cells there is a significant increase in TIGIT, potentially demonstrating that neoadjuvant chemotherapy may diminish the immunosuppressive environment driven by Tregs in the TME.

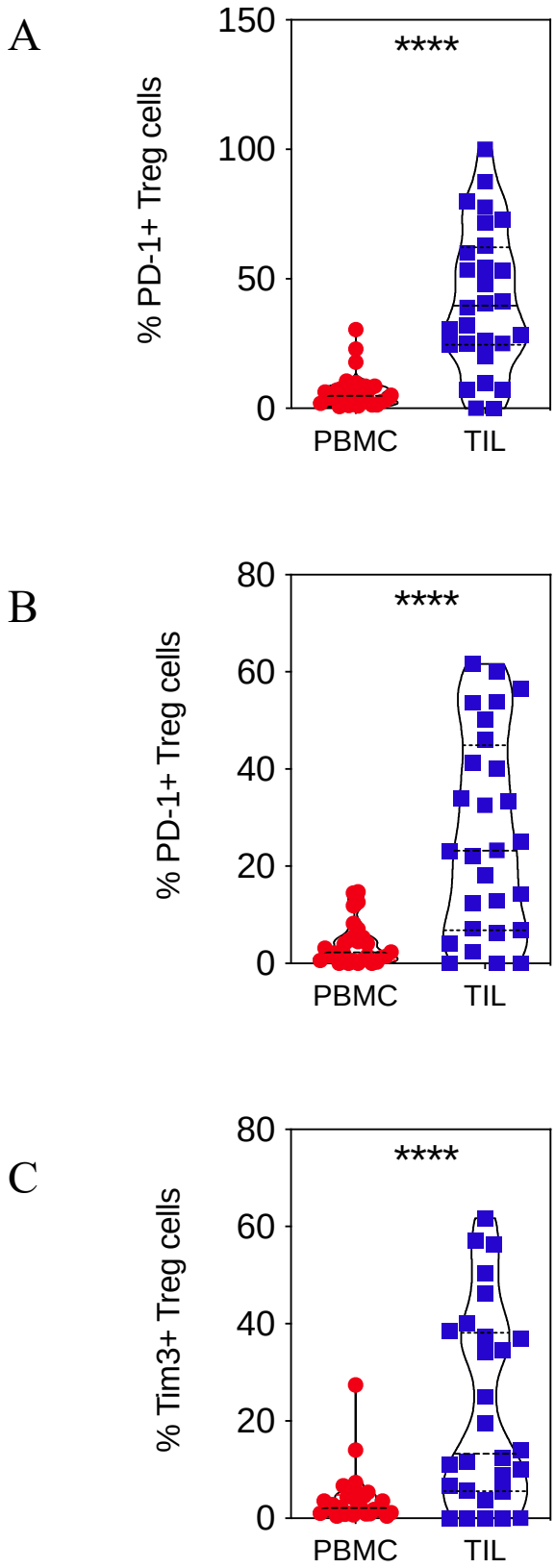

Figure 23. Checkpoint expression in matched PBMC and TIL Treg.
Expression of PD-1, Tigit and Tim-3 was assessed on Treg cells. Proportion of checkpoint positivity PD-1, Tigit and Tim-3 (n=30, A-C) for matched patient PBMC and TIL samples is shown. Each symbol represents an individual patient. Dashed horizontal lines indicate the median and dotted lines indicate the interquartile range. Data analysed by Wilcoxon matched-pairs signed rank test **** denotes $p<0.0001$.

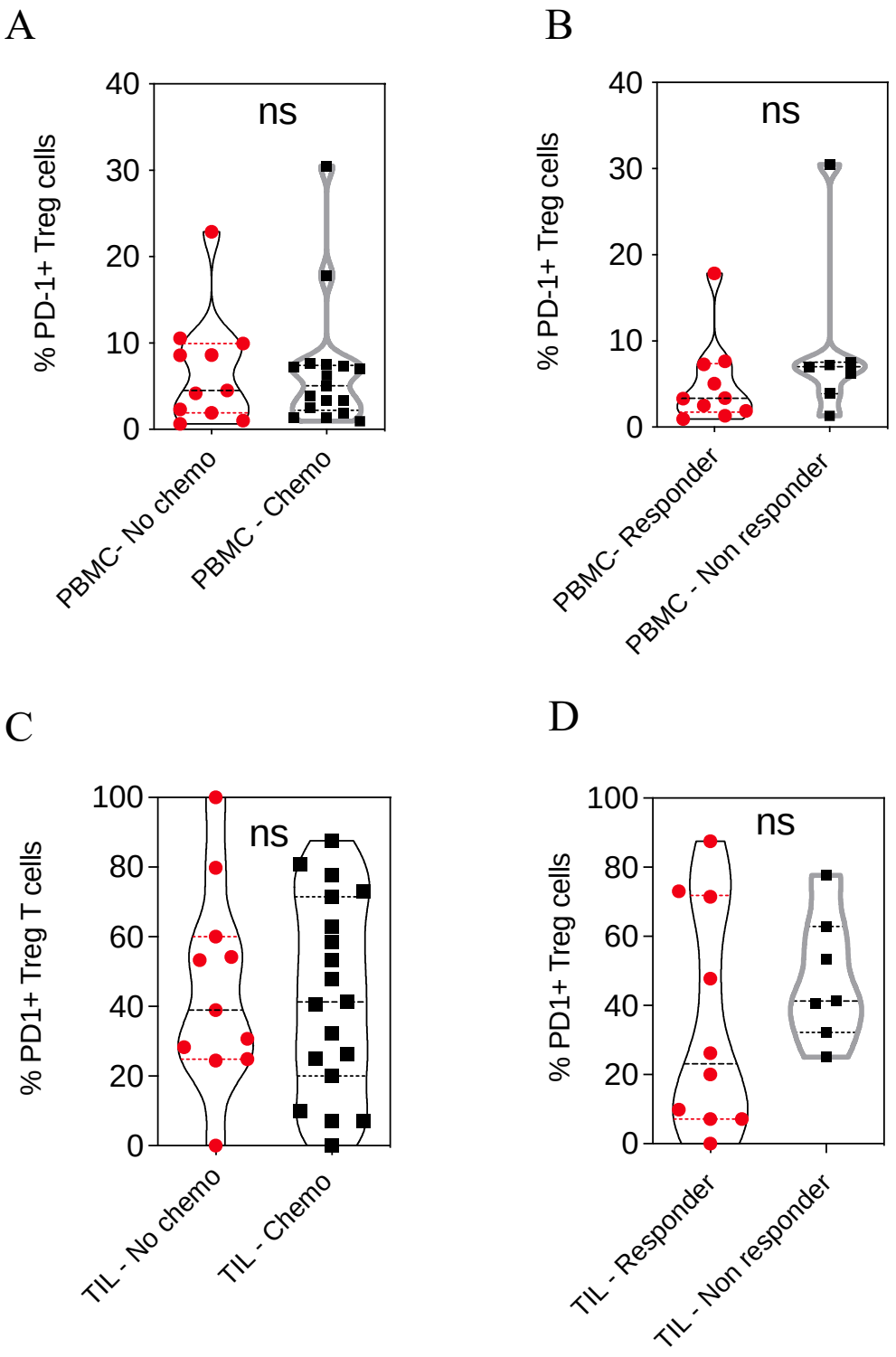

Figure 24. Impact of neoadjuvant chemotherapy on PD-1 expression in matched PBMC and TIL Treg cells.

Expression of PD-1 was assessed on PBMC T-reg cells in patients who had and had not been administered neoadjuvant chemotherapy(No chemo n=10, Chemo n=20, A), subsequently this was assessed according to response to chemotherapy (B, responders defined as Mandard score 1-3, Responder n=13, non-responder n=7). Expression of PD-1 was also assessed on TIL Treg cells in patients who had and had not been administered neoadjuvant chemotherapy(A), subsequently this was assessed according to response to chemotherapy (B, responders defined as Mandard score 1-3). Each symbol represents an individual patient. Dashed horizontal lines indicate the median and dotted lines indicate the interquartile range. Data analysed by Mann Whitney test.

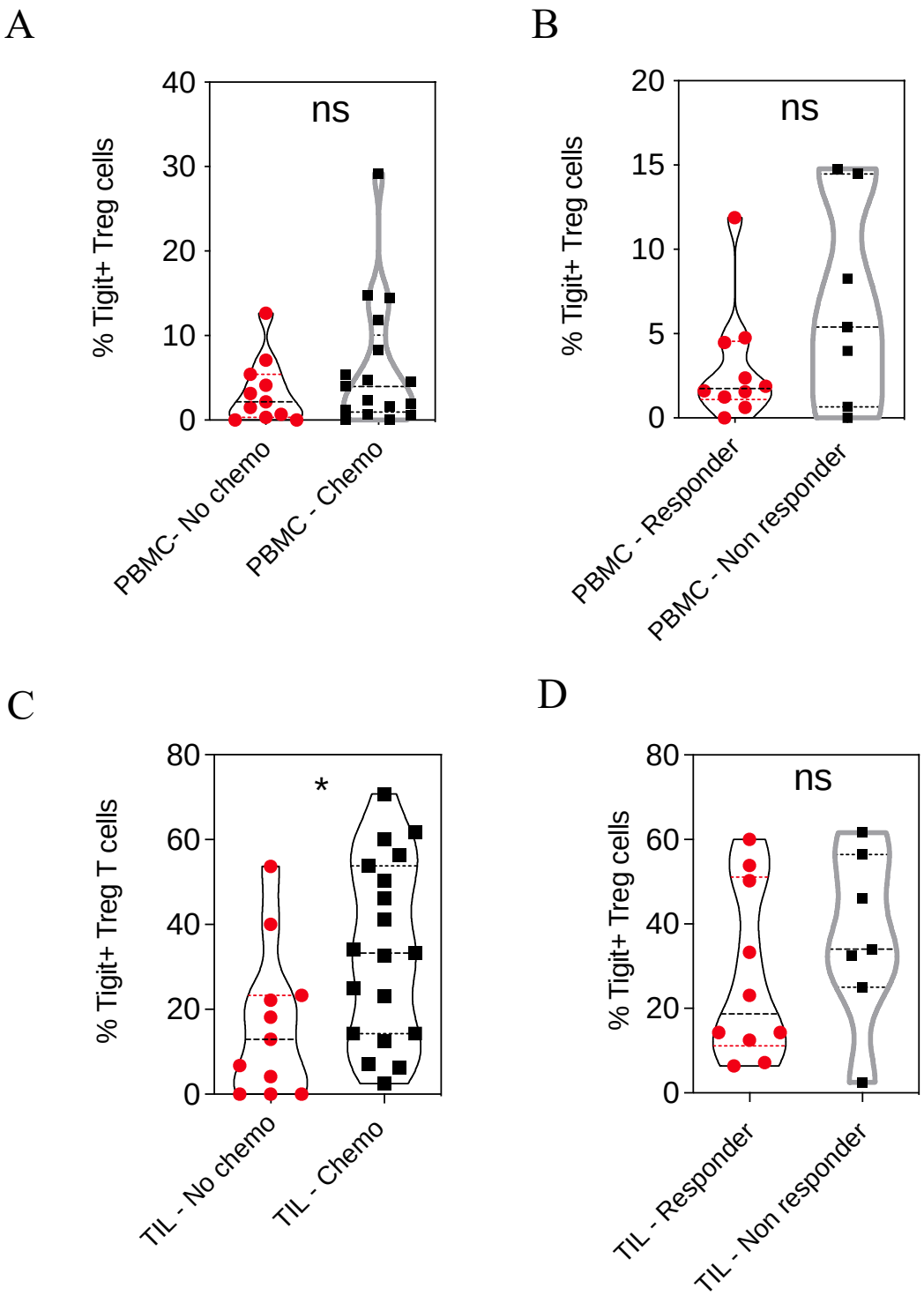

Figure 25. Impact of neoadjuvant chemotherapy on Tigit expression in matched PBMC and TIL CD4+ T cells.

Expression of Tigit was assessed on PBMC Treg cells in patients who had and had not been administered neoadjuvant chemotherapy(No chemo n=10, Chemo n=20, A), subsequently this was assessed according to response to chemotherapy (B, responders defined as Mandard score 1-3, Responder n=13, non-responder n=7). Expression of Tigit was also assessed on TIL Treg cells in patients who had and had not been administered neoadjuvant chemotherapy(A), subsequently this was assessed according to response to chemotherapy (B, responders defined as Mandard score 1-3). Each symbol represents an individual patient. Dashed horizontal lines indicate the median and dotted lines indicate the interquartile range. Data analysed by Mann Whitney test.

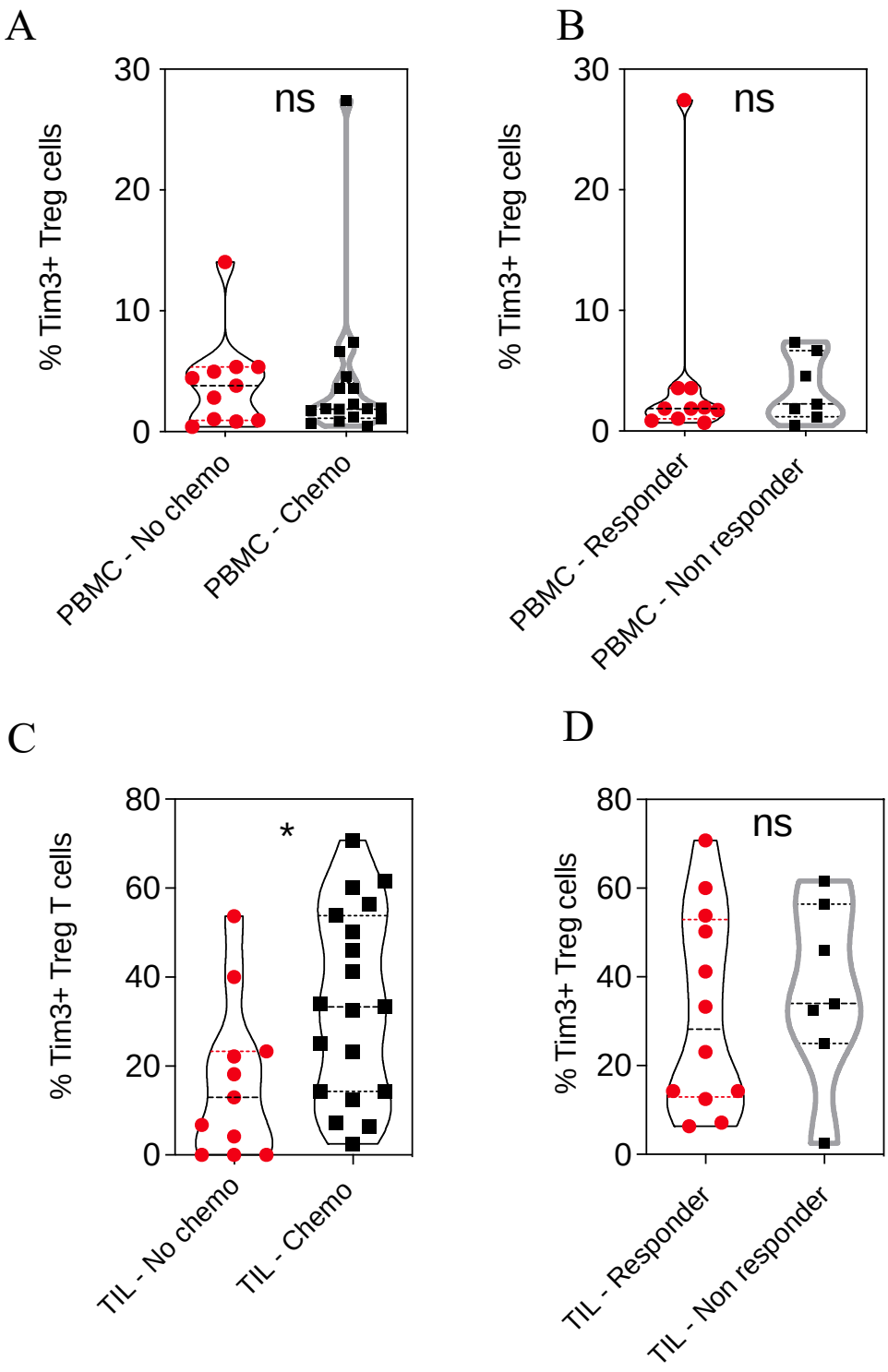

Figure 26. Impact of neoadjuvant chemotherapy on Tim-3 expression in matched PBMC and TIL Treg cells.

Expression of Tim-3 was assessed on PBMC Treg cells in patients who had and had not been administered neoadjuvant chemotherapy(No chemo n=10, Chemo n=20, A), subsequently this was assessed according to response to chemotherapy (B, responders defined as Mandard score 1-3, Responder n=13, non-responder n=7). Expression of Tim-3 was also assessed on TIL Treg cells in patients who had and had not been administered neoadjuvant chemotherapy(A), subsequently this was assessed according to response to chemotherapy (B, responders defined as Mandard score 1-3). Each symbol represents an individual patient. Dashed horizontal lines indicate the median and dotted lines indicate the interquartile range. Data analysed by Mann Whitney test.

NK cells are reduced within the OAC Tumour Microenvironment and have an altered phenotypic profile

Natural killer (NK) and B cells are important effector and regulatory cells within the tumour microenvironment. In order to identify NK and B cells, cells were first gated to remove doublets, before gating on live lymphocytes (Figure 27). Non-T cells were identified by the absence of CD3 expression and subsequently CD3-CD45+ cells were subdivided dependent on their expression of CD56+ and CD19+ to determine NK and B cells respectively.

A four-fold reduction in the proportion of NK cells was seen in TIL as compared to PBMC ($p<0.0001$, Figure 28). In particular, the proportion of NK cells reduced from 16% in PBMC to 3.7% in TIL. This relative proportion was the same within PBMC or TIL irrespective of prior chemotherapy ($p=0.97$, $p=0.69$) and was not related to response to treatment ($p=0.77$, $p=0.44$).

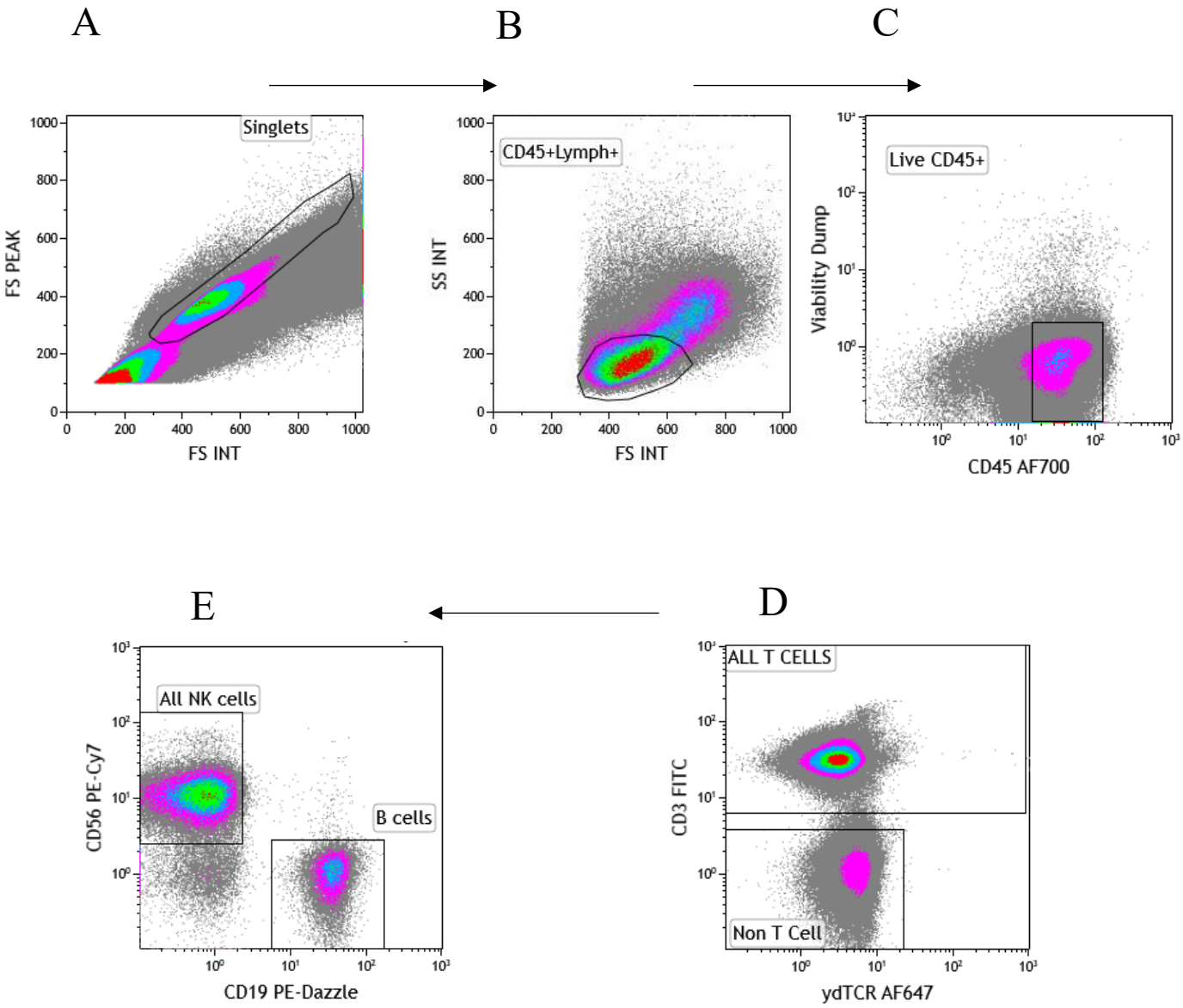

Figure 27. Gating strategies for the identification of NK and B cells.
Cells were first gated to remove doublet cells (A), before gating on lymphocytes based on FSC-A and SSC-A properties (B). Lymphocytes were classified as being propidium iodide (PI) negative and CD45 positive cells C). CD3 negative lymphocytes were isolated (C) and subdivided dependent on CD56/CD19 expression. NK cells were identified as CD56+CD19- and B cells CD56-CD19+. Plots shown are representative of TIL isolated from OAC tissue of a single individual.

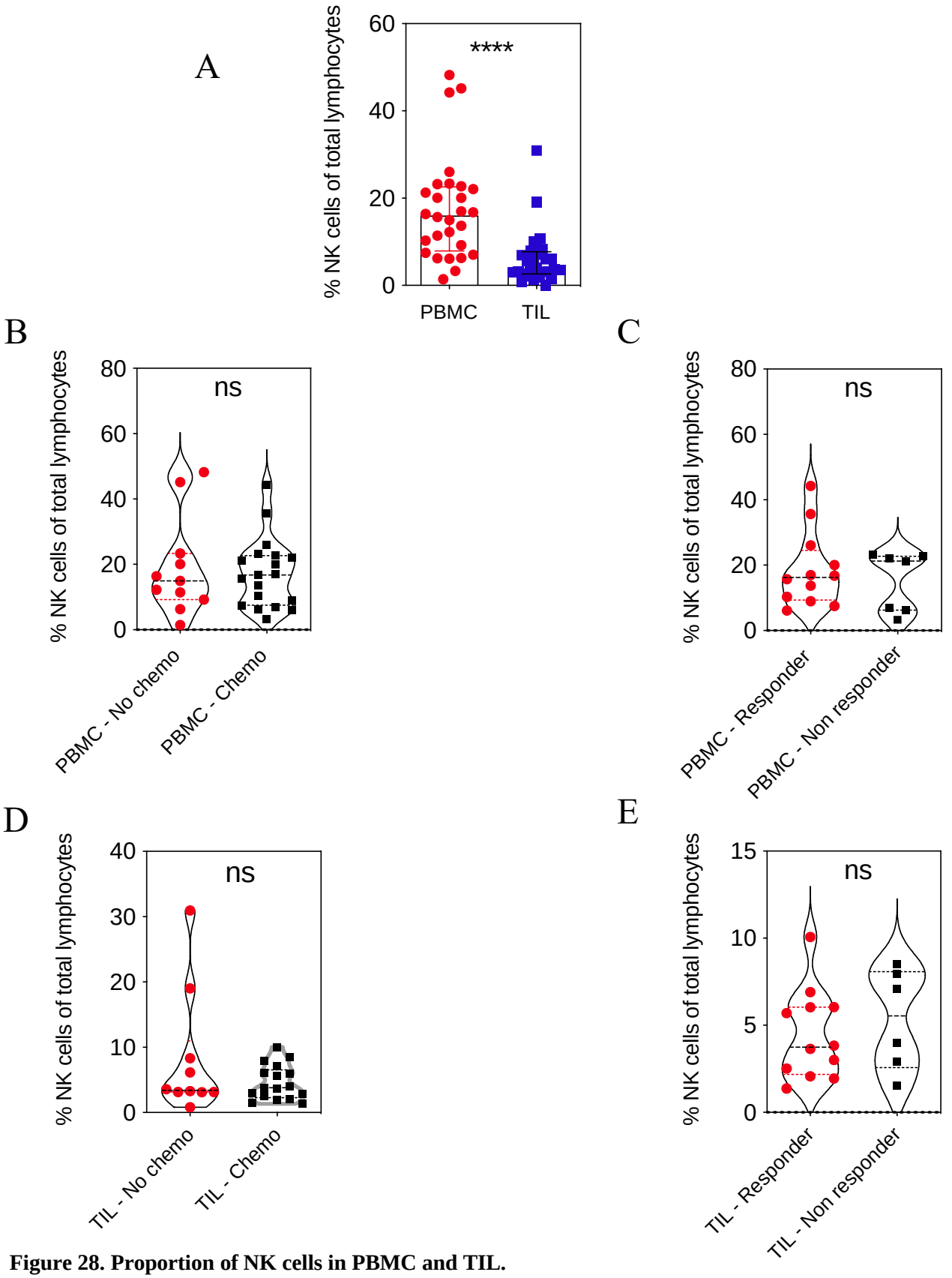

Figure 28. Proportion of NK cells in PBMC and TIL.
The proportion of NK cells in matched PBMC and TIL (n=30, A). Differential proportion of NK cells in PBMC dependent on administration or absence of neoadjuvant chemotherapy (No chemo n=10, Chemo n=20, B) and subsequently dependent on response to chemotherapy (C, responders defined as Mandard score 1-3, Responder n=13, non-responder n=7). Differential proportion of NK cells in TIL dependent on administration or absence of neoadjuvant chemotherapy (D) and subsequently dependent on response to chemotherapy (E). Each symbol represents an individual patient. Dashed horizontal lines indicate the median and Data analysed by Wilcoxon matched-pairs signed rank test for matched samples(A), data analysed by Mann Whitney test for unpaired samples (B-E), **** denotes p<0.0001.

NK Cell Subtypes in Oesophageal Adenocarcinoma

Major subsets of NK cells can be delineated by relative expression of CD56 and CD16. As such, I next defined subsets within PBMC and TIL based on these values.

$CD56^{dim}CD16+$ NK cells predominated within PBMC, comprising 94% of cells (IQR 88.8-96.1, Figure 29). Conversely, $CD56^{bright}CD16-$ cells comprised only 1% of the circulating population (IQR 0.46-2.05). $CD56^{dim}CD16-$ and $CD56^{bright}CD16+$ made up 3.3% and 1% respectively (IQR 1.57-6.05, 0.40-3.2).

The phenotype of NK cells within TIL was markedly different to that of circulating PBMC. Although $CD56^{dim}CD16+$NK cells still predominate they were reduced to only 54% of circulating NK cells (IQR 41.3-70.4, $p<0.0001$, Figure 30) whilst $CD56^{bright}CD16-$ are reciprocally increased to 9.5% (IQR 5.1-16.2, $p<0.0001$). $CD56^{dim}CD16-$ populations are significantly increased, comprising 31% of the total pool (IQR 14.4-44, $p<0.0001$) whilst no difference was seen in the proportion of $CD56^{bright}CD16+$ cells (median 1%; IQR 0.15-2.72, $p=0.62$).

The proportion of these values within PBMC and TIL was not significantly influenced by chemotherapy ($p=0.97$, $p=0.69$, Figure 31) or response to chemotherapy ($p=0.77$, $p=0.44$, Figure 32).

A

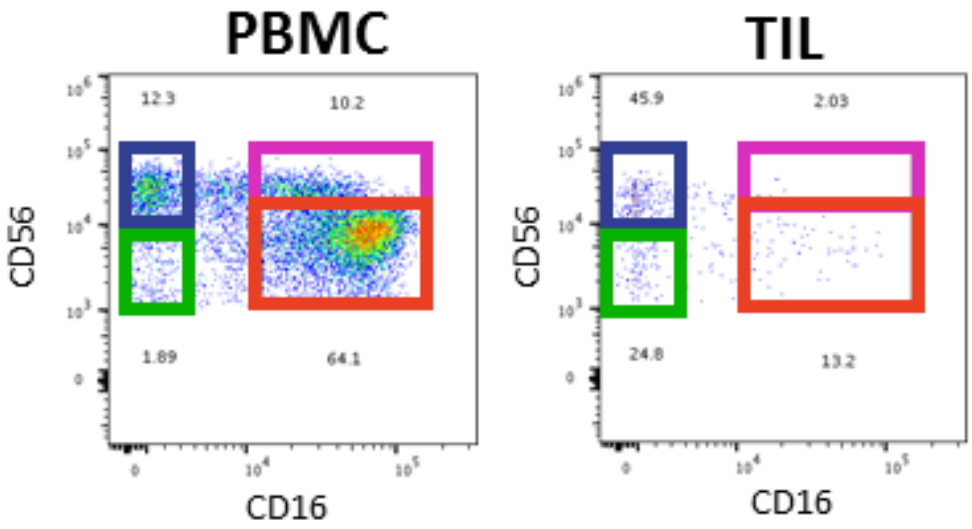

B

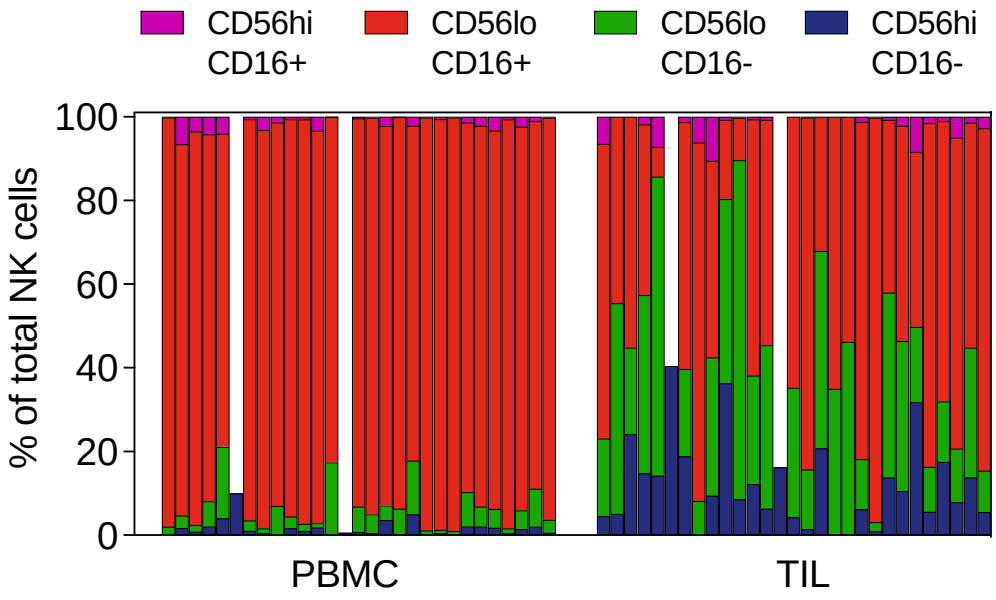

Figure 29. Changing NK populations in PBMC and TIL
Example plot of matched PBMC and TIL demonstrating changing phenotype dependent on location(A). Bar chart showing consecutive matched PBMC and TIL pairs classifies as per CD56 and CD16 expression.

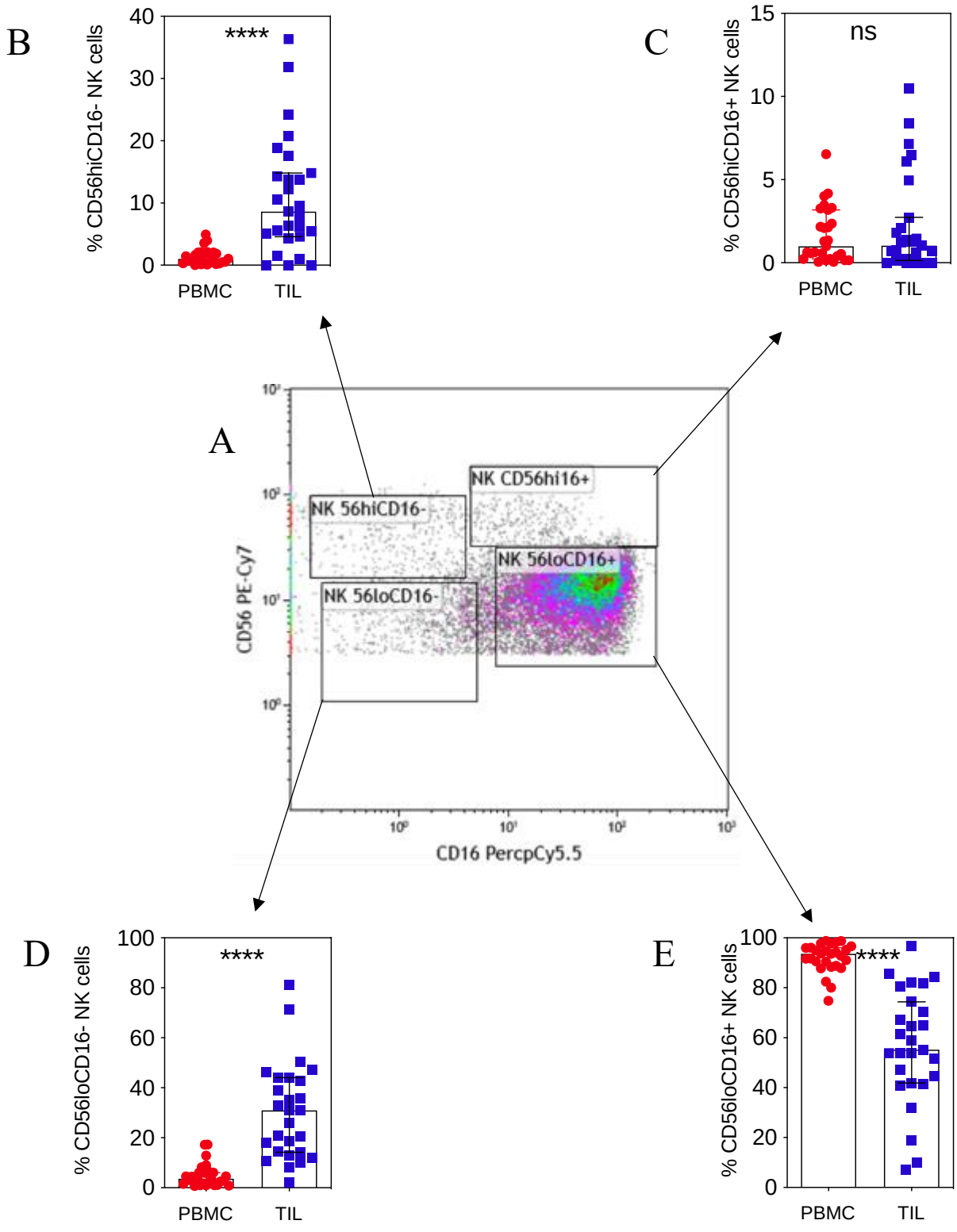

Figure 30. Relative subsets of NK populations within PBMC and TIL from patients with OAC

Representative plot of NK populations in PBMC (A). Changing NK subsets in PBMC and TIL, CD56hiCD16- (B), CD56hiCD16+ (C), CD56loCD16- (D), CD56loCD16+ (E)(n=30).

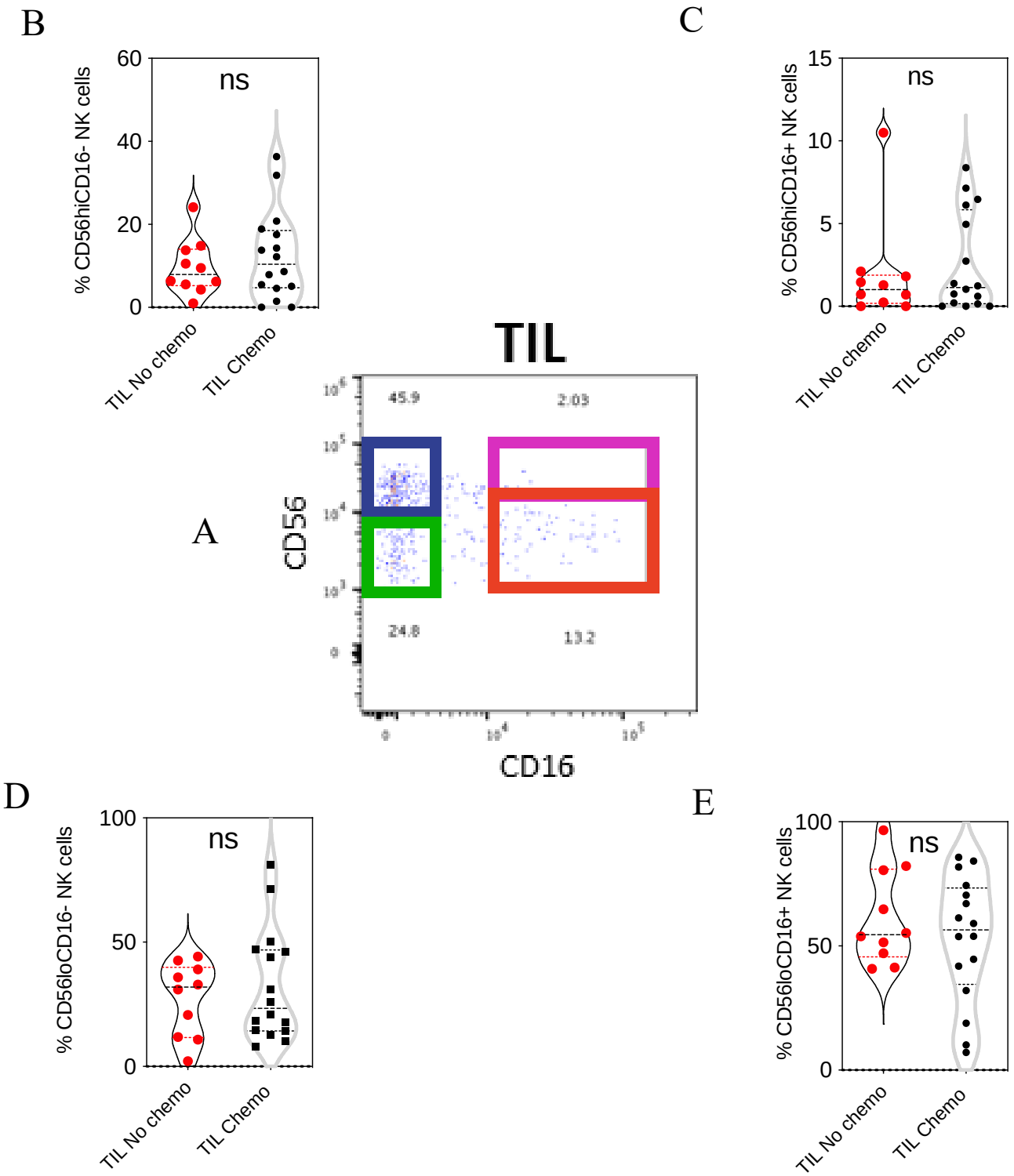

Figure 31. Impact of neoadjuvant chemotherapy on NK populations in matched PBMC and TIL
Representative plot of NK populations in TIL (A). Impact of neoadjuvant chemotherapy on NK TIL subsets, CD56hiCD16- (B), CD56hiCD16+ (C), CD56loCD16- (D), CD56loCD16+ (E)(No chemo n=10, Chemo n=20). Each symbol represents an individual patient. Dashed horizontal lines indicate the median and dotted lines indicate the interquartile range. Data analysed by Mann Whitney test.

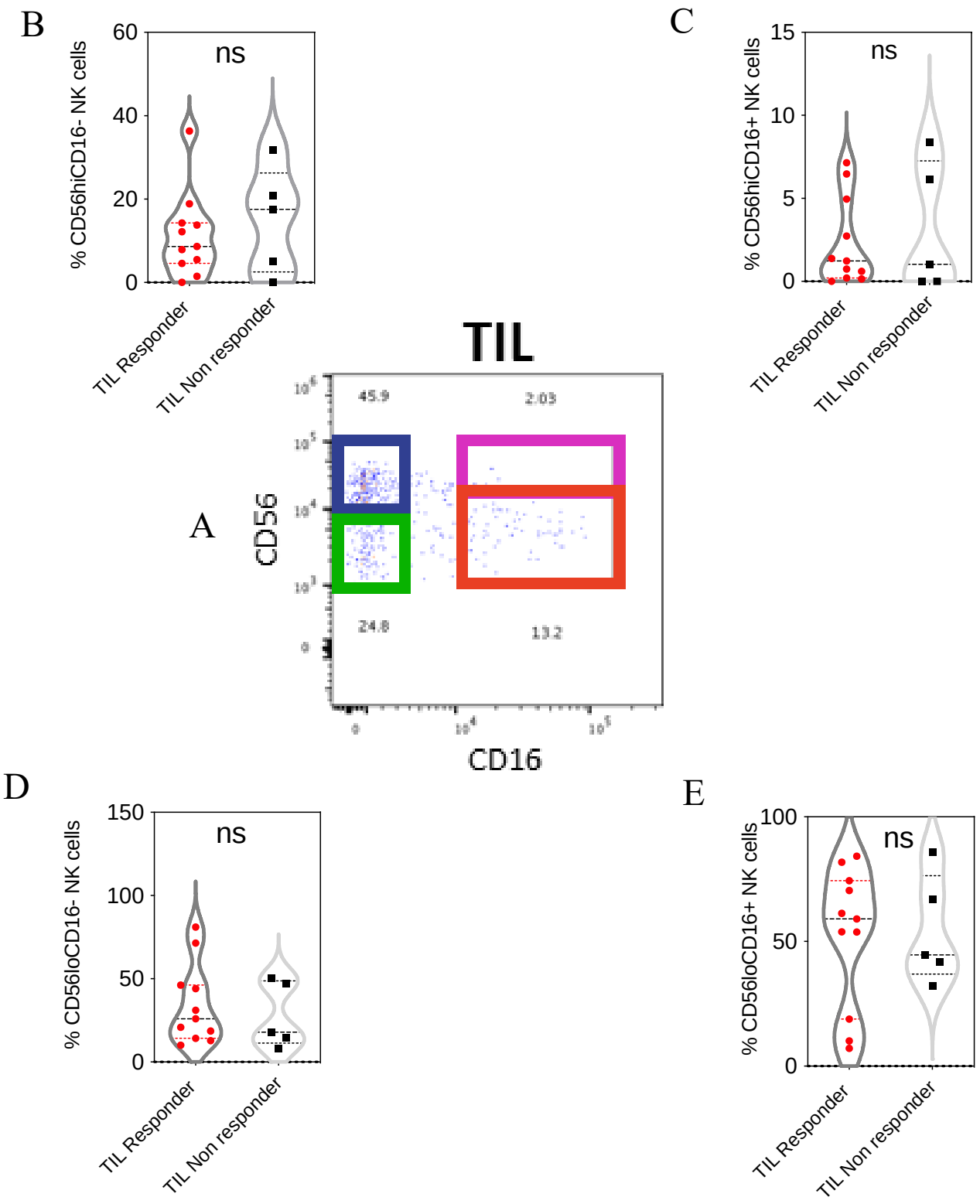

Figure 32. Impact of response to neoadjuvant chemotherapy on NK populations in matched PBMC and TIL

Representative plot of NK populations in TIL (A). Impact of response to neoadjuvant chemotherapy on NK TIL subsets, CD56hiCD16- (B), CD56hiCD16+ (C), CD56loCD16- (D), CD56loCD16+ (E). Responders defined as Mandard score 1-3 (Responder n=13, non-responder n=7). Each symbol represents an individual patient. Dashed horizontal lines indicate the median and dotted lines indicate the interquartile range. Data analysed by Mann Whitney test.

Phenotypic analysis of B Cells in Oesophageal Adenocarcinoma

B cells within the OAC environment were identified through expression of CD19. To further subdivide B cell subsets, memory B cells were identified as CD27+ and naïve B cells as CD27- (Figure 33).

B cells expressed as a proportion of total lymphocytes were comparable between PBMC and TIL (p=0.43, Figure 34). There was also no difference in the proportion of B cells in PBMC after neoadjuvant chemotherapy (p=0.40). There was, however, a three fold increase in B cells within TIL in patients following neoadjuvant chemotherapy (p=0.009) from 2 to 6%. No difference was seen in the proportion of B cells in PBMC or in TIL in those who did and those who did not respond to neoadjuvant chemotherapy (p=0.38, p=0.20).

Although there was no significant difference in the proportion of total B cells within TIL, the proportion of memory B increased from 32% in PBMC to 69% in TIL (p<0.0001, Figure 35). There was no significant difference in the proportion of memory B cells in PBMC or TIL when comparing those who had and had not been given neoadjuvant chemotherapy (p=0.65, p=0.07). Equally there was no significant difference in the proportion of memory B cells in PBMC or in TIL in those who did and those who did not respond to neoadjuvant chemotherapy (p=0.49, p=0.07).

These data show that B cells within the tumour microenvironment of OAC exhibit an increased proportion of memory B cells which may suggest a possible response to tumour antigen. Furthermore, B cell numbers increase within tumour following use of NACT.

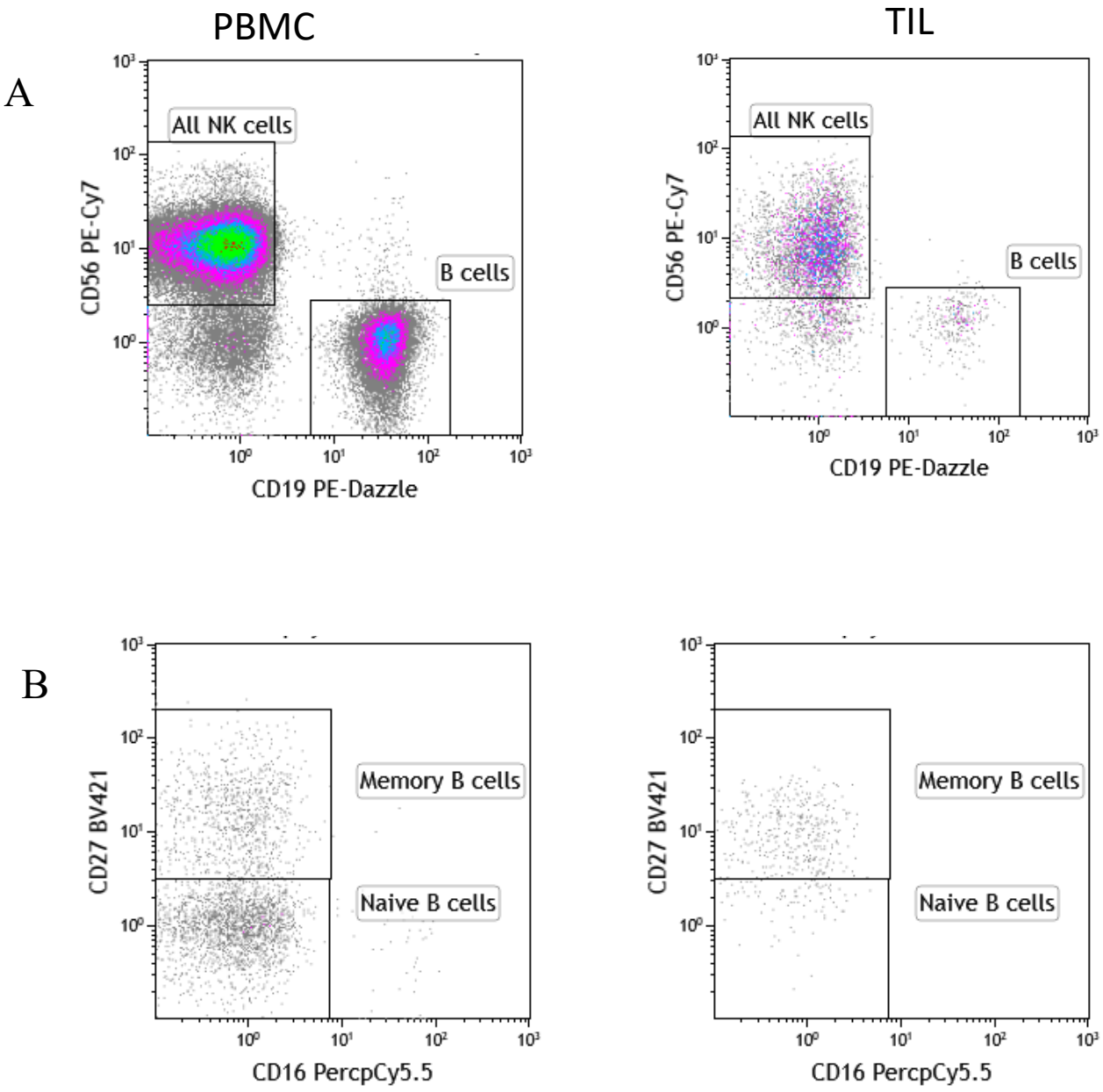

Figure 33. Gating strategies to identify B cells
Example plots of matched PBMC and TIL demonstrating total B cells as CD3-CD19+CD56- lymphocytes (A). Memory B cell were identified as CD19+CD27+ cells.

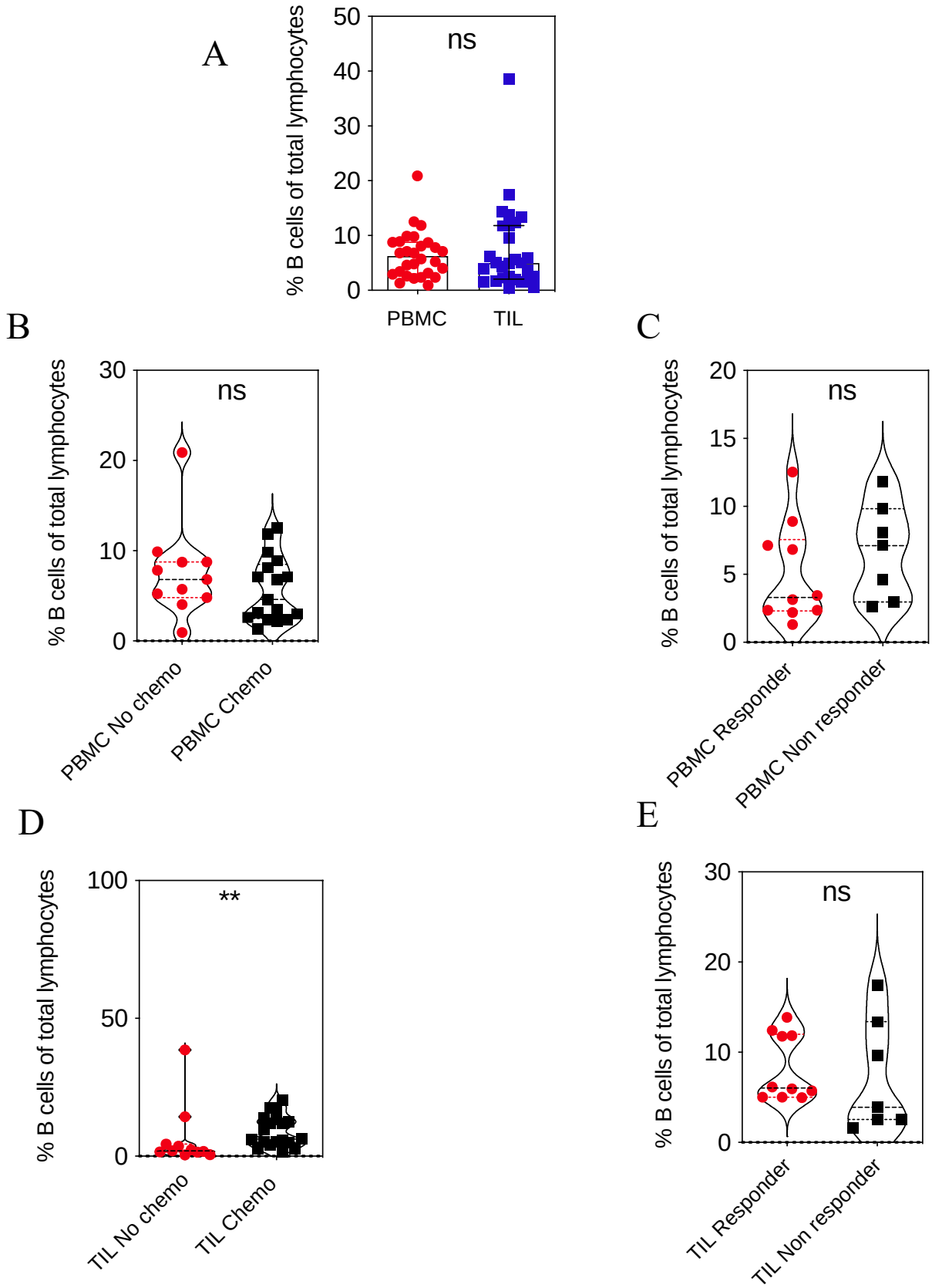

Figure 34. Assessment of proportion of B cells in matched PBMC and TIL
Differential proportion of B cells in matched PBMC and TIL (n=30, A). Differential proportion of B cells in PBMC in relation to administration of neoadjuvant chemotherapy (No chemo n=10, Chemo n=20, B) and subsequently dependent on response to chemotherapy (C, responders defined as Mandard score 1-3, Responder n=13, non-responder n=7). Differential proportion of B cells in TIL dependent on administration or absence of neoadjuvant chemotherapy (D) and subsequently dependent on response to chemotherapy (E). Each symbol represents an individual patient. Dashed horizontal lines indicate the median and Data analysed by Wilcoxon matched-pairs signed rank test for matched samples(A), data analysed by Mann Whitney test for unpaired samples (B-E).

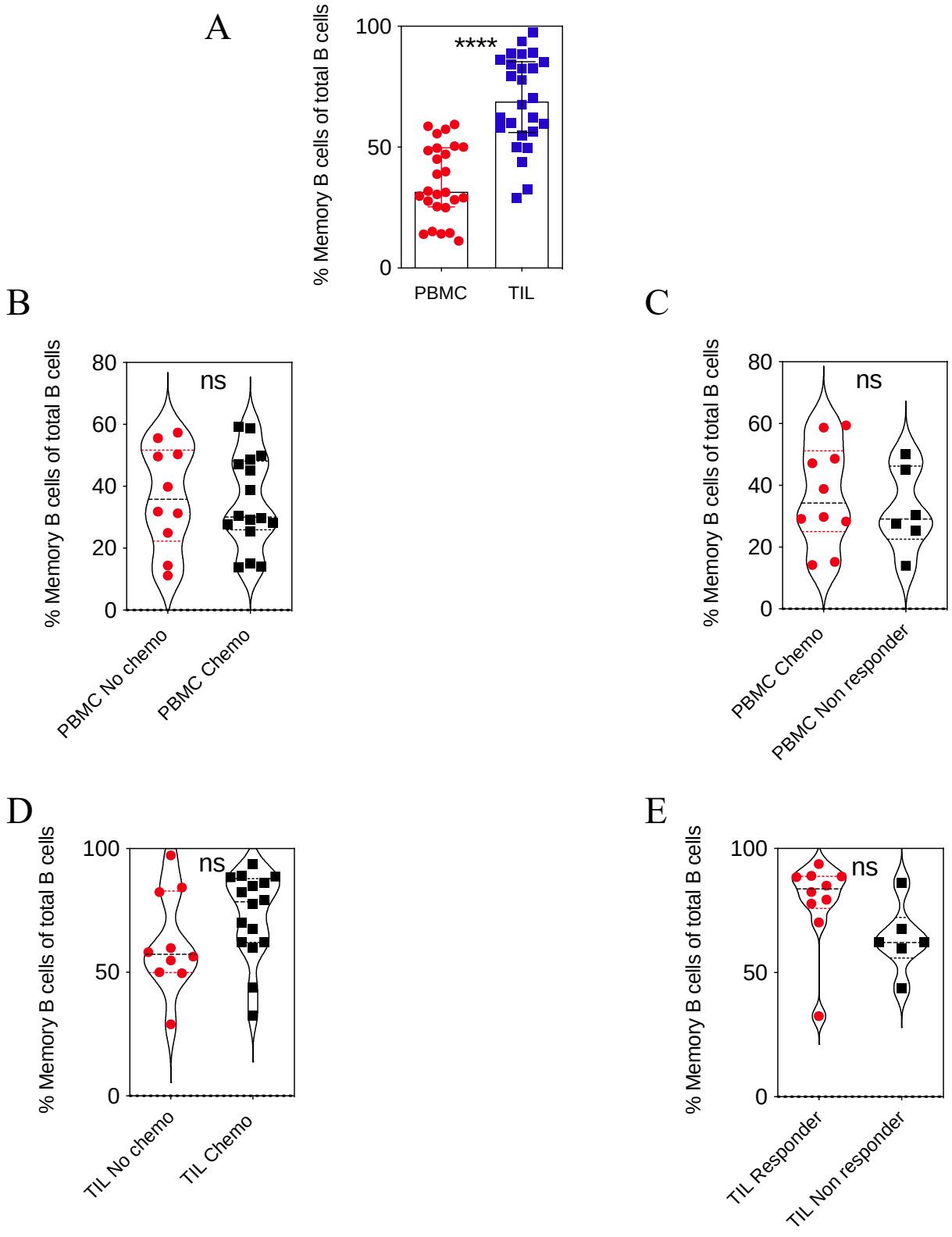

Figure 35. Proportion of memory B cells in matched PBMC and TIL
Differential proportion of B cells in matched PBMC and TIL (n=30, A). Proportion of memory B cells in PBMC dependent on administration or absence of neoadjuvant chemotherapy (B) and subsequently dependent on response to chemotherapy (C, responders defined as Mandard score 1-3). Differential proportion of Memory B cells in TIL dependent on administration or absence of neoadjuvant chemotherapy (D) and subsequently dependent on response to chemotherapy (E). Each symbol represents an individual patient. Dashed horizontal lines indicate the median and Data analysed by Wilcoxon matched-pairs signed rank test for matched samples(A), data analysed by Mann Whitney test for unpaired samples (B-E).

Discussion

In this chapter I investigated the phenotype of major lymphocytes subpopulations within the blood and tumour microenvironment of patients with OAC. My focus was on major T cell lineages, T regulatory cells and the NK and B cell pools. I also assessed the expression of checkpoint proteins on T cell subpopulations.

T cells are critical determinants of the outcome of cancer and within the TME it is believed that they play an important role through direct recognition of malignant cells and the release of inflammatory cytokines or mediation of direct tumour lysis. CD8+ T cells appear particularly critical in this regard and release immunoregulatory cytokines such as IFN-γ and TNF that may induce cytolytic T cell responses in tumours[92,93].

I observed that T cells predominated within both the peripheral blood and tumour infiltrating lymphocytes (TIL) in patients with OAC. The ratio of CD4+ to CD8+ T cells was equivalent in both compartments. Prior studies in squamous cell carcinoma of the oesophagus (OSCC) have shown significant variation in the proportion of CD4+ and CD8+ T cells between patients[94]. This was also seen in my study which is important as immunohistochemistry studies have shown that patients with a high CD4:8 ratio have improved outcome in OAC[95]. The mechanism behind this observation is not clear although downregulation of MHC expression may limit CD8+ recognition of tumour[96]. Indeed, IHC analysis in OAC has shown a 30% reduction in MHC class I expression despite retention of mRNA expression. In this regard it is notable that nanostring analysis identified upregulation of LILRB1, the major receptor in detection and simultaneous inhibition of MHC class I-triggered phagocytosis[97,98]. Paradoxically, poor survival outcomes have also been associated with TAP1-mediated upregulation of MHC I and cell lines with high MHC I expression may have significantly high expression of checkpoint ligands such as PD-L1 and PD-L2[99]. This is in keeping with other solid tumours that have been shown in the context of maintained MHC I expression to

express higher levels of immuno-inhibitory molecules such as PD-1/PD-L1, LAG3 and TIM-3[100].

Current literature investigating T cell infiltration within the OAC TME has sought to further identify the specific density and location of TILs using immunohistochemistry. IHC analysis is limited in the number of markers it can analyse and as such offers a relatively limited view of the TME although contemporary technologies may transform current capability. However, IHC can assess anatomical distribution of cells and can also be applied to large numbers of samples to enhance studies of correlation with clinical outcome.

Prior analyses have shown that high levels of TIL infiltration are an independent prognostic factor for improved cancer-specific survival in a range of tumours[90,91,101]. An early meta-analysis of immunohistochemical prognostic biomarkers in resected oesophageal adenocarcinoma reported that an increased density of CD8+ T cells was associated with improved overall survival[102]. More recently a meta-analysis by Gao et al has reported that both CD4+ and CD8+ T-cell infiltration were associated with improved overall survival[103,104] and CD8+ infiltration in the tumour nest or tumour stroma predicts improved survival in SCC. Insufficient data currently exists to perform subset analysis of adenocarcinoma[103]. Schumacher et al found that intratumoural CD8+ T cell infiltrations in OAC and SCC were proliferative, demonstrated IFN-γ secretion and that intratumoural infiltration was an independent prognostic factor[105]. However, Zingg et al. did not find any independent associations between TIL subsets and survival in OAC patients who received either neoadjuvant chemoradiotherapy or surgery alone. Although univariate analyses demonstrated the importance of some subsets this association was lost on multivariate analysis[106].

□δ T cells were seen to make up only a small proportion of T cells in OAC. Indeed, a proportional reduction was seen in TIL as compared to PBMC and this was not impacted by

NACT. γδ T cell-driven tumour lysis has been linked to recognition of heat shock proteins such as HSP60, HSP70 on the surface of tumour cells[107] and autologous adoptive γδT-cell therapy trials have be shown to be an clinically safe in patients with metastatic OSCC although with mixed clinical outcome results. No improvement in survival was seen in chemotherapy refractory patients with γδT-monotherapy-P1 alone whilst a potential benefit was observed in combination with chemotherapy[108].

MAIT and CD161+ T cells were found to be significantly increased in OAC TIL with no impact from NACT. This is somewhat disappointing as MAIT cells have previously been shown to reduce OAC cell line viability[109] and may have future utility for immunotherapy. CD161+ T cells have also been shown to offer protection and improved survival in murine models through granzyme driven cytotoxicity[110] and demonstrate enhanced cytotoxicity, tissue homing and memory characteristics in human studies[111].

The proportion of T regulatory cells was substantially increased in TIL although this was not influenced by administration of neoadjuvant chemotherapy. The importance of Tregs in oesophageal cancer is poorly understood and contrasting evidence exists with regard to the impact on tumour progression and overall patient survival[106,112,113]. The majority of work has focussed on OSCC but my findings indicate that this is also an important topic for future study in OAC.

Several studies have interrogated the T regulatory tumour microenvironment through IHC analysis. Zingg et al reported higher densities of T reg in the peripheral tumour microenvironment of advanced oesophageal adenocarcinoma and indicated that this may be associated with improved survival. However, no independent influence of TILs and Tregs was seen following multivariate analysis[106,114]. Stein et al reported an association between high intratumoural T-reg density and lower pT stage and node negative disease[115]. Furthermore, high intratumoural T-reg density and high Treg/CD3/CD8 dense tumours were

associated with improved overall survival. Zhu et al have shown in advanced and untreated OSCC that the density of Tregs in isolation does not impact overall survival however the CD8+:Treg ratio was an independent predictor of both disease-free and overall survival[116]. A meta-analysis by Gao et al has reported that FOXP3+ TILs were not associated with overall survival[103].

Nabeki et al showed increased T-reg infiltration to be associated with a reduced overall survival synergistically with IL-32 expression in cancer cells. IL-32 causes local immune suppression and establishes preferential conditions for tumour invasion or metastasis[117]. IL-33 has also been shown to be associated with reduced overall survival and CCL2, which is regulated downstream of IL-33, could potentially promote tumour development and metastasis by recruiting regulatory T-regs[118]. The concentration of T-regs is heavily determined by both tumour and stroma-derived chemokines such as CCL20[119]. T-regs may also be recruited by M2-like tissue associated macrophages (TAM) through secretion of C–C motif ligand 17 (CCL17) and C–C motif ligand 22 (CCL22) [120]. Finally, recent evidence suggests that Eomesodermin (Eomes), a T-box transcription factor that drives the differentiation and function of cytotoxic lymphocytes, may also promote oesophageal cancer progression by recruiting T-reg cells through the CCL20-CCR6 pathway[121].

PD-1, Tigit and Tim-3 were found to be significantly upregulated on CD4+, CD8+ and T-reg TIL. PD1 is upregulated in the presence of chronic antigen exposure and as a result is found in high frequency in the TME and chronic infection. It plays a crucial role in maintaining balance between tumour recognition and breakdown and inadvertent tissue destruction. PD1 binds to PD-Ligand 1 and PD-Ligand 2 (PDL1-/2) which are expressed by tumour macrophages, some activated T cells and B cells, DCs and some epithelial cells, particularly under inflammatory conditions[122]. In addition, PD-L1 is expressed by tumour cells as an adaptive immune mechanism to escape anti-tumour responses[28,29]. PD-1 signalling due to

PD1-PDL1/2 interaction invokes T-cell exhaustion, a reversible inhibition of T-cell activation and proliferation, and blockade of the PD-1 axis has been shown to have a significant anti-tumour effect[30–35]. Functional studies of OSCC cell lines have shown that PD-1/PD-Ls signal pathway was able to downregulate the function of CD8+ T lymphocyte and its function could be restored by blocking the signal pathway[123]. A meta-analysis by Khunger et al shows that tumour and TILs overexpression of PD-L1 is associated with significantly higher response rates to PD-1/PD-L1 axis inhibitors across a range of malignant solid tumours including gastro-oesophageal cancer[124].

Numerous studies have explored the effect of PD1/PD-L axis in relation to OAC immunotherapy. Kollman et al reported that the expression of PD-1 by TILs increases with associated increase in tumour stage and lymph node involvement. However, after adjusting for clinicopathological factors, increased PD-1 expression was not a determinant of survival. PD-L1 was expressed to a greater degree on TIL rather than tumour (69% vs 44% respectively). PD-L1^{+} cancer cells were more common at early tumour stage but no differences were seen in relation to lymph node status. Overall survival was higher in patients with increased cancer cell-PD-L1 expression but this was not the case for PD-L1 expression on TIL. Leng et al reported that in OSCC overall survival for PD-L1-positive patients was significantly worse than that of negative patients whilst PD-L2 expression did not impact overall survival[123]. Okadome et al reported that patients identified to be negative for both PD-L1 and PD-L2 had an improved overall survival on multivariate analsysis[91]. Supporting evidence from Ohigashi et al showed an inverse correlation between PD-L2 expression and CD8+$^{+}$ T cells with no such correlation for PD-L1[125]. Zhao et al have shown that in OSCC PD-1 expression in TILs and PDL-1/2 on tumour have been shown to be independent predictors of a reduced overall survival[126] whilst Tanaka et al reported increased PD-L1 to be associated with worse overall survival.

It is important to consider the role of PD-L expression in metastasis and Svensson et al reported that PD-L1 expression on TIL was significantly higher in lymph node metastases compared to in primary tumours and associated with prolonged survival. A significant stepwise positive association was found between CD+ T cells and categories of PD-L1 expression on TIL[127].

The PD-1:PD-L1 axis is the major target for checkpoint therapy but mixed results have been observed in OAC to date. Checkmate 577 examined the use of adjuvant PD-1 inhibitor Nivolumab for resected oesophageal cancer post neoadjuvant chemoradiation and reported improved disease free survival for both OAC and SCC[79]. Maximal effects were seen in OSCC but this has been licensed by NICE for use after administration of neoadjuvant chemoradiation. However, as the UK predominantly uses a peri-operative FLOT-based neo-adjuvant approach the use of Nivolumab has been limited. The PD-L1 inhibitor pembrolizumab has also been assessed in the neoadjuvant setting but did not meet the pre-specified endpoint[128]. Similarly, the PERFECT trial examined pembrolizumab in the neoadjuvant setting but without clinical success[82]. Further research is required to understand why there is such variation in the response to PD-1:PD-L blockade within patient cohorts. This lack of therapeutic success has led to interest in the potential utility of additional checkpoint blockade approaches, such as targeting of TIGIT or Tim-3. TIGIT can bind to CD155 and can act to enhance T and NK cell exhaustion[129]. TIGIT overexpression has been reported on CD8+ TILs and Tregs in many tumours and this was confirmed in my findings[130–133]. A transition of overexpression has been seen from PBMC, to lymphocytes within adjacent oesophageal tissue, and finally to TIL[134]. TIGIT is highly expressed in OSCC where it is an independent unfavourable prognostic factor[126,135]. Good therapeutic effects have been achieved in many pre-clinical models by blocking the interaction between CD155 and TIGIT however its clinical role in oesophageal cancer is as yet unknown[136,137]. An initial

phase 1 trial has shown that the anti-TIGIT antibody Tiragolomab has appropriate safety and paves the way for a wider expanse of trials[138,139]. Co-expression of TIGIT with PD-1 on CD4 and CD8+ is common, suggesting it may be an appropriate target for dual blockade immunotherapy. Indeed, some murine models have shown a synergistic effect of the inhibition of both pathways in boosting the antitumor immune response[134,140].

TIM-3 expression on CD4+ and CD8+ TILs in OSCC is also markedly increased[202] and Hong et al have reported that high TIM-3 expression was associated with a higher probability of recurrence and death[141]. Co-expression with PD1 is also common in TIM-3+ CD4+ and CD8+ TIL. Of note, TIM-3 expression is significantly upregulated on NK cells in PBMC and TIL of oesophageal cancer patients[142].

I found that NK cells are significantly reduced in TIL as compared to PBMC where they represented only 3.7% of the infiltrate compared to 16% in blood. NK-TIL were seen to undergo significant phenotypic change with increased populations of the $CD56^{bright}CD16^{low}$ subset. The ability of NK cells to kill tumour cells in a non-MHC dependent manner has made them an interesting target for immunotherapy[143] but there is currently very little information on NK-TIL in OAC. Expanded NK cells have been shown to be highly cytotoxic against NKG2DLs-expressing OSCC cells, particularly those with an epithelial mesenchymal transition (EMT) phenotype (down-regulation of E-cadherin and the acquisition of mesenchymal markers including N-cadherin and Vimentin)[144,145]. Furthermore, the density of NK cell infiltration is associated with an improved overall survival[146]. Liu et al reported that peripheral NK cells in OSCC upregulate PD-1 expression as compared to healthy controls. This correlated with the degree of tumour differentiation, lymph node metastasis stage and overall metastasis [147]. These $PD\text{-}1^{+}$ NK cells had higher expression of CD107a and NKG2D and PD1/PD-L1 binding induced apoptosis, thus potentially delineating an additional target cell from PD-1 blockade[147,148]. NK-TIL have also been shown to sometimes express TIM-3,

TIGIT and LAG-3 in addition to PD-1[142]. Zheng et al reported Tim-3 expression to be dominant on $CD56^{bright}$ NK cells in both PBMC and TIL whilst a significant negative correlation was seen in relation to cell frequency. TIM-3+ NK TIL also demonstrate a greater tendency to apoptosis and produce reduced quantities of IFN-gamma[142]. TIM-3 expression on NK TIL is significantly associated with tumour invasion, lymph node metastasis and stage of disease suggesting that it may have an overall impact on survival and in turn may be a promising target for immunotherapy.

The importance of the humoral immune response against cancer is currently of considerable interest and as such I was interested to assess global and memory B cell pools within my study group. I found that the proportion of B cells was comparable within PBMC and TIL but that the percentage of the memory pool was increased within TIL, potentially reflecting local engagement with antigen. NACT acted to increase the proportion of B cells within TIL but this was not related to treatment response. These findings correlate with an IHC study by Svensson et al that confirmed B cells increase after neoadjuvant chemotherapy (EOX, FLOX, FOLFOX)[149] whilst B cell number did not impact survival.

This chapter provides a representative overview into the populations of TIL in OAC using flow cytometry. Flow cytometry provides accurate immunophenotyping information and has been used as a preferred methodology in immunology for decades there are some inevitable limitations. Acquisition of cells for analysis was done by a diffusion technique. This potentially does not maximise the number of cells for analysis as could be improved by tissue degradation techniques however it is known that additional steps within a cell preparation cycle have the potential to impact TIL phenotype potentially distorting the results. Use of the diffusion technique aims to best reflect the TIL populations as they would be found in the tissue. Flow cytometry is an ideal technique to identify specific populations that have been identified pre-testing however converse to this it does not provide the opportunity to identify

novel populations that may previously not have been know. Discovery of novel populations would be better undertaken by transcriptomics as was done in chapter 4. A further potential criticism of flow cytometry relative to other techniques including immunohistochemistry (IHC) is that despite revealing the TIL within the immune landscape it does not provide location. IHC would have been possible however affordable techniques have very limited antibody binding capacity and multispectral panels such as Vectra are increasingly expensive. It was determined that discovery science opportunities in the form of single cell transcriptomics would provide a better use of resources than multispectral IHC.

Conclusion

My work has demonstrated marked variation in the immune landscape between PBMC and TIL. The immune infiltrate is dominated by T cells which comprise a range of different subsets and an increase in the regulatory pool. Cellular populations are largely unaffected by neoadjuvant chemotherapy and, whilst this is somewhat disappointing in relation to potential understanding of how NACT may work, I sought to study this further in chapter 6. Marked inter-patient variability was noted in relation to immune profile and as such greater tailoring of treatment for 'personalised therapy' may improve outcomes, particularly in light of recent PD1/PD-L1 inhibitor trials which are beginning to show some encouraging results. Checkpoint expression is high across all T cell phenotypes and my findings suggest that combinatorial checkpoint blockade, such as targeting PD-1 together with TIGIT or Tim-3, may act to improve OAC treatment pathways.

Chapter 4 - The single cell transcriptional landscape of esophageal adenocarcinoma and its modulation by neoadjuvant chemotherapy

Introduction

Over 570,000 new cases of oesophageal cancer are diagnosed annually and OC remains a tumour of unmet need with high rates of morbidity and mortality and nearly 510,000 annual deaths[150]. OC comprises two major histological subtypes, adenocarcinoma or squamous cell carcinoma, with distinct etiological factors and management pathways. Risk factors for oesophageal adenocarcinoma include high body mass index and gastrointestinal reflux disease and its incidence is rising markedly in many countries. Many cases develop from Barrett's oesophagus which originates from transformation of gastric cardia through c-MYC and HNF4A-driven transcriptional programming. Surgical resection (oesophagectomy) may be curative for some patients without metastatic disease and is usually preceded by administration of chemotherapy or chemoradiotherapy as a 'neoadjuvant' treatment[88,151]. However, patients with metastatic disease are not considered eligible for this approach and the 5-year survival for those who do undergo neoadjuvant chemoradiotherapy and surgery remains below 50%[41].

As such there is considerable interest in the potential utility of immunotherapy regimens to improve OAC clinical outcome. The CheckMate 577 trial demonstrated that adjuvant PD-1 blockade increased disease-free survival from 11 to 24 months in patients with OAC following neoadjuvant chemoradiotherapy and resection[79,152]. Immune checkpoint inhibition (ICI) has also proven of value in the treatment of advanced squamous cell tumors[153,154]. Whilst these findings show the potential power of harnessing the immune system in the treatment of esophageal cancer, clinical responses remain suboptimal. To develop more effective and targeted immunotherapy regimens it is now critical to develop a comprehensive understanding of the immune response within the tumour microenvironment in patients with OAC.

scRNA-Seq analyses have transformed understanding of the complexity and heterogeneity of the tumour microenvironment. Recent interrogation of the scRNA-Seq landscape of squamous

cell OC has revealed a complex microenvironment with many features of immune suppression including accumulation of proliferative and exhausted CD8+ T cells[155,156]. SMART-Seq2 analysis of ~200 cells from two patients with EAC focussed on tumour cells and identified cellular heterogeneity[157].

scRNA-Seq assessment is particularly powerful when applied to samples from clinical pathways that allow correlation of cellular features with disease progression and treatment. This can be used to assess which cellular subtypes associate with treatment response and so help to guide the introduction of novel therapies. We undertook scRNA-Seq analyses of the OAC tumours in patients with both primary disease or those who had undergone neoadjuvant chemotherapy (NAC). Macroscopically normal oesophagus distant to the tumour was also sequenced to provide an appropriate control. Findings from the scRNA-Seq were also correlated with pathological response to NAC to determine whether susceptibility to chemotherapy impacts the immune microenvironment.

Transcriptomic analysis provides many opportunities to understand the complexities of the tumour microenvironment however challenges arise when placing such evidence into the genome-transcriptome-proteome pathway[158]. We will seek to identify key cellular populations within the transcriptome to isolate and confirm in different patient populations using flow cytometrics.

Work within this chapter forms the basis for the published article "The single cell transcriptional landscape of esophageal adenocarcinoma and its modulation by neoadjuvant chemotherapy"[159]. To achieve this novel evaluation of the transcriptomic landscape of oesophageal adenocarcinoma required a team approach from myself and key stakeholders within the Moss Group. It was recognised that to understand the TME of esophageal cancer it would require a multimodal approach and that although flow cytometric analysis as reported in Chapter 3 has demonstrated crucial variations in the checkpoint expression between PBMC

and TIL, the flow work answered predetermined questions as set forth and confirmed by the flow panels. I identified that transcriptomic analyses would provide an opportunity for discovery and potential identification of variances in a greater breadth of cellular populations. Appraisal of the published literature identified that the OCCAMs consortium had performed whole genome, exome, transcriptome and methylation studies of oesophageal and junctional adenocarcinoma yet there was no published work on the transcriptomic immune profiles within OAC. Equally the role of cancer associated fibroblasts (CAFs) within OAC TME is poorly understood. Transcriptomic analyses of TIL and CAFs would potentially provide the opportunity to evaluate interactions within the TME that would benefit from immunomodulation.

As previously highlighted, neoadjuvant treatment is a key component of the gold standard treatment pathway for locally advanced OAC. Although there is debate over the optimum neoadjuvant treatment the UK favours the use of chemotherapy and which differs from many European countries such as the Netherlands which incorporates chemoradiotherapy into their neoadjuvant pathway. UHB currently uses neoadjuvant FLOT in the treatment of locally advanced OAC undergoing treatment with curative intent. Immunotherapy beyond Checkmate 577 has not been incorporated into the curative treatment pathway for OAC. It is likely therefore that introduction of immunotherapy in the neoadjuvant setting will likely arise in concordance with already established chemotherapy or chemoradiotherapy regimens. It is poorly understood however how neoadjuvant treatment impacts the TME. I determined therefore that it would be crucial to examine samples pre and post neoadjuvant treatment.

As highlighted in the methods I was able to gain tumour samples at staging laparoscopy/gastroscopy (pre-neoadjuvant) and post resection (post neoadjuvant). I sought initial financing which facilitated the sequencing of four tumour samples. £15,000 was donated from the Experimental Cancer Medicines Centre (ECMC), University of Birmingham. Due to

the time interval between staging and potential that patients undergoing staging may not progress to resection due to reducing performance status or progressive disease I decided that it would not be possible to sequence matched patient samples. After processing and primary analysis it was identified that despite the depth of sequencing criticism could be directed to the small number of samples and lack of control. I acquired a £8000 donation from the Upper GI Cancer Patients Group, Queen Elizabeth Hospital Birmingham and £8000 from University Hospitals Birmingham Charity which facilitated the sequencing of 6 further samples. A total of 10 tissue samples were obtained from 8 patients. Three chemonaive tumour samples were obtained at pre-treatment gastroscopy. An additional chemonaive tumour and matched normal tissue specimen was from a resectional specimen. The remaining 4 tumour and 1 matched normal samples were obtained from post-chemotherapy (FLOT) resections. Post tissue acquisition samples were prepared in accordance with Genomic Birmingham guidance to facilitate sequencing. Data analysis was performed with the Moss group by my colleague Dr Wayne Croft.

Results

The oesophageal adenocarcinoma microenvironment comprises multiple cellular subtypes which are differentially modulated by response to neoadjuvant chemotherapy. Tumour tissue was obtained from 4 treatment-naive patients and 4 patients who had received neoadjuvant chemotherapy. Unsupervised clustering of 52,387 single cells was undertaken to determine the profile of the cellular composition within the OAC microenvironment. This identified 10 high level cell types (T, NK, B, Plasmablast, Myeloid, Mast, Fibroblast, Myofibroblast, Endothelial, Epithelial) and a small population of cycling lymphocytes (Figure 36A). UMAP profiles were comparable before or after neoadjuvant chemotherapy, and also in comparison of tumour or adjacent normal tissue, thus allowing more detailed transcriptional comparison of homologous populations in different clinical settings (Figure 36B). Expression of canonical cell-type marker genes (Figure 36C) and automated cell-type classification overlaid reliably on to individual cell-types and top cluster marker genes were also defined (Figure 36E).

Epithelial cells comprised a small minority of the TME as a result of primary cell sorting at a tissue that aimed to focus on the immune contexture of OAC. The TME was dominated by immune and stromal subsets with T cells, B cells and fibroblasts by far the largest subsets. Increased proportions of T cells, NK cells and cycling cells were seen in tumour compared to normal tissue although endothelial cells were underrepresented within tumour (Figure 36D,F).

Neoadjuvant chemotherapy modulated cellular populations in several ways. Most notable was a reduction in the proportion of NK and cycling cells after therapy whilst endothelial cells and fibroblast populations were increased (Figure 36F). Response to neoadjuvant chemotherapy was then assessed by Mandard score pathological analysis (Figure 36G) where 1 refers to complete remission and 5 indicates no pathological response. Unsurprisingly, poor pathological response was associated with increased proportions of epithelial cells, whilst

higher proportions of cycling cells, T cells and NK cells were also retained. In contrast, these cells were markedly suppressed within a complete response and replaced by myofibroblasts and endothelial cells.

Differential expression analysis was also assessed to identify differentially expressed genes (DEGs) in relation to exposure to neoadjuvant chemotherapy and comparison to normal tissue. Chemotherapy induced marked transcriptional change in myofibroblasts (705 DEGs), fibroblast (496 DEGs) and epithelial populations (548 DEGs) whilst myofibroblasts also differed most markedly between normal and tumour tissue (763 DEGs).

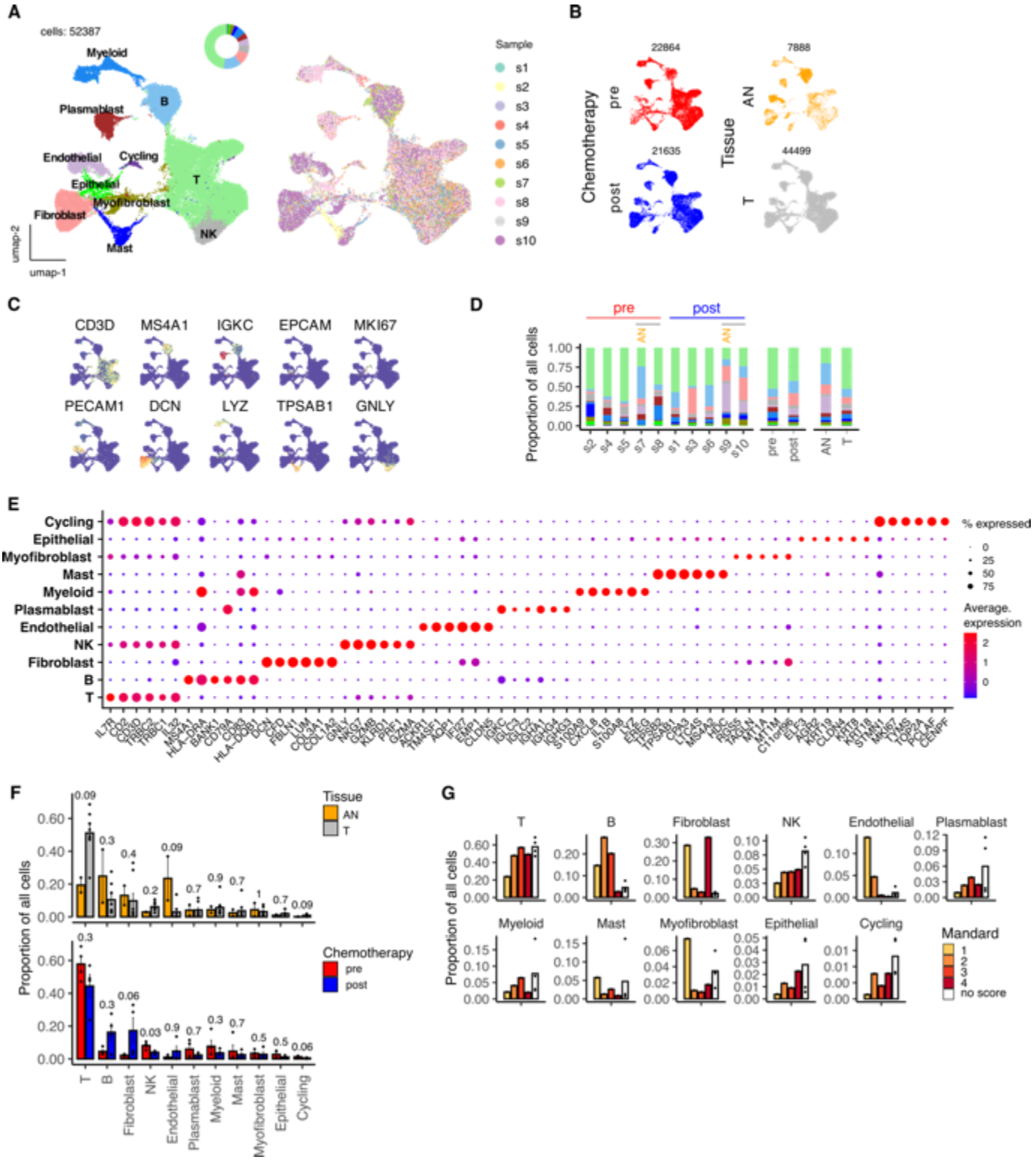

Figure 36 . High level cell type ATLAS of Esophageal Adenocarcinoma. A. Sample processing schematic. **B.** UMAP embedding overlaid with unsupervised cluster cell type annotations (left) and sample label (right). **C.** UMAP embeddings split by treatment and tissue type. **D.** UMAP embeddings overlaid with expression of canonical high level cell type marker genes. **E.** Breakdown of cluster proportions by sample, chemotherapy treatment and tissue type. Grey line indicates matched tumour and Adjacent Normal (AN) samples. **F.** Average expression profile of top cluster marker genes. Dot size indicates the percentage of the cluster showing expression **G.** Comparison by Mann-Whitney test of Adjacent Normal (AN) vs Tumor (T) and pre vs post chemotherapy cluster proportions. **H.** Cluster proportions by Mandard scores. Points represent within-sample cluster proportion of total cells and p values determined by Mann-Whitney test.

Neoadjuvant chemotherapy reduces T regulatory cells and increases the proportion of a range of effector populations

We next went on to determine the transcriptional profile of each major cell subset within EAC and focussed initially on T cells (Figure 37) which were the dominant lymphocyte population. Unsupervised clustering of 25,588 T cells identified 15 distinct populations of which 5 were CD4+, 7 were CD8+ and 3 represented T regulatory populations (Figure 37 A,B,C). Marker gene expression (Figure 37B), automated cell type annotation, enrichment of selected hallmark gene sets (Figure 37D) and signature score distributions (Figure 37E,) was used to interrogate these in further detail.

Very few naïve T cells were present in tissue and effector responses were dominant (Figure 37A,F). A CD8+ T population expressing CXCL13, now recognised as a feature of exhaustion in many tumours, was increased and associated with poor response to chemotherapy[230]. Overall neoadjuvant chemotherapy was found to significantly reduce signature scores assessing cytotoxicity, exhaustion, checkpoint expression and TRM (Figure 37E). CD8+ cells expressing CCL4, a chemoattractant for NK cells and monocytes, showed a similar pattern. CD8+ tissue resident memory cells expressing CD69 and an HSP-positive subgroup were reduced in tumour tissues (Figure 37G).

The CD4:CD8 ratio was 1.1 within tumour tissue prior to chemotherapy but fell to 0.65 following NACT (Figure 37H). However, chemotherapy markedly reduced the proportion of T regulatory cells within the tumour and the ratio of CD4+ effector:CD4+ regulatory cells increased more than 2-fold from 1.6 to 3.4 ($p=0.029$) whilst the CD8+:Treg ratio increased from 4 to 6.5 ($p=0.057$) (Figure 37H). Effector pools after chemotherapy became enriched in a CD8+ subset enriched for granzyme K expression and CD4+ subset characterised by expression of JUNB (Figure 37 F,G).

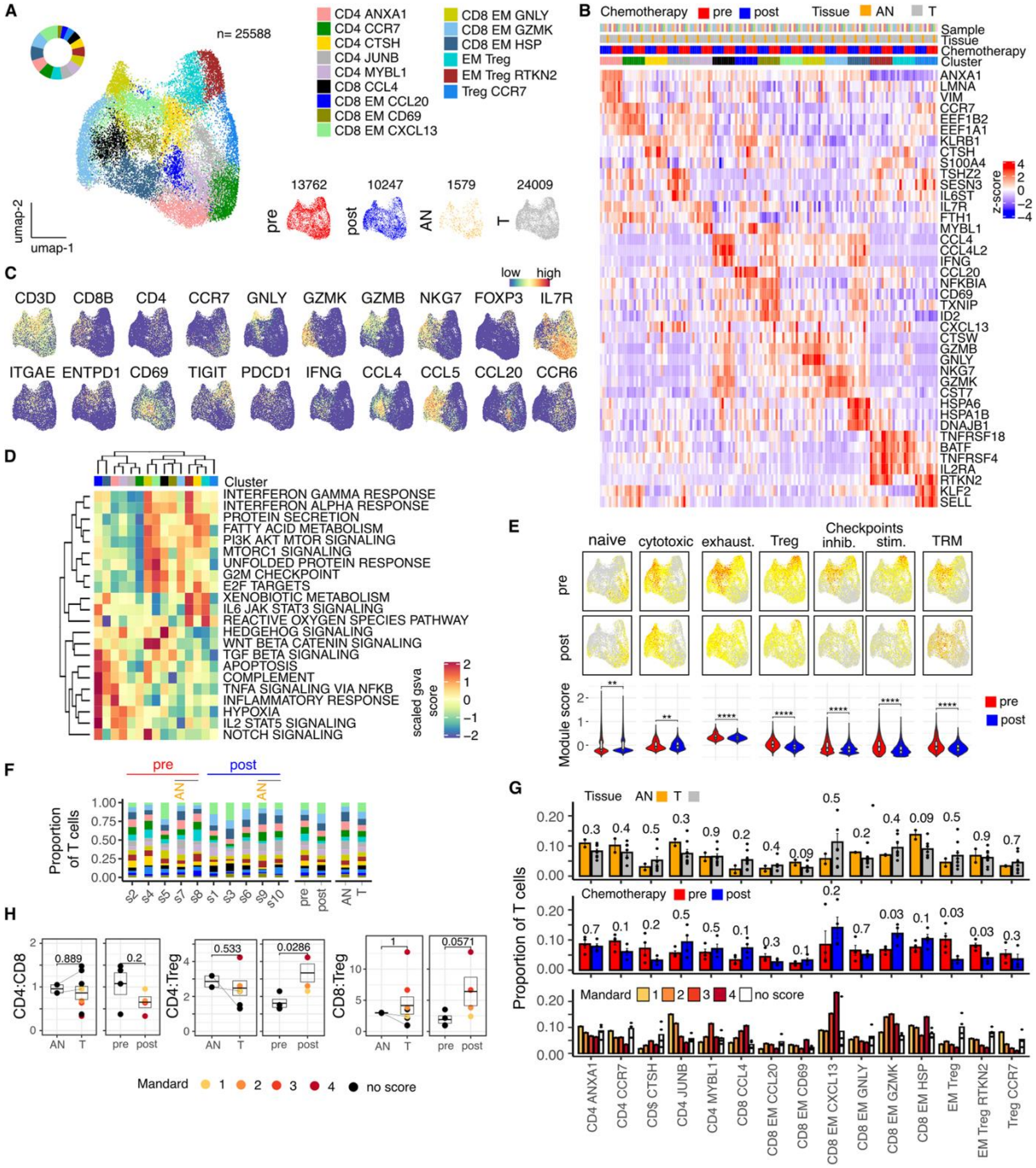

Figure 37. NACT modulation of T cell contexture within the tumour microenvironment of Oesophageal Adenocarcinoma. A. UMAP embedding overlaid with cluster cell type annotations and UMAP embeddings split by treatment and tissue type. **B.** Average expression profile of top cluster marker genes. **C.** UMAP embeddings overlaid with selected canonical T cell type marker genes. **D.** Scaled enrichment score calculated by GSVA for selected MSigDB Hallmark gene sets. **E.** UMAP embeddings overlaid with selected signature module scores and distributions of module scores stratified by chemotherapy treatment. **F.** Breakdown of cluster proportions by sample, chemotherapy treatment and tissue type. **G.** Comparison of Adjacent Normal (AN) vs Tumor (T), pre vs post chemotherapy and Mandard score cluster proportions. Points represent within-sample cluster proportion of total T cells. **H.** CD4:CD8, CD4:Treg and CD8:Treg ratios stratified by tissue type and chemotherapy. p values determined by Mann-Whitney test.

A progenitor NK cells subset is reduced in tumour and increased in patients with chemotherapy response

Unsupervised clustering of 1,671 NK cells identified five distinct subpopulations including 2 mature CD16+ subsets with predominant expression of CCL3 or FGFBP2. NKs expressing CCL3 were significantly reduced after NACT. A population expressing *KIT*, the gene encoding CD117 (c-KIT) and characteristic of NK progenitors, was also seen and expressed high levels of IL-7R, IL-4I1 and TNFRSF25 (DR3) (Figure 38). NK populations within tumour were broadly comparable with normal tissue although the progenitor KIT population was suppressed but increased after chemotherapy in relation to the degree of pathological response, suggesting a potential role in tumour control. In contrast the activated mature populations were reduced following chemotherapy (Figure 38F). DEG analyses were broadly comparable for each subset within different samples with the GZMK-expressing NK cells being most susceptible to transcriptional modulation post chemotherapy (Figure 38I).

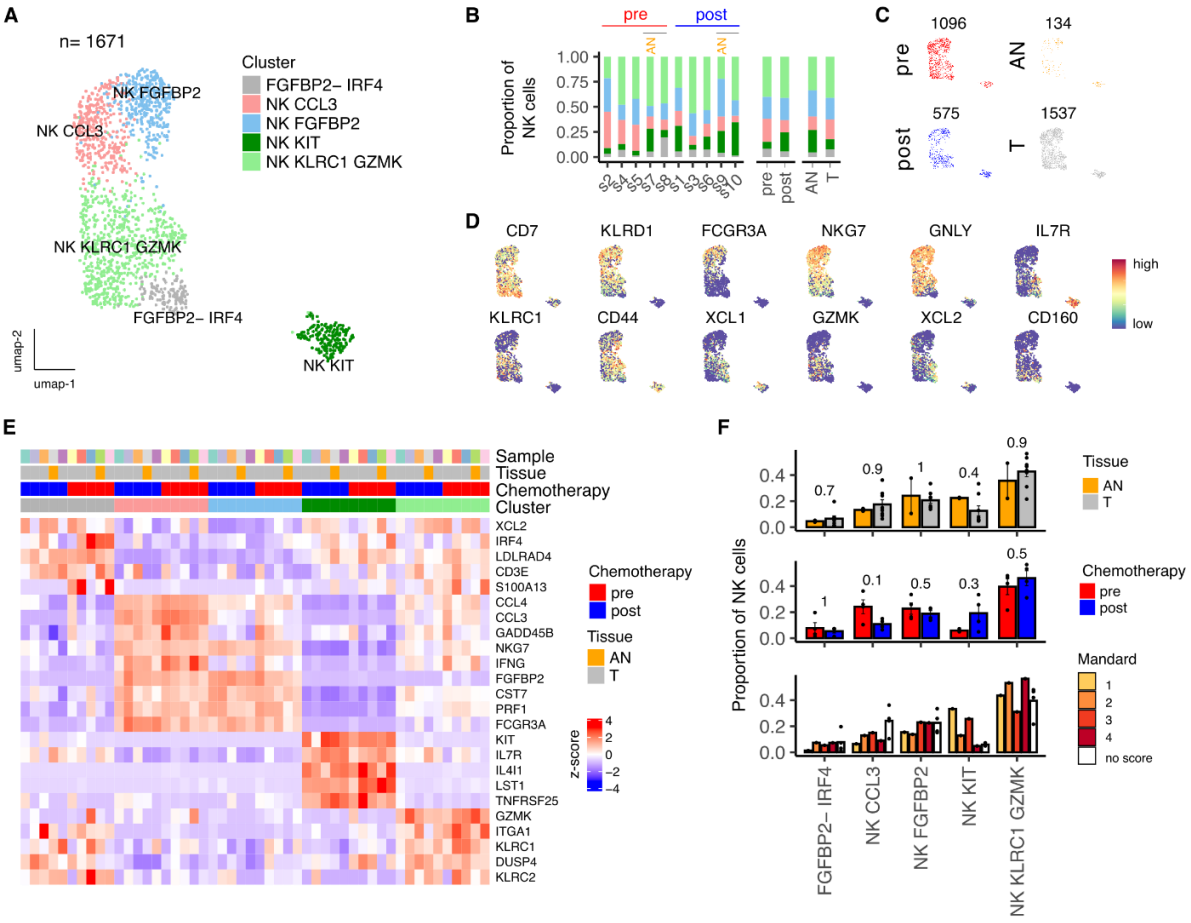
A
n= 1671
Cluster
FGFBP2– IRF4
NK CCL3
NK FGFBP2
NK KIT
NK KLRC1 GZMK
NK FGFBP2
NK CCL3
NK KLRC1 GZMK
FGFBP2– IRF4
NK KIT
umap-2
umap-1
B
pre
post
Proportion of NK cells
1.00
0.75
0.50
0.25
0.00
AN
s2
s4
s5
s7
s8
s1
s3
s6
s9
s10
pre
post
AN
T
C
1096
134
575
1537
pre
post
AN
T
D
CD7
KLRD1
FCGR3A
NKG7
GNLY
IL7R
KLRC1
CD44
XCL1
GZMK
XCL2
CD160
high
low
E
Sample
Tissue
Chemotherapy
Cluster
XCL2
IRF4
LDLRAD4
CD3E
S100A13
CCL4
CCL3
GADD45B
NKG7
IFNG
FGFBP2
CST7
PRF1
FCGR3A
KIT
IL7R
IL4I1
LST1
TNFRSF25
GZMK
ITGA1
KLRC1
DUSP4
KLRC2
Chemotherapy
pre
post
Tissue
AN
T
z-score
4
2
0
−2
−4
F
Proportion of NK cells
0.4
0.2
0.0
0.7
0.9
1
0.4
0.9
1
0.1
0.5
0.3
0.5
0.4
0.2
0.0
0.4
0.2
0.0
Tissue
AN
T
Chemotherapy
pre
post
Mandard
1
2
3
4
no score
FGFBP2– IRF4
NK CCL3
NK FGFBP2
NK KIT
NK KLRC1 GZMK
G
Cell density
0.0015
0.0010
0.0005
0.0000
1000
2000
3000
nFeature_RNA
6e−04
4e−04
2e−04
0e+00
4000
8000
12000
16000
nCount_RNA
0.3
0.2
0.1
0.0
0.0
2.5
5.0
7.5
10.0
percent.mt
s1
s2
s3
s4
s5
s6
s7
s8
s9
s10
H
sample
s1
s2
s3
s4
s5
s6
s7
s8
s9
s10
SingleR hpca coarse
B_cell
Monocyte
NK_cell
T_cell
NA
I
FGFBP2– IRF4 (3,1)
pre
post
LAYN
S100A13
MTRNR2L8
SEC14L1
ZFP36L2
BTG1
FOS
TUBA4A
NK CCL3 (4,1)
JUND
GNLY
TUBB4B
VIM
PPDPF
F2R
KDELR1
NR3C1
NK FGFBP2 (7,4)
VIM
GADD45B
JUND
IER3
PPDPF
HLA-DPB1
SLA
HLA-C
NK KIT (11,2)
CFL1
CD74
C9orf16
DUSP4
PNRC1
PLCG2
ZFAS1
RSL24D1
NK KLRC1 GZMK (48,33)
GNLY
LAYN
GZMB
MTRNR2L8
PLCG2
CXCR4
BTG1
TUBA4A
−Log10(p−value)
Mean Log2 FC
J
FGFBP2– IRF4 (0,0)
AN
T
TSC22D3
ZFP36L2
AREG
GNLY
CCL
SERPINB
ATP6V0E
BCL2A
NK CCL3 (2,0)
MTRNR2L12
PLCG2
CMC1
CCDC186
TUBB4B
SH3BGRL3
SFPQ
HLA-B
NK FGFBP2 (3,0)
MTRNR2L12
PLCG2
DDIT4
AREG
ACTB
PPDPF
SRSF3
HLA-B
NK KIT (3,0)
ZFP36L2
ZFP36
AREG
TNFAIP3
PSMD12
HLA-B
CALR
PBDC1
NK KLRC1 GZMK (8,3)
ZFP36
MTRNR2L12
AREG
PLCG2
HLA-B
ACTB
GAPDH
CD7
−Log10(p−value)
Mean Log2 FC

Figure 38 NACT modulation of NK cell contexture within the tumour microenvironment of Oesophageal Adenocarcinoma. A. UMAP embedding overlaid with cluster cell type annotations. **B.** Breakdown of cluster proportions by sample, chemotherapy treatment and tissue type. **C.** UMAP embeddings split by treatment and tissue type. **D.** UMAP embeddings overlaid with expression of canonical NK cell type marker genes. **E.** Average expression profile of top cluster marker genes. **F.** Comparison of Adjacent Normal (AN) vs Tumor (T), pre vs post chemotherapy and Mandard score cluster proportions. Points represent within sample cluster proportion of total sample NK cells and p values determined by Mann-Whitney test. G, Samplewise distributions of Feature counts (nFeature_RNA), UMI counts (nCount_RNA) and % expression of Mitochondrial genes (percent.mt). H, Automated per-cell annotations of high level cell types using SingleR with the hpca coarse reference dataset. I, Summary of genes identified as differentially expressed in post vs pre NACT EAC tumour sample data. DEG count noted alongside cluster: (pre expressed, post expressed). J, Summary of genes identified as differentially expressed in EAC Tumor (T) vs Adjacent Normal (AN) sample data. DEG count noted alongside cluster: (AN expressed, T expressed) Coloured points indicate DEGs (BH adjusted $p<0.001$ and absolute average log2FC > 0.5).

Profiling of cycling cell population

Expression of cell cycle-associated genes such as *MKi67, TYMS, TOP2A, PCLAF* and CENPF was used to define the presence of cycling cells within tissue. Of note, proliferation was seen almost exclusively within tumour where unsupervised clustering of 436 cells identified 4 subsets (Fig. 39). In contrast only 10 cycling cells were seen within normal tissue and were not analysed further (Fig. 39A).

Cycling cells were predominantly T cells and mostly expressed the tissue residency marker CD103 (*ITGAE*) together with CD39 (*ENTPD1*) which has been associated with tumour specificity (Fig. 39). Proliferation was broadly equivalent in CD4+ and CD8+ subsets.

Chemotherapy reduced the proportion of cycling cells but had no influence on the contexture of the population (Fig. S39A,D). Upregulated DEGs after chemotherapy included MHC class II genes (HLA-DRB1, HLA-DQB1) whilst GITR (TNFRSF18) and the TRM-marker ENTPD1 were reduced (Fig. 39G).

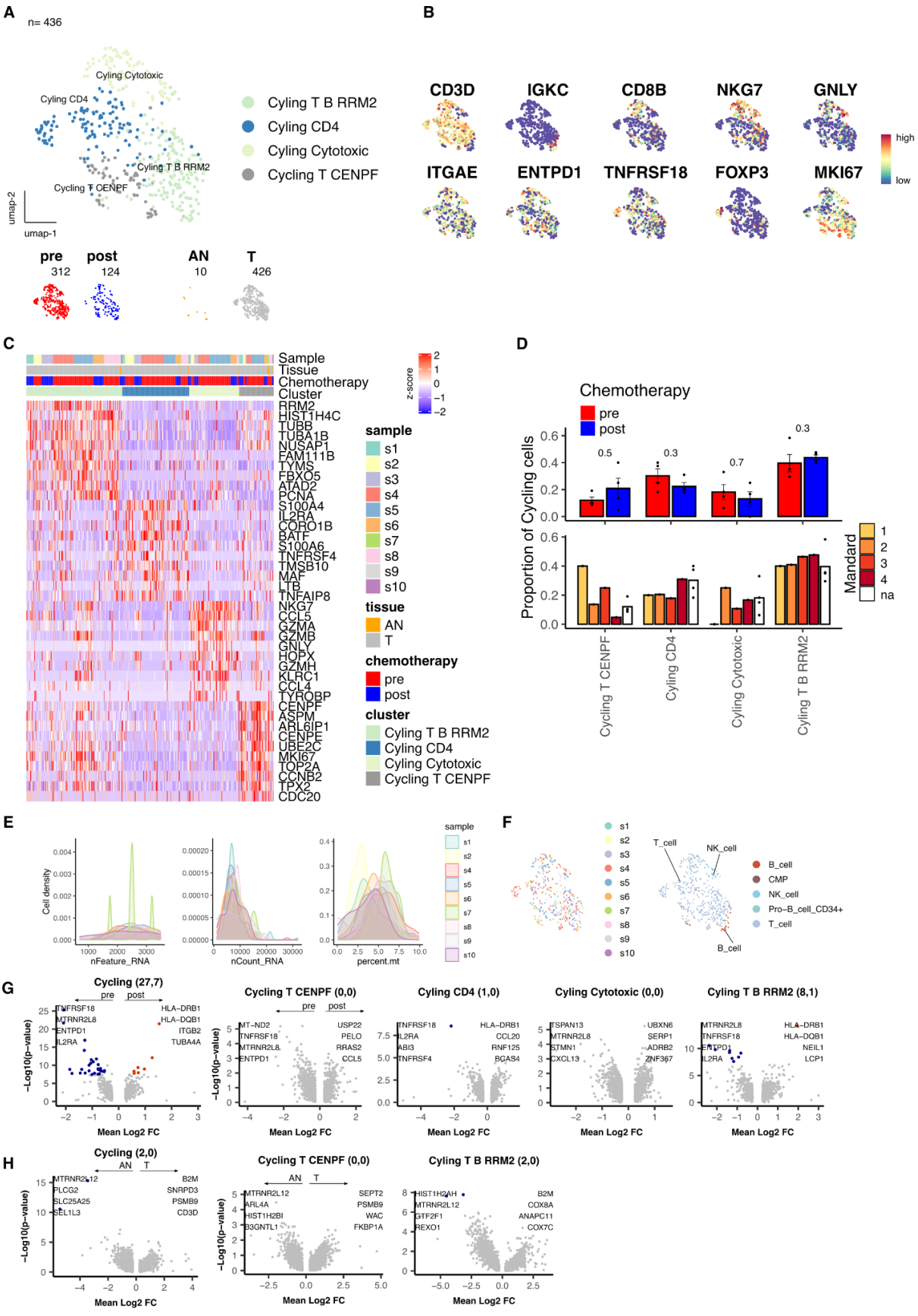
A
n= 436
Cyling Cytotoxic
Cyling CD4
Cyling T B RRM2
Cycling T CENPF
umap-2
umap-1
Cyling T B RRM2
Cyling CD4
Cyling Cytotoxic
Cycling T CENPF
pre 312
post 124
AN 10
T 426
B
CD3D
IGKC
CD8B
NKG7
GNLY
ITGAE
ENTPD1
TNFRSF18
FOXP3
MKI67
high
low
C
Sample
Tissue
Chemotherapy
Cluster
z-score
RRM2
HIST1H4C
TUBB
TUBA1B
NUSAP1
FAM111B
TYMS
FBXO5
ATAD2
PCNA
S100A4
IL2RA
CORO1B
BATF
S100A6
TNFRSF4
TMSB10
MAF
LTB
TNFAIP8
NKG7
CCL5
GZMA
GZMB
GNLY
HOPX
GZMH
KLRC1
CCL4
TYROBP
CENPF
ASPM
ARL6IP1
CENPE
UBE2C
MKI67
TOP2A
CCNB2
TPX2
CDC20
sample
s1
s2
s3
s4
s5
s6
s7
s8
s9
s10
tissue
AN
T
chemotherapy
pre
post
cluster
Cyling T B RRM2
Cyling CD4
Cyling Cytotoxic
Cycling T CENPF
D
Chemotherapy
pre
post
Proportion of Cycling cells
0.5
0.3
0.7
0.3
Mandard
1
2
3
4
na
Cycling T CENPF
Cyling CD4
Cyling Cytotoxic
Cyling T B RRM2
E
Cell density
nFeature_RNA
nCount_RNA
percent.mt
sample
F
T_cell
NK_cell
B_cell
B_cell
CMP
NK_cell
Pro-B_cell_CD34+
T_cell
G
Cycling (27,7)
Cycling T CENPF (0,0)
Cyling CD4 (1,0)
Cyling Cytotoxic (0,0)
Cyling T B RRM2 (8,1)
−Log10(p−value)
Mean Log2 FC
H
Cycling (2,0)
Cycling T CENPF (0,0)
Cyling T B RRM2 (2,0)

Figure 39. Quality metric distributions, SingleR annotations and differential expression analysis of Cycling cells. A, UMAP embedding overlaid with cluster cell type annotations. B, UMAP embeddings overlaid with expression of canonical cell type markers of interest. C, Per-cell expression profile of top cluster marker genes. D, Comparison of pre vs post chemotherapy and Mandard score cluster proportions. Points represent within sample cluster proportion and p values determined by Mann-Whitney test. E, Samplewise distributions of Feature counts (nFeature_RNA), UMI counts (nCount_RNA) and % expression of Mitochondrial genes (percent.mt) for Epithelial (A) and Endothelial (G) cells. F, Automated per-cell annotations of cell types using SingleR with the hpca coarse reference dataset. G, Summary of genes identified as differentially expressed in post vs pre NACT EAC tumour sample data. DEG count noted alongside cluster: (pre expressed, post expressed). H, Summary of genes identified as differentially expressed in EAC Tumor (T) vs Adjacent Normal (AN) sample data. DEG count noted alongside cluster: (AN expressed, T expressed) Coloured points indicate DEGs (BH adjusted $p<0.001$ and absolute average log2FC > 0.5).

Discussion

Recent studies have demonstrated encouraging but suboptimal clinical responses to immune checkpoint blockade in patients with esophageal adenocarcinoma. As such, detailed assessment of the OAC microenvironment is now required and here we undertook comprehensive scRNA-Seq analyses and interrogated the data in relation to neoadjuvant chemotherapy history and pathological response. UMAP transformations were comparable across donors and samples and allowed direct transcriptional comparisons of cell lineages in relation to disease status. This identified a range of findings that may guide future therapeutic approaches.

It was noteworthy that epithelial cells were a minority population in both normal and tumour tissue and as such the microenvironment was dominated by immune and stromal populations. T cells were the majority immune population, a feature also seen in squamous cell pathology [155], and a range of effector and regulatory subsets were identified. This suggests that OAC is broadly immunogenic and induces a tumour-specific cytotoxic cellular response in many cases, a concept supported by the clinical efficacy of PD-1 checkpoint blockade. Intratumoural CD8+ T cells were enriched in CXCL13 and CLL4 expression, mediators of immune cell recruitment, although whether this has a positive or negative influence on tumour growth is unclear. CXCL13 is thought to play a key role in the development of tertiary lymphoid structures through engagement with CXCR5+ follicular helper cells, although CD8+ T cells expressing CXCL13 are observed in many tumours and enriched within exhausted PD-1^{high} s subsets [160]. CCL4 attracts innate cells and its serum level is increased in OAC where it correlates with both the degree of lymphocytic infiltrate and superior clinical outcome[161]. Important modifications of the T cell repertoire were seen after chemotherapy with a marked reduction in T regulatory populations together with relative enhancement of effector pools. This underpins the importance of chemotherapy in overcoming cellular suppression of tumour-

specific immune responses. CD8+ T cells expressing granzyme K were increased after chemotherapy, consistent with the role of this population as a pre-dysfunctional CD8+ subset[162], and potentially explaining the synergy of preoperative neoadjuvant therapy with subsequent checkpoint blockade. In addition, the transcriptional exhaustion signature of CD8+ subsets was reduced after chemotherapy, further supporting a rebalancing of effector responses as a potential mechanism underlying the efficacy of NACT. The potential importance of T cell immunity in OAC was further revealed by the observation that these comprised the majority of proliferating cells, a population which was seen only in tumour tissue. It was noteworthy that this rapidly proliferating population comprised equivalent populations of CD4+ and CD8+ cells and largely comprised of CD69+ and CD103+ cells indicating a tissue resident phenotype. CD39 expression was also enriched on cells and supports their likely role as tumour-specific clones. Chemotherapy was seen to increase the HLA class II-positive activation status of this population, whilst suppressing markers such as GITR that are associated with a regulatory phenotype, further reinforcing the concept that chemotherapy acts to increase the inflammatory balance of the microenvironment within tumours.

There is a reduction in CCL3 expressing NK populations after NACT. CCL3 has been implicated to be pro tumourogenic within the TME. CCL3 expression has been found to be increased in the serum of oeosphageal cancer patients. The reduction in stimulated CCL3 expressing NK cells may result from the reduced tumour burden post NACT. NK subpopulations revealed a KIT+IL-7R+ progenitor subset that was suppressed within tumour but increased in patients who obtained good pathological response to NACT. Of note, these cells expressed high levels of IL4I1, an enzyme which accelerates the expansion of CD8+ T cells[163], and as such this subset may help to support tumour-specific surveillance.

Single cell transcriptomics gives a better understanding of the function of an individual cell and its context within the microenvironment yet it is not without potential limitations. Unlike flow cytometry analyses within this thesis tissue degradation techniques were performed to enable analysis of fibroblasts and epithelial cells which was not possible with diffusion techniques. The phenotypic impact of degradation is limited but should be considered. The data generated by transcriptomics may have high variability, errors and background noise which potentially create technical, methodological and biological complexity when undertaking analysis and interpretation. Using a collaborative approach a bioinformatician with expertise in the analysis of single cell and other transcriptomic modalities was used maximise the analysis and understanding of the data. Equally methodological techniques in analysis of single cell data as previously published in high quality peer reviewed journals was reviewed and incorporated where required. Such understanding was beneficial when trying to translate transcriptome into proteome which is well acknowledged not to be directly replicated despite this measured interpretation and accurate reflection of the data is provided.

Conclusion

This work shows that OAC tumours direct the development of a complex local microenvironment that drives a strong T cell immune response whose efficacy is limited by effector cell exhaustion and expansion of regulatory subsets. This associates with expansion of plasmacytoid dendritic cells and cancer-associated fibroblasts, whilst endothelial cells are markedly suppressed. Effective neoadjuvant chemotherapy was seen to reverse these changes with suppression of T regulatory pools, correction of dendritic subsets, transition of the fibroblast populations and expansion of endothelial cell subsets. This leads to development of pre-dysfunctional effector T cells and a robust B cell expansion. Tumour specific TRM

identified in transcriptional analysis were equally identified in the proteome of OAC. These findings provide insight into the immunological basis of effective checkpoint blockade in EAC and reveal a range of potential novel immunotherapeutic opportunities. Further understanding is required about checkpoint sensitivity in tumour specific lymphocytes.

Chapter 5: Immunophenotypic analysis of tissue resident memory lymphocytes in Oesophageal Adenocarcinoma

Introduction

The transcriptomic analysis of oesophageal TIL discussed in Chapter 4 had identified a population of rapidly cycling T cells which expressed CD69, CD103 and CD39 and thus had the features of a potential cancer-specific T cell population with a tissue residency phenotype. Tissue resident memory cells (TRM) reside within tissues and elicit rapid site-specific immune responses in many organs[164,165]. An increasing body of evidence is evolving to suggest that TRM cells are not only important in responding to exogenous pathogens but may also play a key role in preventing the development and metastasis of solid tumours[166]. Features of tissue residency were first described on CD8 T cells in the context of viral infection[167,168]. Evidence now exists demonstrating that many TILs express phenotypic features of tissue residency, including cell surface markers including CD69 and CD103, and these have been identified in a range of cancers including melanoma, lung, endometrial, ovarian, and breast cancer. Interestingly, an increasing TRM density has been associated with improved patient outcome in several studies[169–173]. Furthermore CD39+ TRM have been suggested to exhibit features of tumour specificity[174].

As such, I next went on to undertake a phenotypic analysis of tissue resident cells in OAC in order to validate and extend the transcriptomic evidence of CD4+ and CD8+ TRM in OAC TIL. Importantly, I also assessed these features on the NK cell population. Features of TRM were further examined in relation to NACT therapy and treatment response (n=10).

Results

Flow cytometric analysis of CD8+ TRM in relation to NACT therapy

Both single expression of CD69 or CD103 (P=0.002, p=0.004) and co-expression were increased on CD8+ TIL in OAC compared to PBMC (p=0.002). Indeed, the population of dual positive cells reached 35% within TIL whilst, as expected (IQR 30.0-42.2), cells with a TRM phenotype were not seen within blood (Figure 40).

I next went on to assess expression of the tumour-associated phenotypic markers CD39 and GITR on the CD8+ TIL. These comprised 1.5% of the total CD8+ TIL pool. Importantly, CD39+ TRM encompassed 13.6% of CD8 TIL (IQR 9.0-16.1, Figure 41). I next assessed TRM percentages on CD8+ TIL in relation to administration of neoadjuvant chemotherapy (NACT). Of note, no changes were observed (p=0.89) and there was also no association seen with treatment response (p=0.39) indicating a stable proportion of TRM despite treatment (Figure 42). However, the co-expression of CD39 and GITR on CD8 TIL increased from less than 0.1% to 2.4% after neoadjuvant chemotherapy (p=0.044), although this did not relate to the treatment response (p=0.79). Similarly, the proportion of CD39+CD8+ TRM in TIL increased from 4.9% to 15% after neoadjuvant chemotherapy (p=0.044) although this was not related to quality of treatment response (p>0.999).

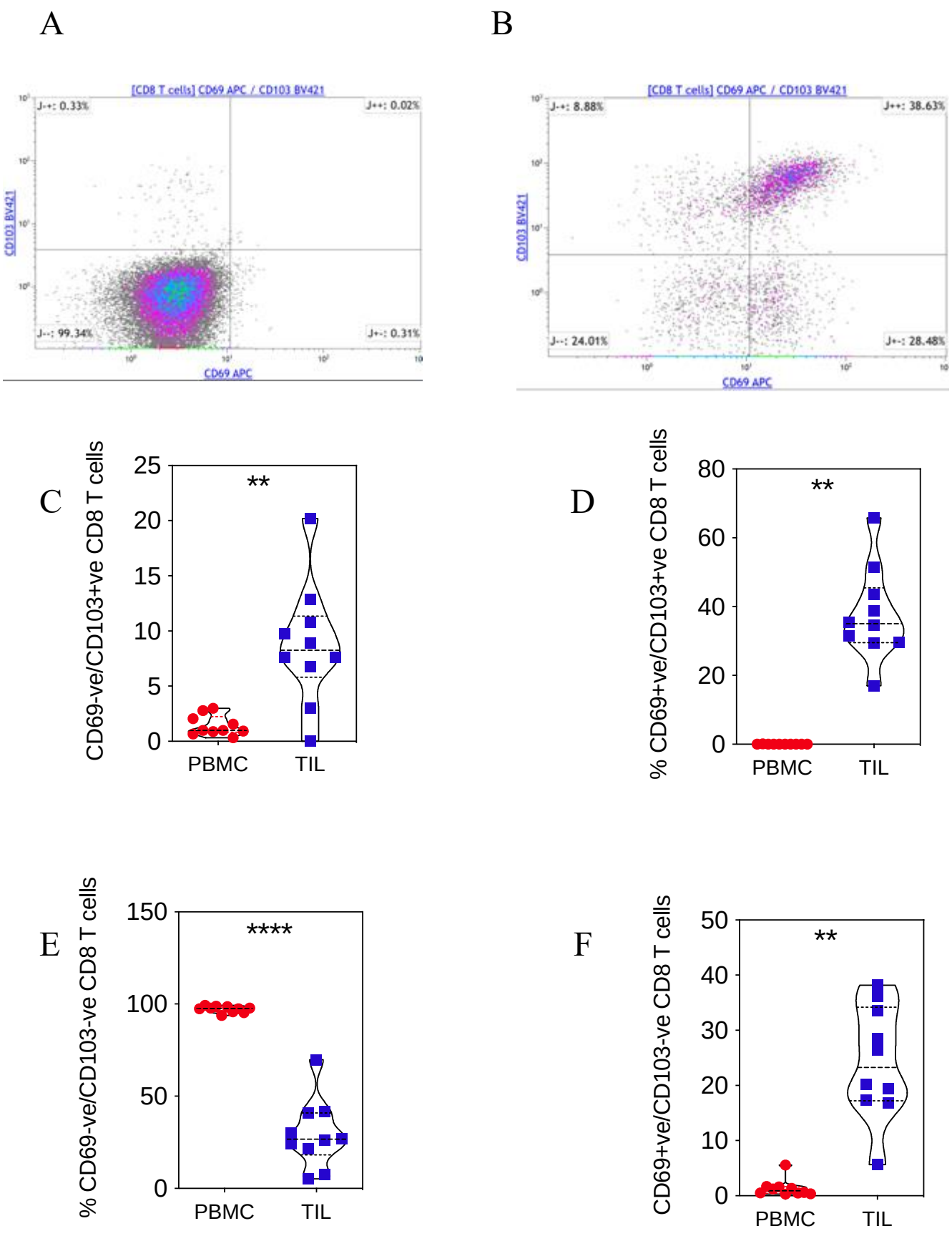

Figure 40. Features of tissue residency in CD8 +T cells.
There was significant upregulation of CD69 and CD103 from PBMC (A) to TIL (B) in matched samples in keeping with tissue residency. Changing CD8 T cell subsets in matched PBMC and TIL, CD69-CD103+ (C), CD69+CD103+ (D), CD69-CD103- (E), CD69+CD103- (F). Data analysed by Wilcoxon matched-pairs signed rank test for matched samples, ** denotes $p<0.01$, **** denotes $p<0.0001$.

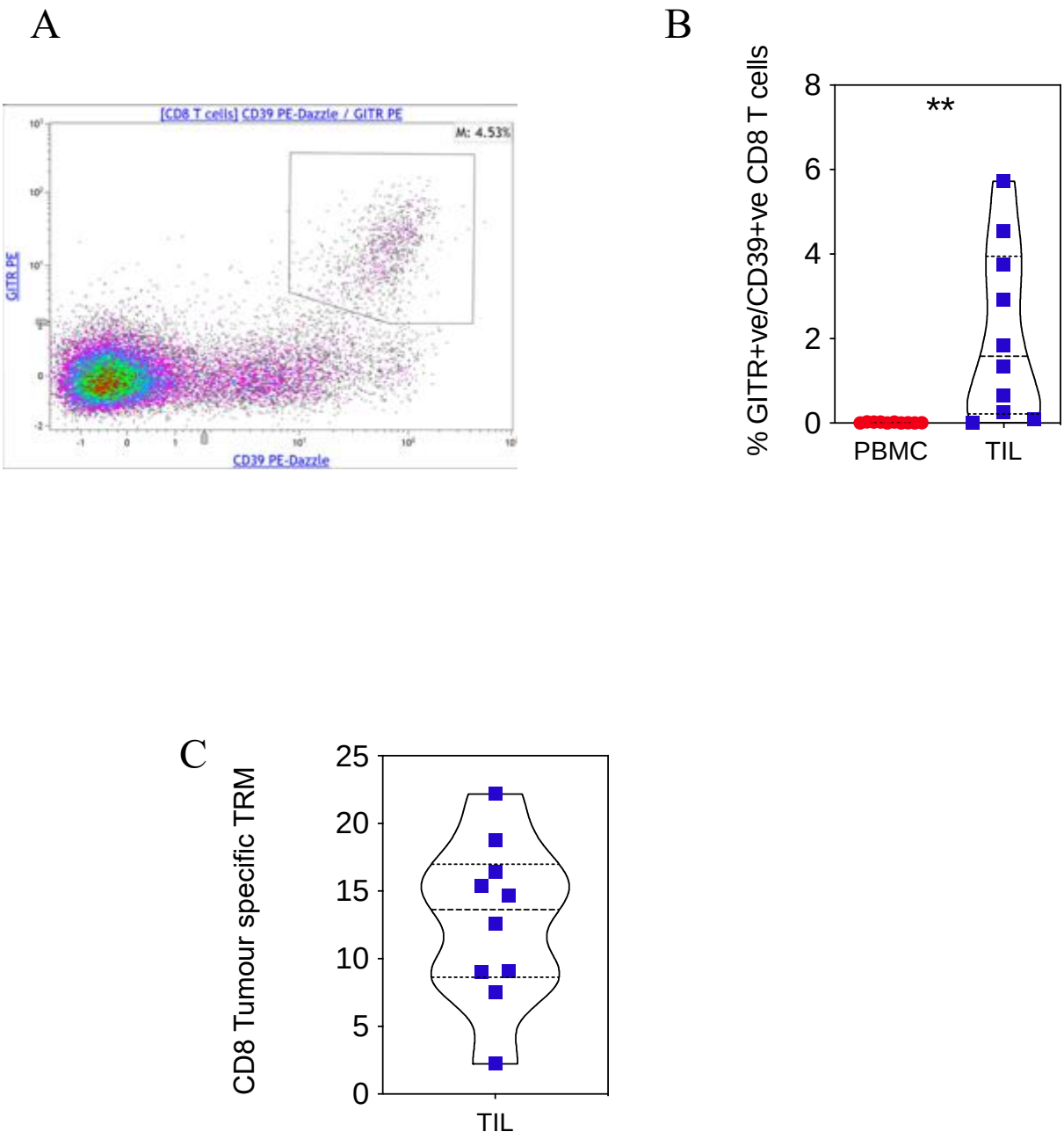

Figure 41. Tissue resident memory CD8+ T cells
An example plot of CD39 and GITR expression in CD8+ T cell TIL(A). There is significant upregulation of CD39 and GITR in matched CD8+ T cell TIL (B). Each symbol represents an individual patient. Dashed horizontal lines indicate the median and dotted lines indicate the interquartile range. Data analysed by Mann Whitney test, ** denotes $p<0.01$. Tissue resident memory (CD69+CD103+CD39+) CD8 T cells are commonly identified in TIL (C).

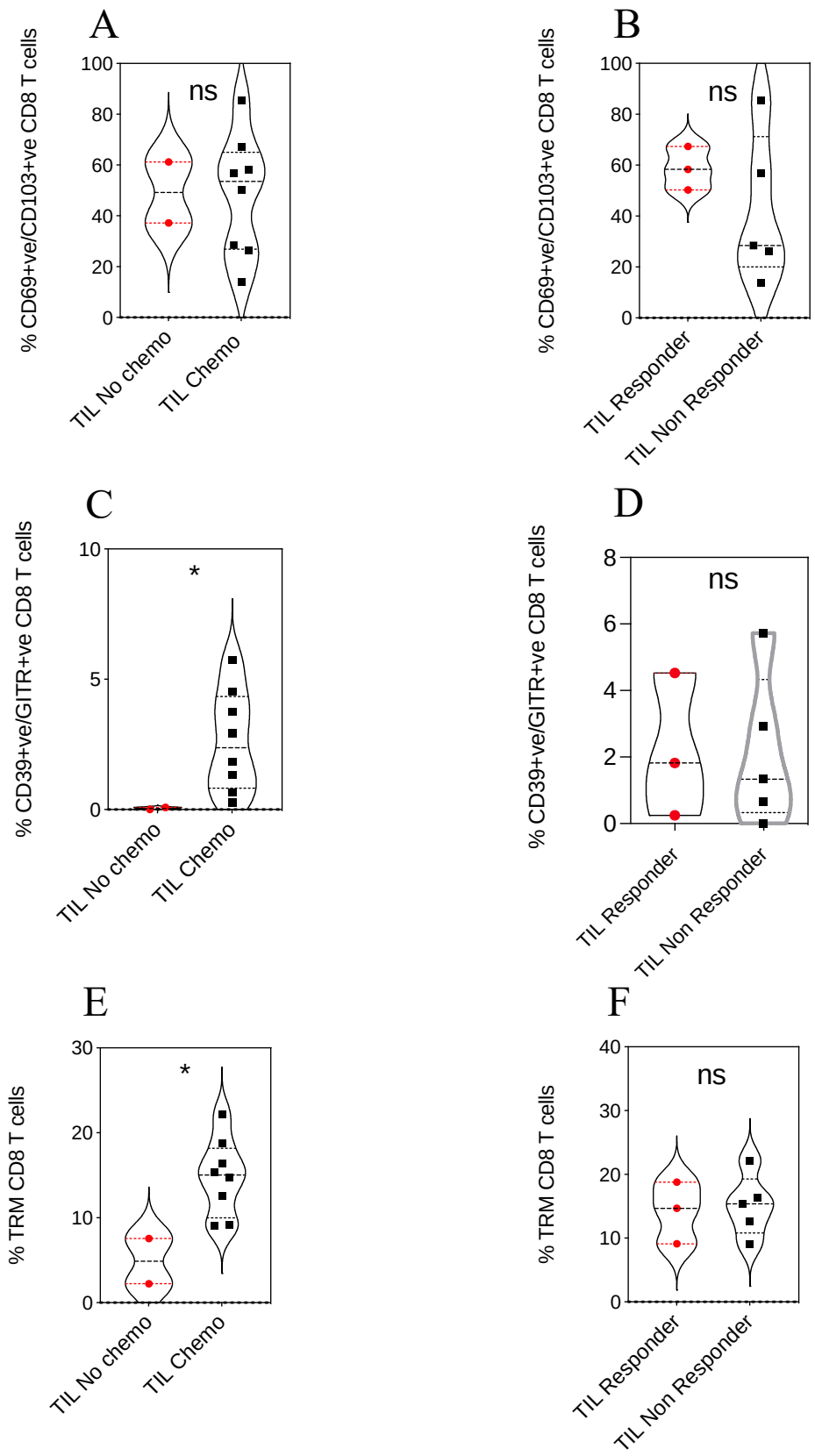

Figure 42. Impact of neoadjuvant chemotherapy on features of tissue residency in CD8+ T cells TIL. Expression of CD69 and CD103 was also assessed on TIL CD8+ T cells in patients who had and had not been administered neoadjuvant chemotherapy(A), subsequently this was assessed according to response to chemotherapy (B, responders defined as Mandard score 1-3). Impact of chemotherapy and response was assessed for GITR and CD39 expression (C,D). This was also performed for tissue resident memory cell as defined as CD69+CD103+CD39+. Each symbol represents an individual patient. Dashed horizontal lines indicate the median and dotted lines indicate the interquartile range. Data analysed by Mann Whitney test.

Flow cytometric analysis of CD4+ TRM in relation to NACT therapy

A distinct CD69+CD103+ TRM population was seen within CD4+ TIL and this represented 15% of the total CD4+ pool (Figure 43). Single expression of CD69 and CD103 was also significantly raised in TIL compared to blood (P=0.002, p=0.002). Co-expression of CD39 and GITR was significantly increased on CD4+ TIL (p=0.02, Figure 44). CD39+ expression on tissue resident memory cells, previously suggested to be a tumour-specific population, was seen on 11.3% of CD4+ TIL (IQR 4.84-15.75).

The proportion of CD4+ TRM within TIL was not altered by the administration of neoadjuvant chemotherapy (p=0.89, Figure 45) and there was no correlation with response to chemotherapy (p=0.79). However, co-expression of CD39 and GITR on CD4+ TIL was significantly increased after neoadjuvant chemotherapy (p=0.044). Response to chemotherapy did not impact CD39 GITR co-expression (p>0.999). Similarly, the proportion of TRM CD4+ TIL was significantly increased after neoadjuvant chemotherapy from 2.3% to 11.7% (p=0.044) yet response to chemotherapy did not alter the proportion of TRM CD4+ TIL in the TME. (p>0.999).

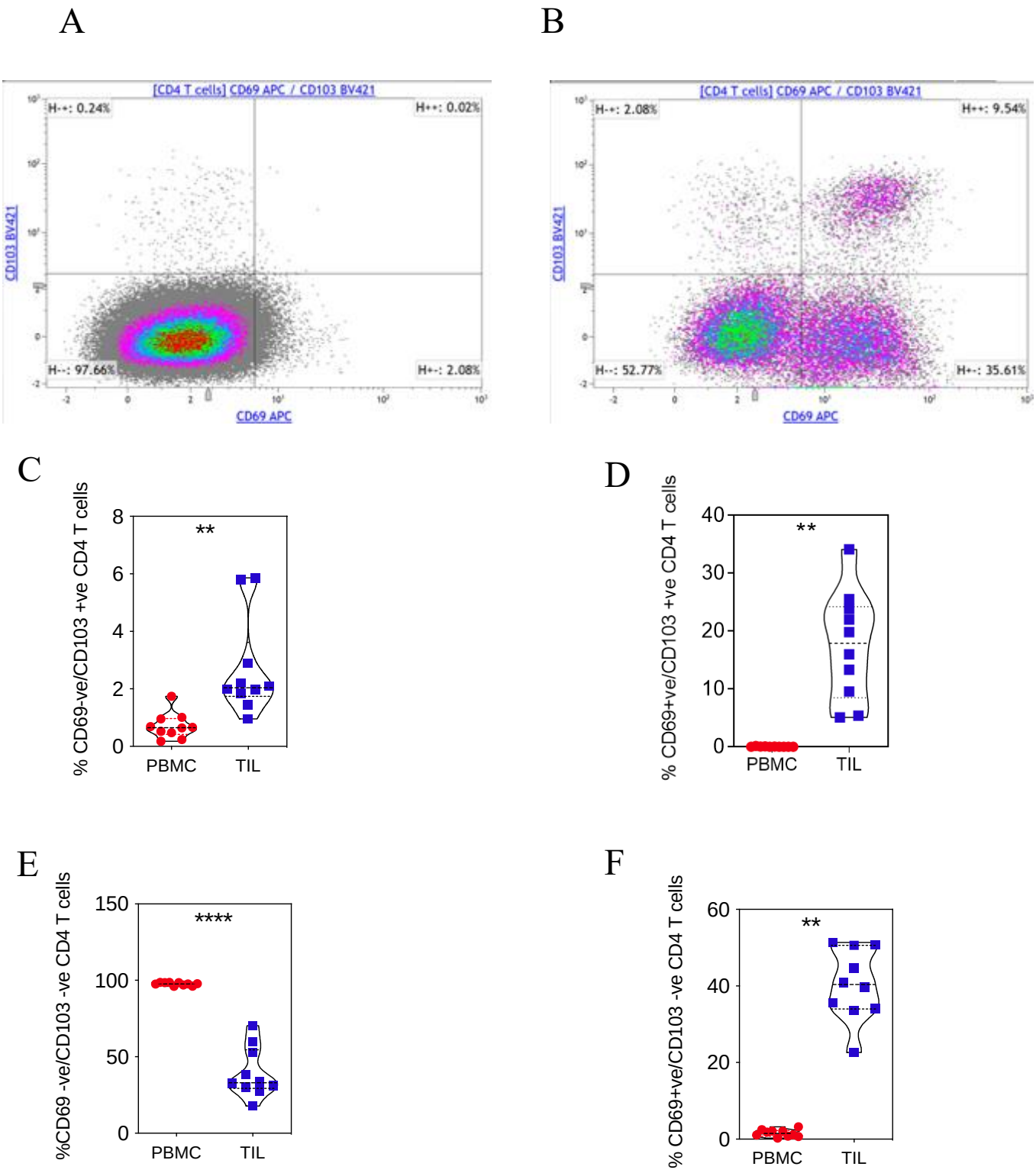

Figure 43. Features of tissue residency in CD4 T+ cells.
There was significant upregulation of CD69 and CD103 from PBMC (A) to TIL (B) in matched samples in keeping with tissue residency. Changing CD8 T cell subsets in matched PBMC and TIL, CD69-CD103+ (C), CD69+CD103+ (D), CD69-CD103- (E), CD69+CD103- (F). Data analysed by Wilcoxon matched-pairs signed rank test for matched samples, ** denotes $p<0.01$, **** denotes $p<0.0001$.

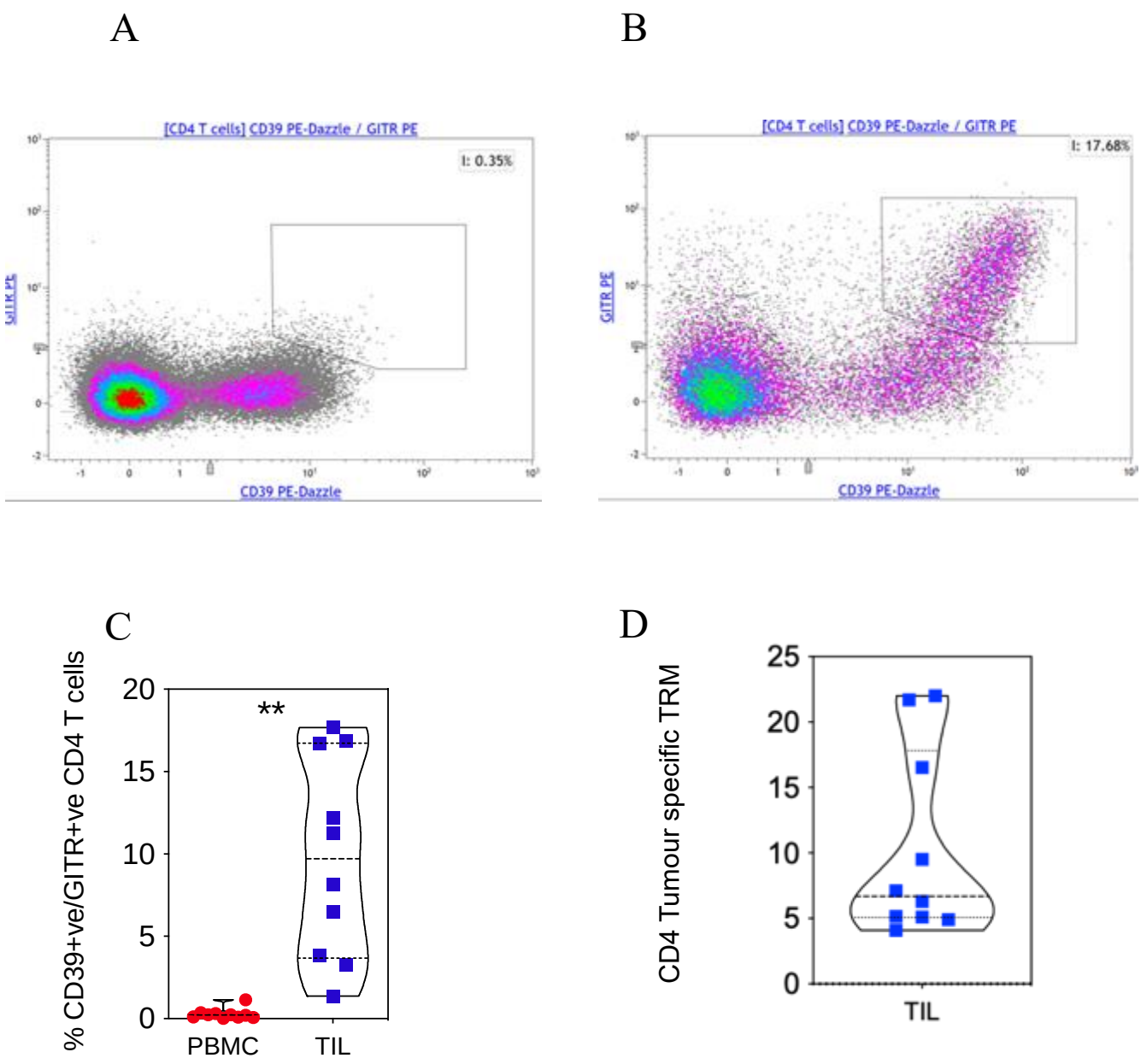

Figure 44. Tissue resident memory CD4+ T cells
An example plot of CD39 and GITR expression in matched CD4 T cell PBMC (A) and TIL(B). There is significant upregulation of CD39 and GITR in matched CD4+ T cell TIL (C). Each symbol represents an individual patient. Dashed horizontal lines indicate the median and dotted lines indicate the interquartile range. Data analysed by Mann Whitney test, ** denotes $p<0.01$. Tissue resident memory (CD69+CD103+CD39+) CD4 T cells are commonly identified in TIL (D).

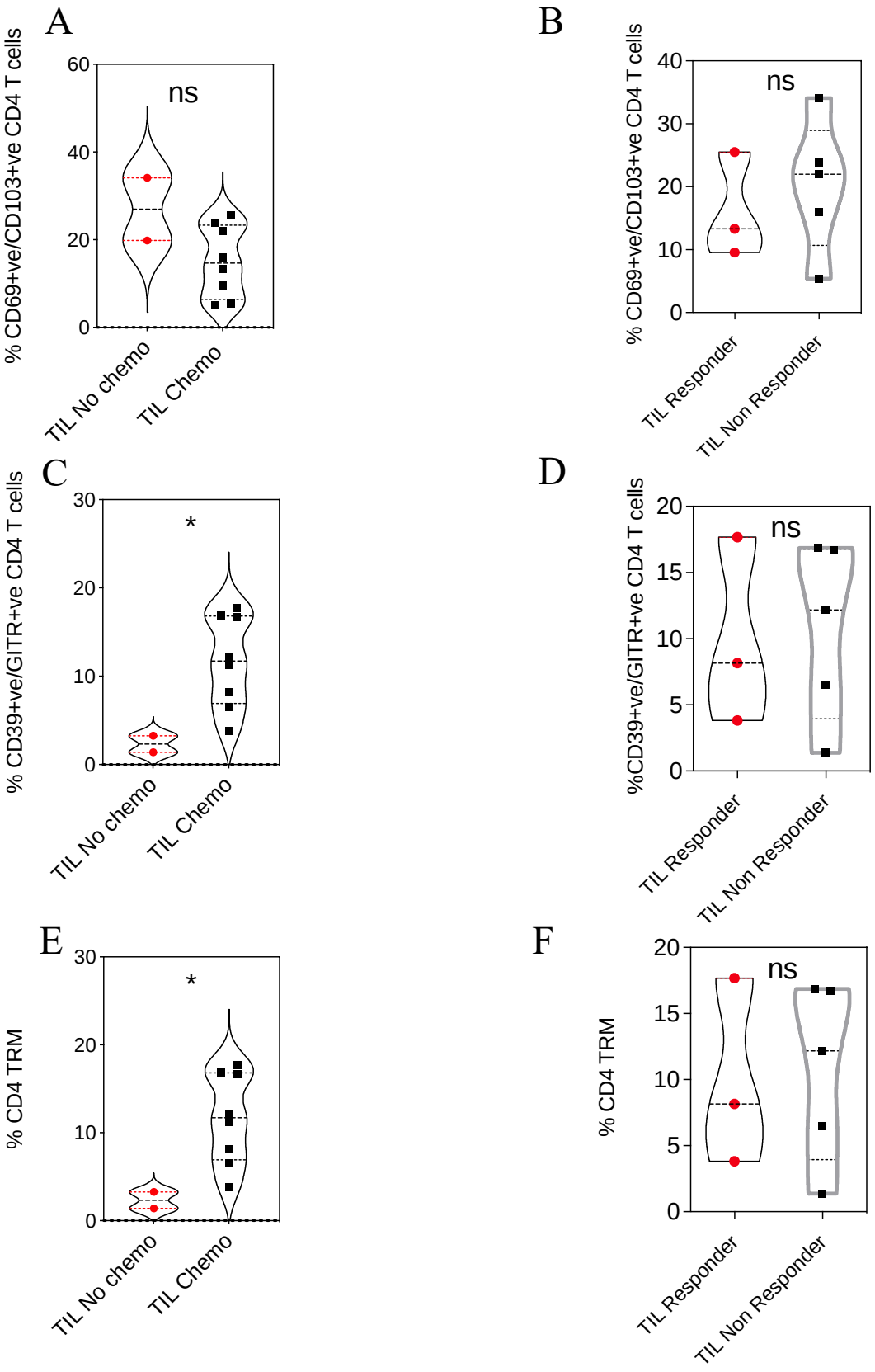

Figure 45. Impact of neoadjuvant chemotherapy on features of tissue residency in CD8+ T cells TIL. Expression of CD69 and CD103 was also assessed on TIL CD8+ T cells in patients who had and had not been administered neoadjuvant chemotherapy(A), subsequently this was assessed according to response to chemotherapy (B, responders defined as Mandard score 1-3). Impact of chemotherapy and response was assessed for GITR and CD39 expression (C,D). This was also performed for tissue resident memory cell as defined as CD69+CD103+CD39+. Each symbol represents an individual patient. Dashed horizontal lines indicate the median and dotted lines indicate the interquartile range. Data analysed by Mann Whitney test.

Flow cytometric analysis of NK TRM in relation to NACT therapy

Co-expression of CD69 and CD103 was significantly increased in NK TIL (p=0.002). Single expression of CD69 and CD103 was also significantly raised in NK TIL (P=0.004, p=0.004)(Figure 46). Co-expression of CD39 and GITR was significantly increased in NK TIL (p=0.002). Tissue resident memory cells were defined as CD69+, CD103+, CD39+ and comprised 15.39% of NK TIL (IQR 8.36-21.05, Figure 47).

The co-expression of CD103 and CD69 on NK TIL was not altered by the administration of neoadjuvant chemotherapy (p=0.89). Equally there was no significant difference in the proportion of CD103+CD69+ co-expression on NK TIL in those who did and those who did not respond to neoadjuvant chemotherapy (p=0.79)(Figure 48). The co-expression of CD39 and GITR on NK TIL was not altered by the administration of neoadjuvant chemotherapy (p=0.57). Equally there was no significant difference in the proportion of CD39+GITR+ co-expression on NK TIL in those who did and those who did not respond to neoadjuvant chemotherapy (p>0.999). The proportion of NK TRM did no differ for those who received neoadjuvant chemotherapy nor did it alter for those who had a response to chemotherapy as compared to non-responders (p>0.999, p=0.57)

Confirmation of CD8, CD4 and NK TRM confirms that novel finding identified with the transcriptome can potentially be confirmed in the proteome of oesophageal adenocarcinoma patients. Crucially chemotherapy had been shown to potentially increase the proportion of TRM within the TME. Neoadjuvant chemotherapy may induce tumour destruction and inflammatory changes within the TME potentially increasing the volume of antigen that can be consumed be tumour specific immune cells.

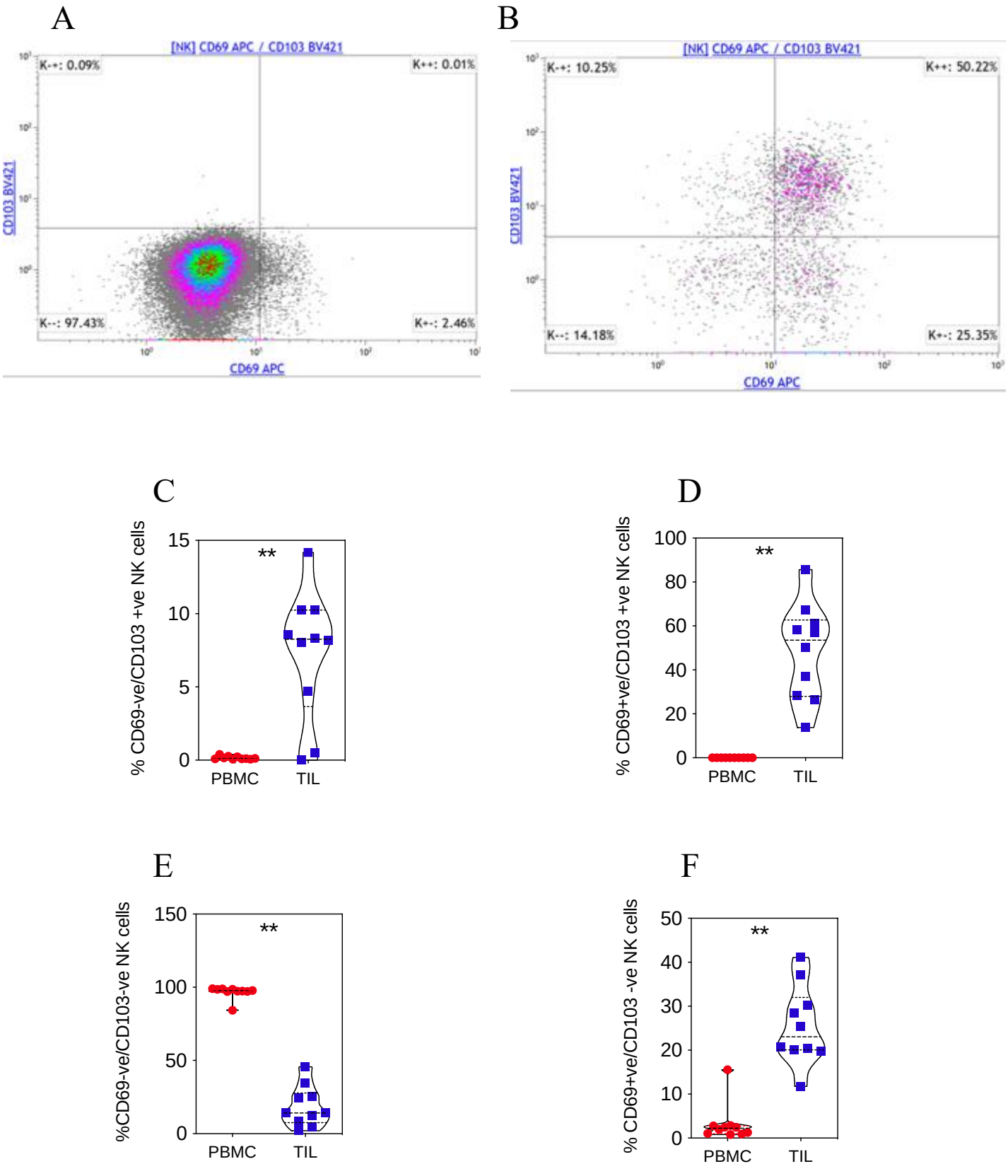

Figure 46. Features of tissue residency in NK cells.
There was significant upregulation of CD69 and CD103 from PBMC (A) to TIL (B) in matched samples in keeping with tissue residency. Changing NK cell subsets in matched PBMC and TIL, CD69-CD103+ (C), CD69+CD103+ (D), CD69-CD103- (E), CD69+CD103- (F). Data analysed by Wilcoxon matched-pairs signed rank test for matched samples, ** denotes p<0.01, ** denotes p<0.01.

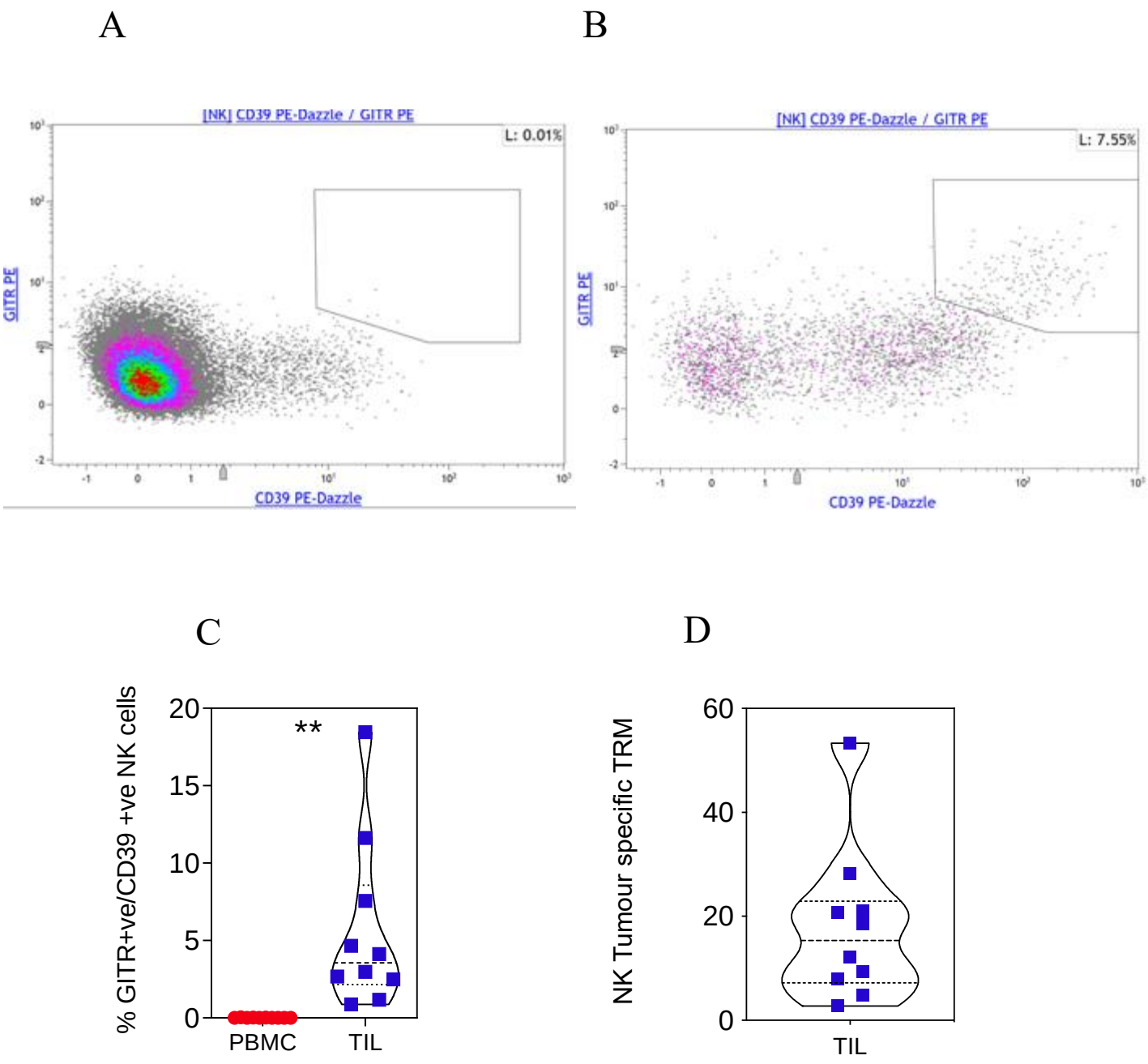

Figure 47. Tissue resident memory NK cells
An example plot of CD39 and GITR expression in matched CD4 T cell PBMC (A) and TIL(B). There is significant upregulation of CD39 and GITR in matched NK TIL (C). Each symbol represents an individual patient. Dashed horizontal lines indicate the median and dotted lines indicate the interquartile range. Data analysed by Mann Whitney test, ** denotes p<0.01. Tissue resident memory (CD69+CD103+CD39+) CD4 T cells are commonly identified in TIL (D).

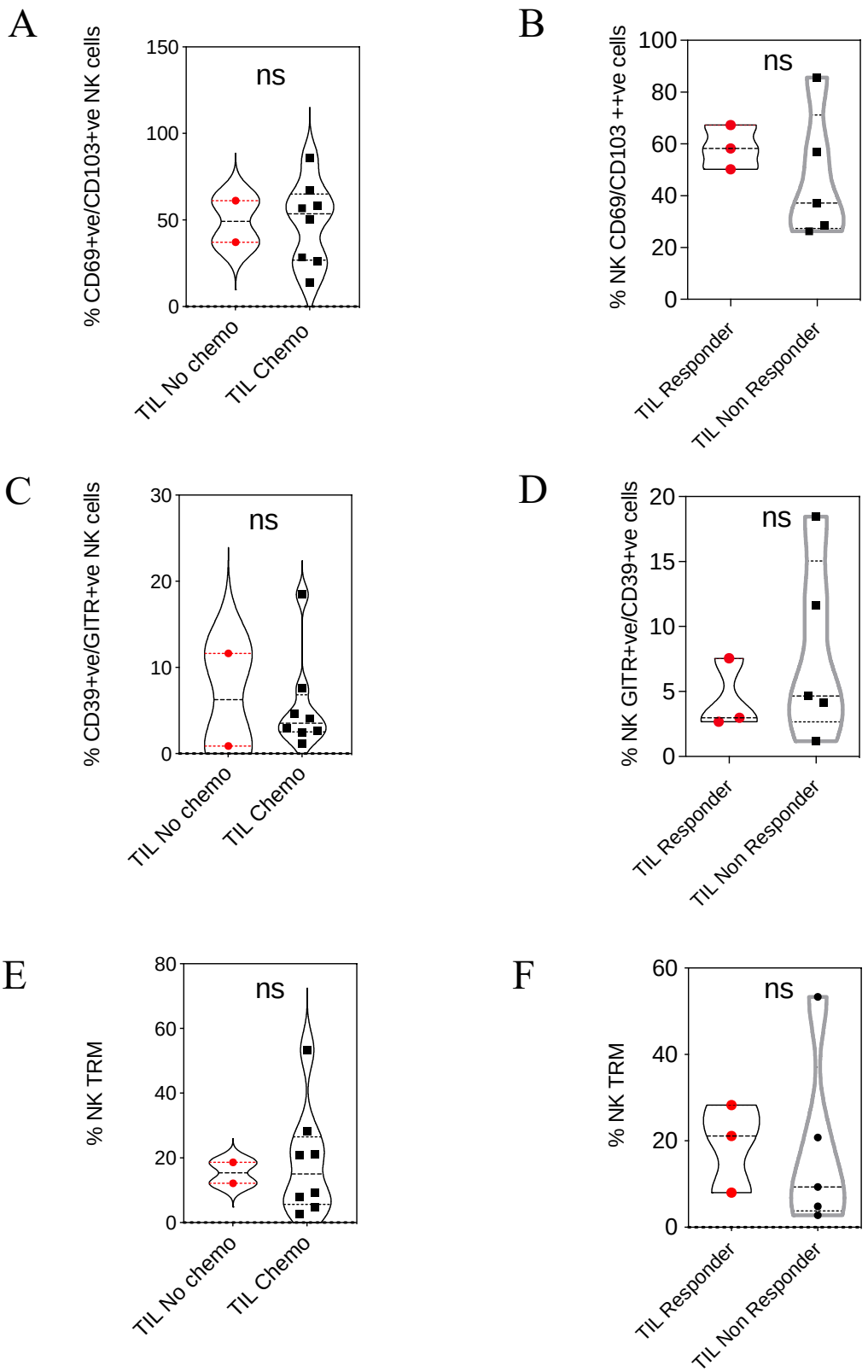

Figure 48. Impact of neoadjuvant chemotherapy on features of tissue residency in NK TIL. Expression of CD69 and CD103 was also assessed on NK TIL in patients who had and had not been administered neoadjuvant chemotherapy(A), subsequently this was assessed according to response to chemotherapy (B, responders defined as Mandard score 1-3). Impact of chemotherapy and response was assessed for GITR and CD39 expression (C,D). This was also performed for tissue resident memory cell as defined as CD69+CD103+CD39+. Each symbol represents an individual patient. Dashed horizontal lines indicate the median and dotted lines indicate the interquartile range. Data analysed by Mann Whitney test.

Discussion

This study confirms that features of tissue residency are common in OAC with a select group of potentially tumour specific lymphocytes accounting for 10-15% of TIL. The ability of TRM to recognise and respond to tumour is as yet undetermined. There are significant increases in the proportion of CD39+, putative tumour-specific, TRM within TIL after chemotherapy. Neoadjuvant treatment may therefore drive an inflammatory response within the TME that enables TRM to recognise tumour antigen driving proliferation of immune response and potential tumour destruction.

CD8+ TRM within TILs in head and neck SCC have been shown to have a distinct T-cell receptor (TCR) repertoire, with T-cell clones expanded in the tumour but present at low frequencies in the periphery. CD8+ TILs have also been shown to efficiently kill autologous tumour cells in a MHC-class I-dependent manner[233] and demonstrate features of exhaustion such as reduced production of TNF and IL2 and increased expression of co-inhibitory receptors PD-1, TIM-3, LAG-3, TIGIT, and 2B4 and CTLA-4[174,175]. GITR has also been suggested to be upregulated in tissue residency and progression of Barrett's to invasive adenocarcinoma[176]. This study further confirms that GITR is upregulated on CD4+, CD8+ and NK TIL. GITR provides a T-cell intrinsic advantage to both CD4+ and CD8+ effector T cells in tissue, as well as for the formation of CD4 and CD8 tissue-resident memory T cells during respiratory formation of CD4 and CD8 tissue-resident memory T cells during respiratory infection[177,178].

Studies of CD8+ TRM T cells in OSCC by Han et al have shown that patients with high density intra-tumoural TRM T cells have improved overall survival. In contrast, increased density of CD8+ TILs and CD103+ TILs did not improve overall survival. The proportion and density of CD103+CD8 T cells was not altered by the administration of neoadjuvant chemotherapy and CD103+CD8 T cells commonly exhibit features of exhaustion with high

expression levels of PD-1 and TIM-3[179]. Chu et al reported similar findings for patients undergoing oesophagectomy for OSCC. Multivariate analysis showed the density of $CD103^+$ TILs was an independent positive prognostic factor for overall and disease free survival. $CD103^+$ TILs were evenly distributed across the advancing edges of intratumoural and adjacent non tumour tissue comprising of a greater proportion of CD8+CD103+ as compared to CD4+CD103+. Phenotypically CD103+demonstrated high levels of CTLA-4 and granzyme B and relatively low levels of PD-1[180]. There is currently no data on tissue residency in oesophageal adenocarcinoma. CD103 expression has been shown to be a potential prognostic biomarker in advanced gastric cancer patients receiving PD-1 inhibitor Nivolumab[181]. Blood sampling 2 weeks after treatment in patients with advanced gastric cancer showed that in multivariate analysis of clinicopathologic variables, the ratio of the frequency of CD103 among PD- 1^+CD8^+ T cells in peripheral blood 2 weeks after treatment to that before treatment was an independent prognostic factor for performance free survival. Circulating $CD103^+PD\text{-}1^+CD8^+$ T cells had lower frequencies of perforin and granzyme than the other subsets at all time points, but higher frequencies of INF-γ, TNF-α, and IL-2 2 weeks after the start of the nivolumab treatment.

Markers of tissue residency have also been identified on NK TIL. Zheng et al reported that NK TIL significantly upregulate CD39[182]. CD39+ NK TIL demonstrate a significant increase in checkpoint expression including PD-1, TIM-3 and TIGIT. An increase in IL-6 within the TME may be one determinant that drives this increase in CD39 expression on NK cells in tumours.

This chapter replicates the methodological techniques as demonstrated in chapter 3 and in turn many of the limitations. More specific to the populations being investigated in this chapter challenges arise when trying to confirm cellular populations of low number. Little was known regarding oesophageal TRM yet due to accuracy of previously demonstrated flow

techniques in OAC this analysis provides accurate information regarding the novel discovery of OAC TRM. The substance of the results may have been better emphasised by increasing the specimen sample number however the primary aim of the chapter was to confirm that cellular populations identified in the transcriptome were present in the proteome which was achieved. Further samples were then better used for complex flow cytometry work as set forth in chapters 6 and 7.

Conclusion

This chapter confirms that lymphocytes with phenotypic features of tumour specificity comprise a major subset of immune cells within the OAC tumour microenvironment. Tumour-specific CD4+, CD8+ and NK-TRM may play a key role in improving immune led tumour destruction. Further evaluation is required to phenotype this population more deeply and to identify whether they exhibit features of exhaustion that may be potentially reversible through immunotherapeutic blockade.

Chapter 6 – Deep Phenotyping of the Immune Landscape in Oesophageal Adenocarcinoma

T cells dominate the lymphocytic immune compartment of oesophageal adenocarcinoma and initial flow cytometric analysis in this study has shown that TIL demonstrate significant features of exhaustion including upregulation of PD-1, TIGIT and TIM-3. Single cell transcriptomic analysis confirmed further evidence of exhaustion with specific CD8+ T cell populations expressing CXCL13, a correlate of T cell functional impairment[159]. In addition, a subset of tissue resident memory (TRM) CD8+ T cells were shown to express CD39, which have been described in other cancers to be enriched for tumour-reactive cells[174,183].

To gain deeper insight into the heterogeneity T cells within OAC, high-dimensional flow cytometry was used to assess a range of additional features. In particular, the profile of activation, exhaustion and differentiation markers on memory T cells subsets was assessed, as well as effect of neoadjuvant chemotherapy on the composition of these subsets. The breadth of the flow cytometry panel also permitted the differentiate between conventional CD4+ effector cells and T regulatory cells in this analysis.

In this chapter we seek to build on the understanding developed in prior chapters to ascertain further phenotypic information to identify improved targets for immunotherapy targeting.

Methods

Blood and matched tumour samples were obtained from 19 patients with OAC. Ten of these were patients who had undergone oesophagectomy whilst nine were obtained from endoscopic biopsies. Ten of these patients had undergone treatment with neoadjuvant chemotherapy (NACT). The neoadjuvant treatment of choice during the study period was FLOT. Seven patients were identified to have responded to NACT (TRG 1-3) whereas three patients failed to demonstrate a response (TRG4-5).

Peripheral blood lymphocytes and tumour infiltrating lymphocytes (TIL) were isolated and frozen prior to use. Samples were defrosted and stained with a panel of antibodies against cell 27 surface markers (Figure 49), including CD14 and CD19 on the same colour as a 'dump' channel to remove B cells and monocytes.

This large panel included markers to assess T cell memory (CCR7, CD45RA) and tissue residency (CD69+CD103+) as well as those that could define conventional CD4+ effector or CD4+ T regulatory subsets (CD127-CD25+). Activation markers included ICOS and CD38 whilst the antibodies were also able to detect checkpoint expression of PD-1, LAG3 and TIGIT.

Instrument / Configuration		BD FACSymphony™ A3	7 UV - 8 Violet - 6 Blue - 4 Yellow/Green - 3 Red	
Excitation Laser Line	Fluorescence Channel	Marker/Antibody	Clone	Cat. No.
UV 355 nm	BUV395	CD4	SK3	563550
	BUV496	CD8	SK1	741199
	BUV563	CD27	M-T271	741366
	BUV615	CD95	DX2	752346
	BUV661	ICOS	DX29	741664
	BUV737	CD38	HB7	612824
	BUV805	CD45	HI30	612891
Violet 405 nm	BV421	CD96	6F9	742794
	BV480	CD28	CD28.2	566110
	BV570-P	CD3	UCHT1	Biolegend
	BV605	BTLA	J168-540	743986
	BV650	CCR7	2-L1-A	566756
	BV711	TIGIT	741182	747839
	BV750	DNAM	DX11	747026
	BV786	CD45RA	HI100	563870
Blue 488nm	BB515	CD57	NK-1	565285
	BB630-P	CD127	HIL-7R-M21	custom
	BB660-P	LAG3	T47-530	custom
	BB700	PD1	EH12.1	566460
	BB755-P			
	BB790-P	CD69	FN50	Custom
Yellow / Green 561nm	PE	2B4	2-69	550816
	PE-CF594	KLRG1	14C2A07	Biolegend
	PE-Cy5	CD14/CD19	M5E2/HIB19	Biolegend/555414
	PE-Cy7	CD25	M-A251	557741
Red 640	AF647	CD160	BY55	562362
	R718	CD103	Ber-ACT8	752007
	FVS780	Viability		565388

Flow cytometry panel used for analysis in Chapter 5 (Figure 49)

Results

T cell memory subsets in oesophageal adenocarcinoma (OAC) and their relationship to response to neoadjuvant chemotherapy (NACT)

Initial analyses were undertaken to assess the memory phenotype of major T cell subsets. Staining with antibodies against the CD45 isoform CD45RA and the chemokine receptor CCR7 is able to distinguish four major subsets defined as antigen-naive (N; CD45RA+CCR7+), central memory (CM; CD45RA-CCR7+), effector memory (EM; CD45RA-CCR7-) and terminally differentiated effector memory with CD45RA reversion (TEMRA; CD45RA+CCR7-).

As shown earlier, a significant difference was observed in the memory phenotype of CD8+ T cells within PBMC and TIL. Compared to blood, naïve and TEMRA CD8+ T cells were reduced in TIL from 6.0% to 0.4 % and 21% to 5.6% respectively ($p<0.0001$, $p=0.0002$) with no difference in central memory CD8+. In contrast, there was a marked increase in the effector memory CD8+ pool within TIL from 69% to 90% ($p=0.38$, $p<0.0001$, Figure 50). The proportion of naïve, central memory, effector memory and TEMRA CD8+ T cells in PBMC and TIL did not differ for patients who did or did not receive chemotherapy ($p=0.39$, $p=0.16$, $p=0.24$, $p=0.29$, Figure 51). Furthermore, these proportions did not differ for patients who did or did not have a significant response to chemotherapy ($p=0.38$, $p>0.999$, $p>0.999$, $p>0.999$, Figure 52).

A similar pattern in the memory phenotype of T cells in PBMC and TIL was seen for the conventional (non-T regulatory) CD127+CD25- CD4+ population. Naïve and TEMRA CD4+ T cells were reduced in TIL from 23% to 0.9 % ($p<0.0001$) and 3.6% to 1.0% ($p<0.0001$), respectively, with no change in the central memory pool. In contrast, the effector memory CD4+ pool was increased from 43% to 78% ($p<0.0001$, Figure 53). Proportions of naïve, central memory, effector memory and TEMRA CD4+ T cells in PBMC and TIL did not differ

for patients who did or did not receive chemotherapy (p=0.84, p=0.45, p=0.32, p=0.21, Figure 54). Equally, proportions of naïve, central memory, effector memory and TEMRA CD4+ T cells in PBMC and TIL did not differ for patients who did or did not have a significant response chemotherapy (p>0.999, p=0.27, p=0.27, p=0.38, Figure 55).

Treg memory PBMC and TIL populations were also compared in order to establish the differential effector function of Treg within the TME. A significant alteration in the proportion of memory subsets of Treg cells (CD127-CD25+) was also seen between PBMC and TIL. Naïve and TEMRA Treg were significantly reduced in TIL from 9.4% to 0.4 % (p<0.0001) and 4.1% to 0.5% (p<0.0001), respectively, whilst there was no change in central memory Treg (p>0.999) but a significant increase in effector memory Treg TIL from 68 to 78%, (p=0.002, Figure 56). Proportions of naïve, central memory, effector memory and TEMRA Treg T cells in PBMC and TIL did not differ for patients who did or did not receive chemotherapy (p=0.38, p=0.96, p=0.78, p=0.28, Figure 57). Equally, proportions of naïve, central memory, effector memory and TEMRA Treg in PBMC and TIL did not differ for patients who did or did not have a significant response chemotherapy (p>=0.19, p=0.52, p=0.52, p>0.999, Figure 58).

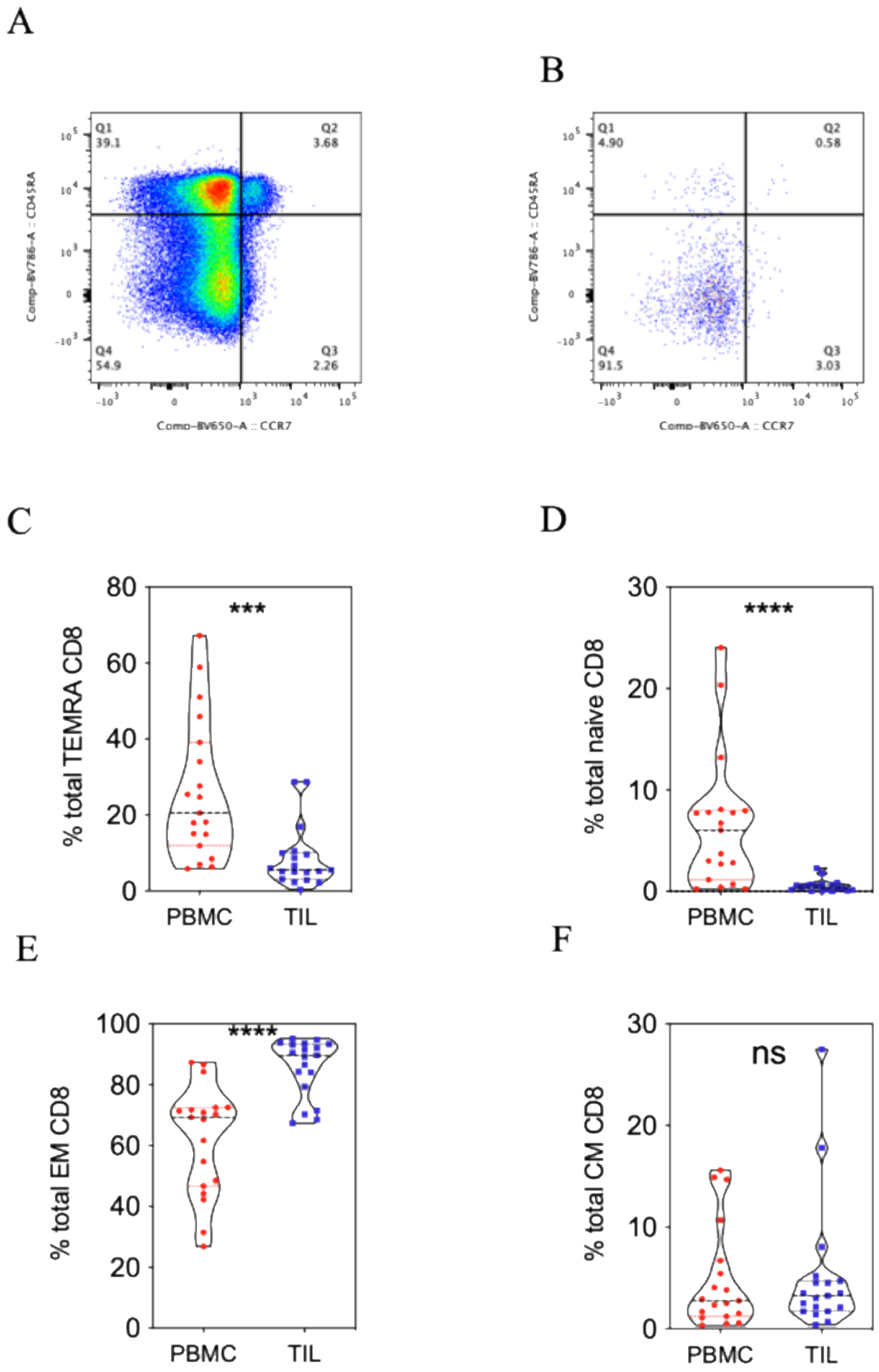

Figure 50. Memory phenotype of CD8+ T cells in matched PBMC and TIL
Expression of CCR7 and CD45RA on CD8+ T cells was determined to show TEMRA (CCR7+CD45RA-), naïve (CCR7+CD45RA+), effector memory (EM, CCR7-CD45RA-) and central memory (CM, CCR7+CD45RA-) T cells. An example plot of CD8 T cell memory is shown in matched PBMC (A) and TIL (B). Comparative analyses are shown for matched patient PBMC and TIL for TEMRA (C), naïve (D), EM (E) and CM (F). Each symbol represents an individual patient. Dashed horizontal lines indicate the median and dotted lines indicate the interquartile range. Data analysed by Wilcoxon matched-pairs signed rank test ** denotes $p<0.01$ and **** $p<0.0001$.

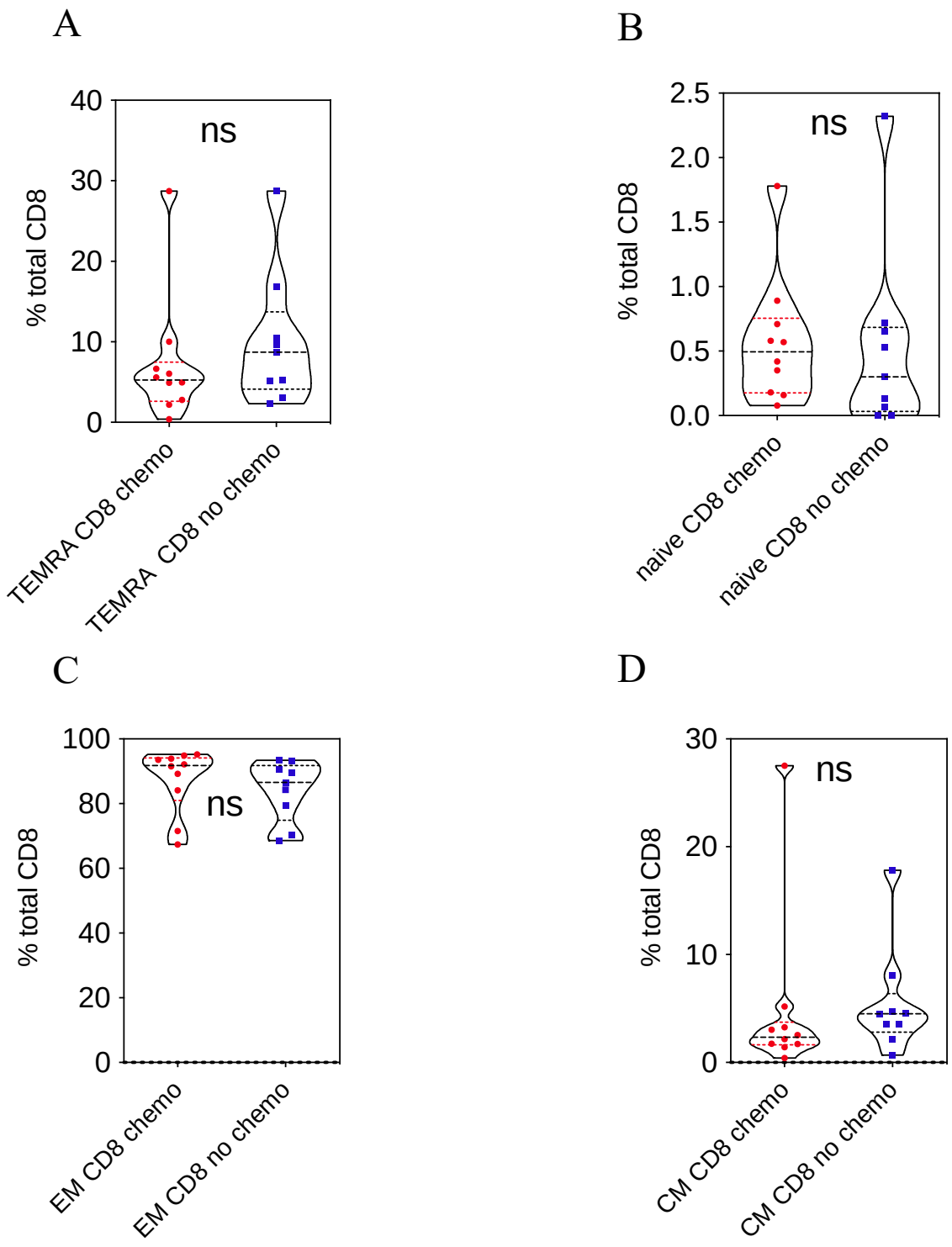

Figure 51. Neoadjuvant chemotherapy has no impact on memory subsets of CD8+ T cells in TIL. Comparative analyses are shown for patients who have and have not received neoadjuvant chemotherapy. TEMRA (A), naïve (B), EM (C) and CM (D). Each symbol represents an individual patient. Dashed horizontal lines indicate the median and dotted lines indicate the interquartile range. Data analysed by Wilcoxon matched-pairs signed rank test.

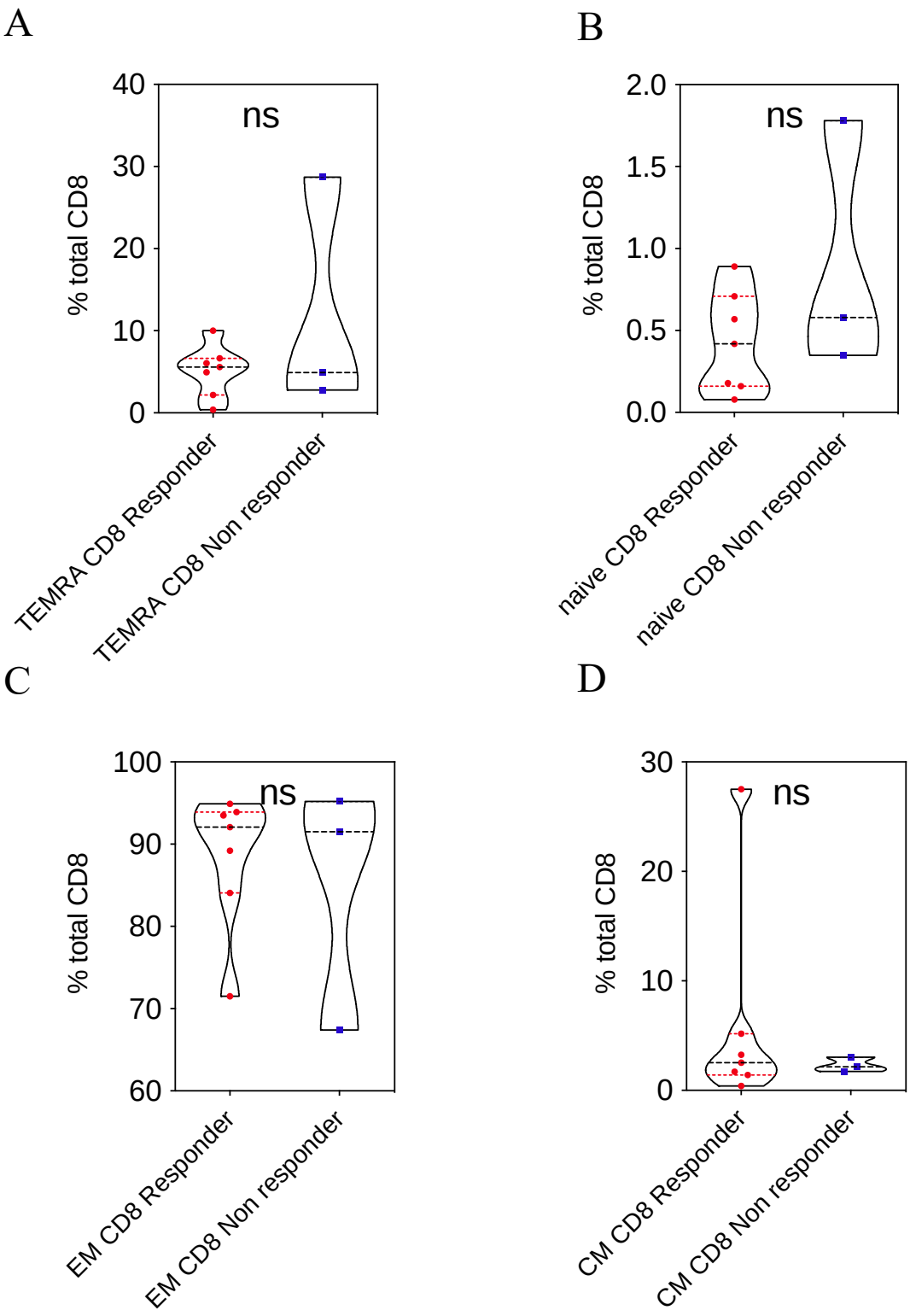

Figure 52. Clinical response to NACT is not related to memory phenotype of CD8+ T cells TIL. Comparative analyses are shown for patients who have or have not responded neoadjuvant chemotherapy (responders are defined as Mandard score 1-3). TEMRA (A), naïve (B), EM (C) and CM (D) subsets are shown. Each symbol represents an individual patient. Dashed horizontal lines indicate the median and dotted lines indicate the interquartile range. Data analysed by Wilcoxon matched-pairs signed rank test.

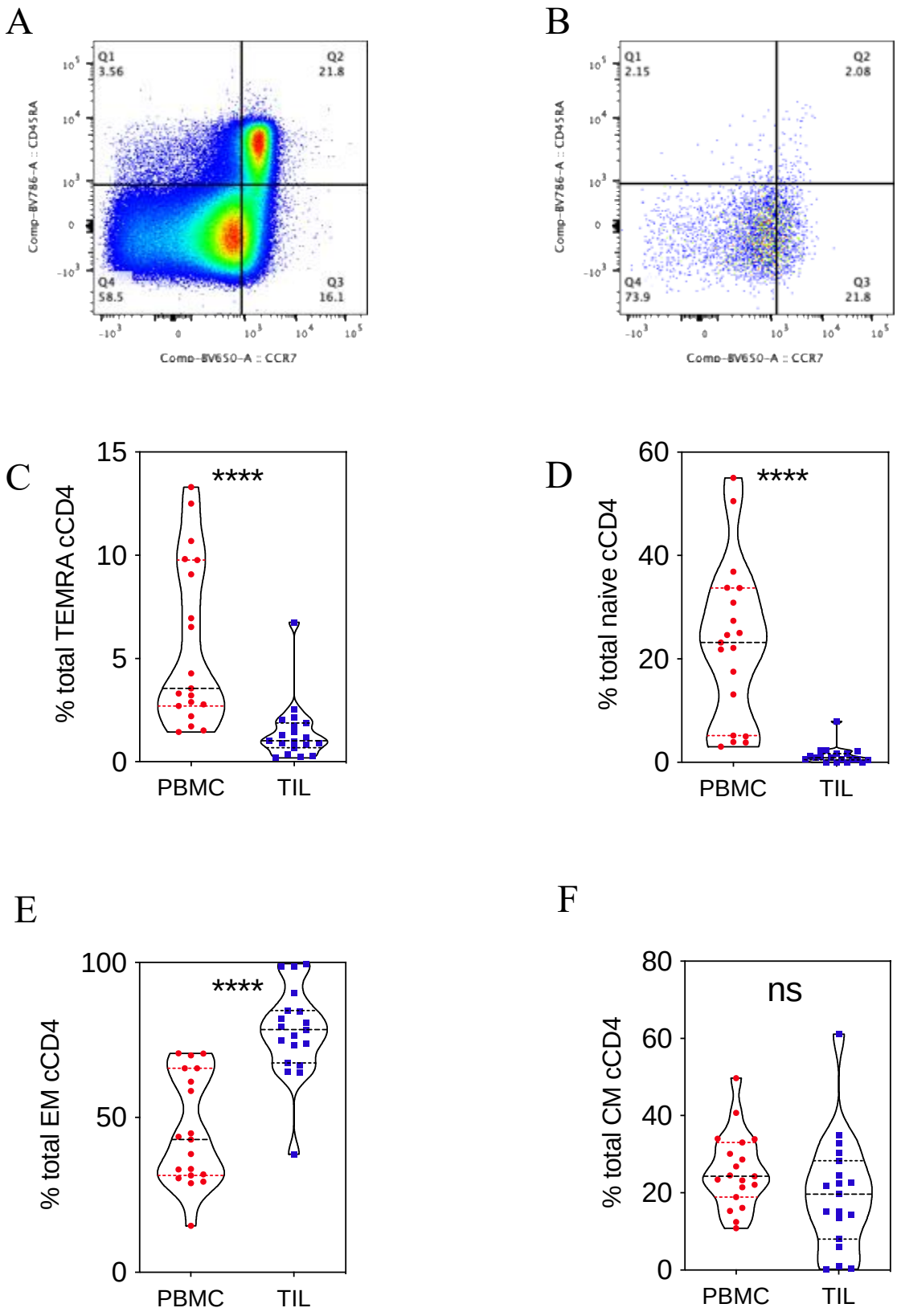

Figure 53. Memory phenotype of conventional CD4+ T cells in matched PBMC and TIL. Expression of CCR7 and CD45RA on CD4+ T cells was determined to show TEMRA, naïve, effector memory and central memory (CM, CCR7+CD45RA-) T cells. An example plot of CD4+ T cell memory is shown in matched PBMC (A) and TIL (B). Comparative analyses are shown for matched patient PBMC and TIL for TEMRA (C), naïve (D), EM (E) and CM (F). Each symbol represents an individual patient. Dashed horizontal lines indicate the median and dotted lines indicate the interquartile range. Data analysed by Wilcoxon matched-pairs signed rank test **** denotes $p<0.0001$.

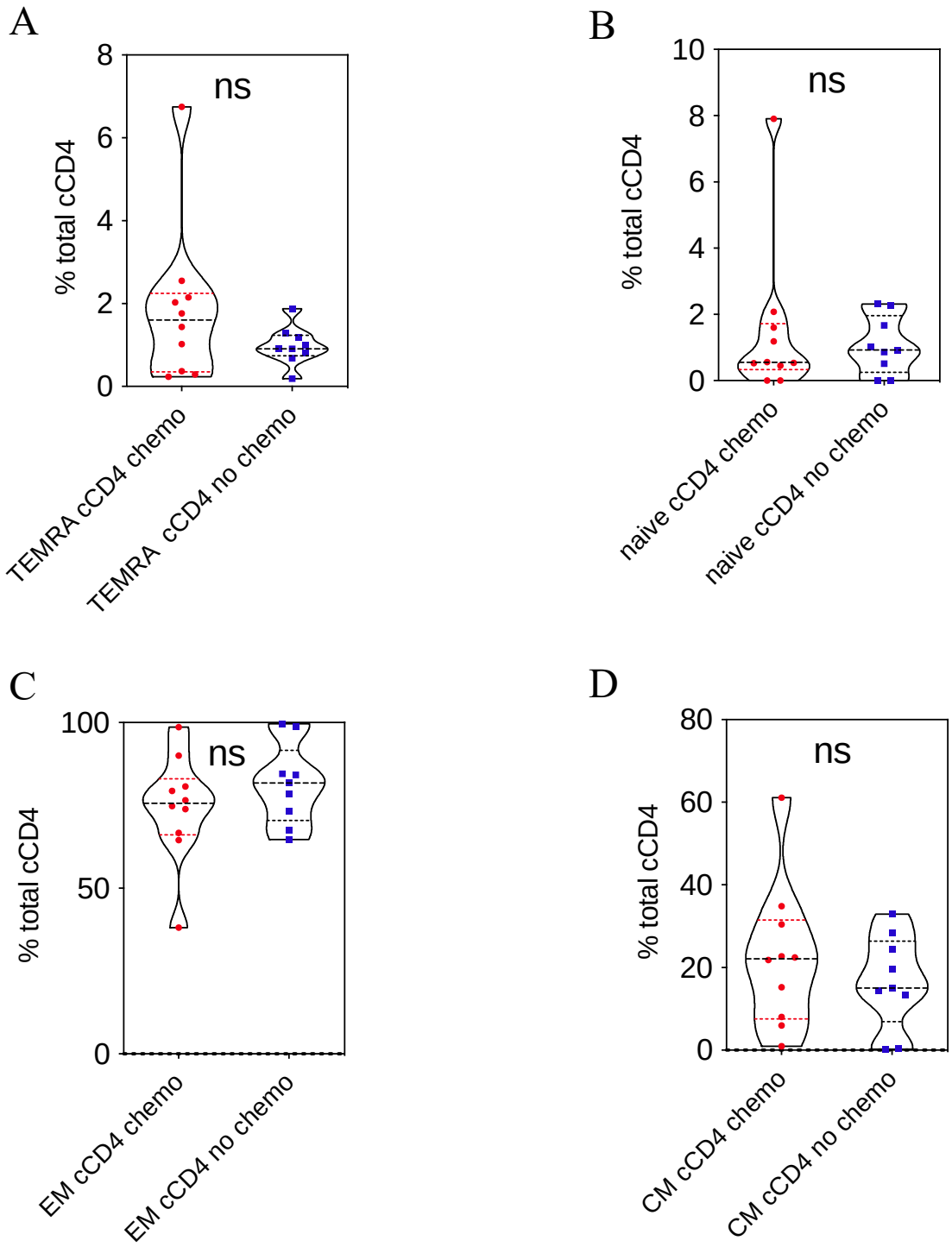

Figure 54. Neoadjuvant chemotherapy does not alter the memory phenotype of conventional CD4+ T cells in TIL

Comparative analyses are shown for patients who have and have not received neoadjuvant chemotherapy. The proportion of TEMRA (A), naïve (B), EM (C) and CM (D) subsets is shown for patients who did, or did not, receive chemotherapy. Each symbol represents an individual patient. Dashed horizontal lines indicate the median and dotted lines indicate the interquartile range. Data analysed by Wilcoxon matched-pairs signed rank test.

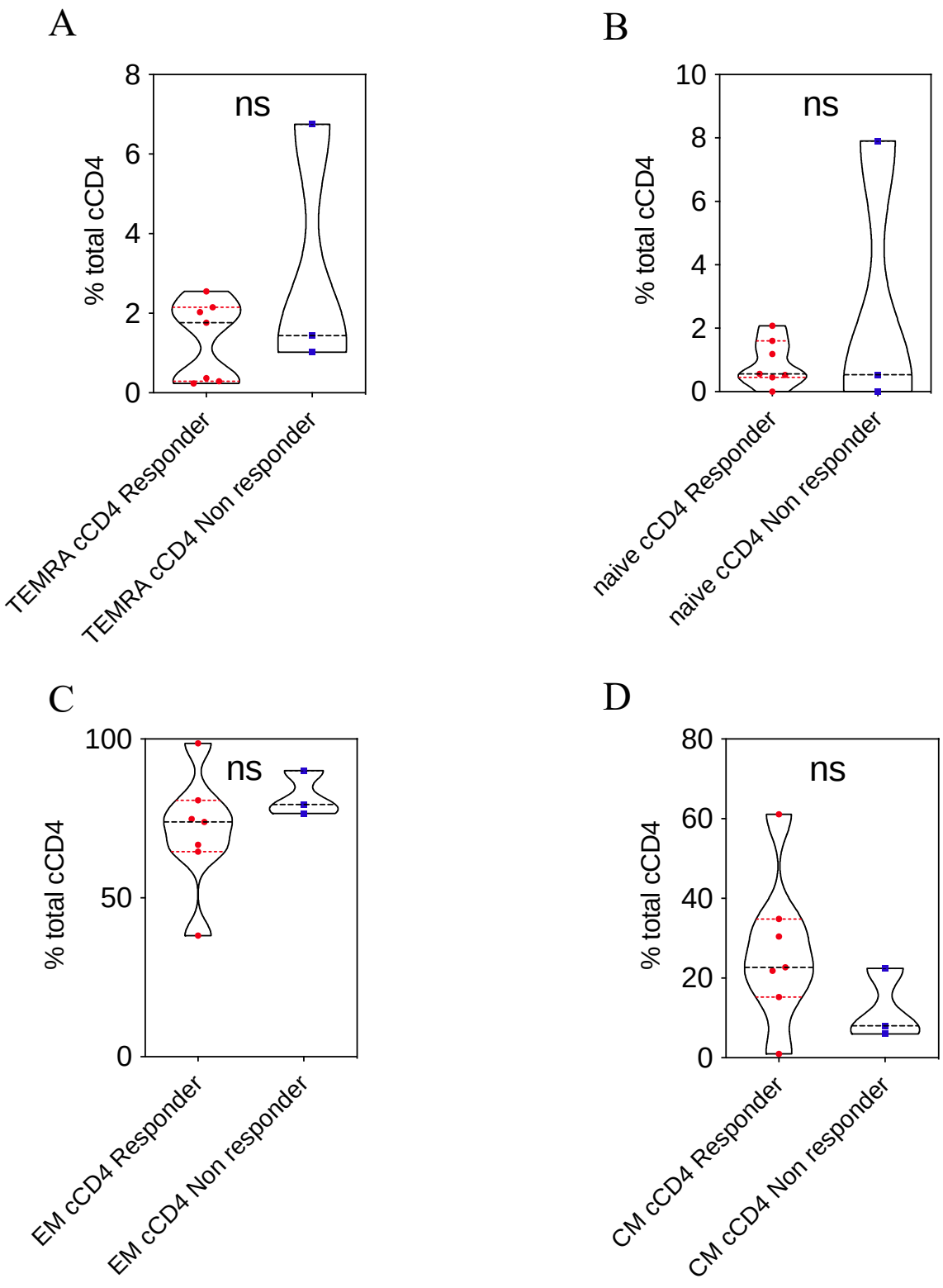

Figure 55. No relationship is observed between pathological response to NACT and memory phenotype of conventional CD4+ T cells within TIL.
Comparative analyses are shown for patients who have or have not responded to neoadjuvant chemotherapy (responders are defined as Mandard score 1-3). TEMRA (A), naïve (B), EM (C) and CM (D) subsets are shown. Each symbol represents an individual patient. Dashed horizontal lines indicate the median and dotted lines indicate the interquartile range. Data analysed by Wilcoxon matched-pairs signed rank test.

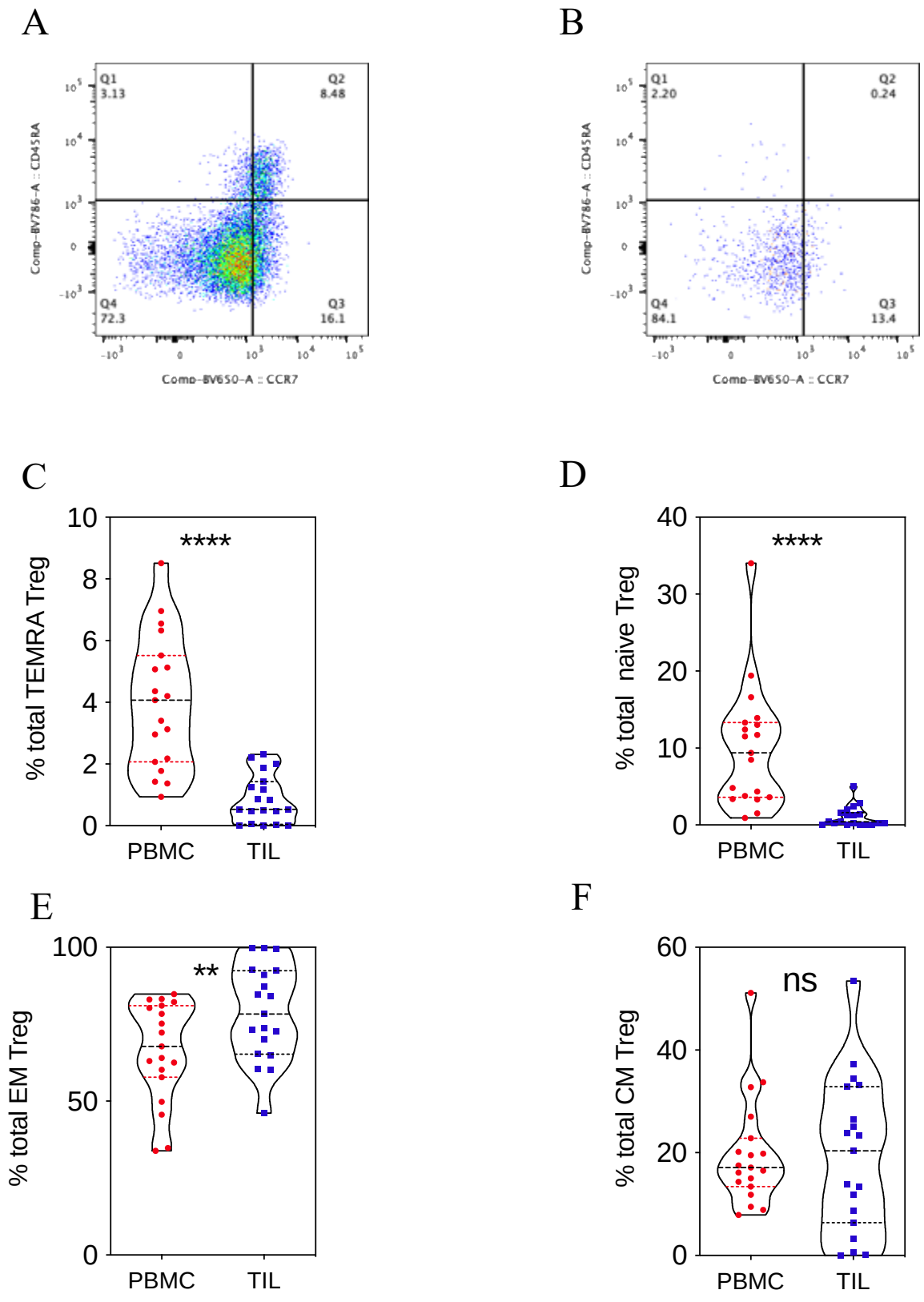

Figure 56. Memory phenotype of T regulatory cells in matched PBMC and TIL.
Expression of CCR7 and CD45RA on CD127-CD25+ CD4+ T cells was determined to show TEMRA, naïve, effector memory and central memory subsets. An example plot of gating is shown for matched PBMC (A) and TIL (B). Comparative analyses are shown for matched patient PBMC and TIL for TEMRA (C), naïve (D), EM (E) and CM (F) subsets. Each symbol represents an individual patient. Dashed horizontal lines indicate the median and dotted lines indicate the interquartile range. Data analysed by Wilcoxon matched-pairs signed rank test ** denotes $p<0.01$ and **** $p<0.0001$.

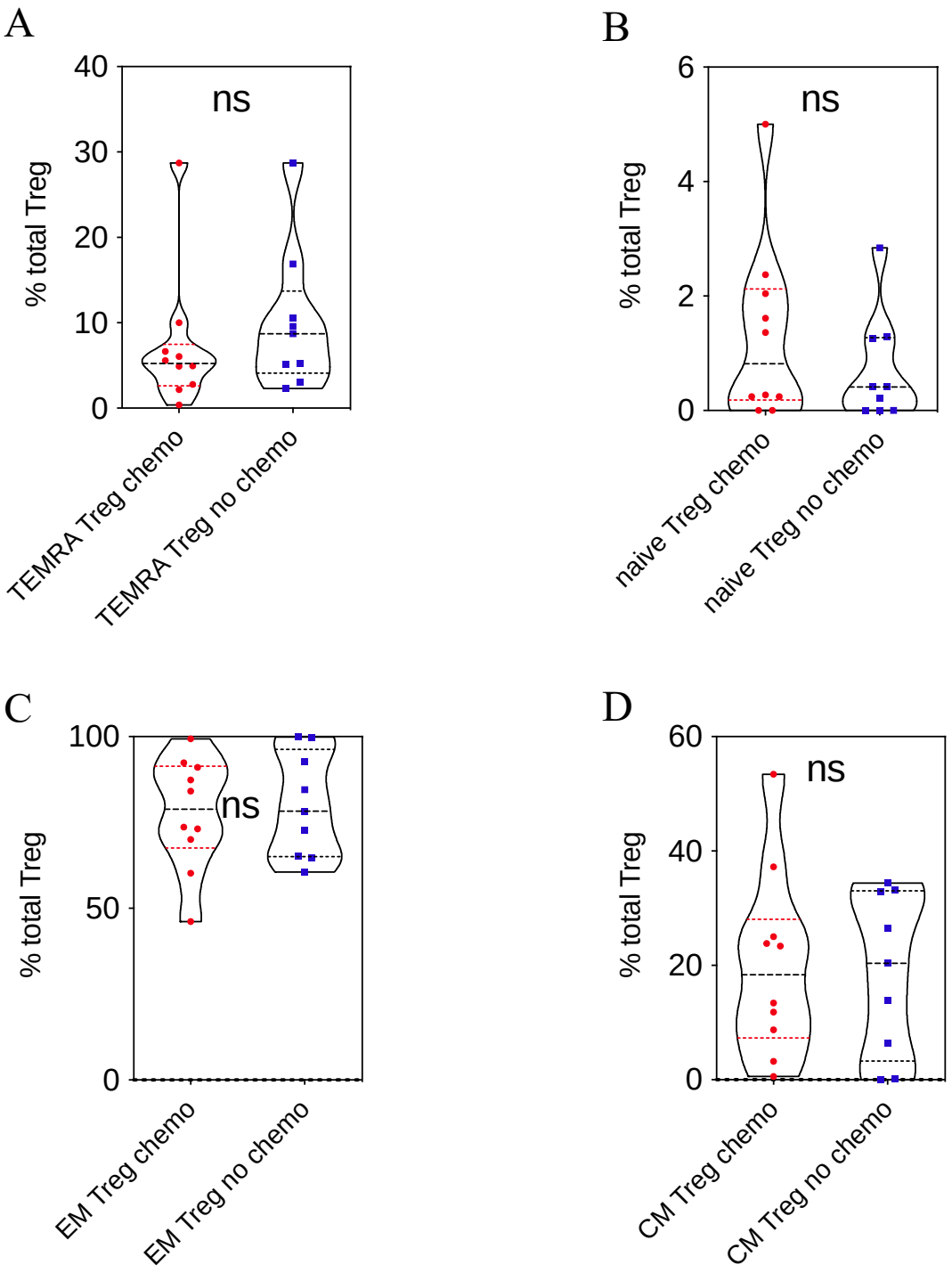

Figure 57. The impact of chemotherapy on memory phenotype Treg TIL.
Comparative analyses are shown for patients who have and have not received neoadjuvant chemotherapy. TEMRA (A), naïve (B), EM (C) and CM (D). Each symbol represents an individual patient. Dashed horizontal lines indicate the median and dotted lines indicate the interquartile range. Data analysed by Wilcoxon matched-pairs signed rank test.

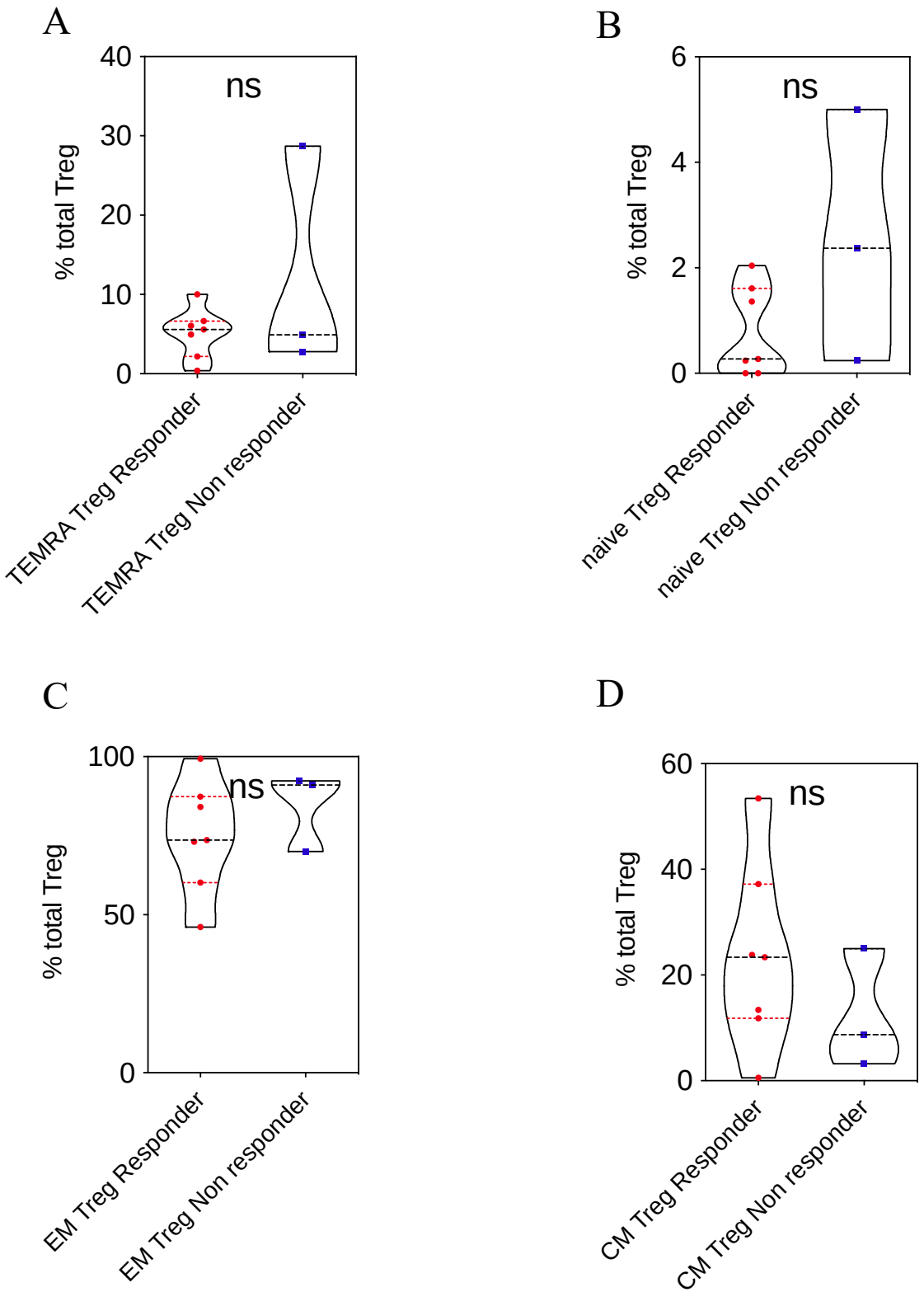

Figure 58. Relationship between pathological response to NACT and memory phenotype of T regulatory cells within TIL

Comparative analyses are shown for patients who have, or have not, responded to neoadjuvant chemotherapy (responders are defined as Mandard score 1-3). TEMRA (A), naïve (B), EM (C) and CM (D) subsets are shown. Each symbol represents an individual patient. Dashed horizontal lines indicate the median and dotted lines indicate the interquartile range. Data analysed by Wilcoxon matched-pairs signed rank test.

Profile of late differentiation of T cells in blood and TIL of patients with OAC

Given that effector T cells were shown to be expanded within the tumour microenvironment, I next assessed if these were driven to a state of late differentiation. CD57 is a carbohydrate epitope and is used as a marker of late differentiation status in T and NK cells[184]. KLRG1 is a coinhibitory receptor that interacts with E-cadherin and N-cadherin and is also a marker of late differentiation of CD8+ T cells and NK cells[185].

Dual expression of staining with these two markers defined four clear subsets of T cells and it was noteworthy that the relative proportion of each of these was different between PBMC and TIL populations.

Expression of KLRG1 was lower on the CD8+ TIL population whilst expression of CD57 was increased. Co-expression was therefore reduced from 24% of CD8+ populations in blood compared to 8.8% in TIL ($p=0.0001$, $p<0.0001$, Figure 59). Double negative and single positive CD57+KLRG1- CD8+ T cells within TIL were significantly increased from 32% to 55% ($p<0.0001$) and 2.7% to 22% ($p=0.0005$), respectively.

No differences were observed in these relative proportions in relation to delivery of NACT or the pathological response to NACT (data not shown).

KLRG1 and CD57 expression on CD4+ T cells is limited. However, there was a marked increase in CD57+KLRG1- cells within TIL from 1.0% to 14% whilst the CD57+KLRG1+ proportion was unaltered ($p<0.0001$, $p=0.013$, Figure 60). The proportion of double negative and CD57-KLRG1+ cells was decreased in TIL from 91% to 73% ($p=0.014$) and 7.5% to 6.1% ($p=0.049$), respectively. No differences were observed in these relative proportions in relation to delivery of NACT or the pathological response to NACT (data not shown).

Expression of KLRG1 and CD57 was also low on CD127-CD25+ T regulatory cells. Almost negligible expression of either marker was seen on Treg cells within PBMC whilst a small, but

non-significant, increase in KLRG1 expression was seen on cells within TIL. However, a marked increase in CD57 expression was seen on T regulatory cells within TIL, at 9.9% compared to 0.7% within PBMC. As such, the proportion of double negative cells was reduced from 97% to 83% within TIL (Figure 61).

No differences were observed in these relative proportions in relation to delivery of NACT or the pathological response to NACT (data not shown).

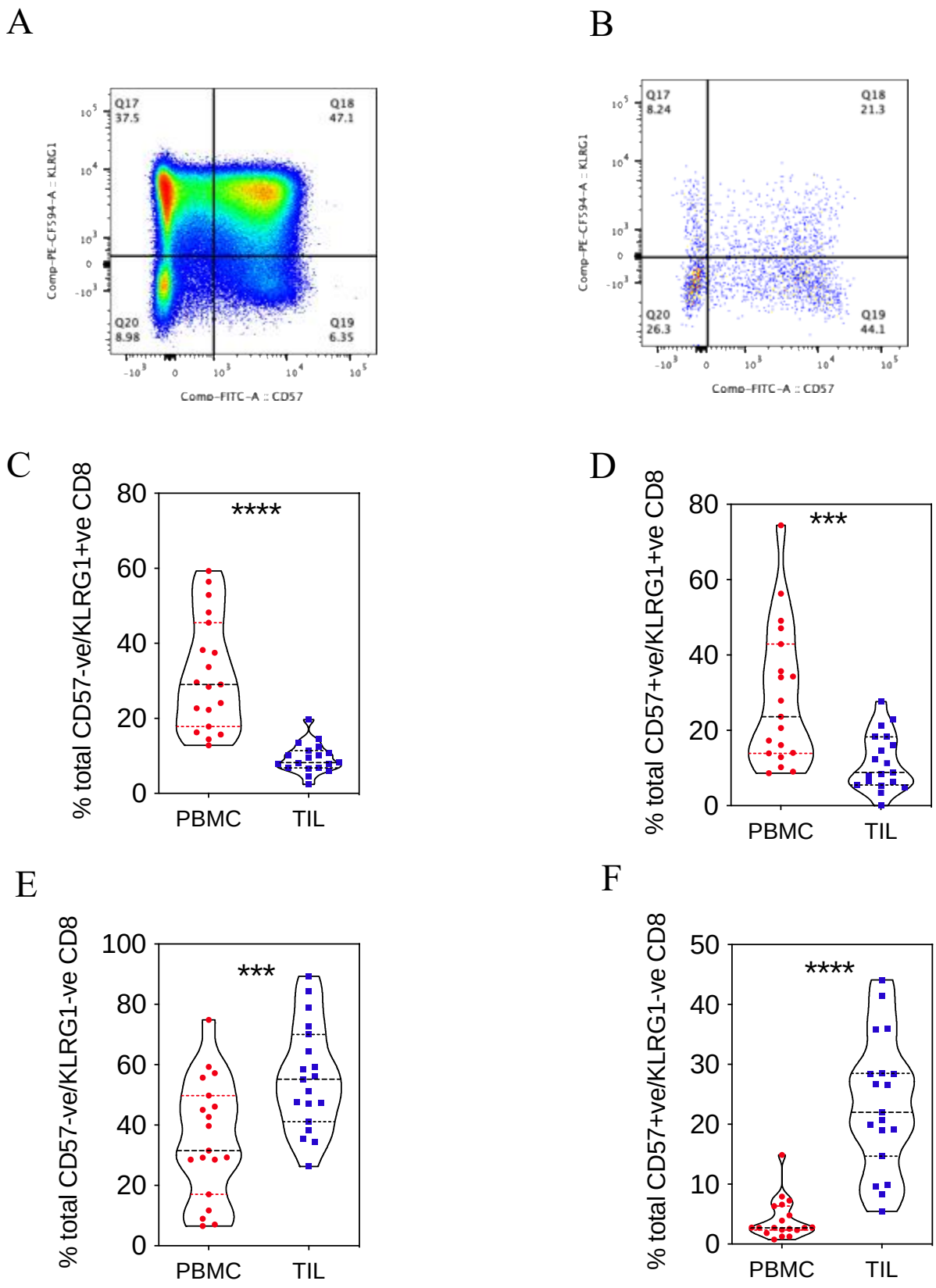

Figure 59. Expression of late differentiation markers on CD8+ T cells in matched PBMC and TIL. Features of terminally differentiation were identified by expression of CD57 and KLRG1, an example plot of CD8 T cells is shown in matched PBMC (A) and TIL (B). Comparative analyses are shown for matched patient PBMC and TIL for CD57-KLRG1+ (C), CD57+KLRG1+ (D), CD57-KLRG1-(E) and CD57+KLRG1- (F). Each symbol represents an individual patient. Dashed horizontal lines indicate the median and dotted lines indicate the interquartile range. Data analysed by Wilcoxon matched-pairs signed rank test, ***denotes $p<0.001$ and **** $p<0.0001$.

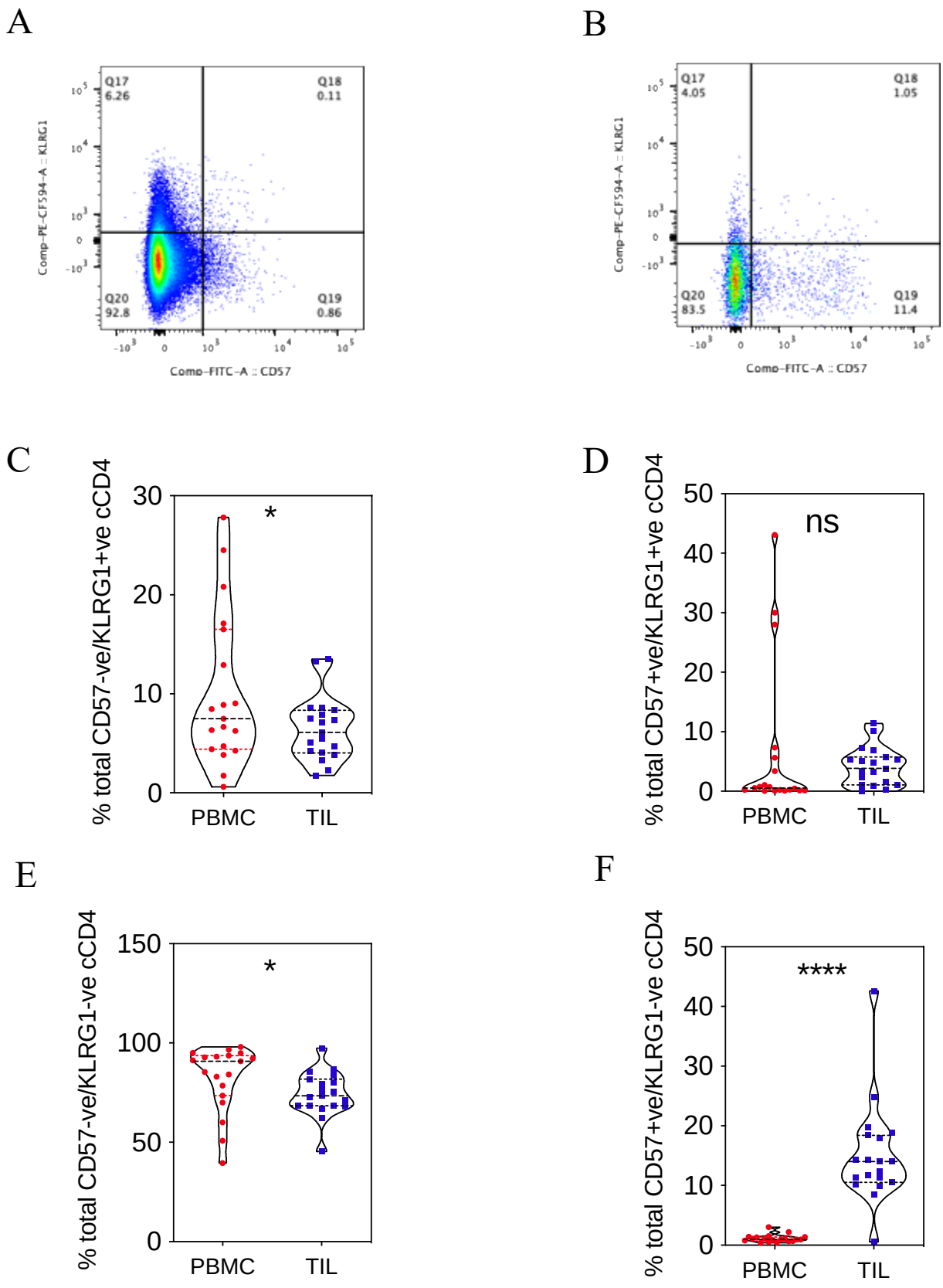

Figure 60. Expression of late differentiation markers on conventional CD4+ T cells in PBMC and TIL. Example plot of CD57 and KLRG1 expression on CD127-CD25+ CD4+ T cells is shown in matched PBMC (A) and TIL (B). Comparative analyses are shown for matched patient PBMC and TIL for CD57-KLRG1+ (C), CD57+KLRG1+ (D), CD57-KLRG1-(E) and CD57+KLRG1- (F). Each symbol represents an individual patient. Dashed horizontal lines indicate the median and dotted lines indicate the interquartile range. Data analysed by Wilcoxon matched-pairs signed rank test *denotes $p<0.05$ and **** $p<0.0001$.

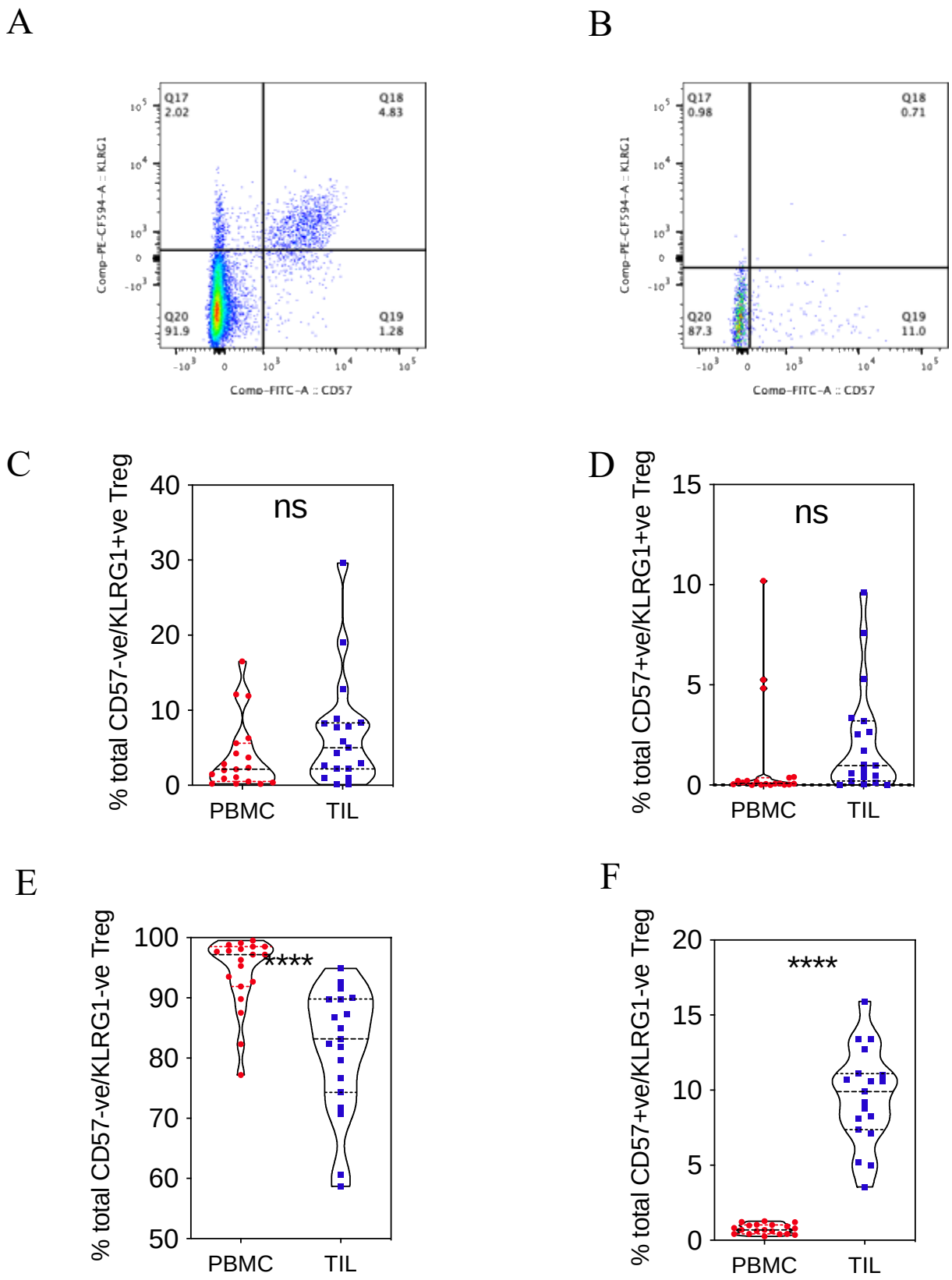

Figure 61. Expression of late differentiation markers on regulatory CD4+ T cells in PBMC and TIL
Example plot of CD57 and KLRG1 expression on CD127+CD25- CD4+ T regulatory cells is shown in matched PBMC (A) and TIL (B). Comparative analyses are shown for matched patient PBMC and TIL for CD57-KLRG1+ (C), CD57+KLRG1+ (D), CD57-KLRG1-(E) and CD57+KLRG1- (F). Each symbol represents an individual patient. Dashed horizontal lines indicate the median and dotted lines indicate the interquartile range. Data analysed by Wilcoxon matched-pairs signed rank test ****denotes p<0.0001.

Checkpoint Expression on Tissue Resident Memory T cells within OAC

The extended flow cytometry panel was able to simultaneously assess the expression of many protein markers and therefore enabled me to examine the detailed phenotype of tissue resident populations. As such, I was initially interested to determine the profile of immune checkpoint receptor expression on these populations.

Tissue resident cells were initially gated and defined through co-expression of CD69+ and CD103+ whilst 'non-tissue resident' cells were measured as the aggregate of CD69-CD103-, CD69+CD103- populations.

Increased expression of PD-1 and LAG-3 was seen on CD8+ TRM compared to non-tissue resident cells (40% vs 62% and 18% vs 24%, respectively ($p<0.0001$, $p=0.01$, Figure 62). In contrast, TIGIT expression did not differ between these two subsets ($p=0.47$) and was seen on a median of 42% of TRM cells.

A trend towards decreased expression of all three checkpoint proteins on both TRM and non-TRM CD8+ T cells was seen following the use of NACT but statistical significance was seen only in relation to LAG-3 expression on non-TRM cells where a fall from 23% to 15% was seen ($p=0.017$), potentially suggesting a reduction in exhaustion phenotype as was also observed within our transcriptional analysis[159]. However, there was no relationship between relative expression and pathological response to NACT treatment (Figure 64).

Tissue resident CD4+ T cells were also seen to upregulate PD-1 and LAG-3 expression compared to non-tissue resident populations from 53% to 71% and 22% to 28%, respectively ($p=0.017$, $p=0.023$, Figure 65) whilst TIGIT expression did not differ ($p=0.42$) and median expression on CD4+ TRM TIL was 24%.

In comparison to CD8+ populations, there was no decrease in checkpoint expression on CD4+ TRM following use of NACT. (Figure 66) and no differences were seen in relation to pathological response to chemotherapy (data not shown).

I next assessed checkpoint expression on T regulatory cells which were defined by CD127-CD25+ phenotype. In contrast to the profile seen on CD8+ and CD4+ effector subsets, expression of PD1, TIGIT and LAG-3 was equivalent between TRM and non-TRM Treg populations ($p=0.11$, $p=0.93$, $p>0.999$, Figure 67). Exposure to NACT treatment did not impact on the expression of PD1 or TIGIT expression on either TRM or non-TRM subsets (PD1-$p=0.15$, $p=0.90$, TIGIT-$p=0.78$, $p=0.50$; Figure 68) although LAG-3 expression on TRM Treg was marginally reduced after NACT from 27% to 24% although no difference was seen in non-TRM Treg ($p=0.042$ vs $p=0.13$). Pathological response to NACT was not related to PD-1 or TIGIT expression any subpopulation. However, LAG-3 expression was markedly higher in patients who responded to neoadjuvant chemotherapy on both the TRM and non-TRM Treg subpopulations, increasing from 0% to 26% and 0.2 to 27% respectively ($p=0.017$, $p=0.017$). This suggests that an increase in LAG-3 on T regulatory cells is associated with good clinical response in OAC patients.

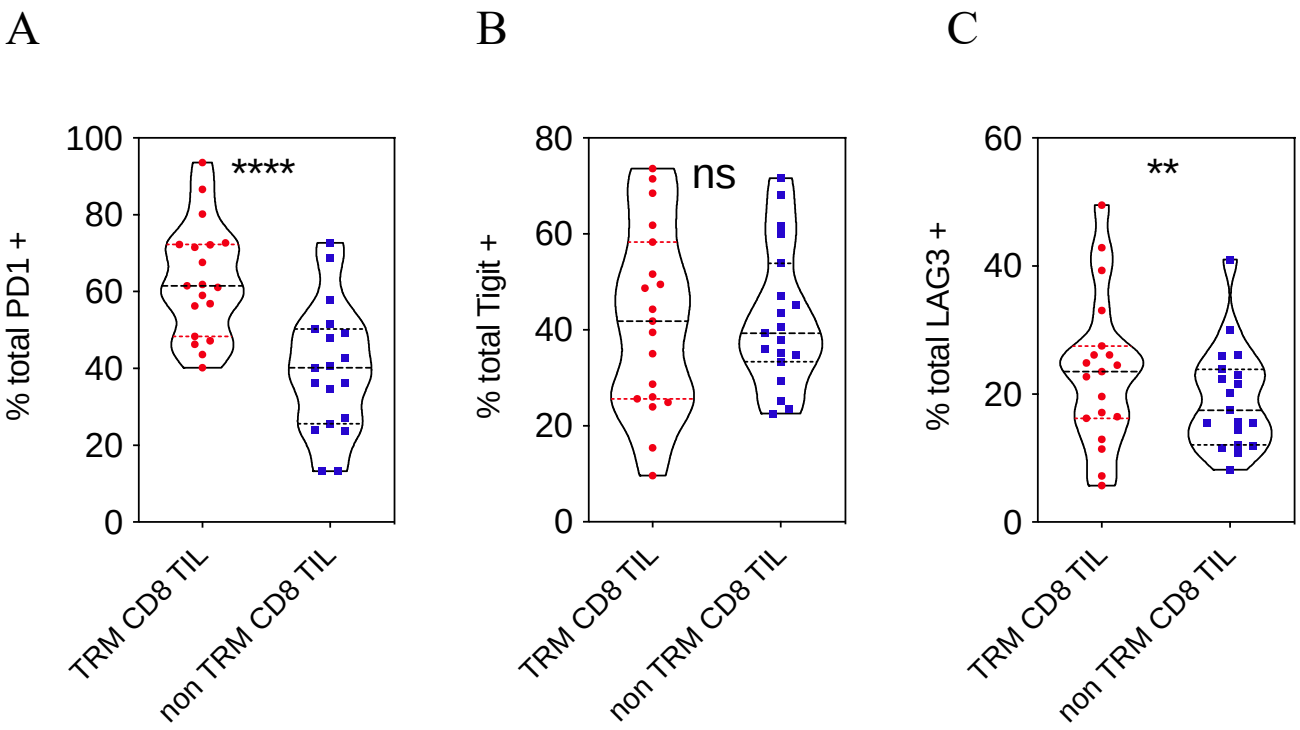

Figure 62. PD-1 and LAG-3 expression is increased on CD8+ TRM cells in OAC
Tissue resident memory (TRM) CD8+ T cells were identified as CD69+CD103+ whilst other populations were defined as non-TRM. Comparative analyses are shown for PD1, Tigit and LAG-3 (A-C respectively). Each symbol represents an individual patient. Dashed horizontal lines indicate the median and dotted lines indicate the interquartile range. Data analysed by Wilcoxon matched-pairs signed rank, **denotes $p<0.01$ and **** $p<0.0001$.

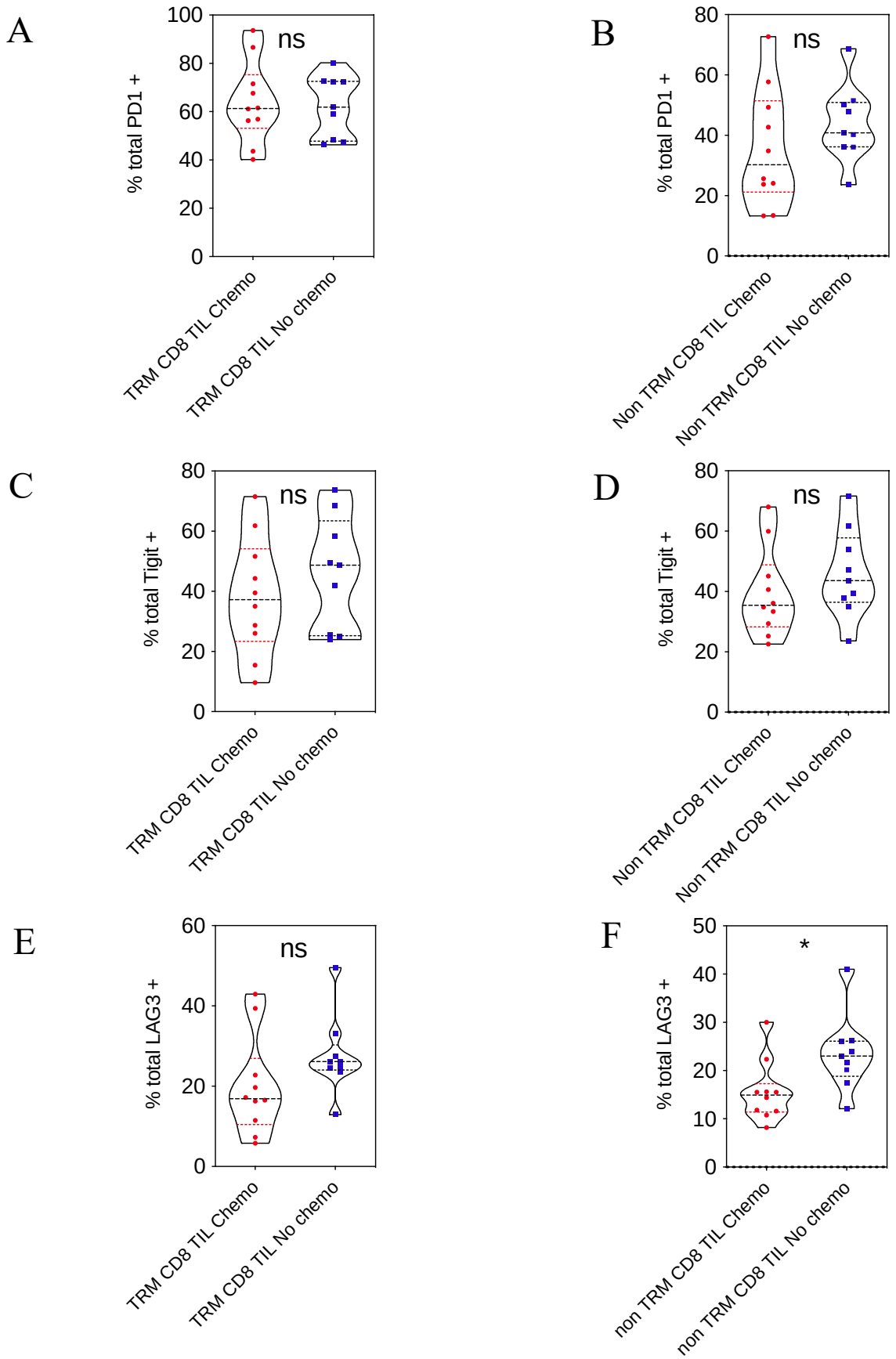

Figure 63. Checkpoint protein expression on tissue resident and non-tissue resident CD8+ TIL in relation to exposure to neoadjuvant chemotherapy

Tissue resident CD8 T cells were identified as CD69+CD103+. Comparative analyses are shown for chemotherapy/no chemotherapy exposure. Checkpoint protein expression is shown on CD8+ TRM (PD-1,A; Tigit,C; and LAG-3,E) and nonTRM. (PD-1,B; Tigit, D; LAG-3, F). Each symbol represents an individual patient. Dashed horizontal lines indicate the median and dotted lines indicate the interquartile range. Data analysed by Wilcoxon matched-pairs signed rank. * denotes $p<0.05$.

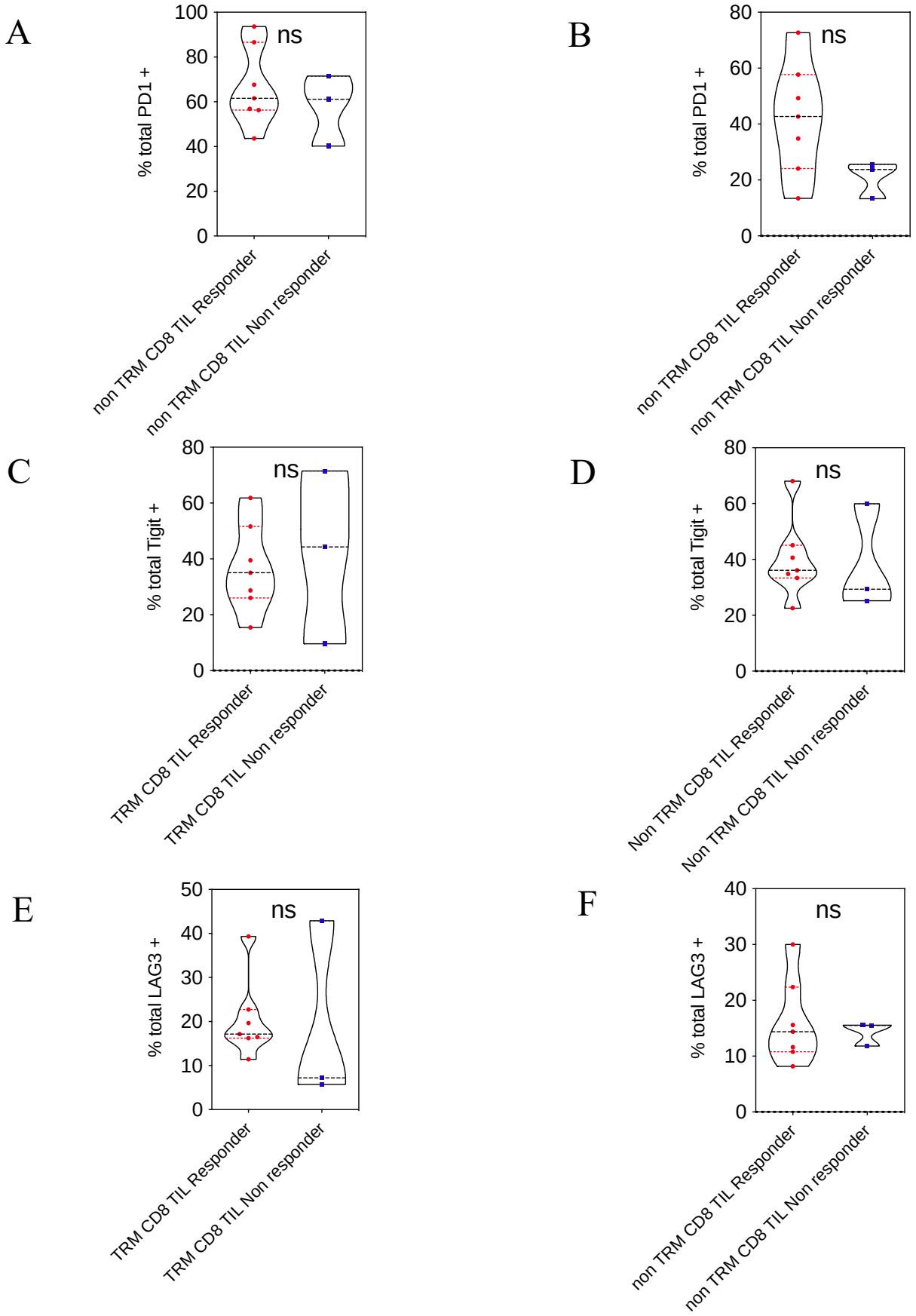

Figure 64. Checkpoint protein expression on tissue resident and non-tissue resident CD8+ TIL in relation to pathological response to neoadjuvant chemotherapy

Tissue resident CD8 T cells were identified as CD69+CD103+. Comparative analyses are shown for response to chemotherapy in relation to checkpoint expression for CD8+ TRM (PD-1, A; Tigit, C; and LAG-3,E) and CD8+ non-TRM. (PD-1, B; Tigit, D; and LAG-3, F) (Responders are defined as Mandard score 1-3). Each symbol represents an individual patient. Dashed horizontal lines indicate the median and dotted lines indicate the interquartile range. Data analysed by Wilcoxon matched-pairs signed rank. * denotes $p<0.05$.

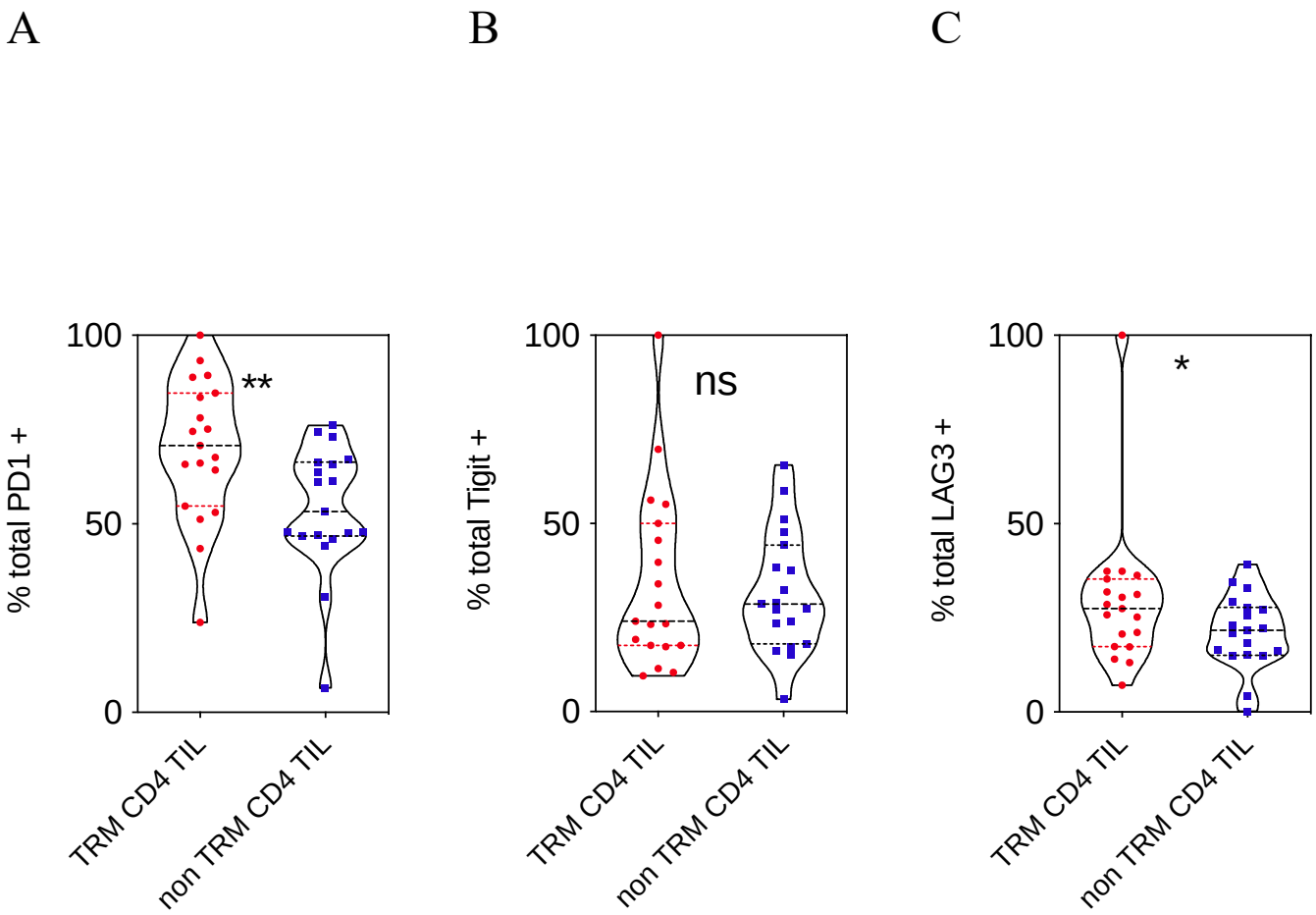

Figure 65. PD-1 and LAG-3 expression is increased on CD4+ TRM cells in OAC
Tissue resident memory (TRM) CD8+ T cells were identified as CD69+CD103+ whilst other populations were defined as non-TRM. Comparative analyses are shown for PD1, Tigit and LAG-3 (A-C respectively). Each symbol represents an individual patient. Dashed horizontal lines indicate the median and dotted lines indicate the interquartile range. Data analysed by Wilcoxon matched-pairs signed rank, *denotes $p<0.05$ and ** $p<0.01$.

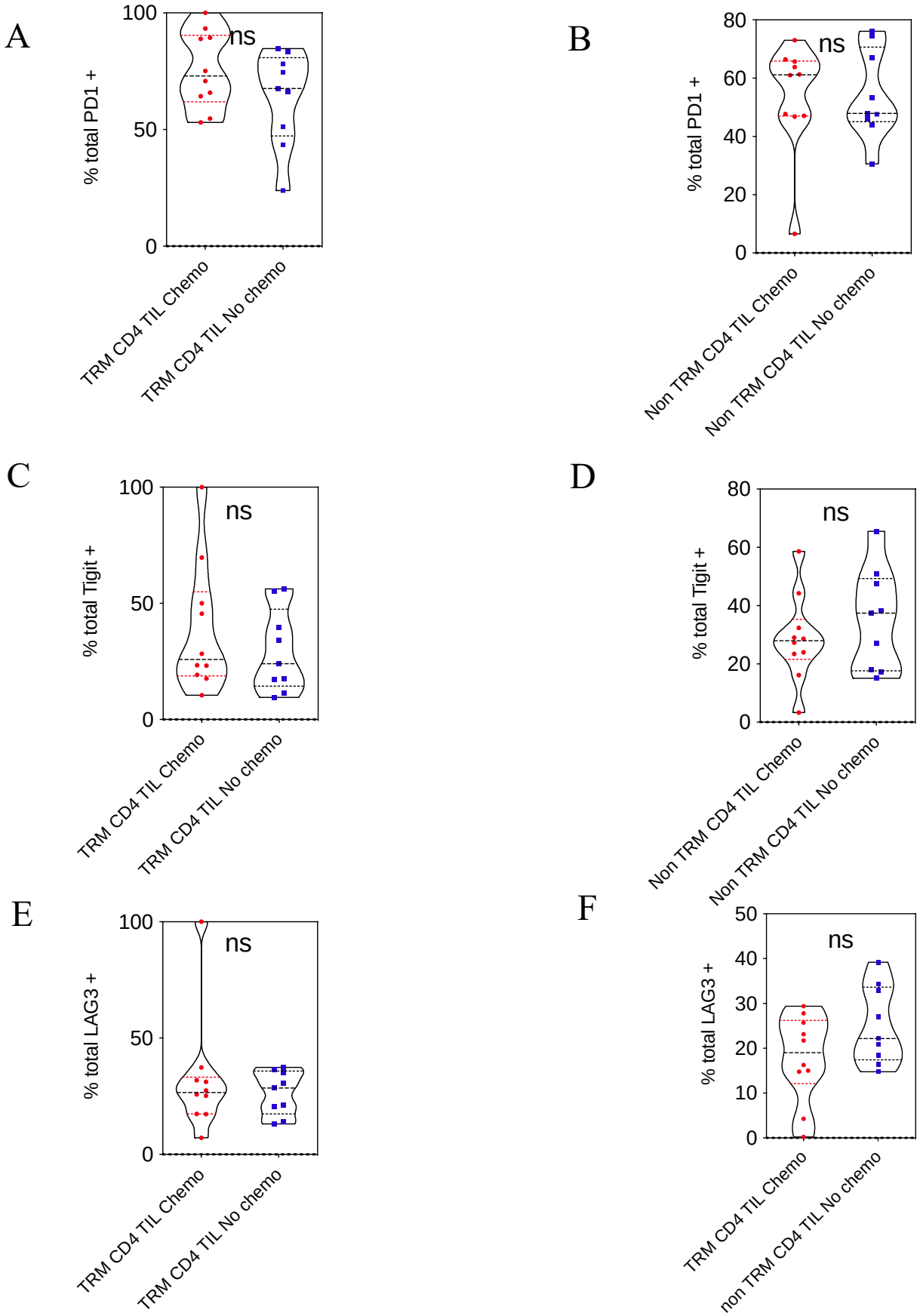

Figure 66. Checkpoint protein expression on TRM and non-TRM CD4+ TIL in relation to exposure to neoadjuvant chemotherapy

Tissue resident CD4 T cells were identified as CD69+CD103+. Comparative analyses are shown for checkpoint expression in relation to chemotherapy/no chemotherapy exposure on CD4+ TRM (PD-1,A; Tigit, C; LAG-3, E) and non-TRM cells (PD-1, B; Tigit, D; LAG-3, F). Each symbol represents an individual patient. Dashed horizontal lines indicate median and dotted lines show interquartile range. Data analysed by Wilcoxon matched-pairs signed rank.

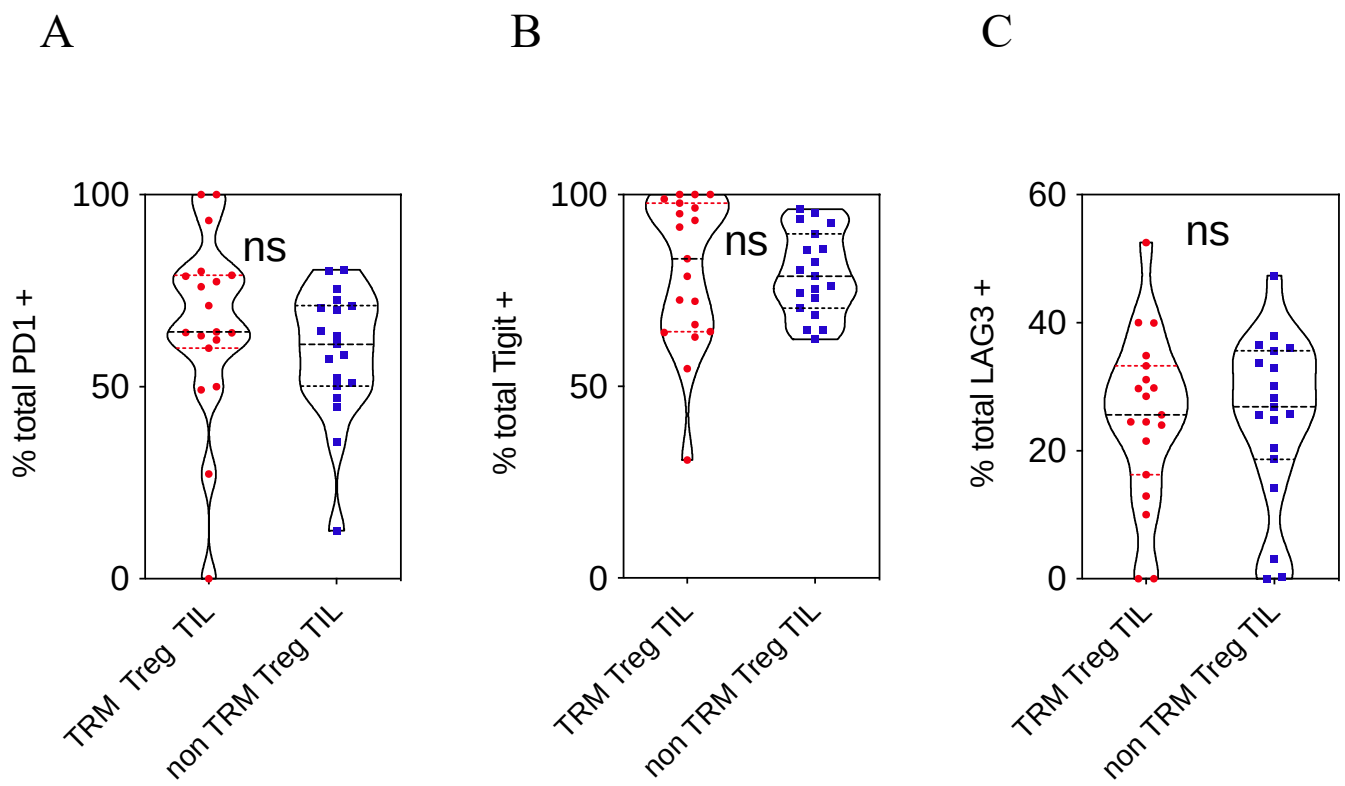

Figure 67. Checkpoint protein expression is comparable on CD4+ T regulatory TRM and non-TRM cells in OAC

Tissue resident cells were identified as CD69+CD103+. T reg were defined as CD127-CD25+CD4+. Comparative analyses are shown for PD1, Tigit and LAG-3 (A-C respectively). Each symbol represents an individual patient. Dashed horizontal lines indicate the median and dotted lines indicate the interquartile range. Data analysed by Wilcoxon matched-pairs signed rank, *denotes $p<0.05$ and ** $p<0.01$.

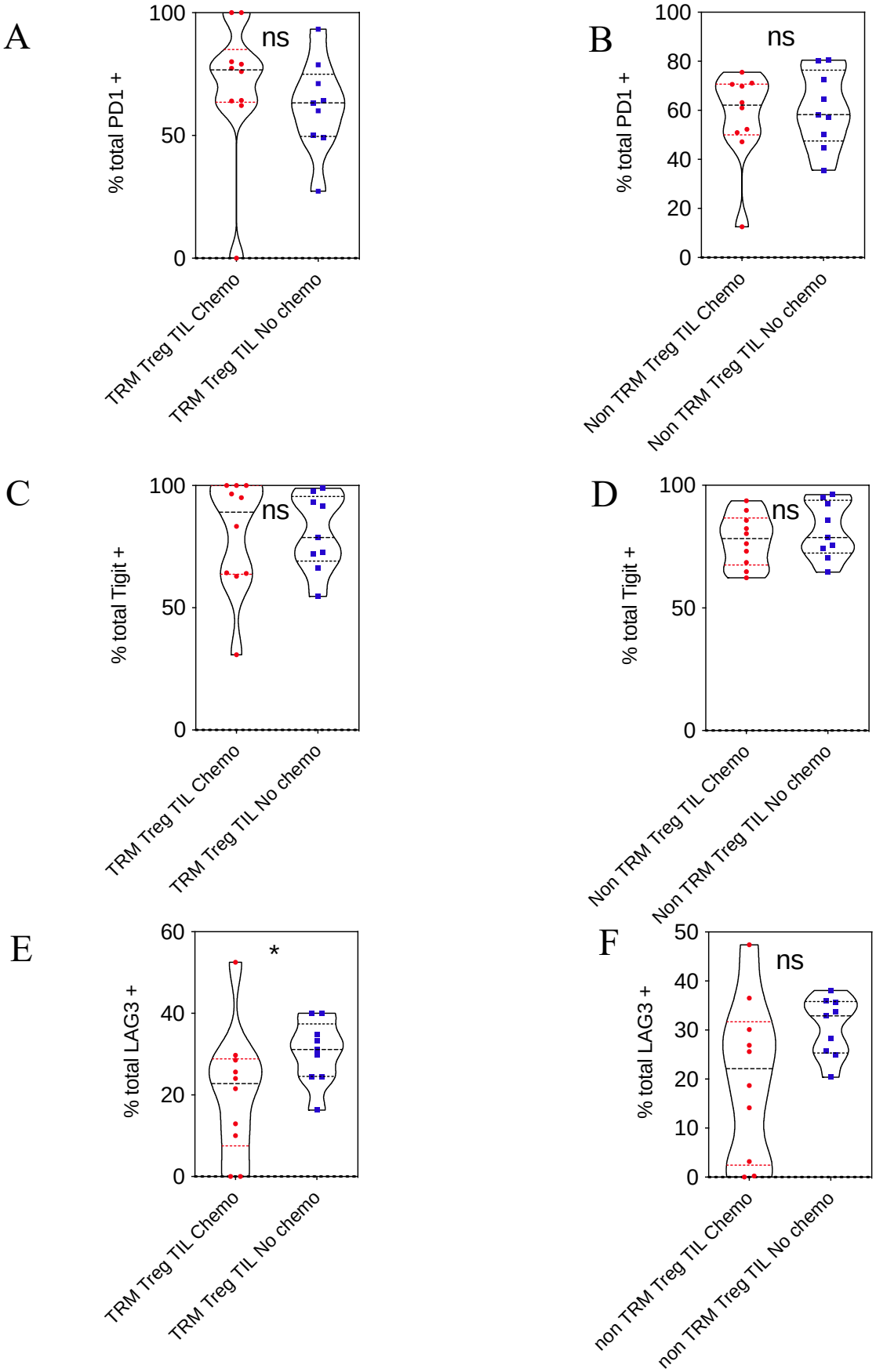

Figure 68. Checkpoint expression on TRM and non-TRM Treg cells in relation to exposure to neoadjuvant chemotherapy.

TRM Treg were identified as CD69+CD103+CD127-CD25+CD4+. Checkpoint expression is shown for Treg TRM (PD-1, A; Tigit, C; LAG-3, E) and non-TRM. (PD-1,B; Tigit, D; LAG-3, F). Each symbol represents an individual patient. Dashed horizontal lines indicate the median and dotted lines indicate the interquartile range. Data analysed by Wilcoxon matched-pairs signed rank. * denotes $p<0.05$.

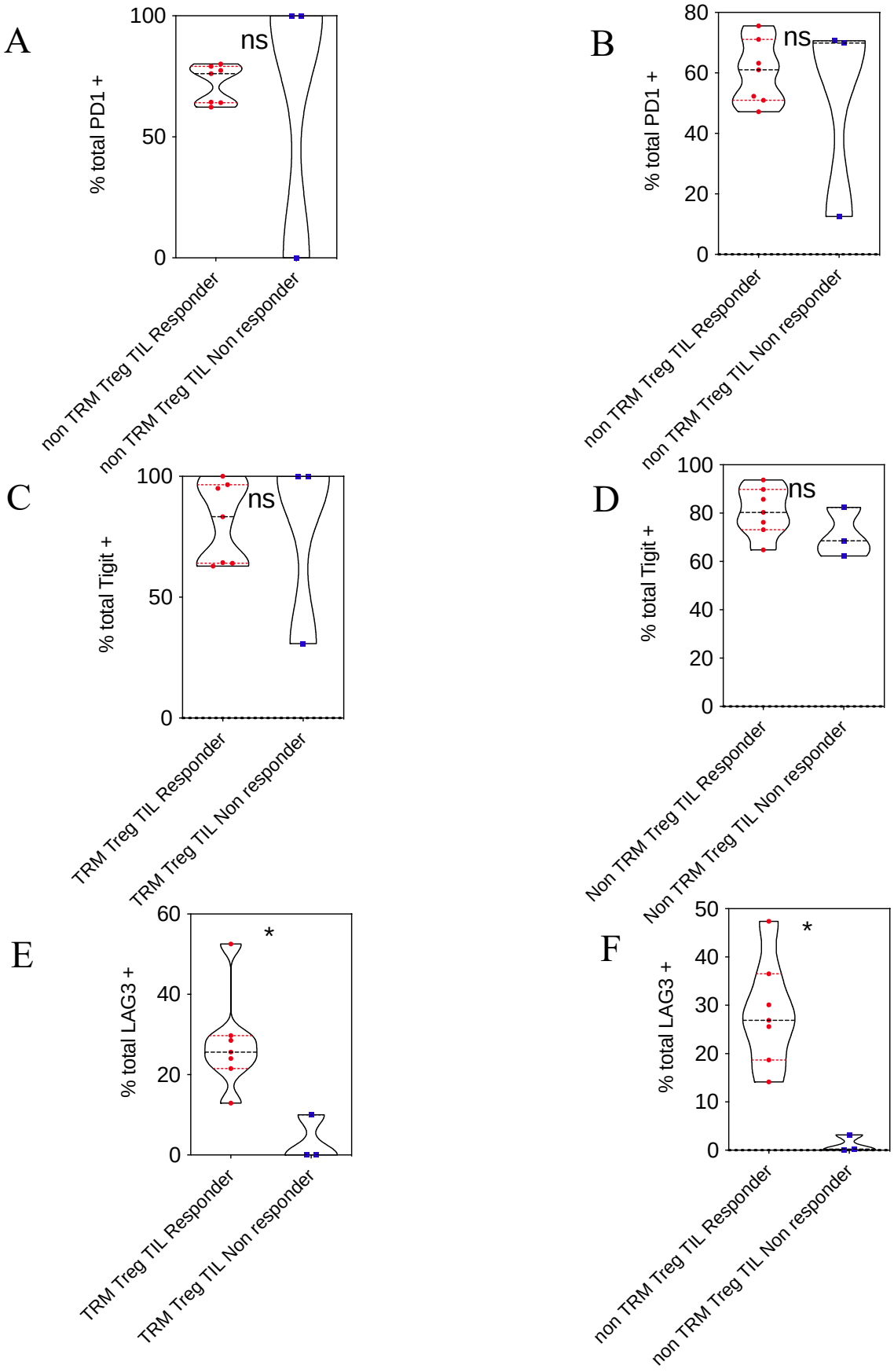

Figure 69. Checkpoint expression on TRM and non-TRM Treg cells in relation to pathological response to neoadjuvant chemotherapy.
TRM Treg were identified as CD69+CD103+CD127-CD25+CD4+. Checkpoint expression is shown for Treg TRM (PD-1, A; Tigit, C; LAG-3, E) and non-TRM. (PD-1,B; Tigit, D; LAG-3, F) Responders are defined as Mandard score 1-3). Each symbol represents an individual patient. Dashed horizontal lines indicate the median and dotted lines indicate the interquartile range. Data analysed by Wilcoxon matched-pairs signed rank. * denotes $p<0.05$.

The profile of terminal differentiation on tissue resident memory T cells and its relationship to NACT

In order to assess the potential proliferative history of TRM cells I next assessed the relative profile of late differentiation markers on this population. As such, I assessed the relative expression of KLRG1 and CD57 on the TRM and non-TRM subsets within OAC.

Within the CD8+ population, an increase in expression of both markers was seen on non-TRM CD8+ TIL where CD57+KLRG1-, CD57-KLRG1+ and CD57+KLRG1+ subsets were all increased ($p=0.04$, $p<0.0001$, $p=0.004$, Figure 70). CD8+ TIL with dual expression represented 2.7% of TRM cells but 18% of non-TRM.

The profile within the CD4+ repertoire was somewhat different. Expression of KLRG1 was increased on the non-TRM subset and this was notable within the single positive CD57-KLRG1+ population. In contrast, CD57 expression was relatively increased on the TRM population. Single positive CD57-KLRG1+ were reduced on CD4+ TRM, from 7% to 3.6%, whereas CD57+KLRG1- were increased on this population from 12% to 21% ($p=0.0002$, $p=0.001$). No differences were seen in relative distribution of the CD57-KLRG1- or CD57+KLRG1+ subsets on CD4+ TRM or non-TRM populations ($p=0.13$, $p=0.77$, Figure 71).

In contrast to these differential findings in effector T cell subsets, no differences in the proportion of subsets with markers of terminal differentiation were seen on TRM and non-TRM T regulatory populations (Figure 72).

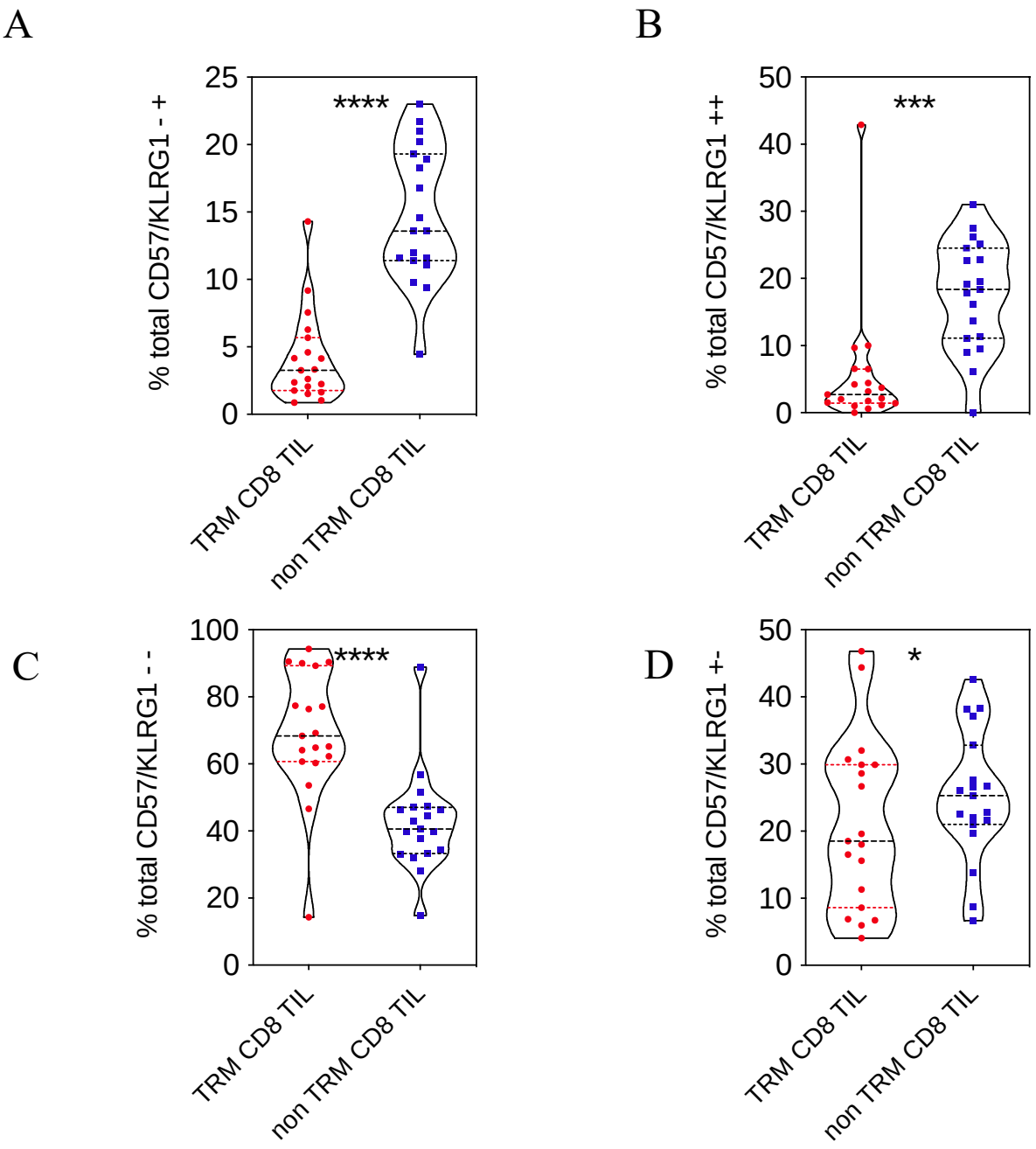

Figure 70. Expression of late differentiation markers on TRM and non-TRM CD8+ cells within TIL
Expression of CD57 and KLRG1: example plot on CD8+ T cells in matched PBMC (A) and TIL (B). Comparative analyses are shown for matched patient TRM and non-TRM TIL for CD57-KLRG1+ (C), CD57+KLRG1+ (D), CD57-KLRG1-(E) and CD57+KLRG1- (F) subsets. Each symbol represents an individual patient. Dashed horizontal lines indicate the median and dotted lines indicate the interquartile range. Data analysed by Wilcoxon matched-pair signed rank test, *denotes $p<0.05$, ** $p<0.01$, *** $p<0.001$ and **** $p<0.0001$.

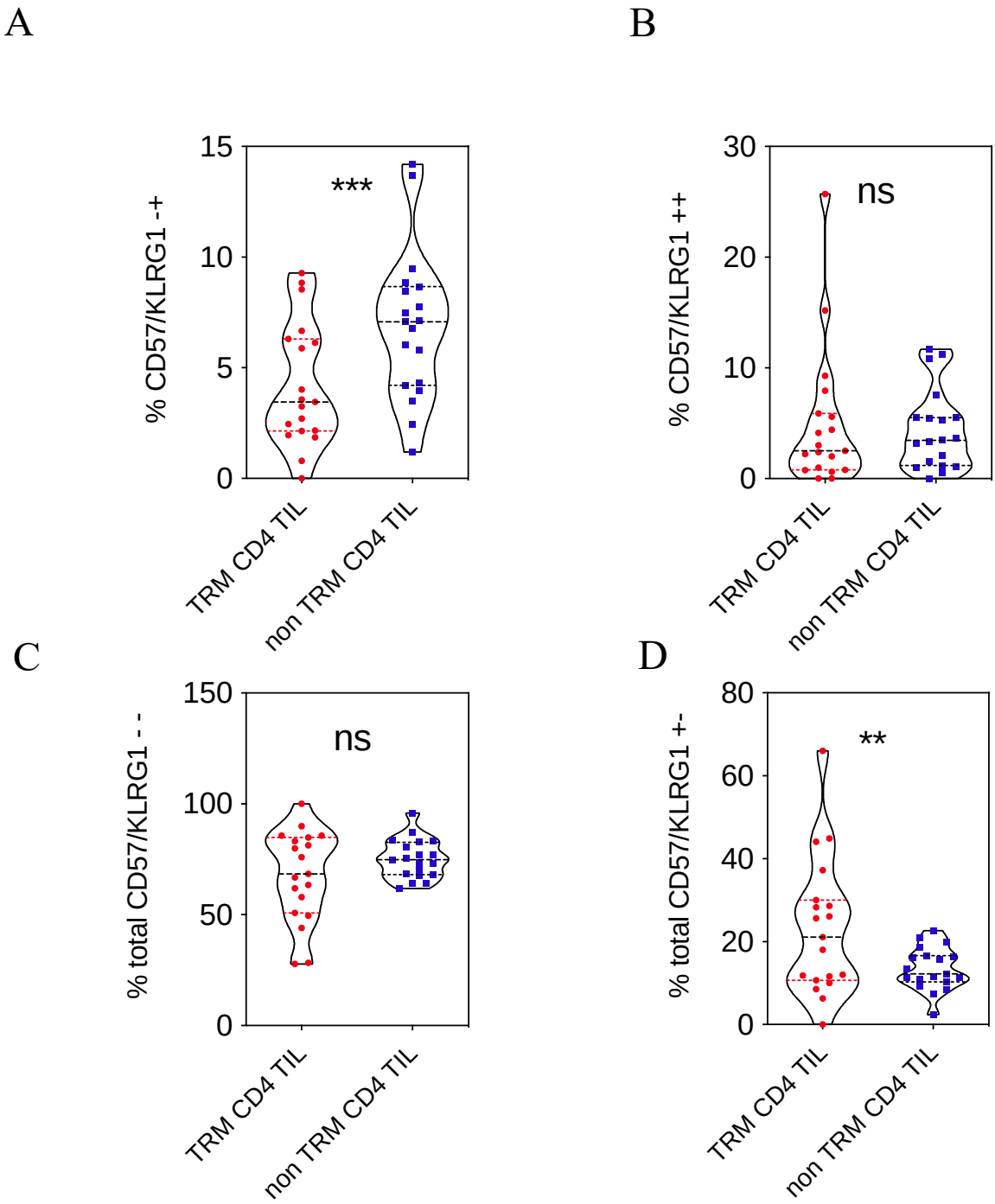

Figure 71. Expression of late differentiation markers on TRM and non-TRM CD4+ cells within TIL Comparative analyses are shown for matched patient TRM and non-TRM TIL for CD57-KLRG1+ (A), CD57+KLRG1+ (B), CD57-KLRG1-(C) and CD57+KLRG1- (D) subsets. Each symbol represents an individual patient. Dashed horizontal lines indicate the median and dotted lines indicate the interquartile range. Data analysed by Wilcoxon matched-pairs signed rank test, *denotes $p<0.05$, ** $p<0.01$, *** $p<0.001$ and **** $p<0.0001$.

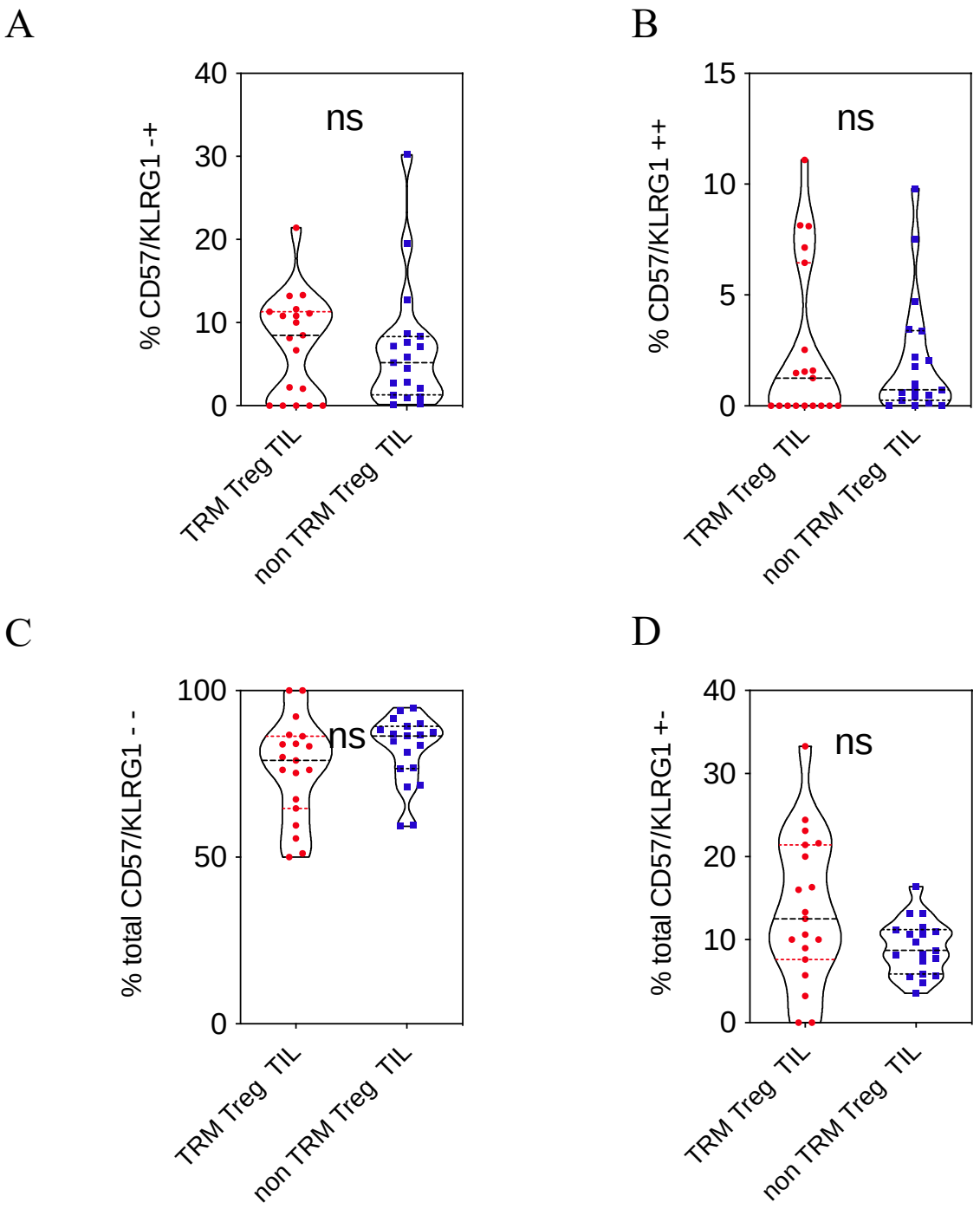

Figure 72. Expression of late differentiation markers on TRM and non-TRM CD4+ regulatory cells within TIL

Comparative analyses are shown for matched patient TRM and non-TRM TIL for CD57-KLRG1+ (A), CD57+KLRG1+ (B), CD57-KLRG1-(C) and CD57+KLRG1- (D) subsets. Each symbol represents an individual patient. Dashed horizontal lines indicate the median and dotted lines indicate the interquartile range. Data analysed by Wilcoxon matched-pairs signed rank test.

Expression of activation markers on tumour infiltrating T cells in oesophageal adenocarcinoma

Markers of cellular activation are a valuable guide to understanding if T cells have undergone recent antigenic stimulation within the tumour microenvironment. As such, I next went on to determine relative expression of a range of activation-related markers on T cell subsets.

Initially, expression of a range of proteins that are upregulated on T cells following activation was measured on the bulk CD8+ T cell pool. Expression of DNAM, and the DNAM homologue CD96, which competes with DNAM for binding to CD155, and whose expression is increased on T cell activation, was also assessed. Expression of the activation markers CD25, CD38, CD96 and ICOS were all higher on CD8+ TILs as compared to PBMC ($p=0.002$, $p<0.0001$, $p<0.0001$). In contrast, DNAM expression was reduced on CD8+ TIL ($p=0.009$). Increased expression of PD-1 and TIGIT, and reduction of KLRG1, was confirmatory of prior analyses ($p<0.0001$, $p<0.0001$, $p<0.0001$).

Memory CD8+ T Cell subsets

These findings were then contrasted to the profile seen on CD8+ T cell memory subsets. Of note, increased expression of CD28 , CD38, CD95, CD96, PD1 and TIGIT was seen on naive T cell subsets ($p=0.02$, $p=0.02$, $p<0.0001$, $p=0.03$, $p<0.0001$, $p=0.0003$), suggesting either that this expression may reflect non antigen-dependent stimulation, potentially through cytokines, or that this 'naive' pool contained revertant memory cells. In contrast, expression of CD27 and KLRG1 expression was reduced ($p=0.005$, $p=0.0042$).

Within the memory pool a key feature was increased expression of CD38 and CD96 in all subsets, whilst KLRG1 and DNAM were reduced.

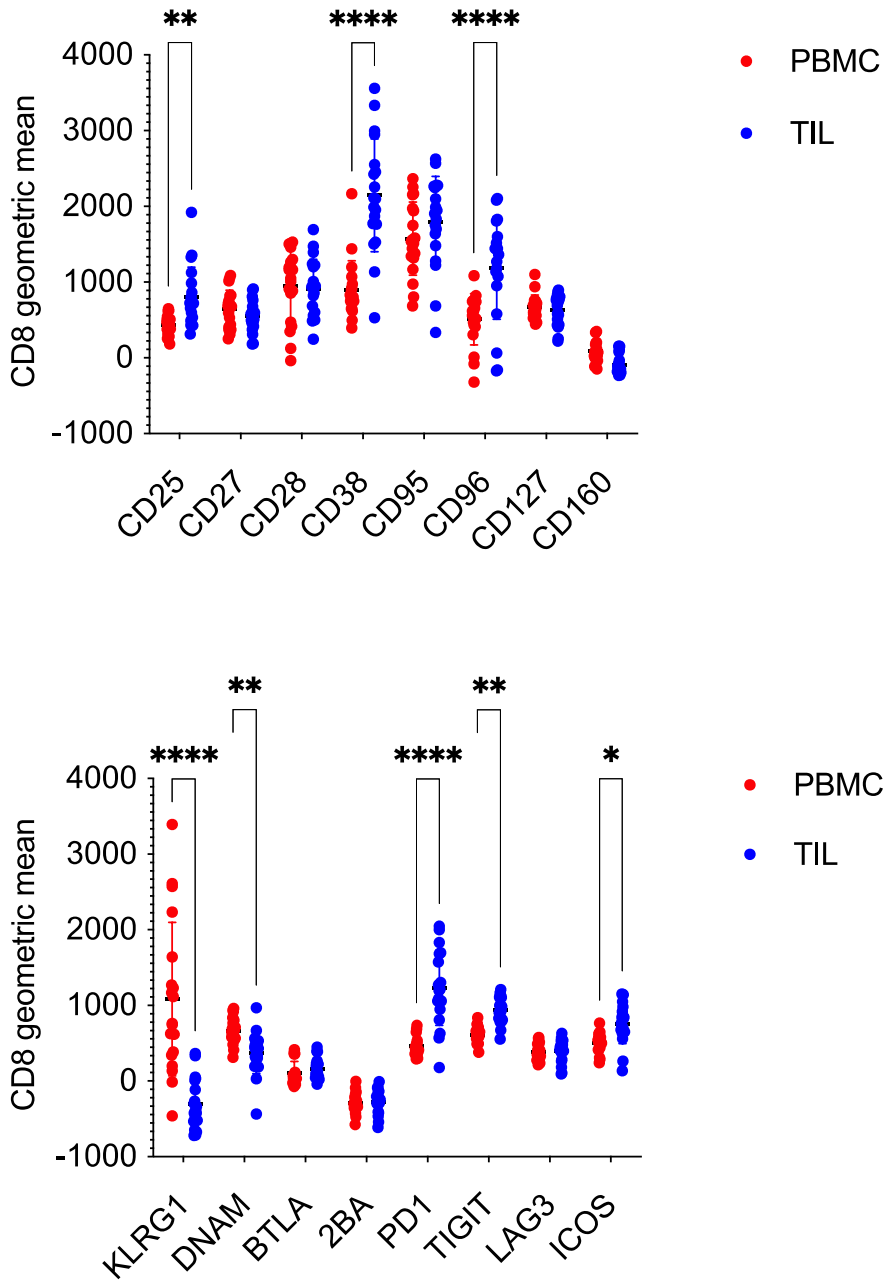

Figure 73. Phenotypic profile of matched PBMC and TIL CD8+ T cells.
Geometric mean expression of cell surface markers of CD8+ T cells. Each symbol represents an individual patient. Data analysed by Sidak's multiple comparison test, *denotes $p<0.05$, ** $p<0.01$, *** $p<0.001$ and **** $p<0.0001$.

A

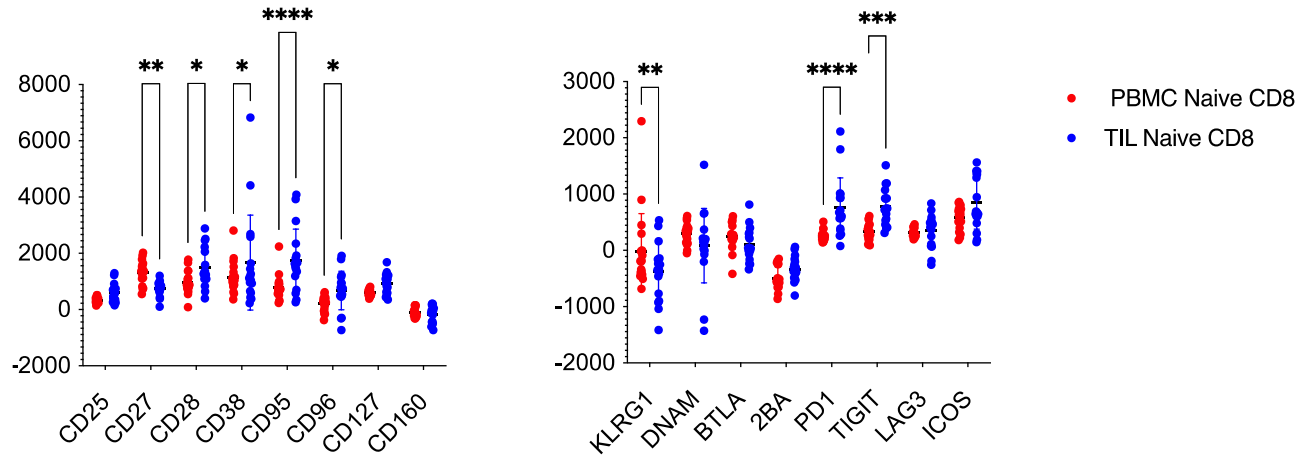
8000
6000
4000
2000
0
-2000
**
*
*
****
*
CD25
CD27
CD28
CD38
CD95
CD96
CD127
CD160
3000
2000
1000
0
-1000
-2000
**
****
***
KLRG1
DNAM
BTLA
2BA
PD1
TIGIT
LAG3
ICOS
PBMC Naive CD8
TIL Naive CD8

B

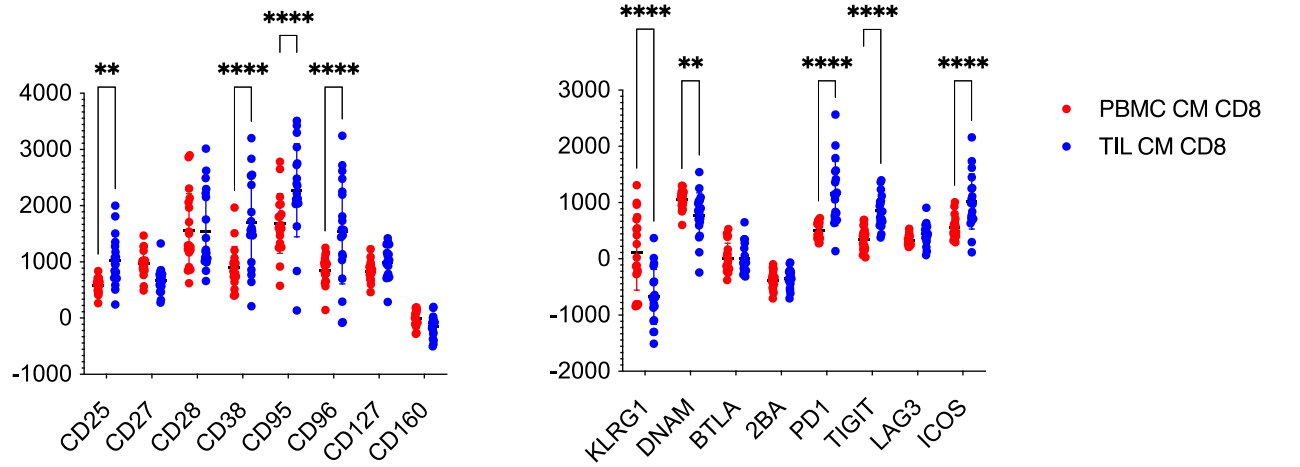
4000
3000
2000
1000
0
-1000
**
****
****
****
CD25
CD27
CD28
CD38
CD95
CD96
CD127
CD160
3000
2000
1000
0
-1000
-2000
****
**
****
****
****
KLRG1
DNAM
BTLA
2BA
PD1
TIGIT
LAG3
ICOS
PBMC CM CD8
TIL CM CD8

C

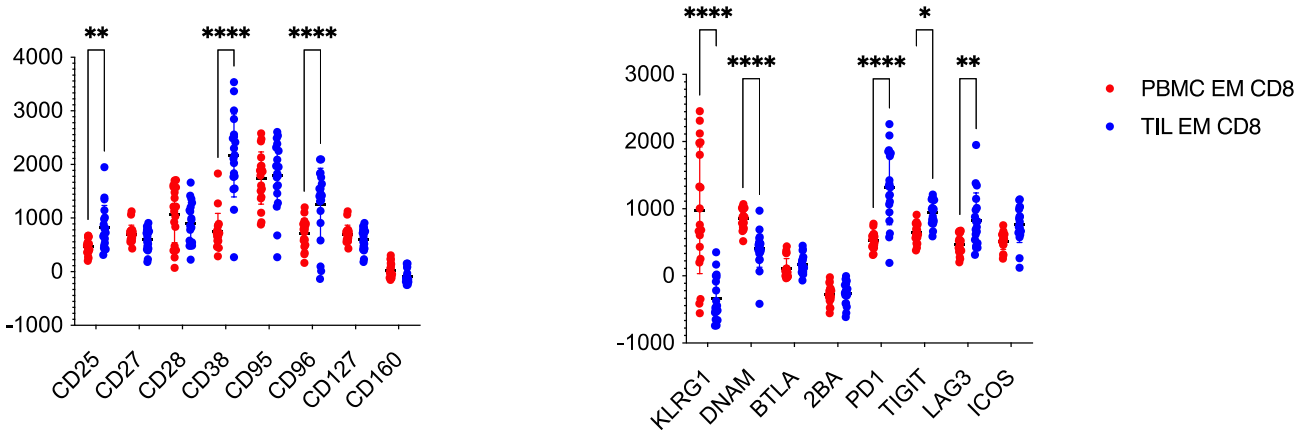

D

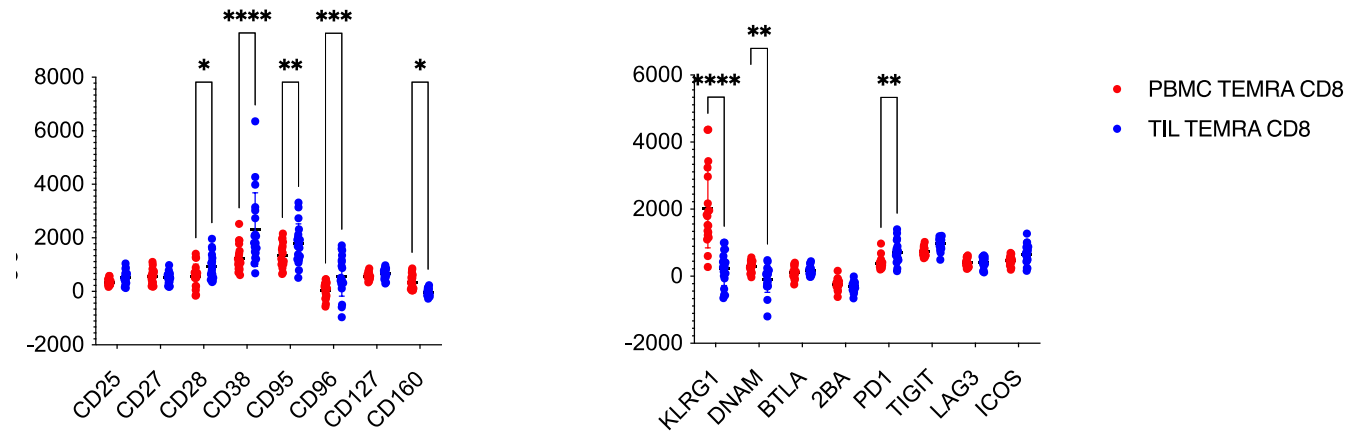

Figure 74. Phenotypic profile of matched PBMC and TIL CD8+ T cell memory subsets
Geometric mean expression of cell surface markers on CD8+ T cell memory subsets. Comparative assessment of matched patient PBMC and TIL for naïve CD8 T cells (A), central memory CD8 T cells (B), effector memory CD8 T cells (C) and TEMRA CD8 T cells (D). Each symbol represents an individual patient. Data analysed by Sidak's multiple comparison test, *denotes $p<0.05$, ** $p<0.01$, *** $p<0.001$ and **** $p<0.0001$.

Co-expression of checkpoint and activation molecules on CD8+ T cells in relation to differentiation status

In order to assess if the pattern of checkpoint and activation expression was related to differentiation phenotype, their expression was next examined in relation to CD57 and KLRG1 expression. A wide range of differences in expression was seen between TIL and PBMC populations. However, these were broadly comparable between the 4 different subsets and, whilst some differential patterns were observed, no major distinguishing features were apparent.

In order to focus on the late differentiated 'double positive' KLRG1+CD57+ population I assessed expression on this subset in relation to the combined aggregate of the other 3 subsets. Interestingly, relative expression of CD38, CD96 and DNAM was somewhat lower on this KLRG1+CD57+ pool whilst CD28 expression was maintained at a higher level (Figure 74). Delivery of NACT and response to chemotherapy did not influence these proportions (data not shown).

A

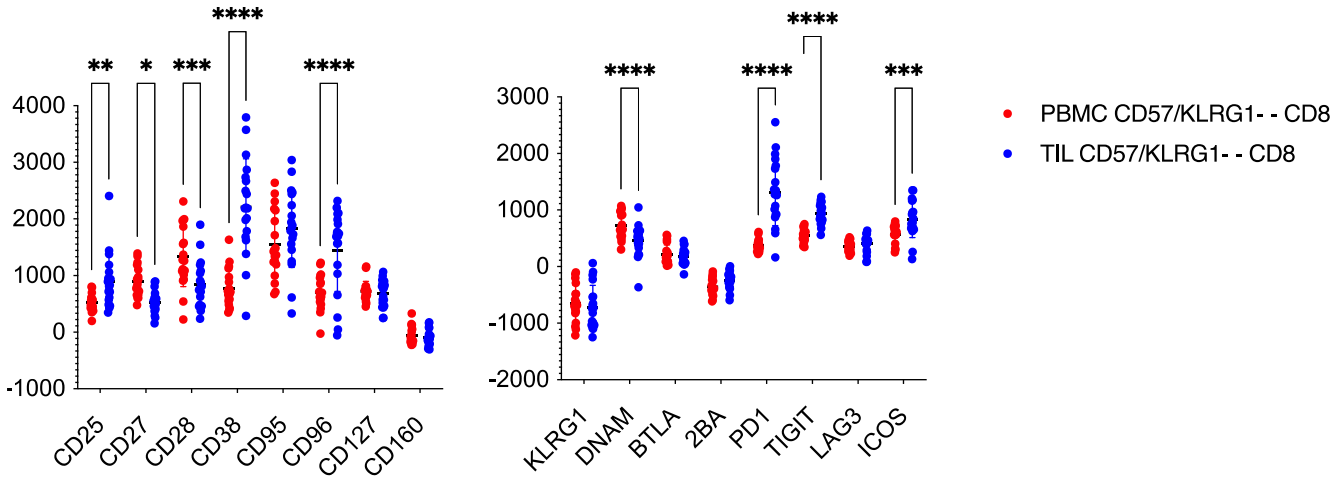
**
*
***
****
****
4000
3000
2000
1000
0
-1000
CD25
CD27
CD28
CD38
CD95
CD96
CD127
CD160
****
****
****
***
3000
2000
1000
0
-1000
-2000
KLRG1
DNAM
BTLA
2BA
PD1
TIGIT
LAG3
ICOS
PBMC CD57/KLRG1- - CD8
TIL CD57/KLRG1- - CD8

B

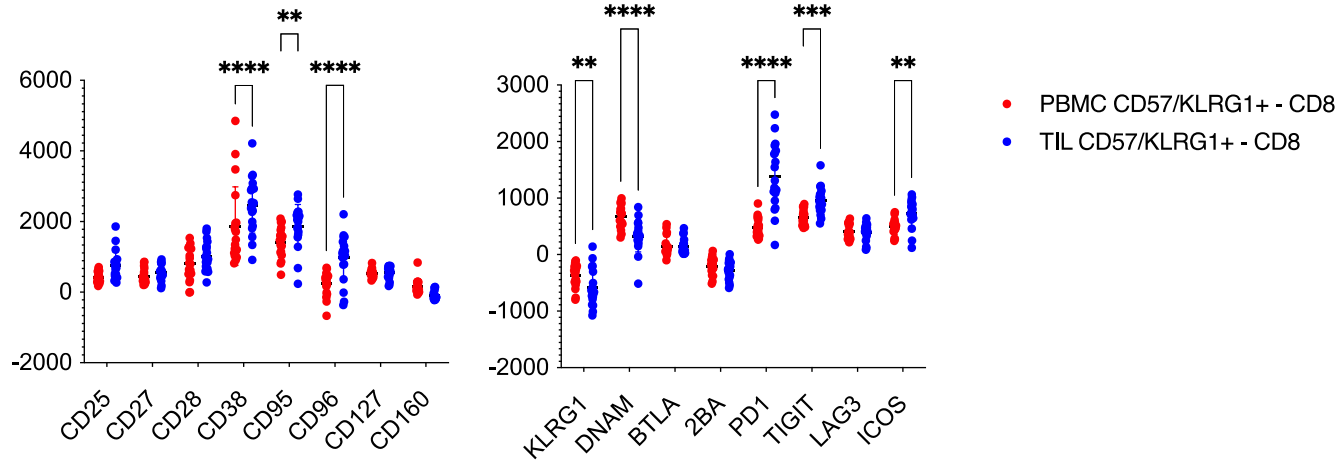
**
****
****
6000
4000
2000
0
-2000
CD25
CD27
CD28
CD38
CD95
CD96
CD127
CD160
**
****
****
***
**
3000
2000
1000
0
-1000
-2000
KLRG1
DNAM
BTLA
2BA
PD1
TIGIT
LAG3
ICOS
PBMC CD57/KLRG1+ - CD8
TIL CD57/KLRG1+ - CD8

C

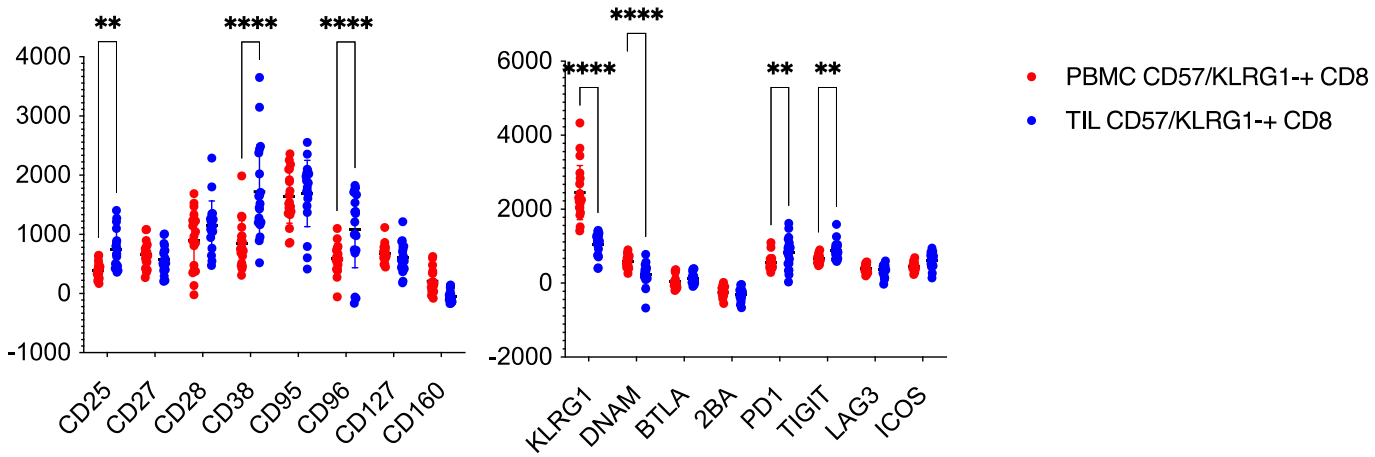

D

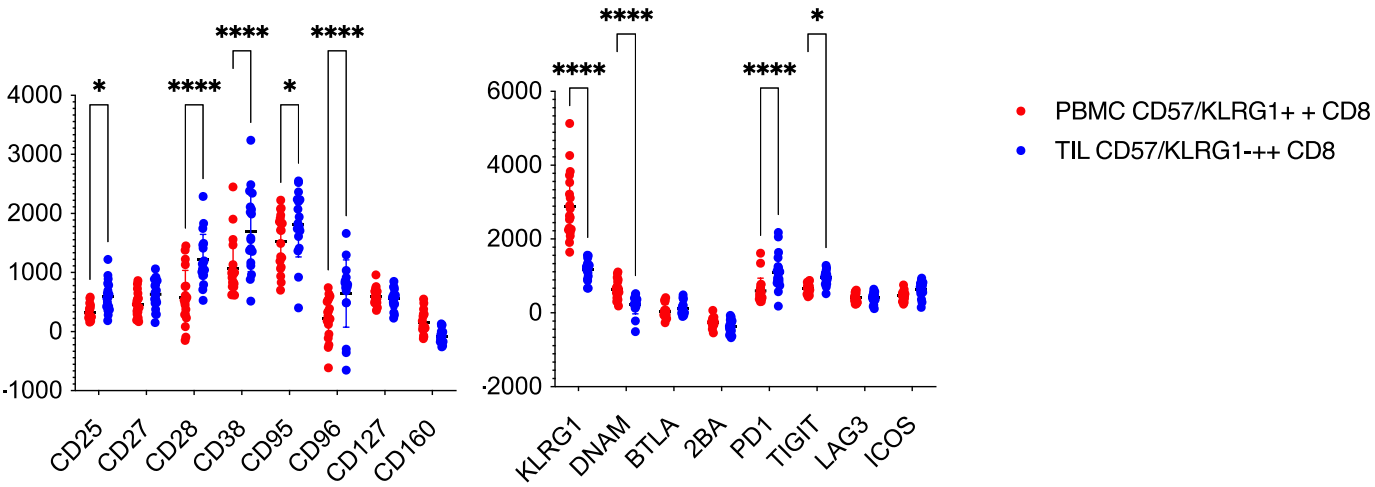

Figure 75. Co-expression of checkpoint and activation molecules on CD8+ T cells in relation to differentiation status

Geometric mean expression of cell surface markers of CD8+ T cells. Comparative assessment of matched patient PBMC and TIL for CD57-/KLRG1- T cells (A), CD57+/KLRG1- CD8+ T cells (B), CD57-/KLRG1+ T cells (C) and CD57+/KLRG1+ CD8+ T cells (D).

Each symbol represents an individual patient. Data analysed by Sidak's multiple comparison test, *denotes $p<0.05$, ** $p<0.01$, *** $p<0.001$ and **** $p<0.0001$.

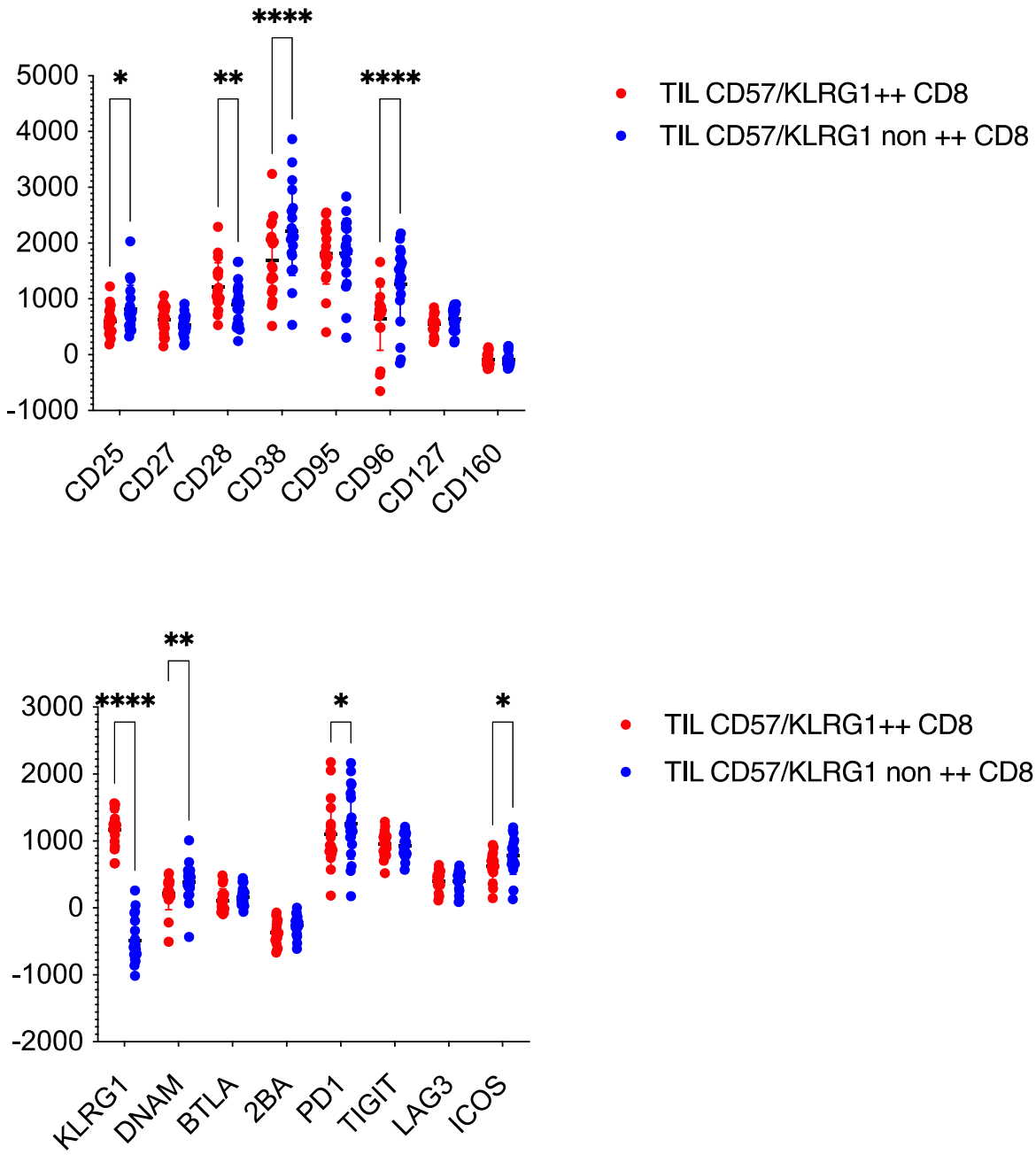

Figure 76. Phenotypic profile of CD8+ T cells in terminally differentiated CD8+ T cell TIL. Geometric mean expression of cell surface markers of CD8+ T cells. Comparative assessment of CD57+/KLRG1+ T cells and non CD57+/KLRG1+ CD8+ T cells (CD57-/KLRG1- ,CD57+/KLRG1- CD57-/KLRG1+) subsets. Each symbol represents an individual patient. Data analysed by Sidak's multiple comparison test, *denotes $p<0.05$, ** $p<0.01$, *** $p<0.001$ and **** $p<0.0001$.

Co-expression of markers of differentiation and checkpoint expression on Tissue Resident Memory CD8+ T cells

I next went on to assess the profile of co-expression of differentiation and checkpoint expression markers on tissue resident memory CD8+ populations.

TRM expressed higher levels of several activation markers including CD25, CD38, CD95, CD96 and ICOS compared to non-TRM ($p<0.0001$, $p<0.0001$, $p=0.03$, $p<0.0001$, $p<0.0001$). whilst expression of CD28 and KLRG1 was reduced ($p=0.01$, $p<0.0001$). Differences in CD95, ICOS and CD28 expression between TRM and non-TMR populations were not maintained after neoadjuvant chemotherapy ($p=0.14$, $p=0.24$, $p= 0.82$) and no difference was seen in membrane phenotype of TRM CD8+ T cells in relation to delivery of chemotherapy or response to chemotherapy (data not shown).

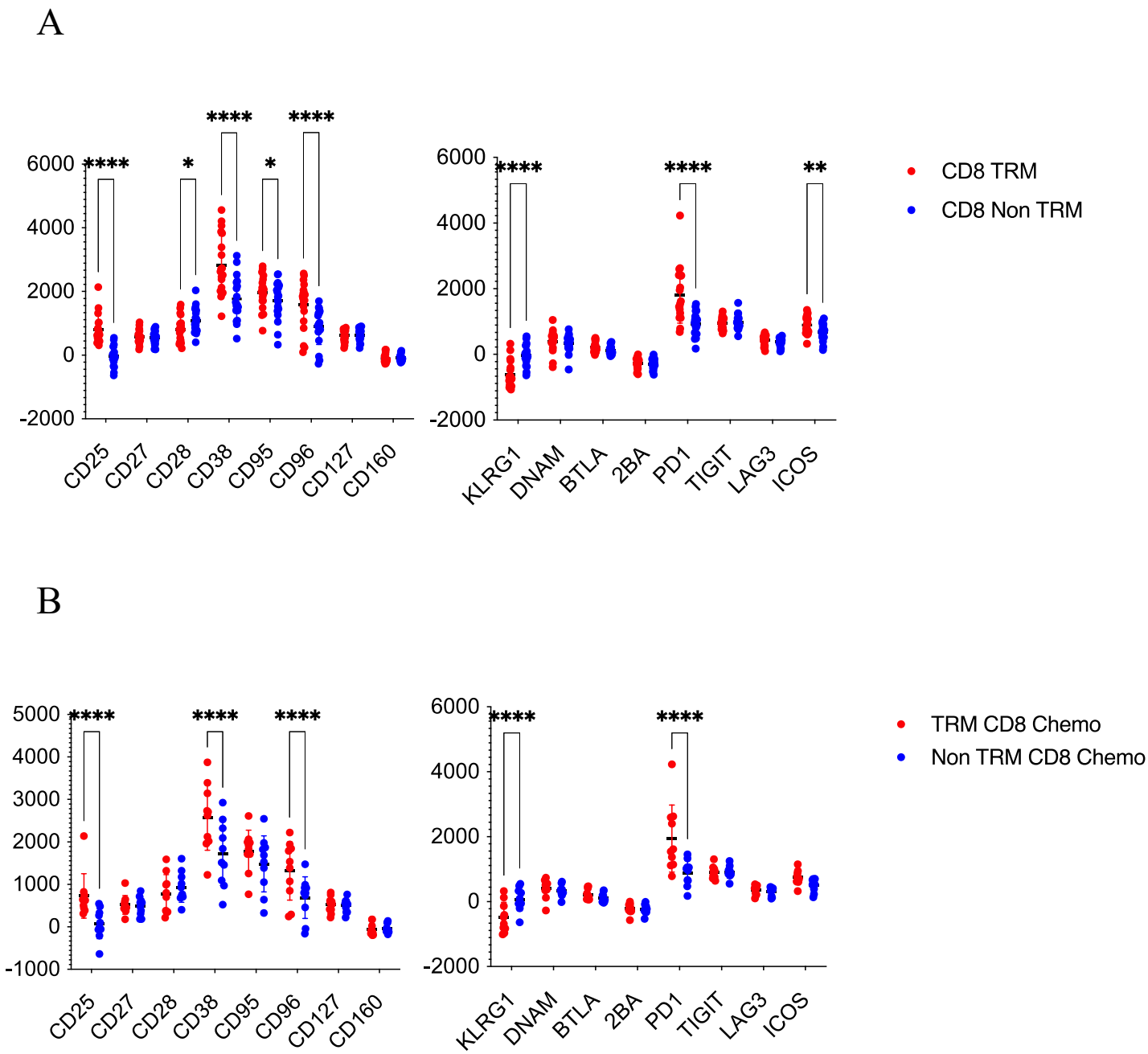

Figure 77. Phenotypic analysis of TRM CD8+ T cells, assessed in relation to NACT treatment. Geometric mean expression of cell surface markers of CD8+ TIL. Comparative assessment of TRM CD8 TIL and non-TRM CD8+ TIL(A) and specifically for patients who had received neoadjuvant chemotherapy (B).
Each symbol represents an individual patient. Data analysed by Sidak's multiple comparison test, **denotes $p<0.01$, **** $p<0.0001$.

Expression of checkpoint and differentiation markers on CD4+ TIL

Following analysis of the CD8+ pool I next went on to assess the profile of expression on the CD4+ T cell repertoire.

The profile of activation was somewhat different from that seen on CD8+ T cells with higher levels of CD95, CD96, PD1 and ICOS compared to PBMC ($p<0.0001$, $p<0.0001$, $p<0.0001$, $p<0.0001$) whilst CD27 and KLRG1 expression was lower ($p=0.003$, $p<0.0001$). The increase in CD96 and ICOS was particularly pronounced whilst CD38 expression was not increased. Higher level expression of PD-1 and TIGIT was confirmed in correlation with prior gating analysis ($p<0.0001$, $p<0.0001$). The reduction in KLRG1 expression on CD4+ TIL differed from prior analysis which did not demonstrate any difference.

CD95 expression was particularly high and this pattern was particularly striking on the two effector subsets. Increased CD38 expression also reached significance on the effector memory pool (Figure 78).

A

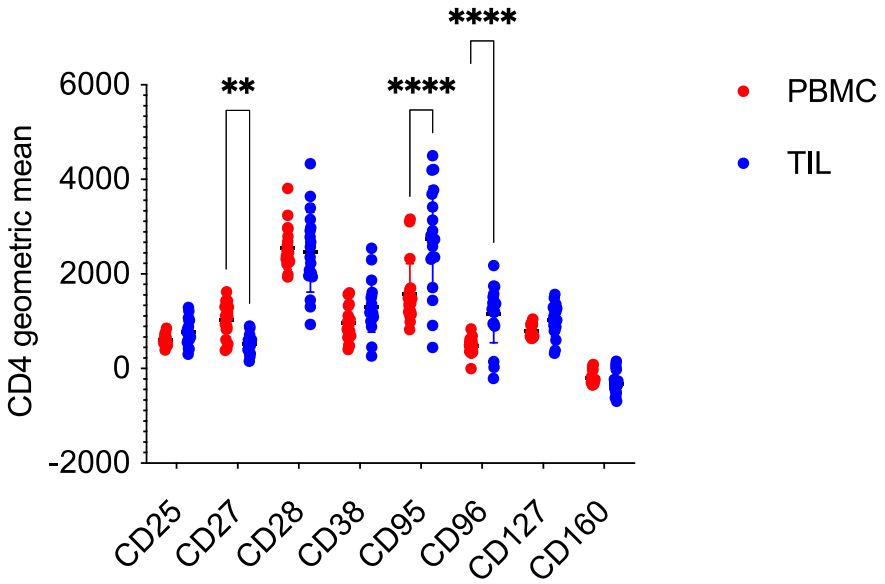

B

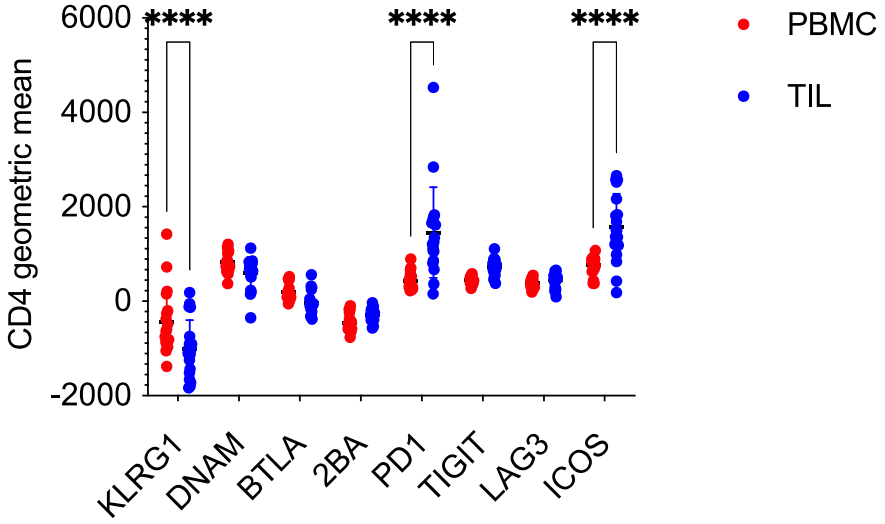

Figure 78. Phenotypic analysis of matched PBMC and TIL CD4+ T cells within OAC
Geometric mean expression of cell surface markers of CD4+ T cells. Each symbol represents an individual patient. Data analysed by Sidak's multiple comparison test, *denotes ** $p<0.01$ and **** $p<0.0001$.

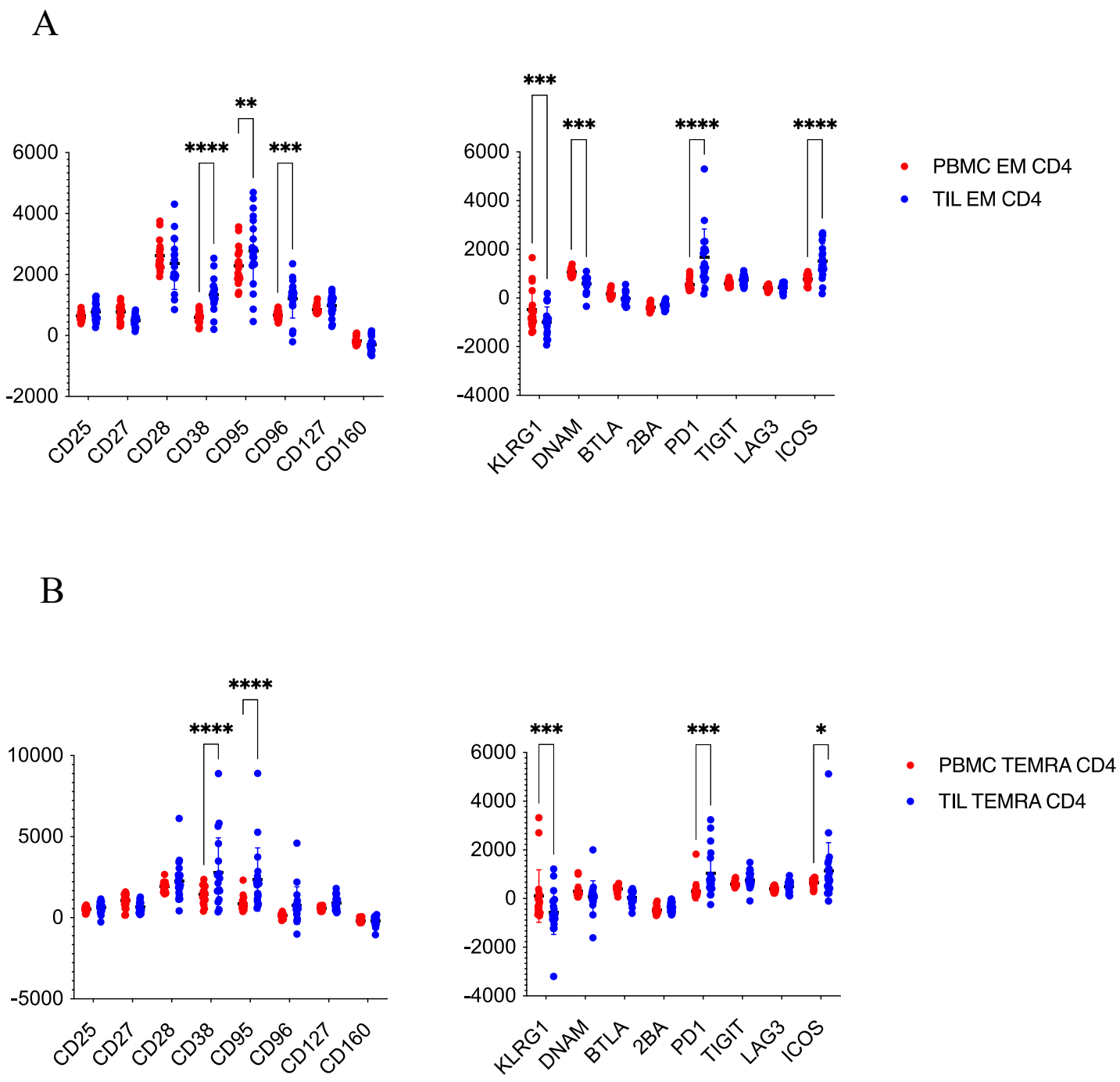

Figure 79. Phenotypic analysis of matched PBMC and TIL effector CD4+ T cells
Geometric mean expression of cell markers of CD4+ T cells. Comparative assessment of matched patient PBMC and TIL for effector memory CD4+ T cells (A) and TEMRA CD4+ T cells (B). Each symbol represents an individual patient. Data analysed by Sidak's multiple comparison test, *denotes $p<0.05$, ** $p<0.01$, *** $p<0.001$ and **** $p<0.0001$.

Phenotypic expression of CD4+ TIL in relation to late differentiation status

Co-expression of inhibitory and stimulatory checkpoints was next examined on CD4+ T cells in relation to the pattern of CD57 and KLRG1 expression.

A range of differences were observed between the four subsets of CD4+ T cells in relation to differentiation status (Figure 80). Overall comparison of 'terminally differentiated' CD57+KLRG1+ CD4+ T cells with 'non-terminally differentiated' CD4+ T cells showed that PD-1 expression was markedly increased within the terminally differentiated pool whilst the other activation markers were increased on the 'non-terminally differentiated' CD4+ TIL subsets ($p=0.0004$, $p<0.0001$, $p=0.0003$, $p<0.0001$, $p<0.0001$; Figure 81). The delivery of NACT, and the response to this, had no influence on these values (data not shown).

A

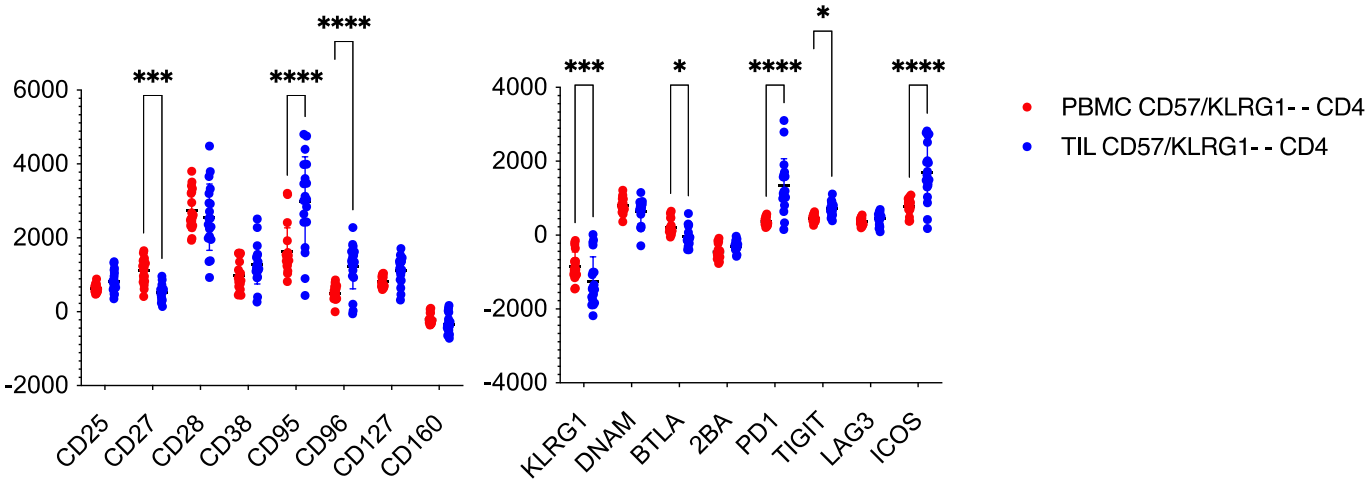
***
****
****
***
*
****
*
****
6000
4000
2000
0
-2000
4000
2000
0
-2000
-4000
CD25
CD27
CD28
CD38
CD95
CD96
CD127
CD160
KLRG1
DNAM
BTLA
2BA
PD1
TIGIT
LAG3
ICOS
PBMC CD57/KLRG1- - CD4
TIL CD57/KLRG1- - CD4

B

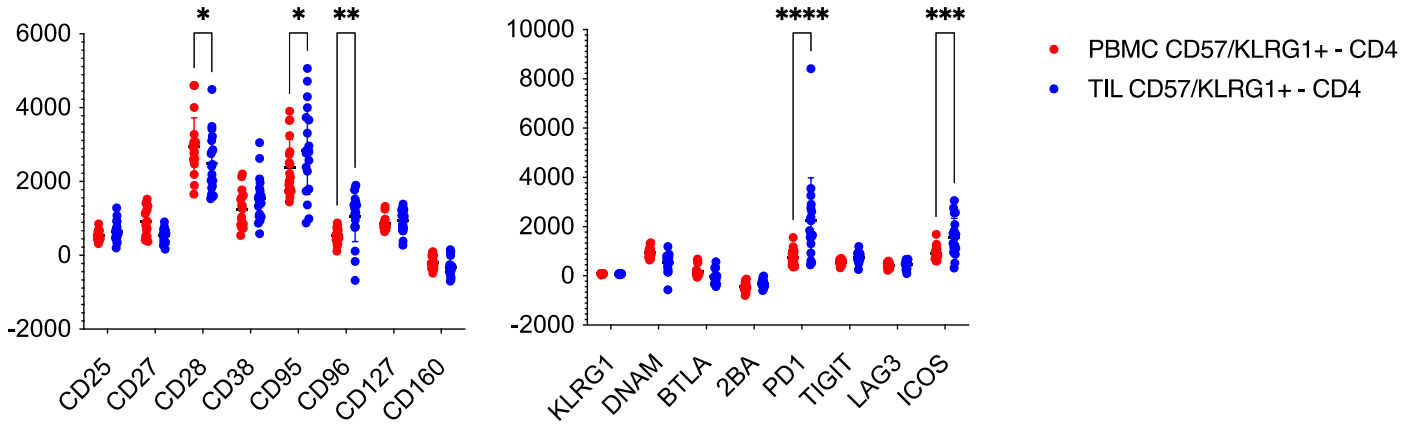
*
*
**
****
***
6000
4000
2000
0
-2000
10000
8000
6000
4000
2000
0
-2000
CD25
CD27
CD28
CD38
CD95
CD96
CD127
CD160
KLRG1
DNAM
BTLA
2BA
PD1
TIGIT
LAG3
ICOS
PBMC CD57/KLRG1+ - CD4
TIL CD57/KLRG1+ - CD4

C

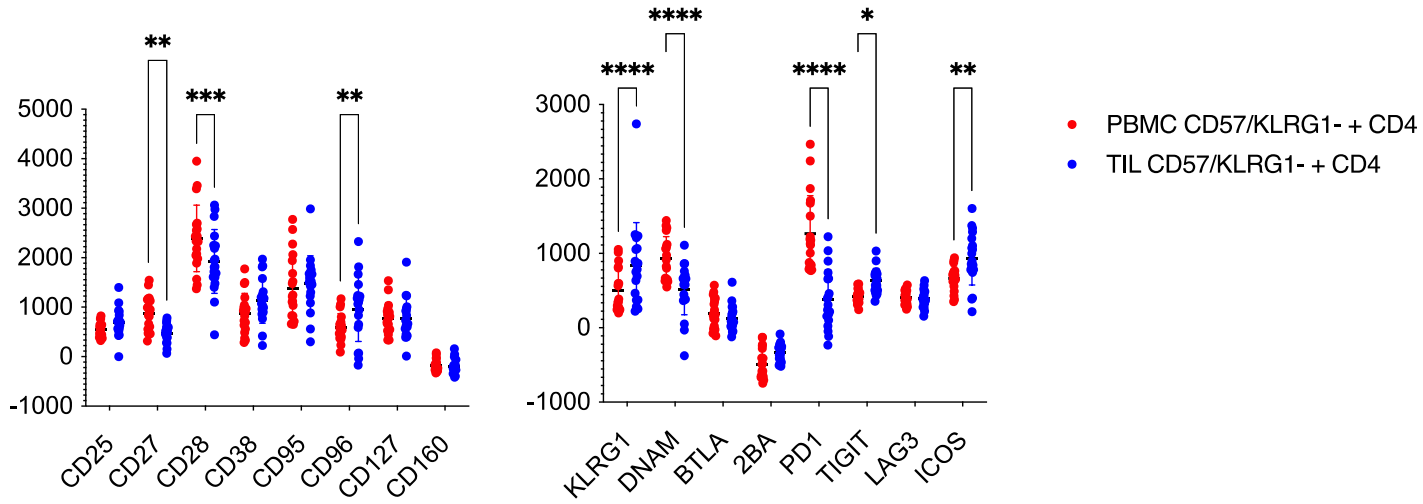

D

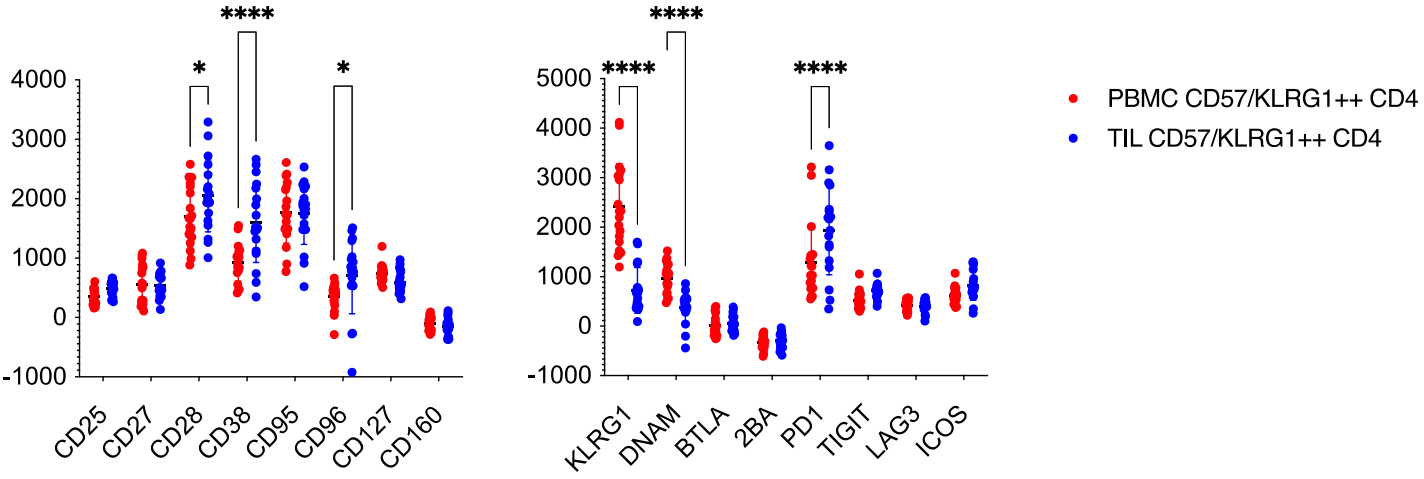

Figure 80. Phenotypic analysis of matched CD4+ PBMC and TIL in relation to differentiation status

Geometric mean expression of cell surface markers of CD4+ T cells. Comparative assessment of matched patient PBMC and TIL for CD57-/KLRG1- CD4+ T cells (A); CD57+/KLRG1- CD4+ T cells (B); CD57-/KLRG1+ T cells (C); and CD57+/KLRG1+ CD8+ T cells (D). Each symbol represents an individual patient. Data analysed by Sidak's multiple comparison test, *denotes $p<0.05$, ** $p<0.01$, *** $p<0.001$ and **** $p<0.0001$.

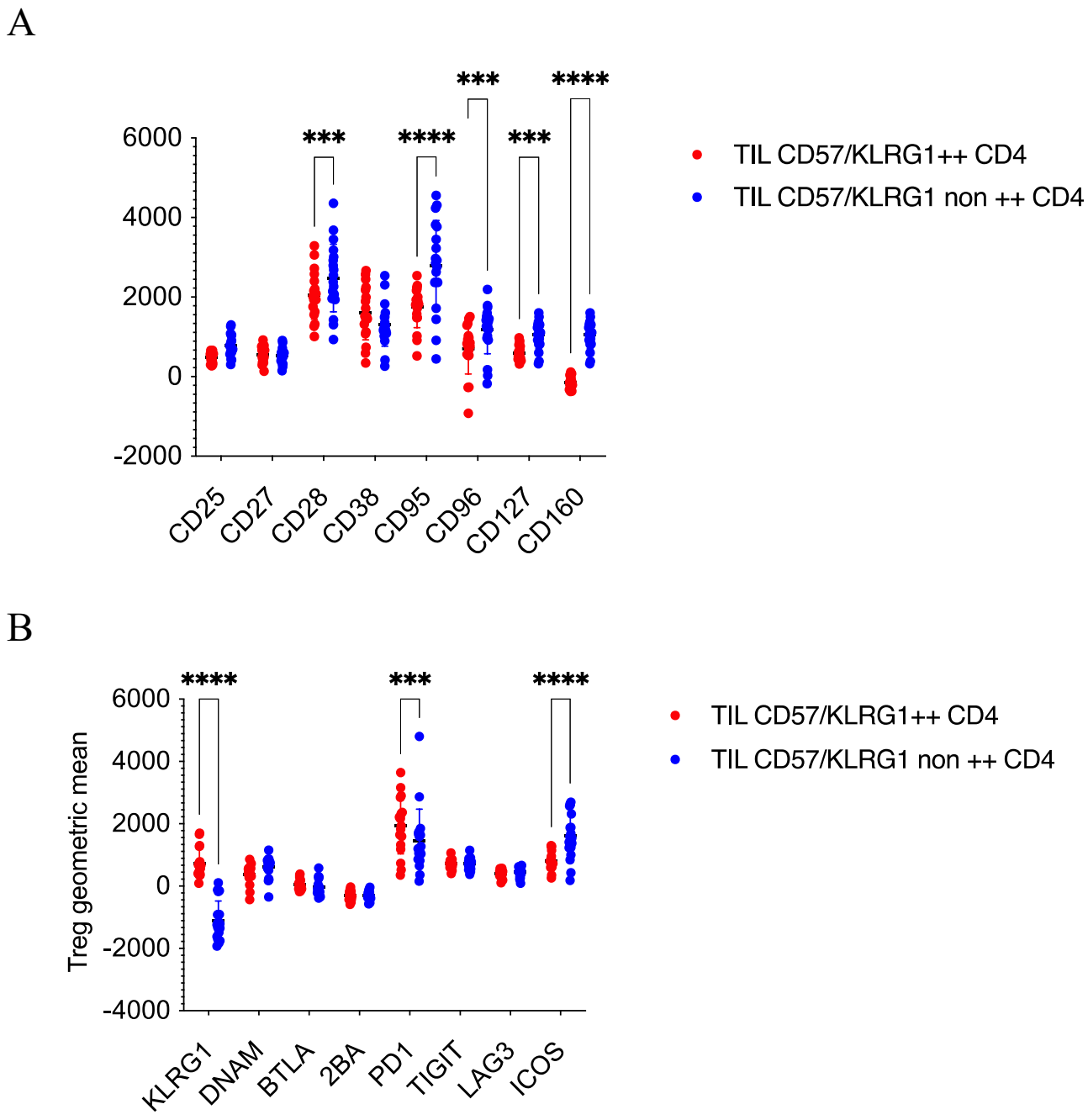

Figure 81. Deep phenotypic variation in terminally differentiated CD4 TIL.
Geometric mean expression of cell surface markers of CD4+ TIL. Comparative assessment of CD57+/KLRG1+ T cells and non CD57+/KLRG1+ Treg (CD57-/KLRG1- ,CD57+/KLRG1- CD57-/KLRG1+). Each symbol represents an individual patient. Data analysed by Sidak's multiple comparison test, *denotes $p<0.05$, ** $p<0.01$, *** $p<0.001$ and **** $p<0.0001$.

Phenotypic Analysis of Tissue Resident Memory CD4+ T cells

Next, I analysed data from the extended flow cytometry panel in relation to expression on TRM CD4+ T cells. Of note, the activation-associated markers CD38, CD96 and PD-1 were all increased on the TRM subset ($p<0.0001$, $p<0.0001$, $p<0.0001$) whilst CD28 expression was reduced ($p<0.0001$). These differences were maintained after neoadjuvant chemotherapy. No phenotypic differences were seen on TRM or non-TRM CD4+ T cells in relation to exposure to chemotherapy or response to chemotherapy (data not shown).

\

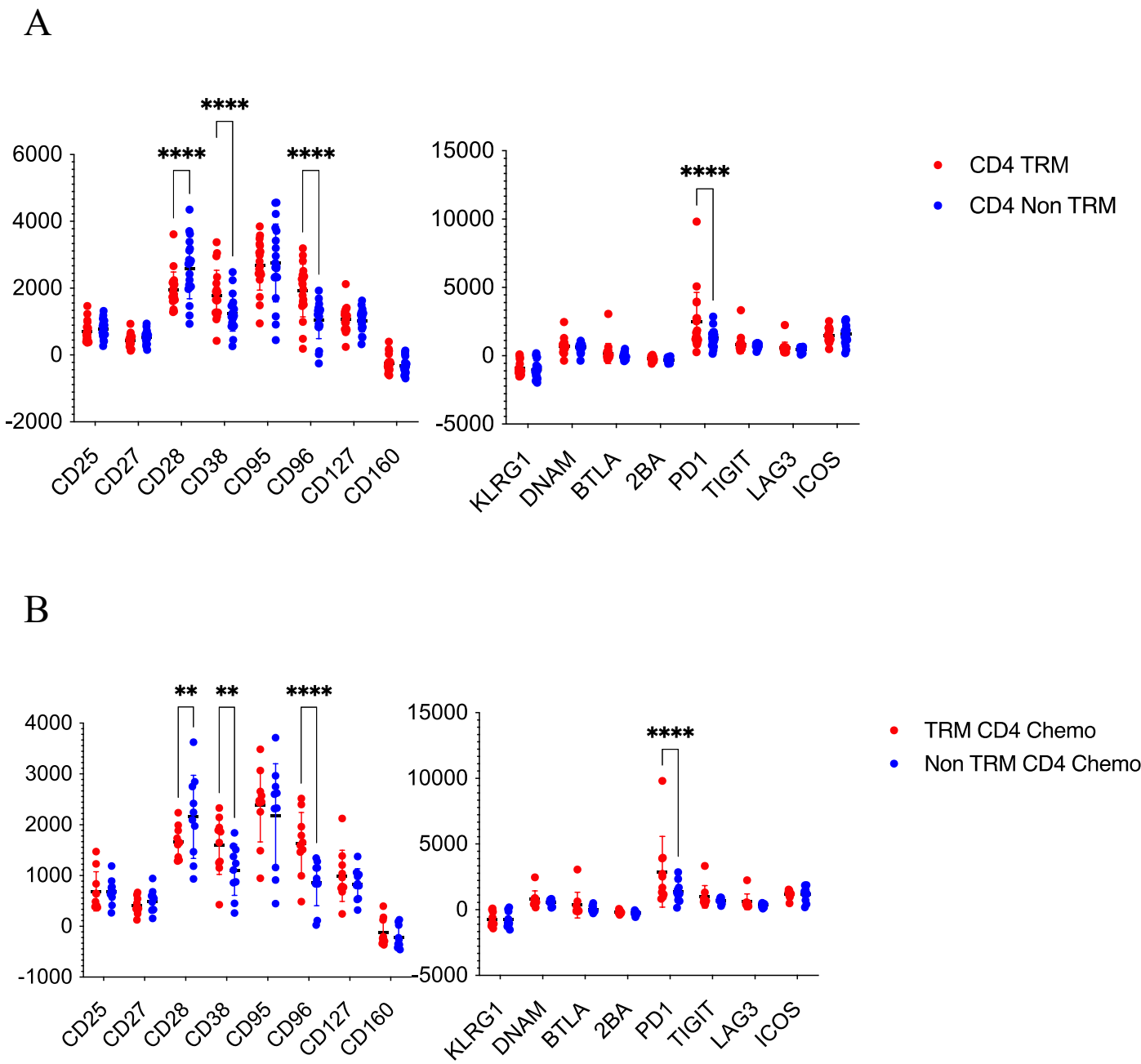

Figure 82. Phenotypic analysis of tissue resident memory CD4+ TIL.
Geometric mean expression of expression of cell surface markers on CD4+ TIL. Comparative assessment of TRM CD4+ TIL and non-TRM CD4+ TIL(A) and specifically for patients who had received neoadjuvant chemotherapy (B). Each symbol represents an individual patient. Data analysed by Sidak's multiple comparison test, **denotes $p<0.01$, **** $p<0.0001$.

Phenotypic analysis of T regulatory CD4+ T cells

The next analysis was an assessment of the extended membrane phenotype of T regulatory cells. Striking differences in the phenotype of Treg TILs were seen in comparison to Treg within PBMC. In particular, CD38, DNAM, PD-1, TIGIT and ICOS were markedly increased on TIL populations ($p=0.004$, $p<0.0001$, $p=0.001$, $p<0.0001$, $p<0.0001$).

This profile was broadly maintained in all Treg memory subsets whilst CD95 expression was selectively increased on the TEMRA subset (Figure 84).

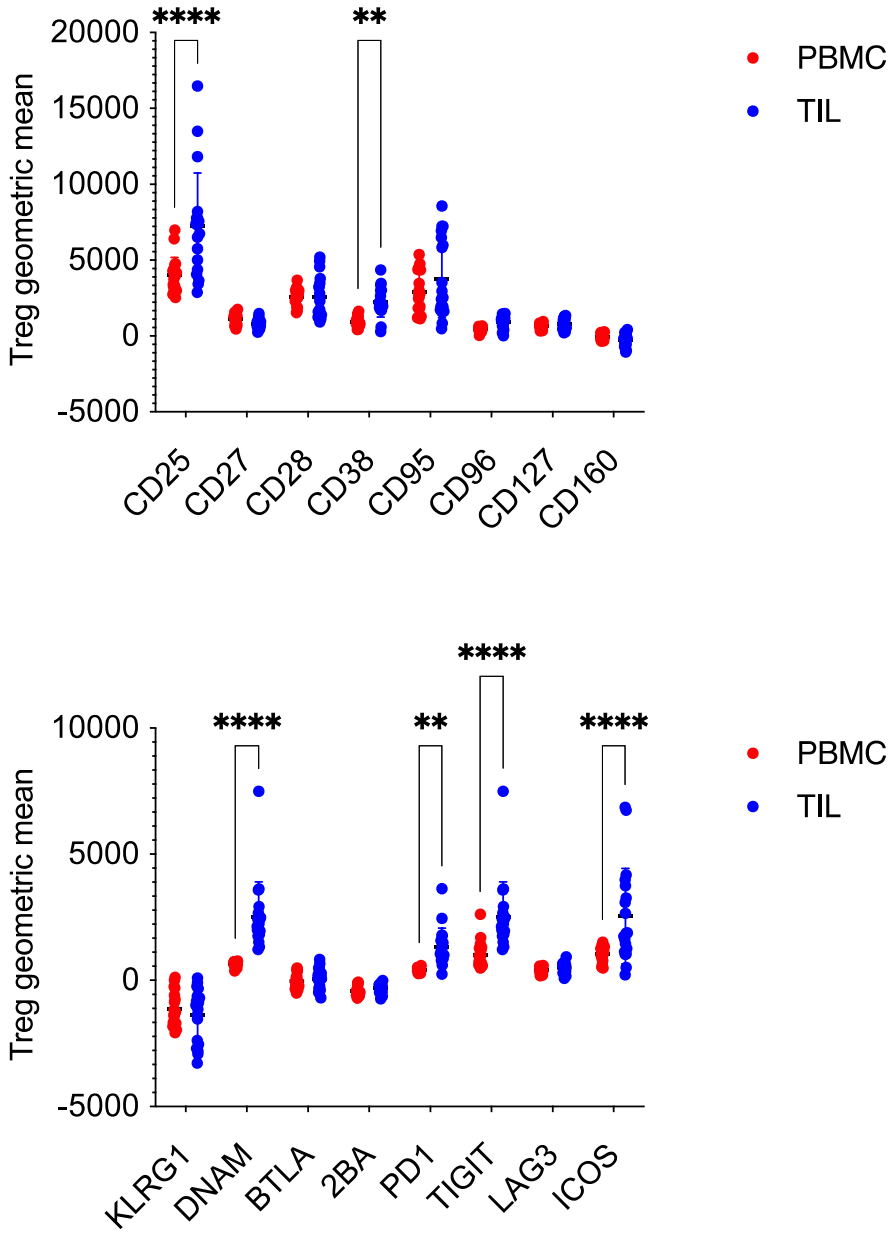

Figure 83. Phenotypic analysis of matched PBMC and TIL T regulatory cells
Geometric mean expression of cell surface markers of Treg cells. Each symbol represents an individual patient. Data analysed by Sidak's multiple comparison test, *denotes ** $p<0.01$ and **** $p<0.0001$.

A

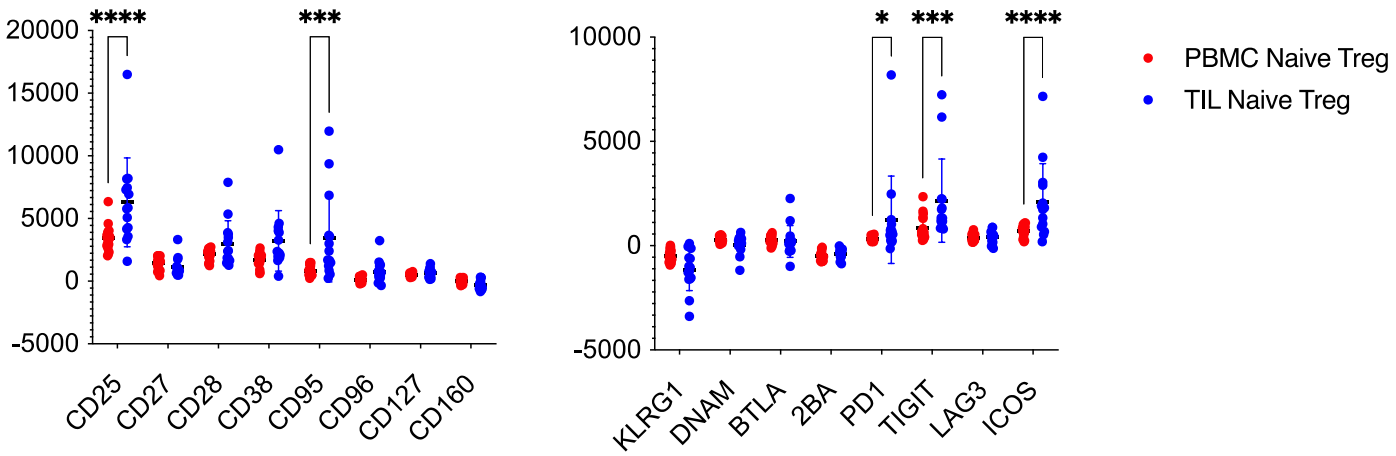
20000
15000
10000
5000
0
-5000
****
***
CD25
CD27
CD28
CD38
CD95
CD96
CD127
CD160
10000
5000
0
-5000
*
***
****
KLRG1
DNAM
BTLA
2BA
PD1
TIGIT
LAG3
ICOS
PBMC Naive Treg
TIL Naive Treg

B

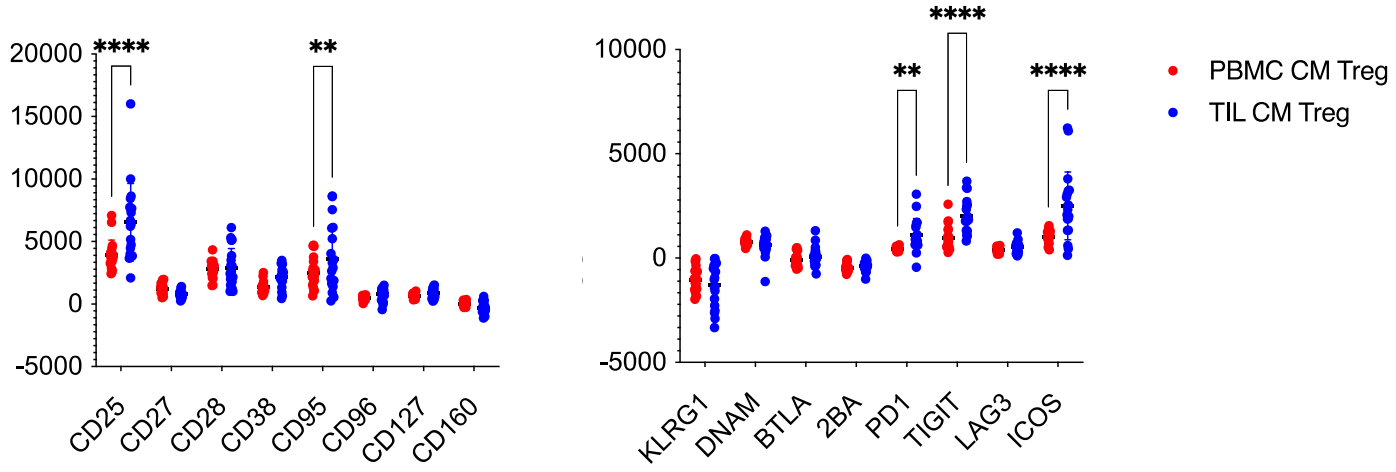
20000
15000
10000
5000
0
-5000
****
**
CD25
CD27
CD28
CD38
CD95
CD96
CD127
CD160
10000
5000
0
-5000
**
****
****
KLRG1
DNAM
BTLA
2BA
PD1
TIGIT
LAG3
ICOS
PBMC CM Treg
TIL CM Treg

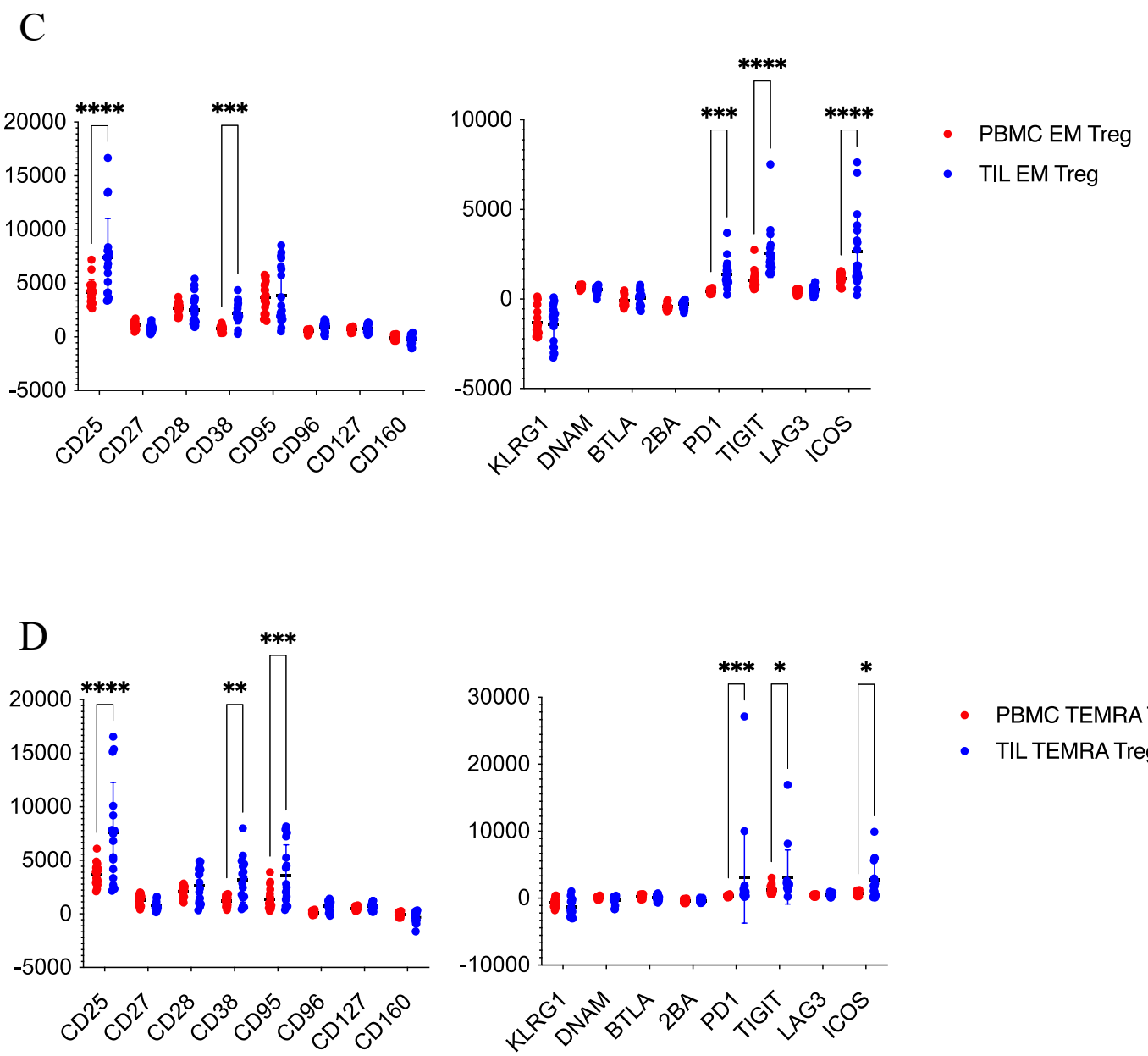

Figure 84. Phenotypic analysis of matched PBMC and TIL T regulatory cells in relation to memory phenotype.

Geometric mean expression of cell surface marker expression on T reg. Comparative assessment of matched patient PBMC and TIL for naïve (A), central memory (B), effector memory (C) and TEMRA (D) subsets.

Each symbol represents an individual patient. Data analysed by Sidak's multiple comparison test, *denotes $p<0.05$, ** $p<0.01$, *** $p<0.001$ and **** $p<0.0001$.

Phenotypic expression of T regulatory cells in relation to markers of terminal differentiation

Co-expression of inhibitory and stimulatory checkpoints was next examined in relation to expression of CD57 and KLRG1 on Treg. A range of minor differences were observed within these four subsets (Figure 85). Comparison of 'terminally differentiated' Treg cells (defined as CD57+KLRG1+) and 'non-terminally differentiated' Treg (defined as phenotypes CD57-KLRG1-, CD57+KLRG1- and CD57-KLRG1+) showed that the former upregulated PD-1 ($p=0.005$) whereas expression of CD95 and ICOS was lower ($p<0.0001$, $p<0.0001$).

Administration of chemotherapy, and response to chemotherapy, did not influence the phenotypic profile of the regulatory T cell pool (data not shown).

A

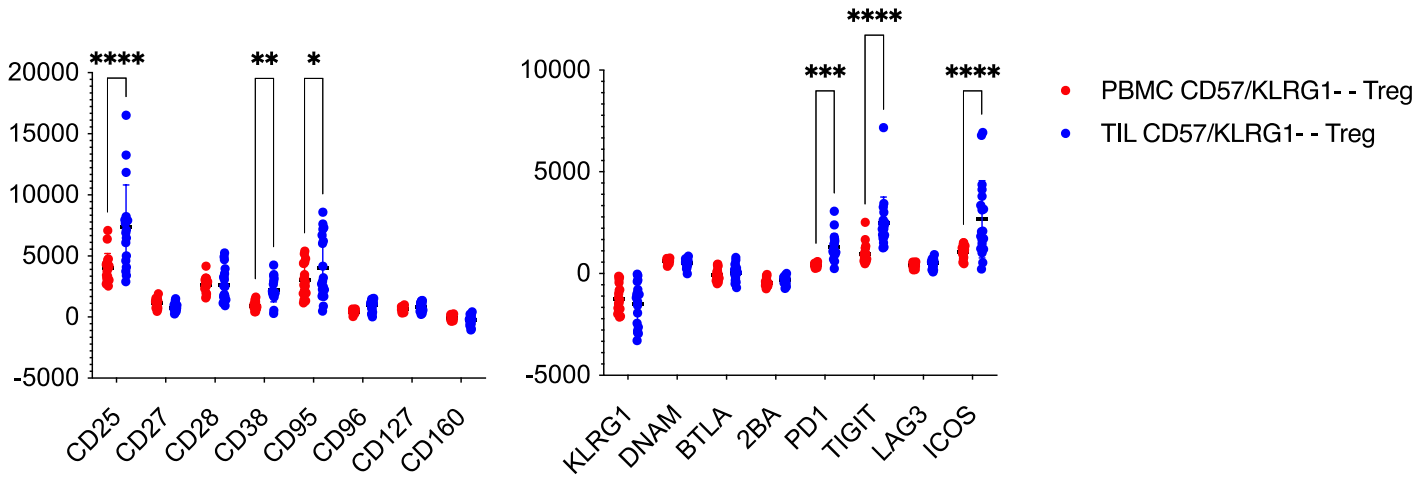
20000
15000
10000
5000
0
-5000
****
**
*
CD25
CD27
CD28
CD38
CD95
CD96
CD127
CD160
10000
5000
0
-5000
***
****
****
KLRG1
DNAM
BTLA
2BA
PD1
TIGIT
LAG3
ICOS
PBMC CD57/KLRG1- - Treg
TIL CD57/KLRG1- - Treg

B

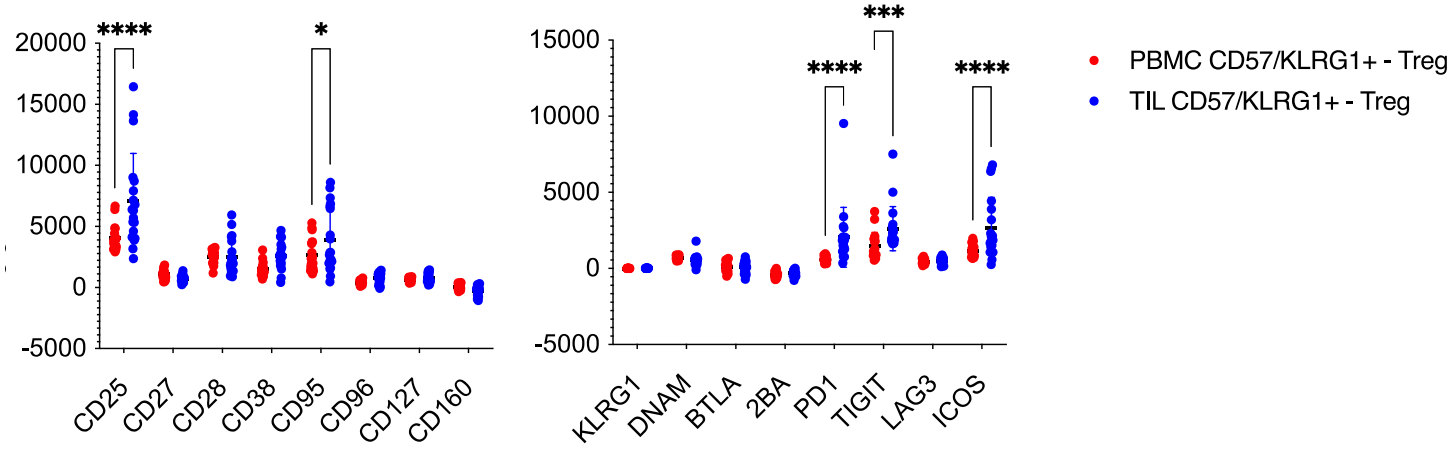
20000
15000
10000
5000
0
-5000
****
*
CD25
CD27
CD28
CD38
CD95
CD96
CD127
CD160
15000
10000
5000
0
-5000
***
****
****
KLRG1
DNAM
BTLA
2BA
PD1
TIGIT
LAG3
ICOS
PBMC CD57/KLRG1+ - Treg
TIL CD57/KLRG1+ - Treg

C

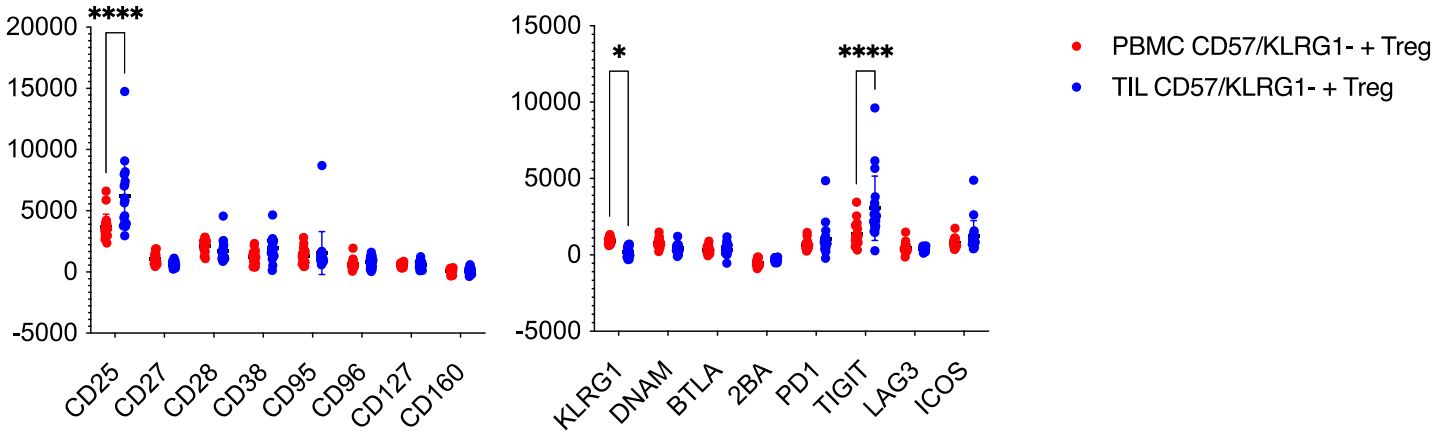

D

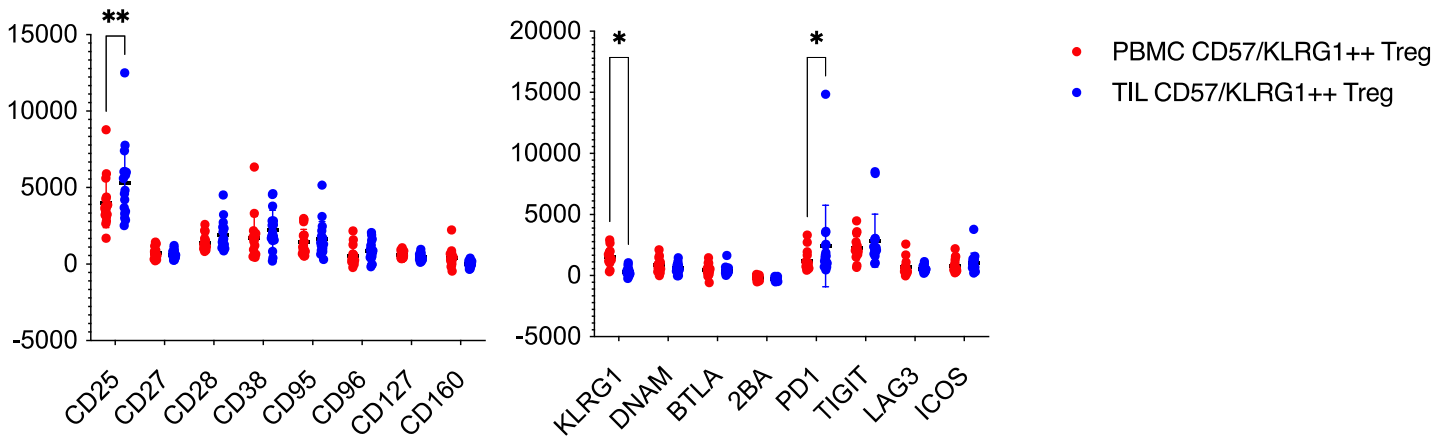

Figure 85. Phenotypic analysis of matched PBMC and TIL T reg in relation to profile of terminal differentiation

Geometric mean expression of cell surface markers of Treg. Comparative assessment of matched patient PBMC and TIL for CD57-/KLRG1- (A); CD57+/KLRG1- (B); CD57-/KLRG1+ (C) and CD57+/KLRG1+ (D). Each symbol represents an individual patient. Data analysed by Sidak's multiple comparison test, *denotes $p<0.05$, ** $p<0.01$, *** $p<0.001$ and **** $p<0.0001$.

A

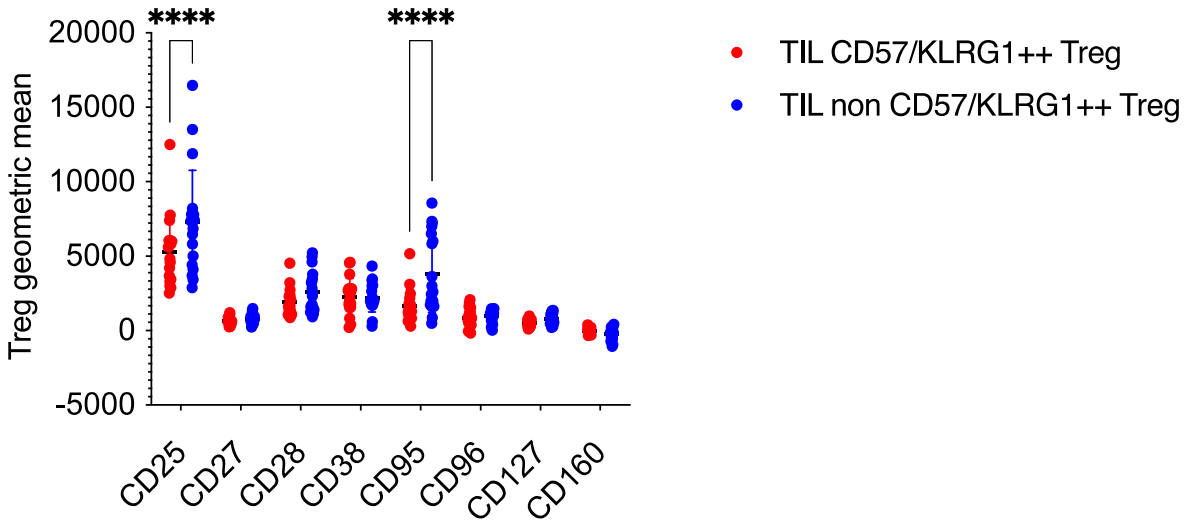

B

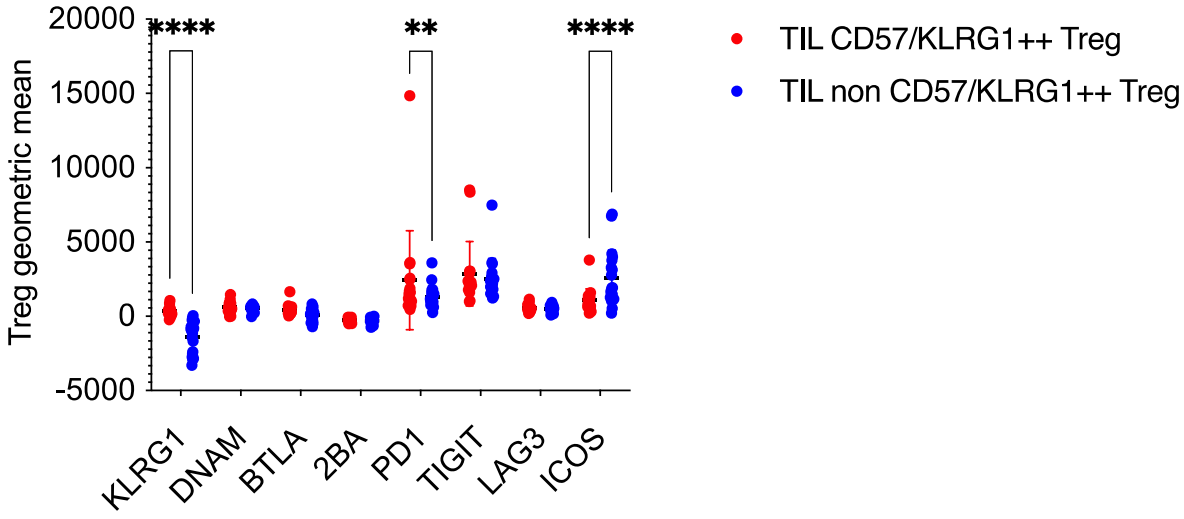

Figure 86. Phenotypic analysis of terminally differentiated T reg TIL in relation to differentiation status

Geometric mean expression of cell surface markers of T reg. Comparative assessment of CD57+/KLRG1+ T cells and 'non-CD57+/KLRG1+' T reg (CD57-/KLRG1- ,CD57+/KLRG1- CD57-/KLRG1+). Each symbol represents an individual patient. Data analysed by Sidak's multiple comparison test, *denotes $p<0.05$, ** $p<0.01$, *** $p<0.001$ and **** $p<0.0001$.

Phenotypic analysis of Tissue Resident Memory T regulatory cells

Analysis of phenotype of T regulatory cells in relation to TRM status showed that TIGIT expression was increased on the TRM ($p=0.0001$) and this was not altered by chemotherapy status (Figure 87). When the TRM subset was analysed specifically it was clear that there was no difference in TIGIT expression in relation to chemotherapy delivery. However, patients who gained a pathological response showed a significant reduction in TIGIT expression ($p=0.047$).

A

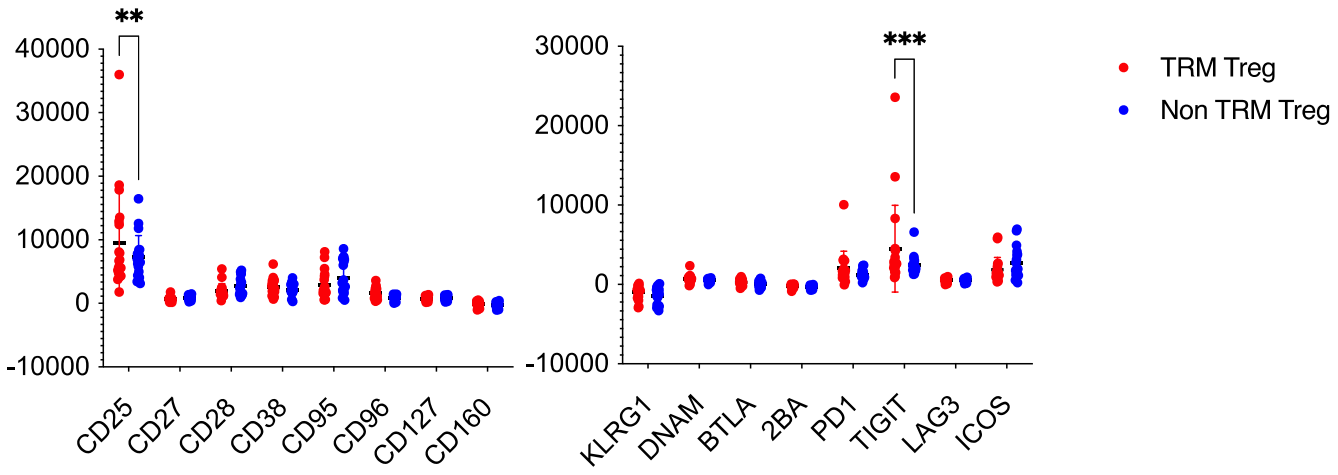
**
***
40000
30000
20000
10000
0
-10000
CD25
CD27
CD28
CD38
CD95
CD96
CD127
CD160
KLRG1
DNAM
BTLA
2BA
PD1
TIGIT
LAG3
ICOS
TRM Treg
Non TRM Treg

B

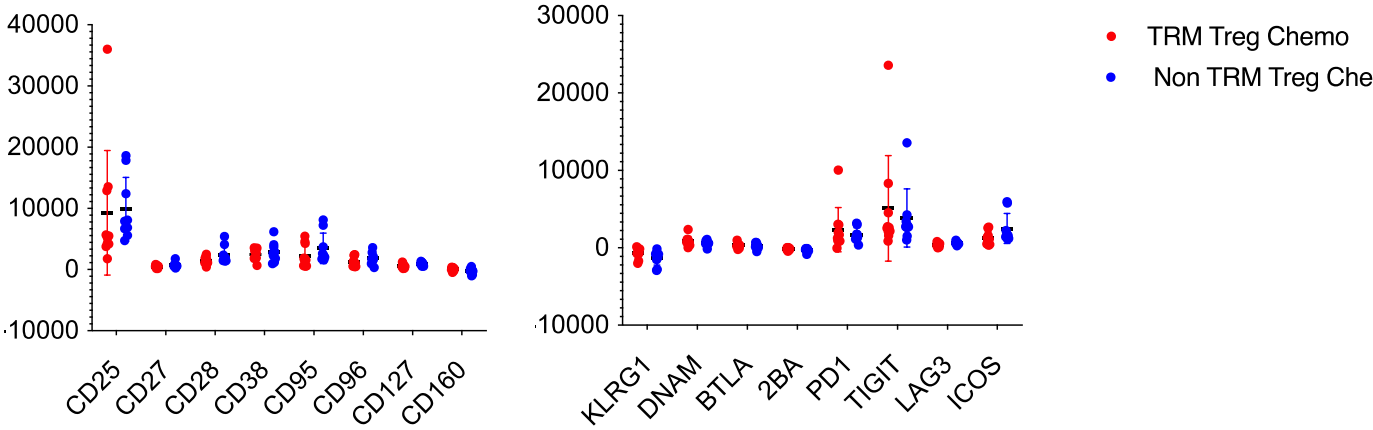
40000
30000
20000
10000
0
-10000
CD25
CD27
CD28
CD38
CD95
CD96
CD127
CD160
KLRG1
DNAM
BTLA
2BA
PD1
TIGIT
LAG3
ICOS
TRM Treg Chemo
Non TRM Treg Che

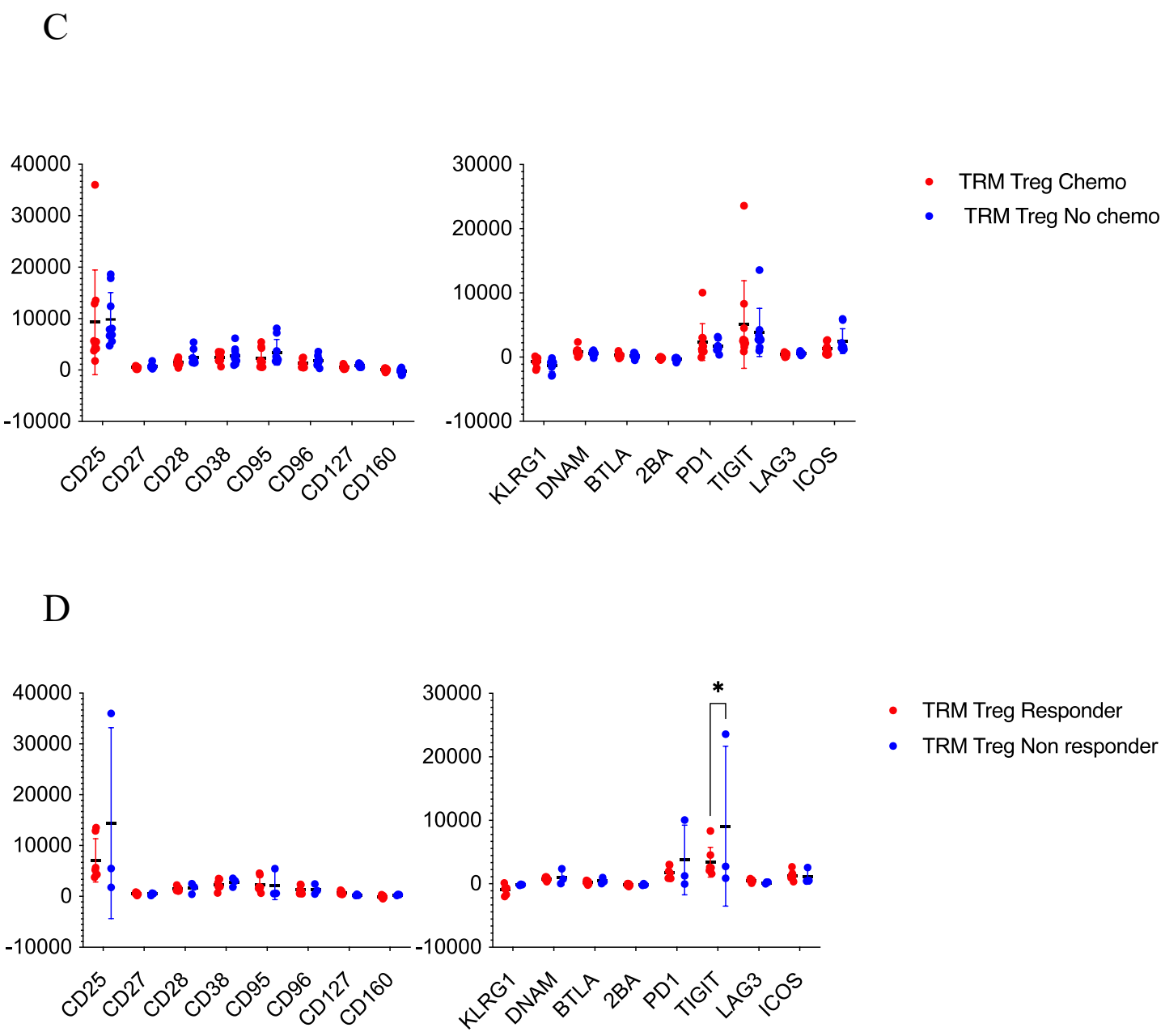

Figure 87. Phenotypic analysis of tissue resident memory T regulatory cells
Geometric mean expression of cell surface markers of T reg TIL. Comparative assessment of TRM Treg and non-TRM Treg (A) and specifically for patients who had received neoadjuvant chemotherapy (B). Each symbol represents an individual patient.
Comparative assessment of TRM Treg TIL for patients who have and have not received neoadjuvant chemotherapy(C) and for patients who have and have not responded to neoadjuvant chemotherapy when administered (D, responders are defined as Mandard score 1-3).
Each symbol represents an individual patient. Data analysed by Sidak's multiple comparison test, *denotes $p<0.05$, ** $p<0.01$.

Discussion

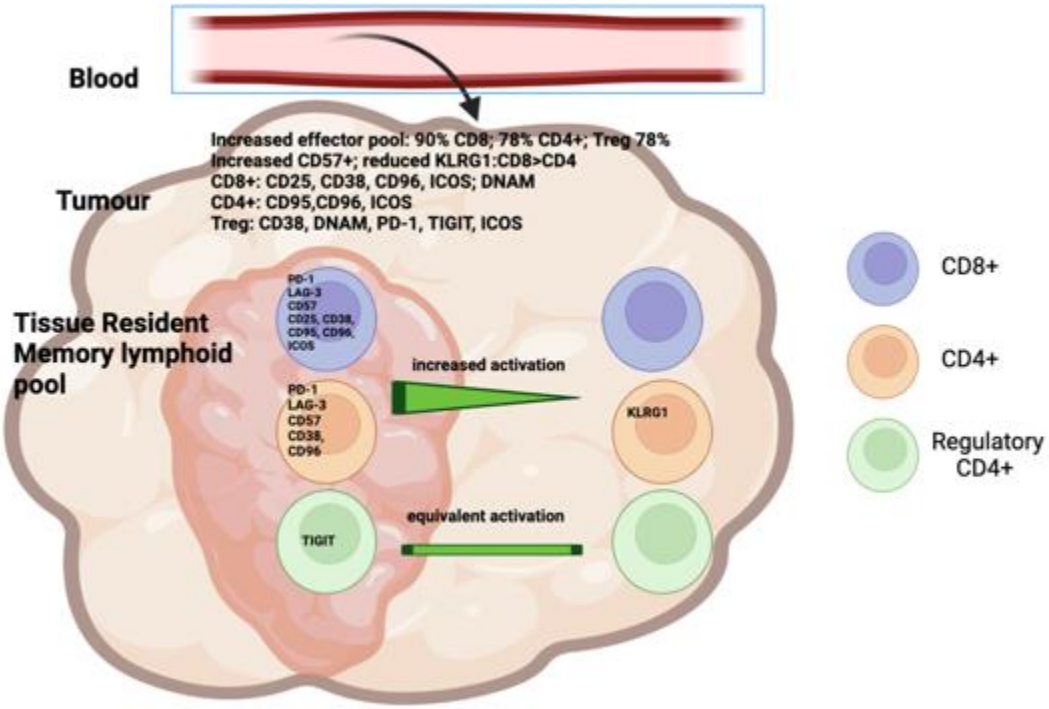

Figure 88- Phenotypic variances in oesophageal adenocarcinoma PBMC and TIL

Within this chapter I took advantage of the development of a broad flow cytometry panel that contained antibodies against a wide range of membrane proteins. I had already established CD4+, CD8+ and T reg cells all upregulate phenotypic features of exhaustion including PD1, TIGIT and TIM-3. Furthermore, highly proliferative cells identified in transcriptional analysis have shown phenotypic features of tissue residency.

Through this extended panel I was able to interrogate a range of phenotypic features of CD8+, CD4+ and T regulatory cells within the tumour micro environment. Specifically, I was interested to focus in further on tissue resident memory populations and view their phenotype in relation to T-cells outside the tissue resident pool.

In my initial studies I assessed the memory phenotype of T cell populations within the tumour microenvironment compared to blood. For all cell types there is a significant reduction in naïve cells, equivalent numbers of central memory cells, and increased effector memory cells in TIL. In contrast the proportion of effector cells that express CD54RA, potentially as a reflection of lack of recent peptide engagement, was markedly lower within tumour and indicates a pattern of ongoing engagement with antigen. Multispectral Vectra analysis has shown increased populations of CD45R0+memory TIL in intraepithelial regions of OAC although more detailed correlations with my study are limited partly as some markers are shared by the subpopulations of memory and effector T cells[186]. Interestingly, the infiltration level of memory T cells was found to be positively correlated with that of the DCs, but negatively with that of PD-L1-expressing subpopulations, potentially suggesting that activation classical DC populations is a mediator of T cell enrichment and expansion. Furthermore, CD45R0+ density has been shown in IHC studies to correlate with an improved outcome independent of clinicopathological factors[187,188]

Comparable studies in squamous cell oesophageal cancer have also shown that effector memory T cells comprise the largest memory population although we find central memory cells to predominate in OAC whilst TEMRA were dominant in OSCC[94]. The CCR7 axis plays a significant role in controlling the migration of tumour cells toward the lymphatic system and metastasis and can therefore contribute to cancer progression. The increased prevalence of CCR7+CD45RA- central memory CD4 and CD8 T cells in OAC opens up opportunities for CCR7-mediated immunotherapy as has been suggested in the literature[189].

An important aspect of this chapter was my ability to interrogate the phenotype of T cells in OAC in relation to the prior use of neo-adjuvant chemotherapy. Analysis of circulating T cells post-oesophagectomy has demonstrated a switch in balance towards a Th2 and

potentially M2 phenotype[190]. M2 reprogramming toward an M1 phenotype and similarly shifting the balance in favour of a Th1 phenotype would offer a potent therapeutic approach for augmenting tumourigenesis and promoting cancer regression. In combination such improved peri-operative understanding of immune variance can augment the design of perioperative immunotherapy trials. Of interest, my findings showed broadly that the use of neo-adjuvant chemotherapy did not have a marked impact of the profile of T cells within the OAC microenvironment.

Tumour infiltrating lymphocytes contained a much higher percentages of effector populations although these varied somewhat between the CD8+ and the CD4+ T cell pool. In particular, 90% of CD8+ T cells had an effector phenotype whilst this value was 78% within the CD4+ effector and regulatory populations. This may potentially indicate that CD8+ T cells are more driven to differentiation within the tumour microenvironment, although CD4+ populations may reside to a higher level within the central memory pool. The latter is able to gain entry to lymphoid tissue, and can provide the basis for subsequent differentiation of effector populations.

The selective distribution of T cell memory subsets within tumour and lymphoid tissue, in untreated cancer patients and after therapy, has been shown in several studies. Following the use of PD-1 checkpoint inhibition in advanced gastric cancer a population of central memory CD103+PD1+ $CD8^+$ T cells in blood was associated with good outcome whilst effector cells with a similar phenotype were observed among TILs [181]. Circulating PD1- CD T cells showed limited variation in memory phenotype transition after Nivolumab treatment. PD1+CD8 however showed significant variation, CM CD8 increased progressively over time (pre-treatment, 2 then 6 weeks post-treatment), EM initially increased and subsequently

declined and TEMRA reduced progressively from pre-treatment levels. Treg have been highlighted as immunosuppressive component of the TME and treatments have developed to target Treg and reverse features of exhaustion within the TME.

A particular focus was on the relative distribution of markers of late differentiation on the T-cell subsets. I choose CD57 and KLRG1 as appropriate markers to assess this. CD57 is a carbohydrate epitope that is expressed on late differentiated lymphoid subsets, although its physiological significance remains uncertain. KLRG1 is also a marker of late differentiation and has a well established role as a ligand for E-cadherin and N-cadherin.

The use of multi parametric flow cytometry allowed me to look at the co-expression of these two proteins and I took dual CD57 and KLRG1 expression to represent a late differentiated pool. Indeed, CD57 and KLRG1 expression is increasingly understood to infer immune sensecence[184,191,192]. Although expression of CD57 and KLRG1is associated with cells of a limited proliferative capacity, a finding of high checkpoint protein expression suggests the potential requirement to suppress ongoing functional activity, such as cytotoxicity or cytokine production[185,193,194]. Infiltration of CD57+ in TIL has been shown to potentially be associated with an improved overall survival in patients with cancer[195].

The use of these markers revealed that CD57 was expressed to a higher level on tumour infiltrating lymphocytes compared to peripheral lymphoid cells, whilst the reciprocal pattern was seen in respect to KLRG1 which was reduced on all memory phenotypes in CD8+ TIL. Low level expression of KLRG1 has also been shown in other immunosensitive cancers such as renal cell carcinoma[196] although breast, colon and melanoma tumour models suggest that 16–48% of $CD8^+$ TIL can express this molecule[197]. Murine models of melanoma and breast cancer have shown that KLRG1 inhibition promotes greater local and distant control of metastatic disease[198] and inhibition has also been shown to further improve tumour control in

conjunction with PD-1 blockade. As such, despite low levels of KLRG1 on T cells in TIL its presence in association with PD1 upregulation may make it a suitable target in oesophageal adenocarcinoma.

I was also interested to assess the expression of activation markers within blood and the tumour microenvironment. The CD8+ population within the tumour expressed a wide range of activation markers including CD25, CD38, CD 96 and ICOS. Of note, expression of DNAM was reduced on the CD8+ pool. High level expression of the checkpoint proteins PD-1 and TIGIT confirmed previous findings from my work.

This broad pattern of activation marker expression was seen on most memory subsets within the CD8+ pool. Indeed, it was notable that increased activation markets were seen on the naive CD8+ population. This may indicate that these cells are not truly 'naïve' but have reverted to a naive phenotype following antigen engagement. Alternatively, this may represent engagement with inflammatory cytokines within the tumour microenvironment. CD38, and CD96 were particularly elevated markers on CD8+ populations and were seen on all memory subsets

Effector CD4+ T cells were also examined and defined as CD4+ T cells which did not have a CD25+CD127- phenotype. Again, there was evidence of strong activation within the tumour microenvironment although the pattern was somewhat different from that seen on CD8+ populations. In particular, CD4+ cells express higher levels of CD95, CD96, and ICOS with the last two markers being particularly high on the effector CD4+ pool.

It was notable that the activation profile on T regulatory cells was somewhat different. Increased markers of activation included CD38 and ICOS whilst the checkpoint markers PD-1 and TIGIT were also elevated. A marked difference with the effector pool was that expression of DNAM-1 was increased on regulatory cells whilst its expression on the effector pool had been low.

I then went on to assess how markers of late differentiation were co-expressed in relation to this activation profile. There was relatively little difference between the subsets although expression of activation markers was reduced on the CD57+KLRG+ dual population. potentially indicating that late differentiated cells were resistant to activation.

Within the CD4+ pool it was also notable that activation markers were generally less expressed on the late differentiated pool although PD-1 was actually higher on dual positive cells within the regulatory pool, suggesting that PD-1 may be a marker of late differentiation.

Finally, I assessed expression of these activation markers on the tissue resident memory population. In order to do this, I defined tissue resident memory lymphocytes (TRM) through co-expression of CD103 and CD69. Within the CD8+ pool there was strong increased expression of activation markers on the TRM pool, including CD25, CD38, CD95, CD96, and ICOS. A similar profile was seen on the effector CD4+ TRM population with high levels of CD38, CD96 and PD-1.

However, comparison of the T regulatory pool showed that it was notable that there was no major difference in the activation status of regulatory cells within the TRM or non-TRM pools. Indeed, the only difference was a higher level of the inhibitory TIGIT protein on the TRM pool. There was also an indication that a decrease in the expression of this protein was associated with good pathological response to chemotherapy.

These observations raise a number of interesting questions regarding the tumour microenvironment in OAC. Broadly, they indicate that the tissue resident memory (TRM) effector T cell pool is more highly activated than the non-TRM population.

The reasons for this are not clear, but it may suggest that the antigenic specificity of TRM cells is more focussed on tumour specificity and therefore receives continual antigenic engagement. TRM populations can be retained within tissue for many years and it is unclear

if this tumour-specificity has been maintained over the long term or if the TRM phenotype reflects capture of recently circulating effector cells into a tissue residency pool.
As such, the effectiveness of checkpoint blockade may therefore be particularly determined by its ability to reverse exhaustion within the TRM pool and enhance effector function. A focussed ability to target checkpoint blockade towards TRM populations could be aspiration for future therapy.

To what extent non TRM T cells contribute to tumour regression is less well understood. Data shows that tumours can possess a wide range of frequencies and phenotypes of bystander infiltrating $CD8^+$ T cells[174,175,183]. Bystander memory $CD8^+$ T cells are specifically recruited to sites with activated antigen-presenting cells (APCs) in a CXCR3-dependent manner as CXCR3 is necessary both for T cell clustering around APCs and for activation of bystander lymphocytes[199]. T cells within the TME are typically refractory to stimulation with tumour antigen and chronic antigen stimulation markedly impairs their ability to respond to PD-1 blockade [200].
There is increasing interest in the biological importance of 'bystander' activated T cells and they appear to have an important role in many settings, including infection. Expression of NK-associated receptors such as NKG2D can overcome the need for antigenic specificity and these cells typically show significant functional capacity with upregulation of Granzyme B and IFN-g secretion[201–203]. CD8 memory T cells are also susceptible to negative feedback and evidence suggest they may be increasingly sensitive to anti-inflammatory cytokines such as IL-10 rather than TCR mediated pathways[204]. TCR-mediated pathways are still relevant in CD8 memory T cells albeit to a lesser degree exhibiting PD-1 and CTLA-4 upregulation[205]. Further study is required to determine the opportunities for bystander T cells to promote tumour regression through immunotherapy modulation.

Treatment of OAC with PD1/PD-L1 checkpoint blockade has proven effective but there remains considerable scope for improvement[82,153]. CD38 was seen to be expressed at high level on T cells within OAC tumours and it is noteworthy that upregulation of CD38, which acts both as a receptor and an enzymatic regulator of NAD+ levels, may represent a potential mechanism of resistance to checkpoint therapy[206]. CD38 expression was particularly high on TRM populations, in all CD8+ memory subsets, and in non-senescent populations. Inhibition of CD38 may therefore be a potential mechanism for limiting immunotherapy resistance.
An additional notable feature was that CD28 expression was reduced on TRM subsets of both CD4+ and CD8+ effector cells. CD28 is an important co-stimulatory molecule and interacts with directly with PD-1. Studies in non small cell lung cancer have shown that CD28-PD1+ CD8 TIL are relatively resistant to PD1 blockade and exhibit characteristics of terminally exhausted $CD8^+$ T cells with low TCF1 expression. This study also showed that this population was responsive to IL-15 and as such treatment with this cytokine may potentially act to enhance PD1 inhibitor efficacy[207]. CD27 expression was also reduced on CD4+ TIL which is notable as CD27 agonism is currently undergoing phase 1 trials in cancer therapy [208].

TRM also upregulated expression of Fas (CD95) which can induce apoptosis following engagement with FasL. This might suggest that TRM cells are susceptible to increased levels of apoptosis although the significance of Fas expression on T cells in relation to cell survival is uncertain and depends on cellular context[209]. The level of CD95L expression in OAC is currently unknown but now represents an important topic for future investigation.

ICOS was also upregulated on effector cells in tumour and, although little is known about the relevance of ICOS in OAC, data in OSCC indicate that upregulation of ICOS correlates strongly with improved overall survival[141]. Initial reports in OAC indicate that ICOS expression can decrease after neoadjuvant chemotherapy although I did not see any

alterations in checkpoint expression in my study[210]. Indeed, this absence of significant change differs somewhat from our transcriptomic analysis which did identify an upregulation of checkpoint and exhaustion cell signatures. The transcriptomic data is consistent with prior evaluation of immune related genes using the NanoString PanCancer Immune Profiling Panel which showed increased expression of PD-1, CTLA-4 and TIM-3 within OAC tumours although no difference was seen when comparing treatment naïve TIL and post neoadjuvant TIL[98]. Overall neither flow cytometry analysis or transcriptomics have shown checkpoint reduction after oncological treatment leaving the door open for combined chemotherapy/immunotherapy trials.

In contrast, T regulatory cells were highly expressed in both the TRM and non-TRM populations. T regulatory populations are thought to have a different profile of antigenic recognition compared to effector cells and it is possible that this is a determinant of this more broadly dispersed activation profile within the tumour. T regulatory cells also have a higher basal proliferation rate which may mediate IL-7R downregulation.

T regulatory cells are key modulators of the efficacy of the tumour-specific immune response and the impact of immunotherapy. The mechanisms that underlie the efficacy of PD-1 are uncertain but may include downregulation of intracellular FOXP3, within Treg[211]. PD inhibition has also been shown to both suppress thymus derived Treg but also peripheral Treg as PD1 regulates expression, maintenance and suppressive function of pTreg[212]. I*n vitro* studies has shown that nivolumab can abolish the suppressive effects of Tregs on naive $CD4^+$ T-cell proliferation and also partially restored IFNγ production[213]. Similarly inhibitory checkpoint TIGIT has been shown to maintain the immunosuppressive phenotype of Th1 Tregs[214]. In the setting of melanoma, TIGIT+ Tregs have been shown to have increased immunosuppressive capacity compared to Treg cells without TIGIT expression[215]. Treg profiles in OAC are a key contributor to the exhausted TME and demonstrate potentially

targetable checkpoint for immunotherapy. A range of additional approaches to suppress T reg function are currently being assessed. The anti-CCR4 antibody mogamulizumab is one such approach and has been shown to significantly reduce circulating and TIL Treg in phase 1 trials.[216]

An interesting finding was in relation to checkpoint protein expression where PD-1 and LAG3 were highly expressed on effector populations. In contrast no difference was found in TIGIT expression in relation to tissue resident status although this remained consistently high across both TRM and non-TRM cells. As such, a combinatorial blockade against these markers may potentially act to increase T cell function and act as a valuable therapy in oesophageal cancer.

Expression of DNAM was found to be differentially regulated in the effector and regulatory lymphoid populations. In particular, expression was decreased on effector cells, whilst increased on the regulatory population. These reasons for this are not clear, yet potentially effector populations are increasingly susceptible to antigen specific transcriptional regulator Eomesodermin mediated downregulation as demonstrated in both human and mouse models[217]. NK Downregulation of DNAM has also been attributed to tumour secreted soluble CD155 in hepatic cellular carcinoma. The impact of soluble CD155 on effector T cell populations or within the context of OAC is unknown[218].

The progression in time from chapter 3 to chapter 6 led to further technological improvements and acquisition of equipment with greater analytical potential. The Symphony flow cytometer enabled a 27 colour panel as compared to a 10 colour panel as was possible on the Gallios flow cytometer (chapters 3 and 5). Due to the increased spectral overlap and limited potential fluorophores the panels for chapters 6 and 7 were designed in coordination with BD panel experts. Despite this a number of antibodies conjugations had to made

bespoke for each panel. Despite the technical accuracy of this process and prior testing the antibody binding capacity of not previously well tested antibodies may be questioned. Comparable results in cell types and checkpoint expression did reflect high levels of comparability between Symphony and Gallios panels. The results of the chapter would have been further reinforced by greater specimen numbers and potentially matched pre and post chemotherapy samples which was not possible due to logistic reasons but should be considered when designing further studies.

Overall, this work has helped to define the phenotypic profile of TRM cells within OAC and reveals these to be highly activated, with combinatorial checkpoint expression and low levels of DNAM. A potential therapeutic approach in this disorder may be to target checkpoint molecules within the TRM pool whilst acting to inhibiting T regulatory function.

Conclusion

The differential memory profile in OAC has previously been poorly understood. This study has identified key variation in the PBMC and TIL confirming a phenotypic shift of T cell profiles to effector profiles. T cells however within the TME increasingly progress to a terminally differentiated state that may be limited in their effector capacity. Further confirmation of TRM in OAC TME has been recognised which again show significant features of exhaustion. Tumour specific T cells show significant upregulation of checkpoint which may be susceptible to immunotherapy. A more complex appraisal of stimulatory and inhibitory profiles further emphasises a limited host capacity to eradicate tumour. Despite this however potential pathways of immunotherapy resistance have been identified which could be targeted to deliver a multimodal efficacious treatment regimen.

Chapter 7 – Identification and Recognition of Transcriptomic Profiles in Oesophageal Adenocarcinoma

Introduction

Transcriptomic interrogation and clustering of tumour infiltrating lymphocytes enables greater in depth assessment of the functional and phenotypic profiles in oesophageal adenocarcinoma. Challenges remain in navigating the progression of transcriptome to proteome. We have been able to confirm features of tissue residency identified in the transcriptomic profile of cycling cells irrespective of prior neoadjuvant treatment in the proteome of an additional patient cohort. It was important therefore to further establish whether transcriptomic T and NK phenotypes could be confirmed in additional patient groups.

Immunotherapeutics in solid tumours currently focus on checkpoint inhibition to reverse the changes of an immunosuppressive tumour microenvironment. Less however is understood about the extent to which the immune infiltrate is functionally impaired. Cytotoxic T and NK destruction of tumour is often directed by granzyme and perforin delivery however quantitative assessments of immune mediated cytotoxicity have not been performed in oesophageal adenocarcinoma. Transcriptomic analysis has shown that T cell profiles can be granzyme specific and this study seeks to gain further understanding of the cytotoxic capacity of tumour infiltrating lymphocytes.

The current assessment of the tumour microenvironment in oesophageal cancer confirms that the immune infiltrate upregulates significant features of exhaustion. Despite this cycling cells remain that phenotypically show properties of tumour recognition. It is undetermined however to what extent the immune infiltrate remains activated, and a greater understanding is required

to determine whether there are phenotypic indicators of functional resilience. This chapter will report the analysis of flow cytometrics designed to confirm key populations identified in the transcriptomic TME and the propensity to which they can maintain an immune response.

Methods

Blood and matched tumour samples from obtained from 14 patients with OAC. Seven of these were patients who had undergone oesophagectomy whilst seven were obtained from endoscopic biopsies. Seven of these patients had undergone treatment with neoadjuvant chemotherapy (NACT). Six patients received neoadjuvant FLOT, of which one patient received 8 pre-operative cycles in order to accommodate for lack of theatre access during COVID. One patient was deemed to have excessive comorbidity and subsequently was administered raltitrexed and oxaliplatin (TOMOX). Five patients were identified to have responded to neoadjuvant treatment (TRG 1-3) whereas as two patients were identified to be non responders (TRG4-5).

Peripheral blood lymphocytes and tumour infiltrating lymphocytes (TIL) were isolated and frozen prior to use. Samples were defrosted and stained with a panel of antibodies against cell 27 surface markers (Figure 89), including CD14 and CD19 on the same colour as a ‘dump’ channel to remove B cells and monocytes. This large panel included markers to assess T cell phenotypes as recognised within scRNA-seq analysis. This included differential T and NK granzyme expression (Gzm A,B, K) and features suggestive of functional activity within the TME (HSP70, Ki-67, HLA-DR, CD94).

Instrument / Configuration		BD FACSymphony™ A3	7 UV - 8 Violet - 6 Blue - 4 Yellow/Green - 3 Red	
Excitation Laser Line	Fluorescence Channel	Marker/Antibody	Clone	Cat. No.
UV 355 nm	BUV395	CD4	SK3	563550
	BUV496	CD8	SK1	741199
	BUV563	CD16	3G8	748851
	BUV615	CD94	HP-3D9	751525
	BUV661	TCRgd	11F2	750019
	BUV737	CD56	NCAM16.2	612766
	BUV805	CD45	HI30	612891
Violet 405 nm	BV421	GITR	V27-580	566423
	BV480	HLA-DR	G46-6	566113
	BV570-P	CD3	UCHT1	Biolegend
	BV605	CD161	DX12	747762
	BV650	CCR7	2-L1-A	566756
	BV711	Ki-67	B56	563755
	BV750	CD39	TU66	747079
	BV786	CD45RA	HI100	563870
Blue 488nm	AF488	HSP70	W27	Biolegend
	BB630-P	CD127	HIL-7R-M21	custom
	BB660-P	GrzB	GB11	custom
	PerCP-Cy5.5	GPR183	SA313E4	Biolegend
	BB755-P			
	BB790-P	CD69	FN50	Custom
Yellow / Green 561nm	PE	GrzA	CB9	Biolegend
	PE-CF594	FoxP3	259D/C7	562421
	PE-Cy5	CD14/CD19	M5E2/HIB19	Biolegend/555414
	PE-Cy7	CD25	M-A251	557741
Red 640	AF647	GrzK	G3H69	566655
	R718	CD103	Ber-ACT8	752007
	FVS780	Viability		565388

Flow cytometry panel used for analysis in Chapter 7 (Figure 89)

Results

Granzyme Profiles of CD8+ TIL

My initial studies focussed on the relative expression of different granzyme proteins within T cells in blood and tumour. I used antibodies against granzyme A, B and K as these have been shown to be differentially expressed within lymphocyte subsets[159].

Comparative assessment of matched PBMC and TIL in CD8+ T cells demonstrated a reduction in Granzyme A and B expression within TIL, from values of 52% to 38% and 59% to 49% respectively (p=0.049, p=0.03, Figure 91). However, it was noteworthy that expression of Granzyme K was nearly doubled within the tumour, where this was present in 50% of cells compared to 27% within blood (p=0.03).

Next, combinatorial staining against CD69 and CD103 was used to define the TRM (CD69+CD103) and non-TRM subsets (CD69-CD103-;CD69+CD103-;CD69-CD103+) and to assess granzyme levels within CD8+ T cells in these two subsets. Substantial differences in granzyme expression were seen within these populations. Granzyme A was observed in only 19% of non-TRM CD8+ cells but this increased to 43% within the TRM pool (p=0.0001). Again, a reciprocal pattern was observed for granzyme K where there was markedly increased expression in the non-TRM pool at 72% vs 37% in TIL (p=0.0009). Granzyme B expression was comparable within the two populations (p=0.86).

I was also interested to assess granzyme expression in different CD8+ memory subsets. Naïve CD8+ T cells (CD45RA+CCR7+) showed a comparable pattern in blood and tumour with high levels of granzyme B, moderate levels of granzyme A and low levels of granzyme K (p=0.058, p=0.24, p=0.17, Figure 92). The central memory CD8+ pool showed a similar overall pattern although Granzyme B expression was lower in TIL (98% vs 79% respectively) whilst Granzyme K was increased (17% to 96%). Granzyme A expression was comparable (p=0.02,

p=0.02, p=0.058 for all three). Granzyme A and B expression was reduced in effector PBMC and TIL subsets but was comparable between PBMC and TIL (Gzm A, p=0.43; Gzm B, p=0.46). A trend towards higher level expression of Gzm K was seen but this was not significant (p=0.09, Figure 92). Reversion of effector cells to re-expression of CD45RA isoform (TEMRA subset; CD45RA+, CCR7+) led to robust expression of granzyme A and B in CD8+ T cells in blood whilst these were reduced within TIL (64% to 36% and 77% to 42% respectively; p=0.003, p=0.002). In contrast, Granzyme K expression was substantially increased within TIL (16% vs 50% respectively; p=0.0001).

Overall these findings show a marked increase in granzyme K expression within the tumour although this is mainly observed within the non-TRM population. Analysis on memory subsets reveals higher level expression within the central memory and TEMRA pools.

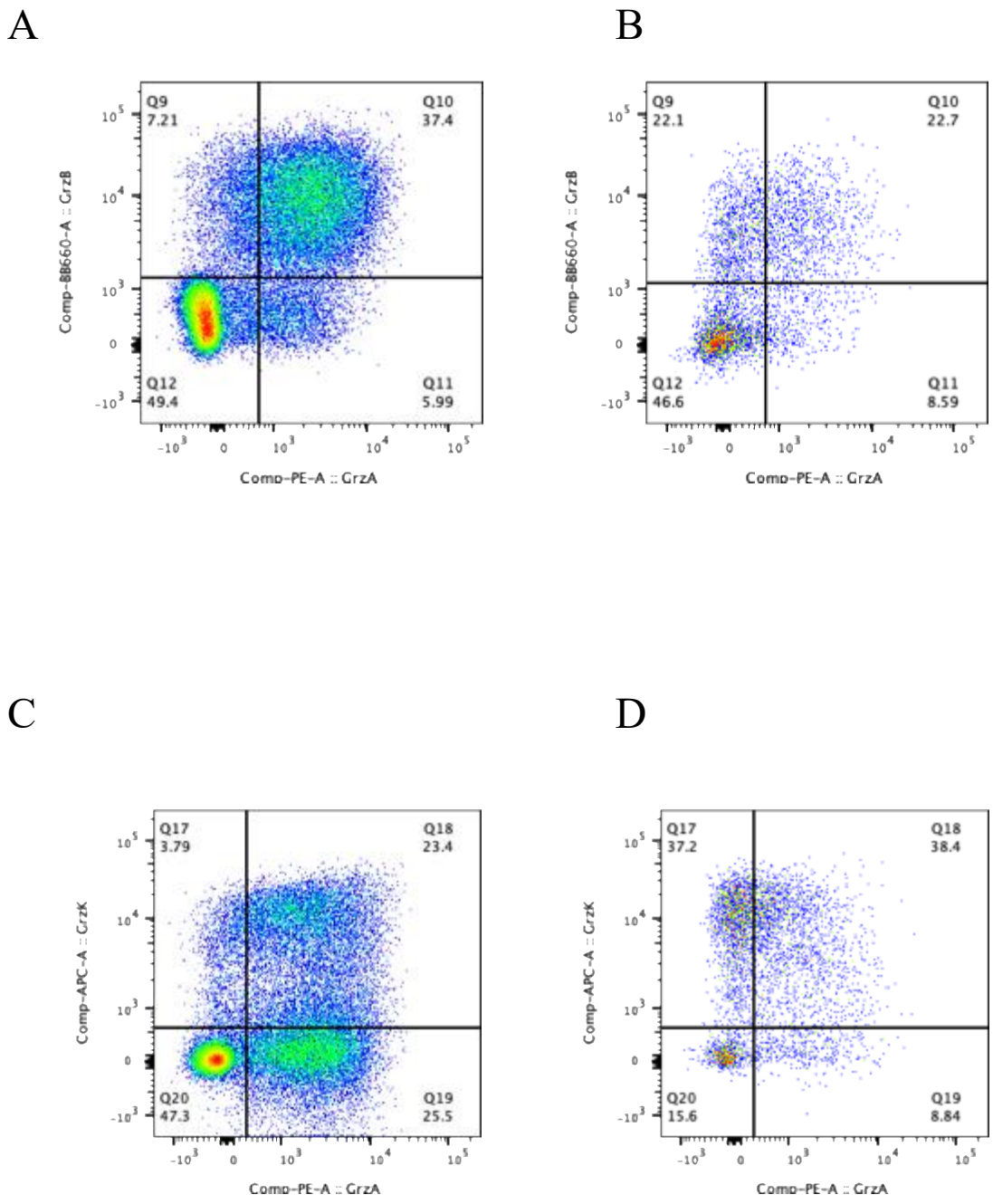

Figure 90. Representative flow plot of granzyme expression on CD8+ TIL
Granzyme expression was assessed in matched PBMC and TIL CD8+ T cells. Expression of Gzm A and Gzm B is shown in a representative sample on PBMC (A) and TIL (B). Expression of Gzm A and Gzm K is shown in a representative sample on PBMC (C) and TIL (D).

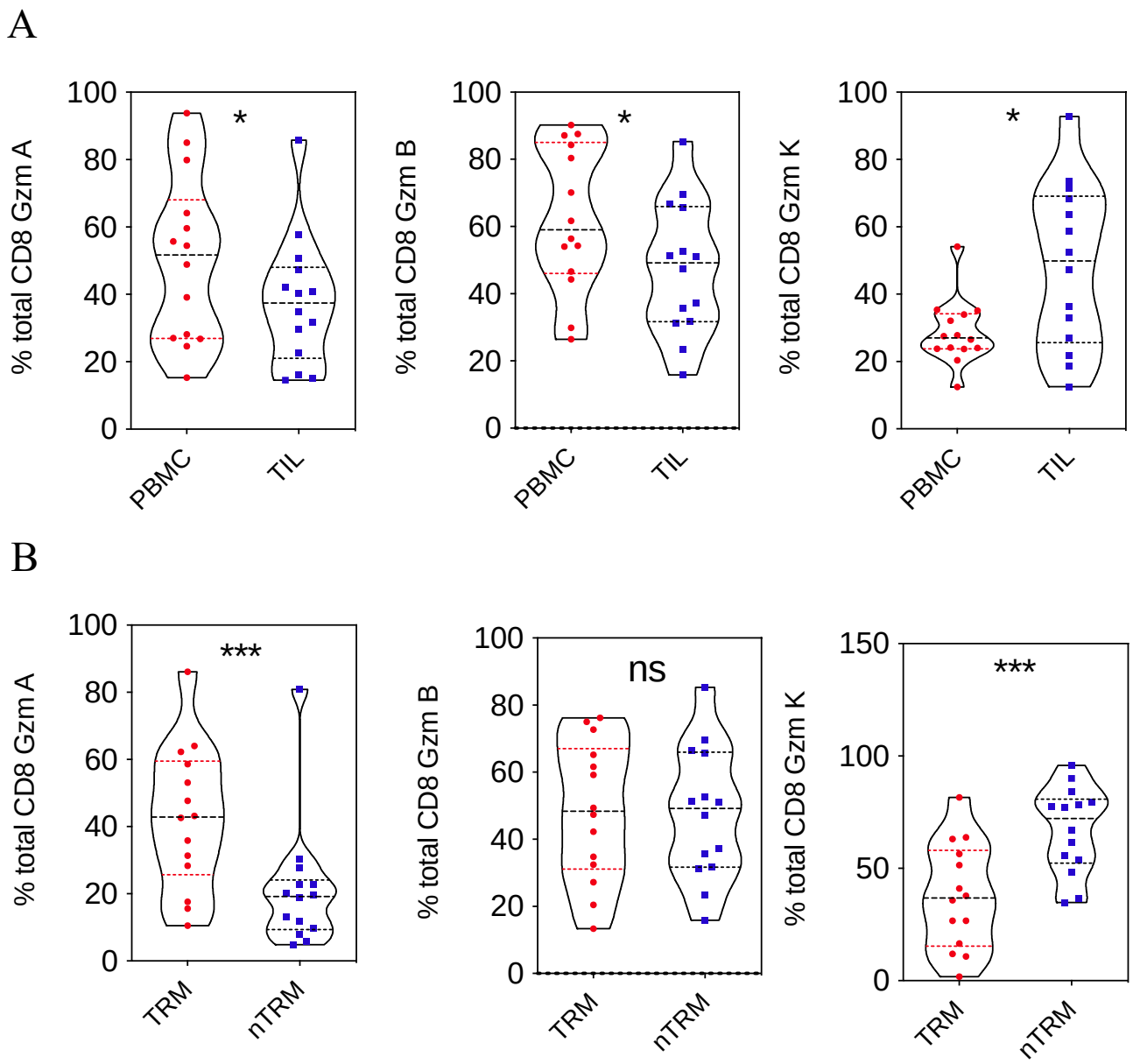

Figure 91. Pattern of granzyme expression in matched PBMC, TIL and TRM subsets
Granzyme expression (Gzm A, B and K) was assessed in matched PBMC and TIL CD8+ T cells (n=14, A). Granzyme expression (Gzm A, B and K) was also examined in tissue resident memory (CD69+CD103+) and non-TRM cells CD8+ T cells (n=14, B).
Each symbol represents an individual patient. Dashed horizontal lines indicate the median and dotted lines indicate the interquartile range. Data analysed by Wilcoxon matched-pairs signed rank test, * denotes $p<0.05$ and *** 0.001.

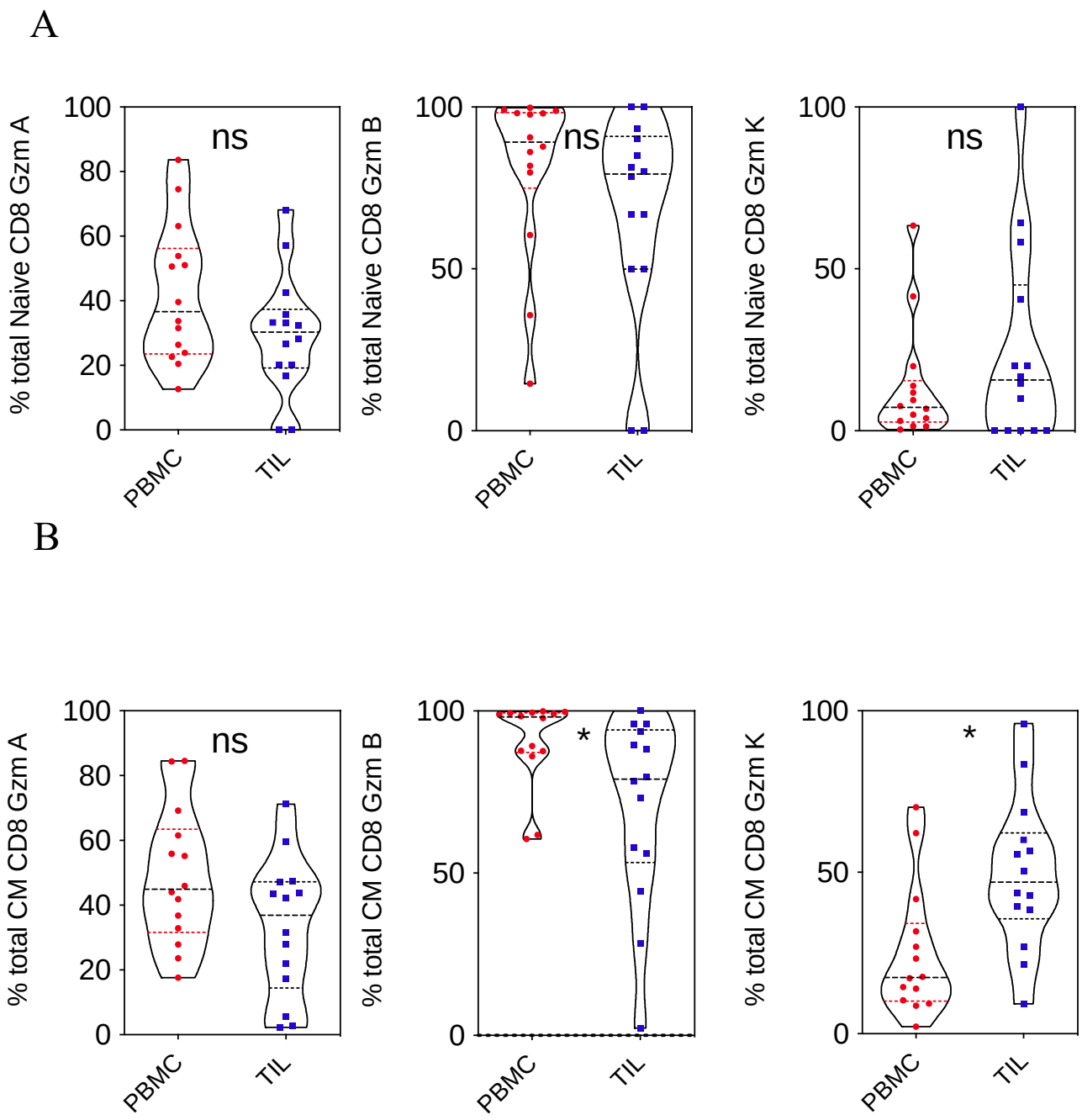

Figure 92. Pattern of granzyme expression in matched PBMC and TIL naïve and central memory CD8+ T cells.

Granzyme expression (Gzm A, B and K) was determined in matched PBMC and TIL naïve (n=14, A) and central memory CD8+ T cells (n=14, B). Each symbol represents an individual patient. Dashed horizontal lines indicate the median and dotted lines indicate the interquartile range. Data analysed by Wilcoxon matched-pairs signed rank test, * denotes $p<0.05$.

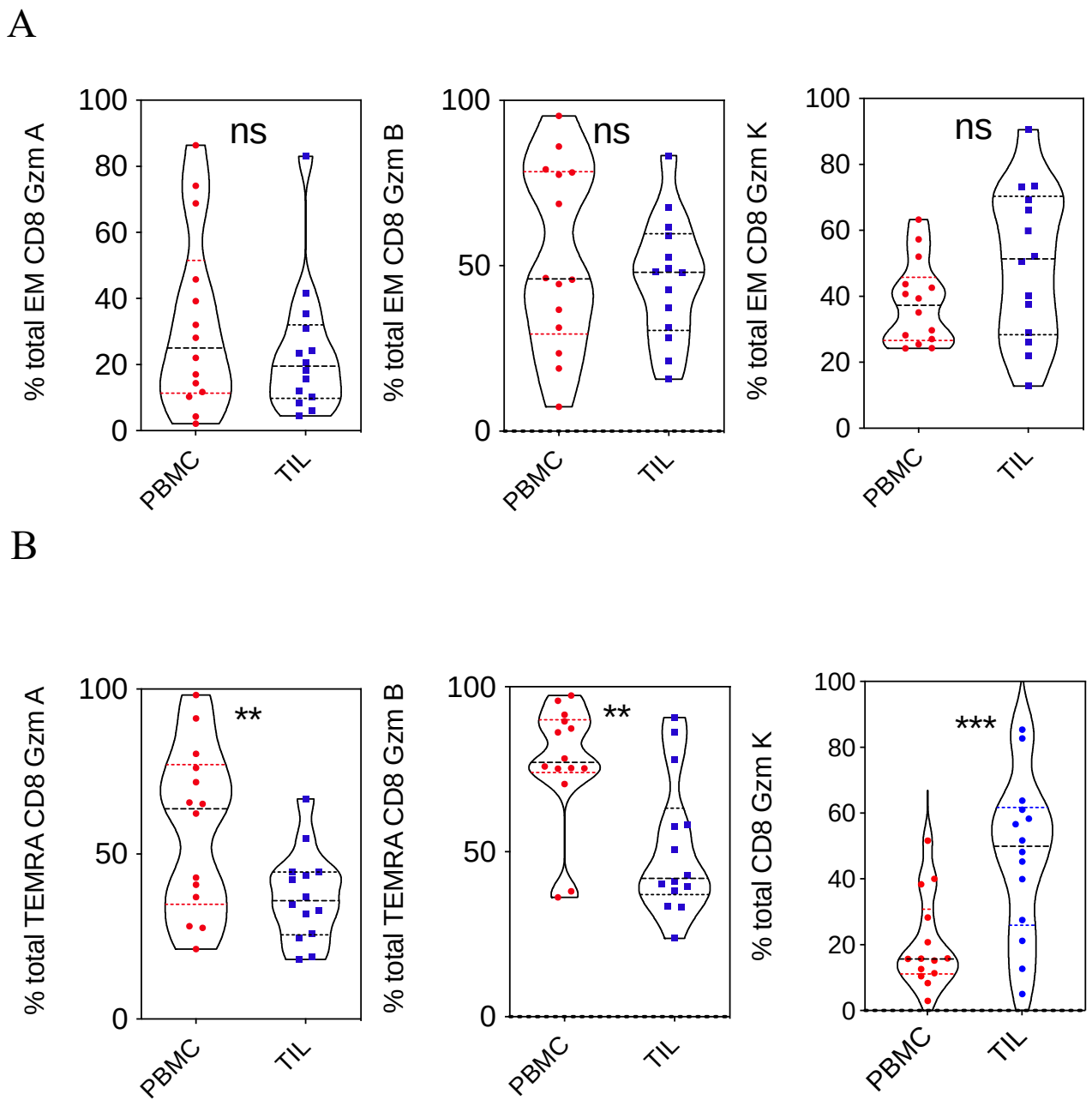

Figure 93. Pattern of granzyme expression in matched PBMC and TIL effector CD8+ T cells.
Granzyme expression (Gzm A, B and K) in matched PBMC and TIL effector memory (n=14, A) and TEMRA CD8 T cells (n=14, B). Each symbol represents an individual patient. Dashed horizontal lines indicate the median and dotted lines indicate the interquartile range. Data analysed by Wilcoxon matched-pairs signed rank test, ** denotes p<0.01, ***denotes p<0.001.

Expression of stimulatory and Inhibitory markers on CD8+ TIL in relation to tissue resident status

Next, the expression of a range of activating and inhibitory proteins on T cells within OAC were assessed.

I initially studied levels of the ectoenzyme CD39 on CD8+ TIL both within the tissue resident and non-tissue resident pools (p=0.0001, Figure 94). Expression of this marker has previously been associated with tumour specificity in tumour infiltrating lymphocytes.

Of interest, CD39 was expressed on 9.3% of TRM compared to only 0.5% of those within blood (IQR: 9.3-33.9%). Then, expression of the inhibitory receptor GITR on the TRM and non-TRM pools was assessed. Expression here was low overall, but comparable (p=0.73) with GITR observed on 0.47% of the TRM population (IQR: 0.35-1.10%).

Ki-67 is a marker of cell proliferation whilst HLA-DR is expressed on activated cells. Comparative assessment of matched PBMC and TIL CD8+ T cells demonstrated upregulation of both Ki-67 (p=0.02) and HLA-DR on TIL subsets (p=0.001). Ki-67 increased from 1.3% to 3.3% and HLA-DR increased from 3.4% to 11.3%. I also assessed expression of HSP70 and CD94 but here the values were comparable (p=0.43, p=0.95, Figure 95).

Comparison of matched TRM and non-TRM CD8+ T cells within TIL demonstrated upregulation of HSP70, HLA-DR and CD94 on the TRM pools whilst no change was seen in Ki-67 expression (p=0.006, 0.004, p=0.003, p=0.43, Figure 96). Median expression of HSP70, HLA-DR and CD94 on TRM populations was 56%, 8.4% and 24%, respectively.

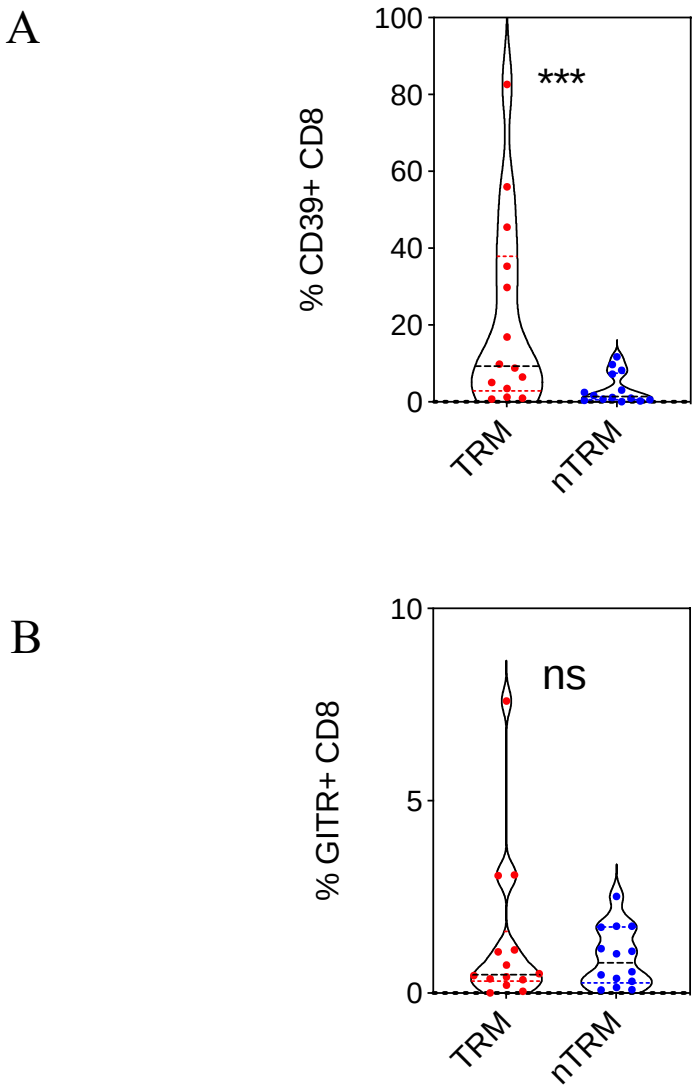

Figure 94. CD39 and GITR expression in matched tissue resident and non-tissue resident TIL CD8+ T cells.

Expression of CD39 (A) and GITR (B) on TRM and non-TRM CD8+ TIL (n=14). Each symbol represents an individual patient. Dashed horizontal lines indicate the median and dotted lines indicate the interquartile range. Data analysed by Wilcoxon matched-pairs signed rank test, *** denotes $p<0.0001$.

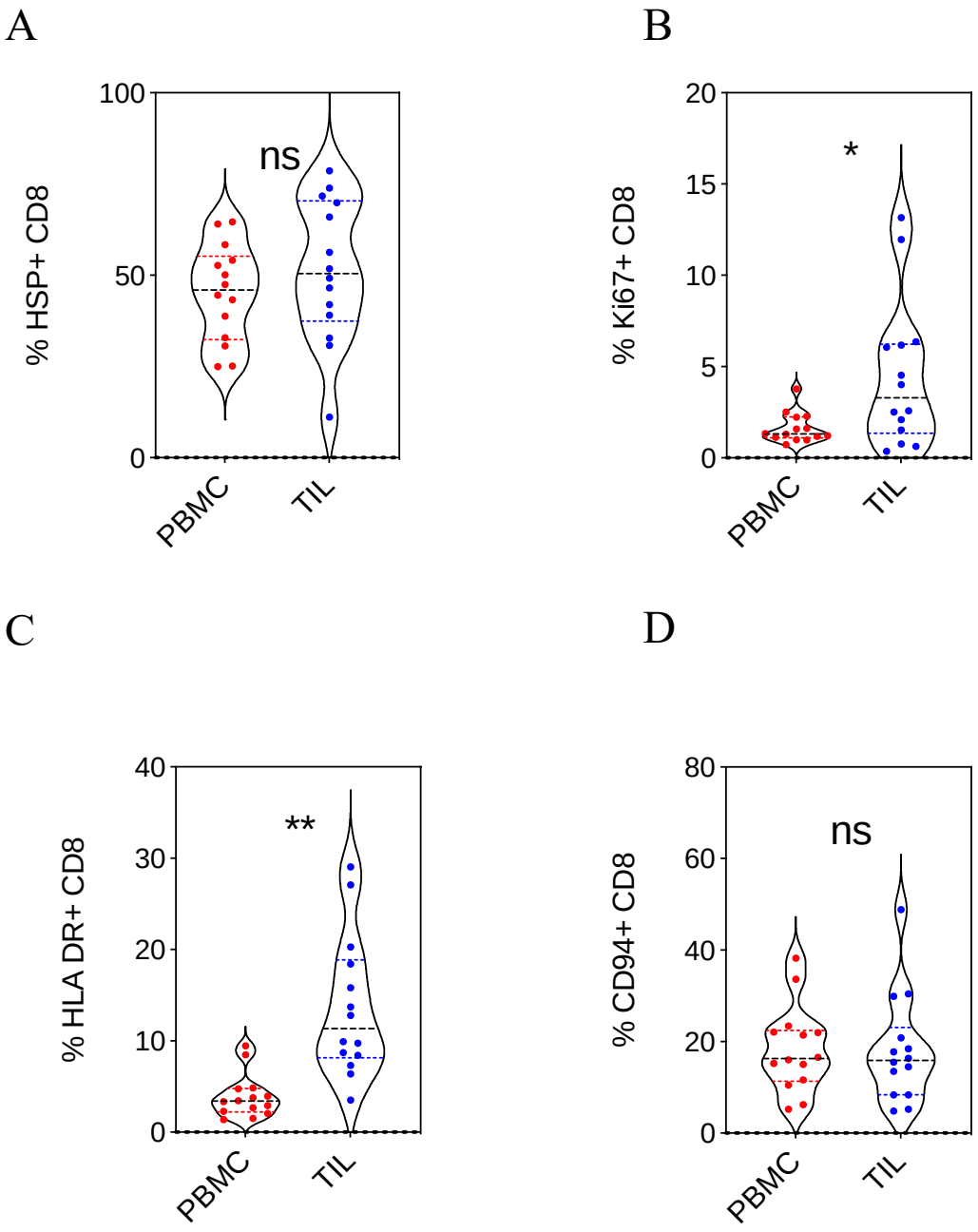

Figure 95. Phenotypic variation of matched PBMC and TIL CD8+ T cells.
Expression of heat shock protein (A), Ki-67 (B), HLA-DR (C) and CD94 (D) in matched PBMC and TIL CD8 T cells (n=14). Each symbol represents an individual patient. Dashed horizontal lines indicate the median and dotted lines indicate the interquartile range. Data analysed by Wilcoxon matched-pairs signed rank test, * denotes $p<0.05$ and ** $p<0.01$.

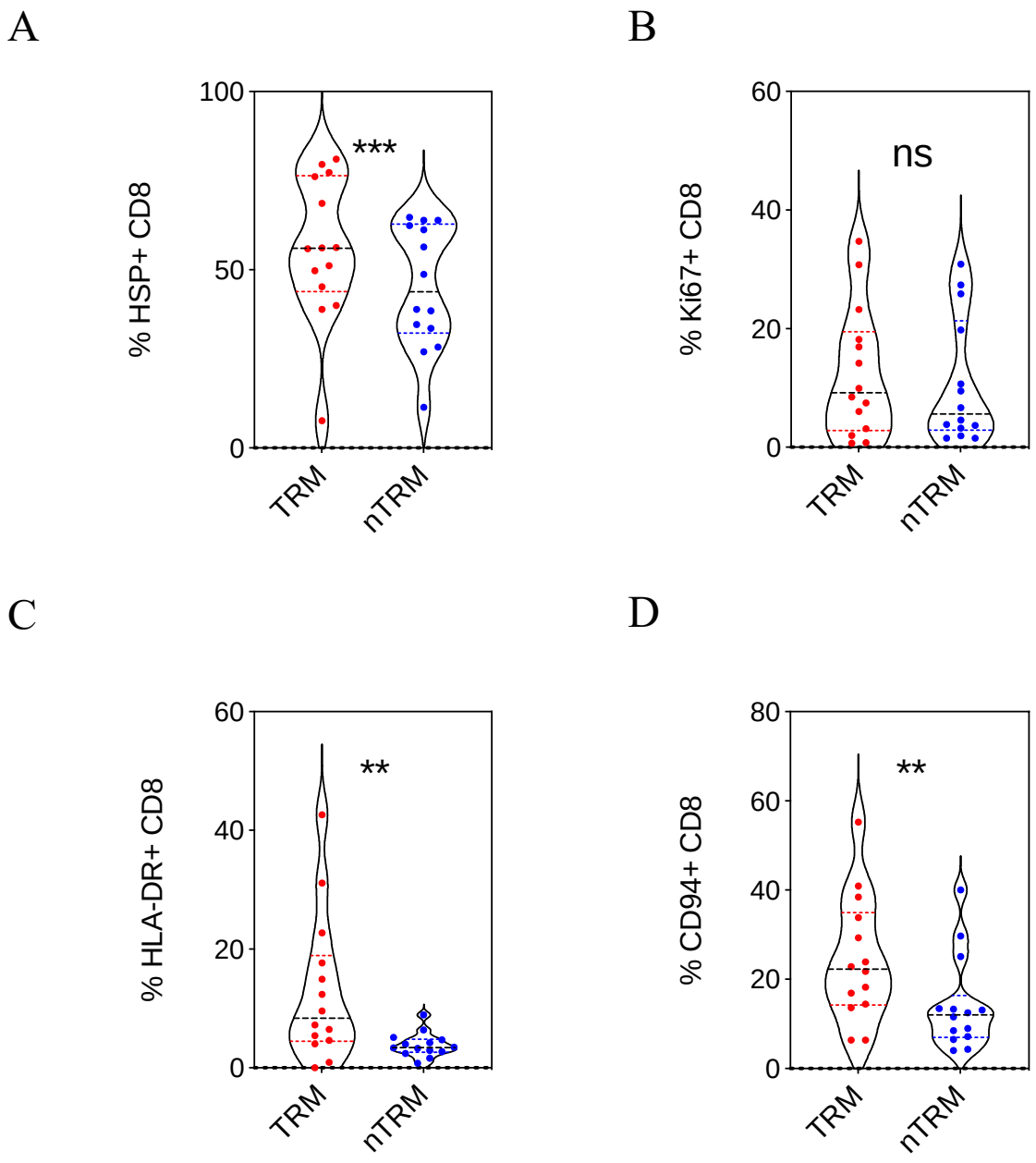

Figure 96. Expression of activation and inhibitory markers in relation to tissue residency on CD8+ T cells in OAC

Expression of heat shock protein (A), Ki-67 (B), HLA-DR (C) and CD94 (D) on matched TRM and non-TRM CD8+ T cells (n=14). Each symbol represents an individual patient. Dashed horizontal lines indicate the median and dotted lines indicate the interquartile range. Data analysed by Wilcoxon matched-pairs signed rank test, ** denotes $p<0.01$ and *** $p<0.001$.

Expression of phenotypic markers on CD8+ memory subsets within the tumour microenvironment.

The expression of activating and inhibitory proteins could differ between CD8+ T cell memory compartments. As expected, no difference in HSP70, Ki-67, HLA-DR or CD94 expression was seen on matched naïve CD8+ T cells from PBMC and TIL which is likely to reflect the fact that naïve cells have not undergone antigenic activation (Figure 97).

In contrast HSP70 levels were higher on central memory CD8+ within TIL (46%) compared to PBMC (32%) (p=0.01). Ki-67 (PBMC 1.2% vs TIL 3.5%; p=0.009) and HLA-DR (PBMC 4.5% vs TIL 16.5%; p=0.0009) were also higher. In contrast, CD94 was lower on the TIL CM pool (PBMC 28% vs.TIL 14%; p=0.02) Figure 98).

Effector memory CD8+ TIL showed upregulation of Ki-67 from 5.2% in PBMC to 8.3% in TIL (p=0.03) and HLA-DR from 1.9% in PBMC to 4.9% in TIL (p=0.005) whereas there was no change in HSP70 or CD94 (p=0.24, p=0.63, Figure 99). In contrast TEMRA CD8+ TIL upregulated HSP70 from 48% in PBMC to 61% in TIL (p=0.02) and downregulated CD94 from 40% in PBMC to 22% in TIL (p=0.01) whereas there was no change in Ki-67 or HLA-DR (p=0.63, p=0.35, Figure 100).

These observations show that central and effector memory CD8+ T cells are more proliferative (Ki-67) and activated (HLA-DR) within TIL although this is lost in the CD45RA-revertant pool. In contrast, within TIL, HSP70 is increased on CM and TEMRA pools whilst CD94 shows a reciprocal reduction in these subsets.

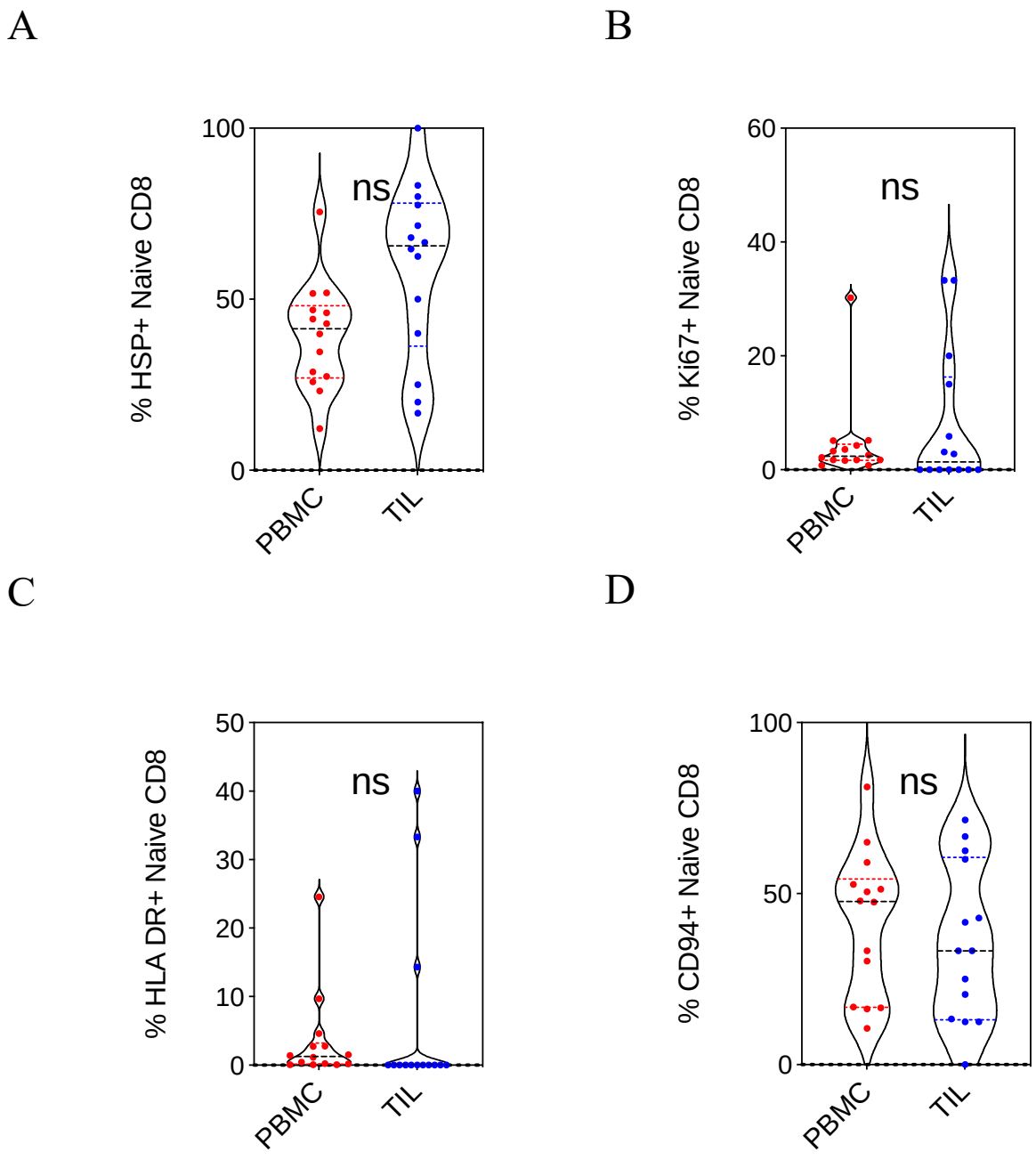

Figure 97. Phenotypic expression of matched PBMC and TIL naïve CD8+ T cells
Expression of heat shock protein (A), Ki-67 (B), HLA-DR (C) and CD94 (D) on matched PBMC and TIL naïve CD8 T cells (n=14, naïve- CCR7+CD45RA+). Each symbol represents an individual patient. Dashed horizontal lines indicate the median and dotted lines indicate the interquartile range. Data analysed by Wilcoxon matched-pairs signed rank test.

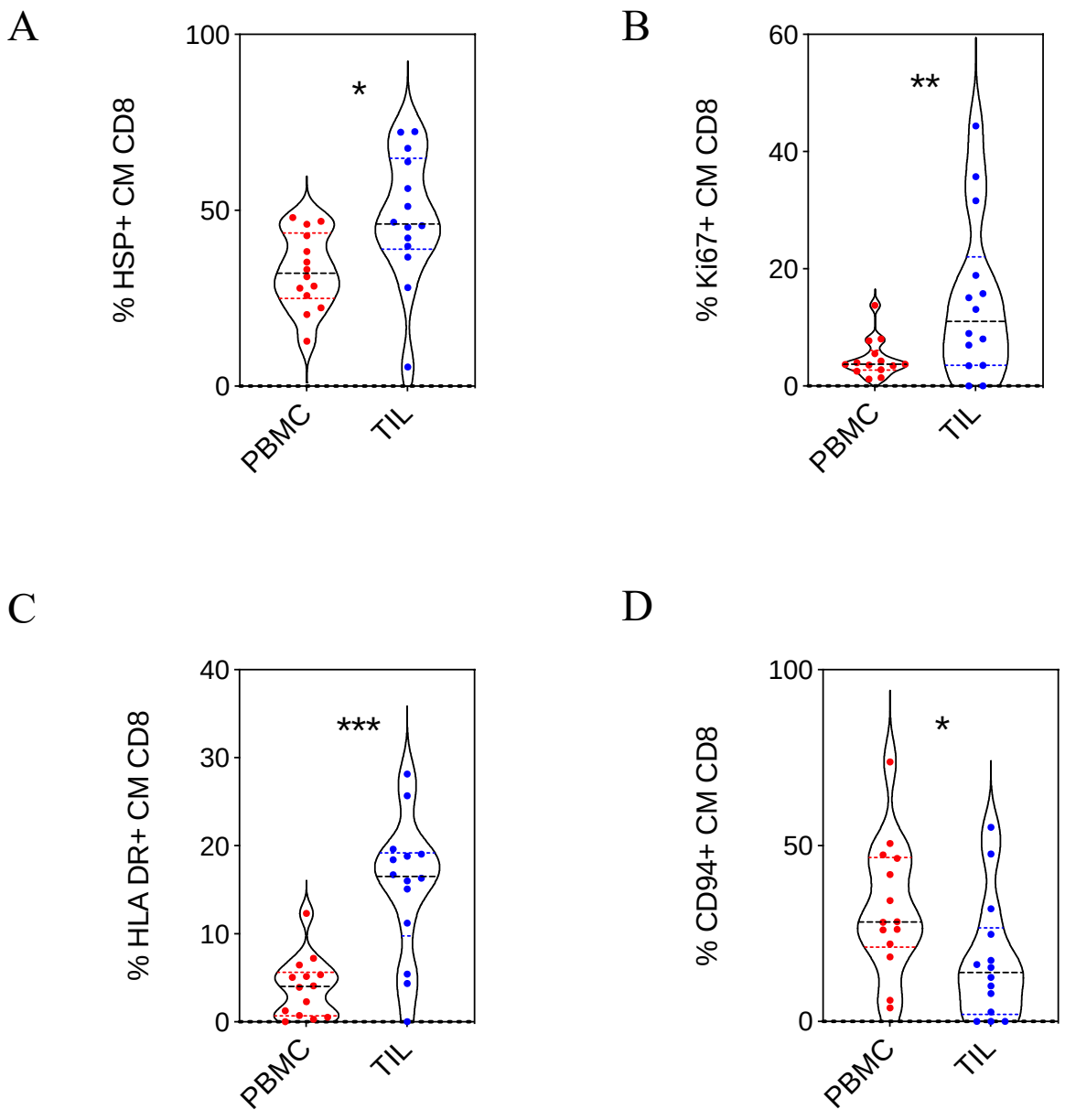

Figure 98. Phenotypic expression of matched PBMC and TIL central memory CD8+ T cells
Expression of heat shock protein (A), Ki-67 (B), HLA-DR (C) and CD94 (D) on matched PBMC and TIL central memory (CM) CD8+ T cells (n=14, CM:CCR7+CD45RA-). Each symbol represents an individual patient. Dashed horizontal lines indicate the median and dotted lines indicate the interquartile range. Data analysed by Wilcoxon matched-pairs signed rank test, * denotes $p<0.05$ and ** $p<0.01$, *** denotes $p<0.001$.

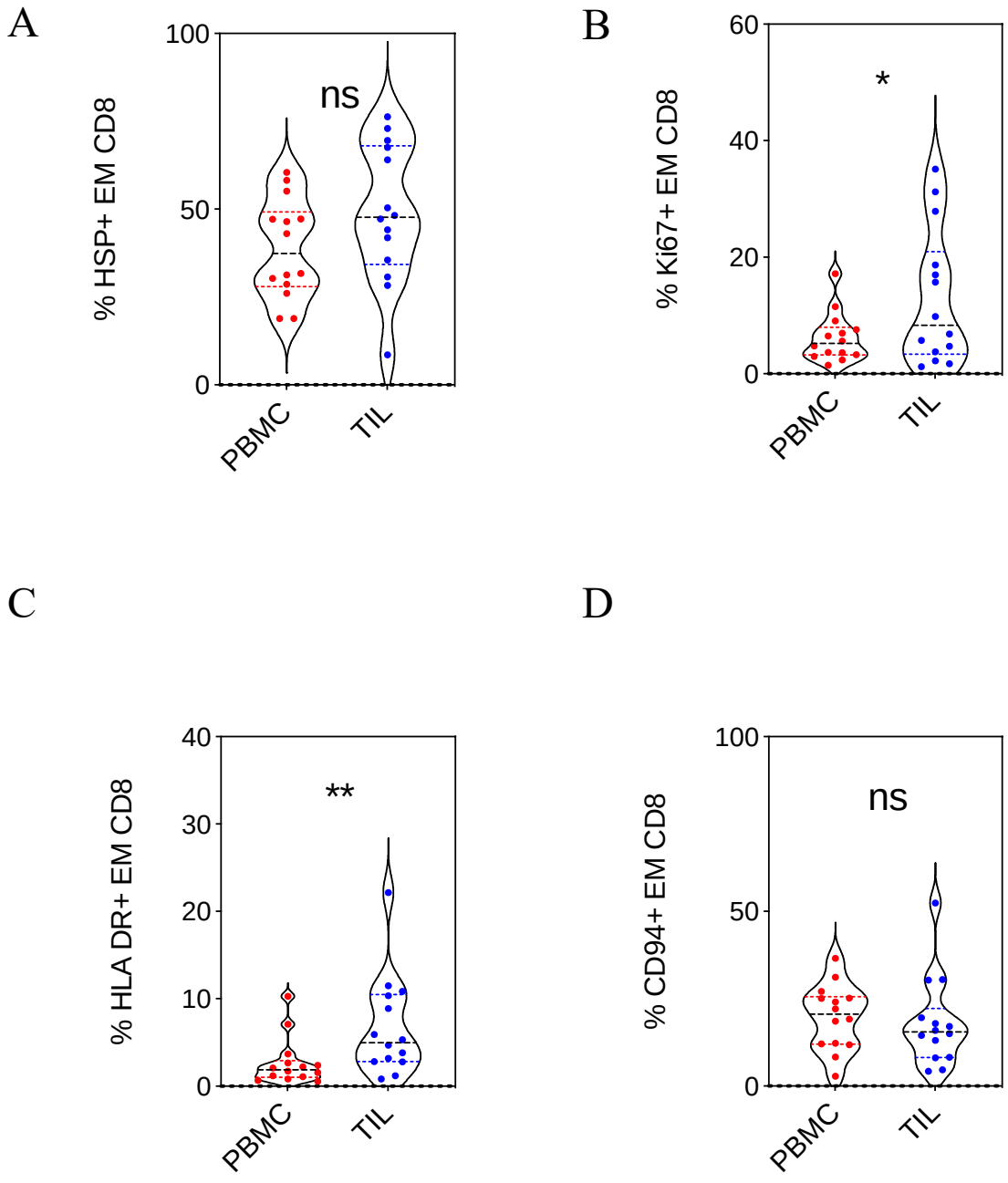

Figure 99. Phenotypic expression of matched PBMC and TIL effector memory CD8+ T cells
Expression of heat shock protein (A), Ki-67 (B), HLA-DR (C) and CD94 (D) on matched PBMC and TIL EM CD8 T cells (n=14, EM; CCR7-CD45RA-). Each symbol represents an individual patient. Dashed horizontal lines indicate the median and dotted lines indicate the interquartile range. Data analysed by Wilcoxon matched-pairs signed rank test, * denotes $p<0.05$ and ** $p<0.01$.

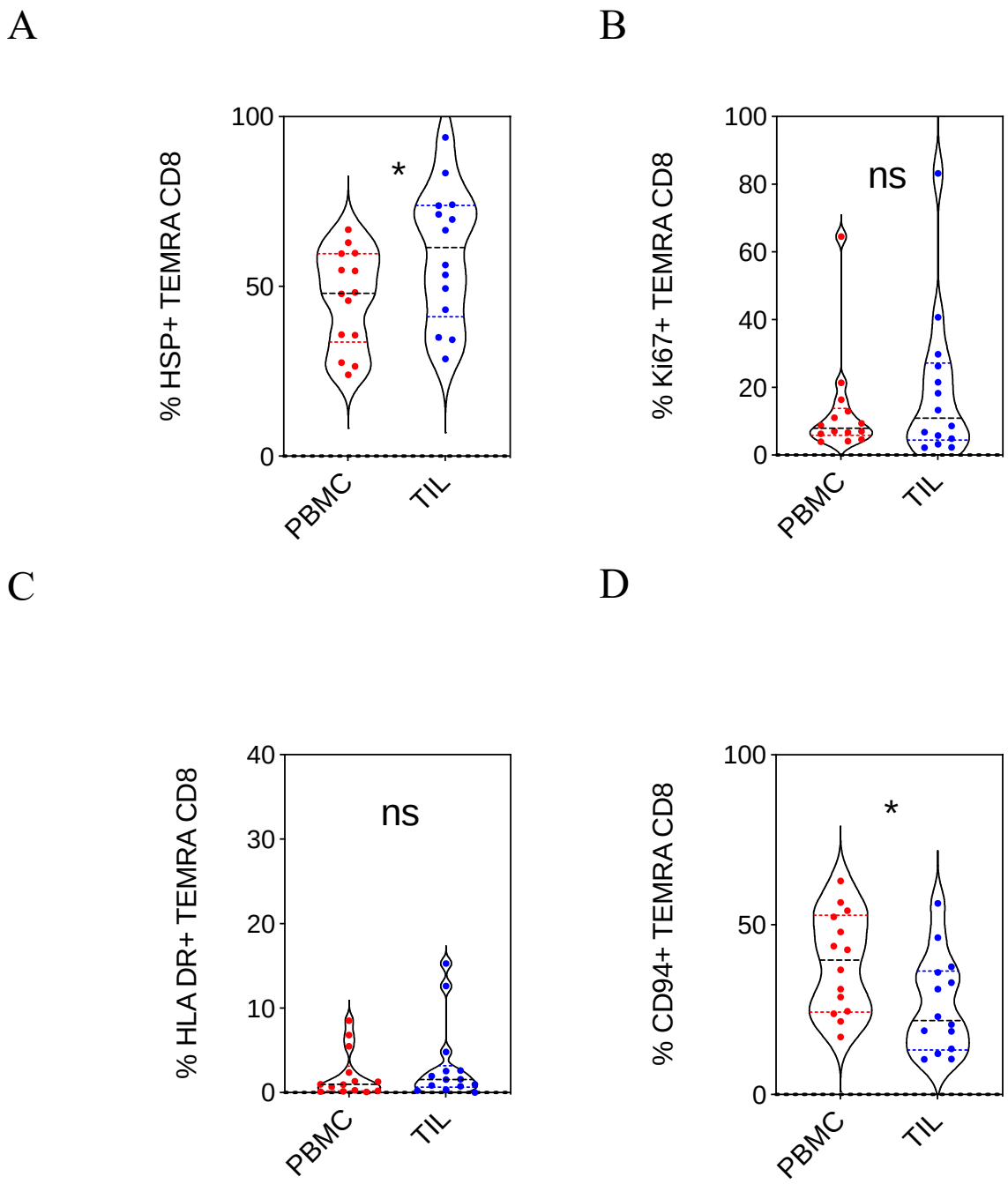

Figure 100. Phenotypic expression of matched PBMC and TIL effector memory CD45RA+ CD8+ T cells. Expression of heat shock protein (A), Ki-67 (B), HLA-DR (C) and CD94 (D) in matched PBMC and TIL effector memory CD45RA (EMRA) CD8+ T cells (n=14, CM- CCR7-CD45RA+). Each symbol represents an individual patient. Dashed horizontal lines indicate the median and dotted lines indicate the interquartile range. Data analysed by Wilcoxon matched-pairs signed rank test, * denotes $p<0.05$ and ** $p<0.01$.

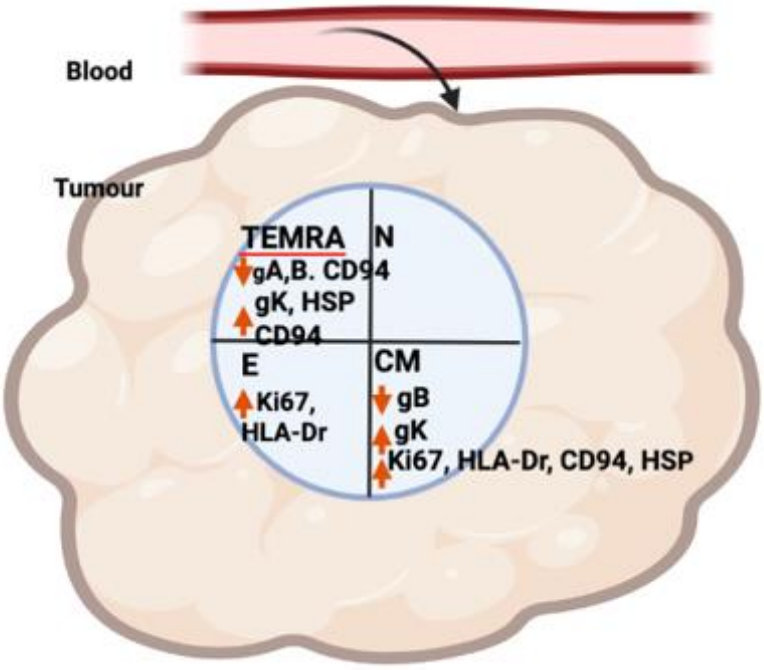

Figure 101. Model of relative expression of proteins in CD8+ T cell memory subsets in the OAC tumour microenvironment. N=naïve, CM = Central memory, E=Effector, TEMRA=CD45RA+ effector. gA=granzyme A, gB=granzyme B, gK=granzyme K.

Impact of neoadjuvant chemotherapy on the expression of granzyme and activation markers on CD8+ TRM populations

Administration of neoadjuvant chemotherapy did not significantly alter expression on HSP70, Ki-67, HLA-DR or CD94 expression on CD8+ TIL although a trend was observed towards lower levels of HSP70 on the TIL population (Figure 102).

I was also able to assess how chemotherapy influenced the expression of granzyme proteins and here there was also no difference observed although a modest non-significant increase in granzyme K was seen following chemotherapy.

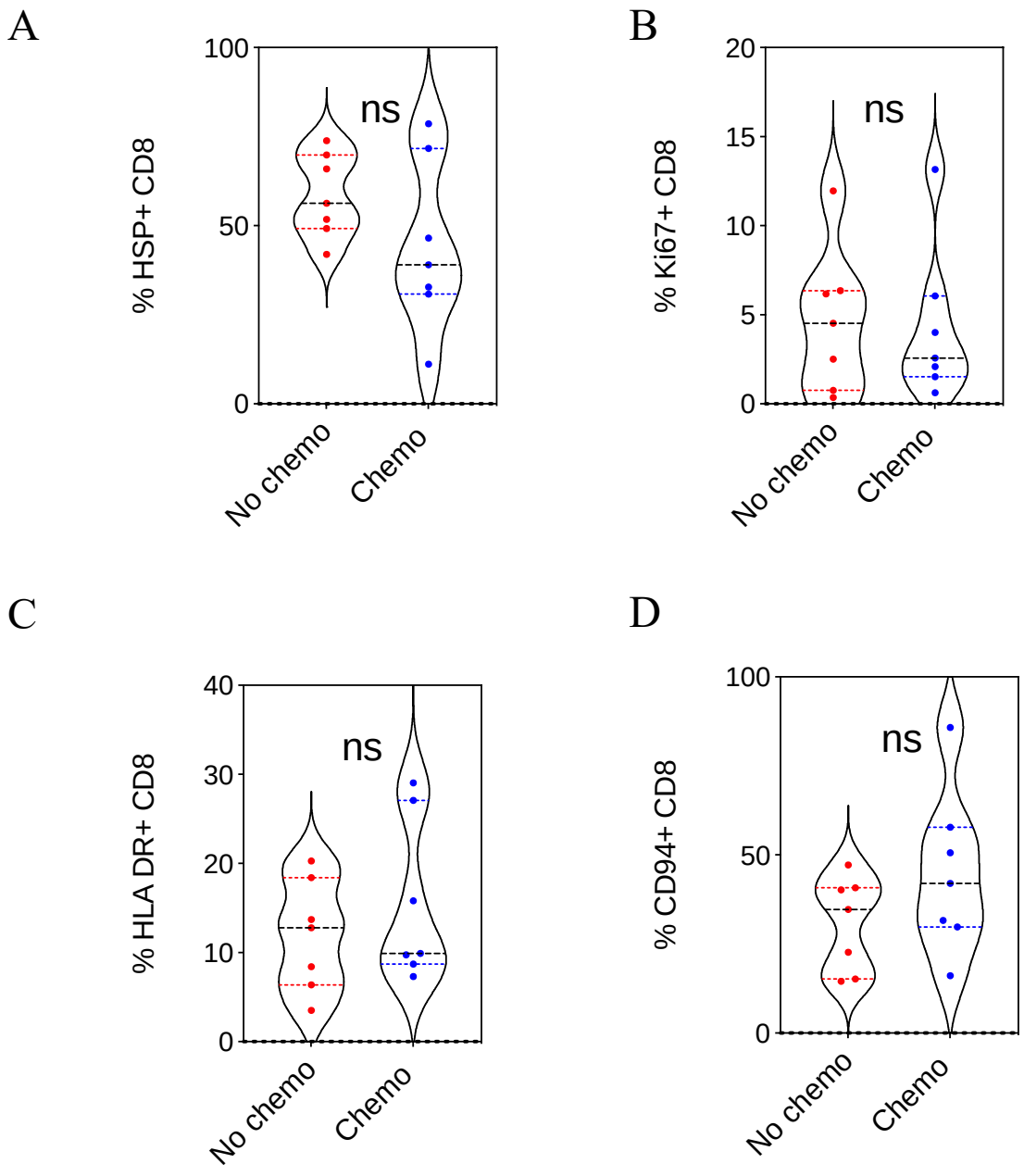

Figure 102. Phenotypic profile of CD8+ TIL in relation to administration of neoadjuvant chemotherapy
Expression of heat shock protein (A), Ki-67 (B), HLA-DR (C) and CD94 (D) on CD8+ TIL for patients who have and have not received neoadjuvant chemotherapy (No chemo n=7, chemo n=7). Each symbol represents an individual patient. Dashed horizontal lines indicate the median and dotted lines indicate the interquartile range. Data analysed by Mann Whitney Test.

A

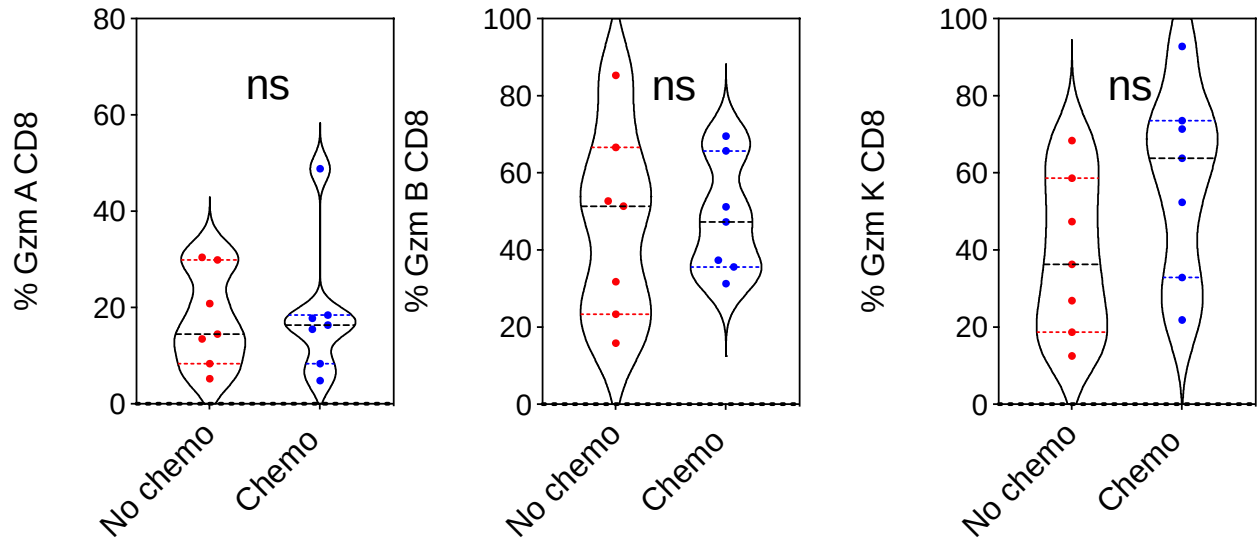

Figure 103. Granzyme expression within CD8+ TIL in relation to administration or absence of neoadjuvant chemotherapy

Granzyme expression (Gzm A, B and K) in CD8 TIL for patients who have, or have not, received neoadjuvant chemotherapy (No chemo n=7, chemo n=7), A). Each symbol represents an individual patient. Dashed horizontal lines indicate the median and dotted lines indicate the interquartile range. Data analysed by Mann Whitney Test (unpaired chemo analysis), Wilcoxon matched-pairs signed rank test (paired CD39 analysis), * denotes $p<0.05$.

Expression of CD39 on CD8+ T cells within subsets of CD8+ T cells within the OAC tumour microenvironment

There is considerable interest in the relative expression of CD39 as it has been described to be expressed on tumour-reactive/non-bystander T cells within tumour microenvironments. As such, I interrogated the co-expression of other markers on CD39+ CD8+ T cells within the tumour.

I focussed specifically on the tumour resident memory T cell population and found Granzyme A to be modestly increased on the CD39+ subset (25% vs 19% (p=0.02, Figure 105). Expression of Granzyme B and K were similar between compartments (p=0.10, p=0.17, Figure 105).

Strikingly, expression of HSP70, Ki-67, HLA-DR and CD94 were all increased on CD39+ TRM (p=0.0001, p=0.02, p=0.0006, p=0.01, Figure 106). Specifically, relative to the CD39- pool, HSP70 expression increased from 27% to 65%, Ki-67 increased from 0.8% to 3.1%, HLA-DR increased from 7.8% to 31% and CD94 increased from 12% to 21%.

These data show that CD39+ cells within the TRM population have heightened activation status, express increased levels of granzyme A, and may be constrained by expression of regulatory proteins.

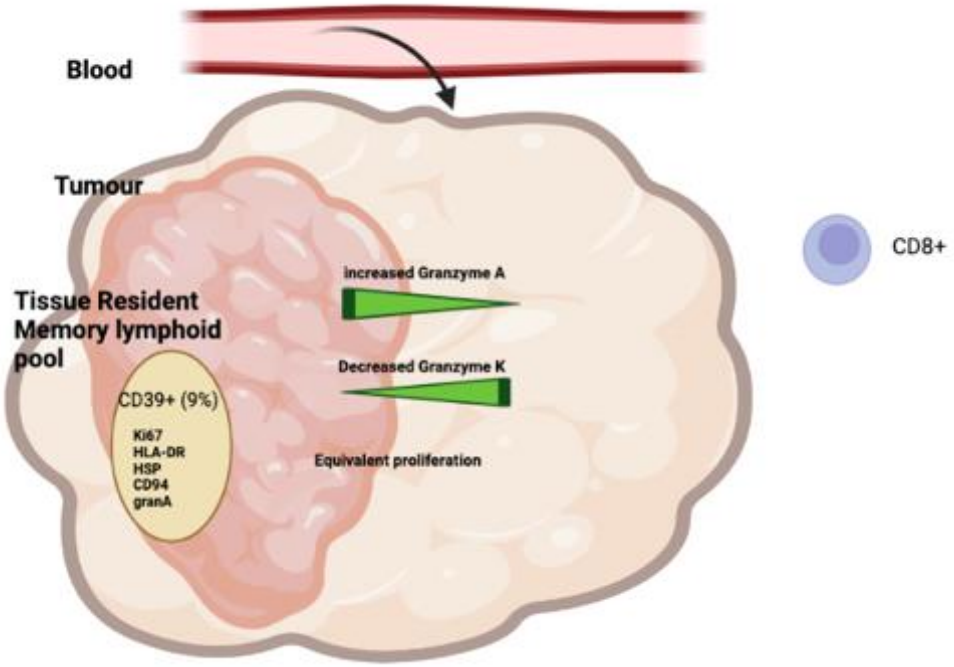

Figure 104. Model of CD8+ T cell phenotype in TRM and CD39+ subsets within OAC tumour

TRM cells show equivalent levels of proliferation but increased levels of granzyme A and lower levels of granzyme K. CD39 expression is seen only within the TRM subset where it comprises 9% of cells. These show increased levels of proliferation, activation and granzyme expression. Created with Biorender

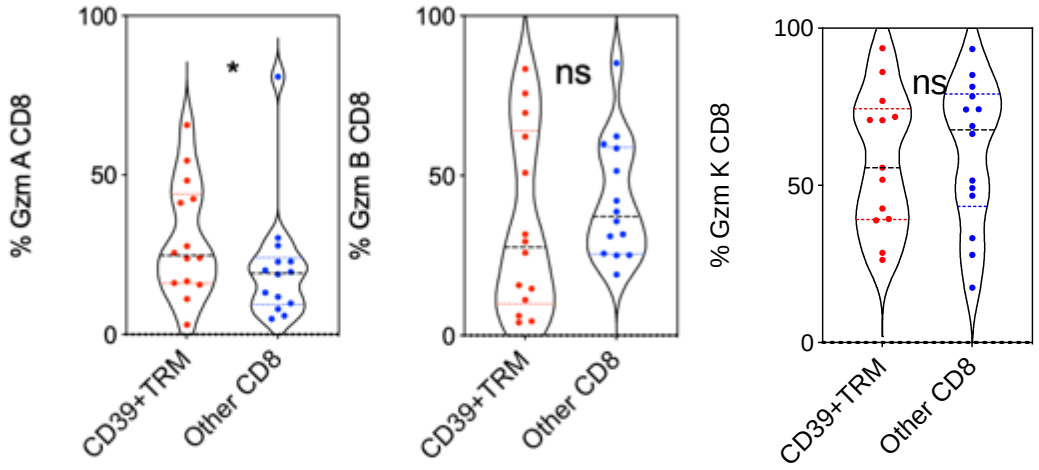

Figure 105. Granzyme expression within CD8+ TIL in relation to expression of CD39+ TRM subsets

Granzyme expression (Gzm A, B and K) within CD39+ TRM CD8 TIL (CD8+CD69+CD103+ CD39+) as compared to all other CD8 T cell TILs (n=14). Each symbol represents an individual patient. Dashed horizontal lines indicate the median and dotted lines indicate the interquartile range. Data analysed by Mann Whitney Test (unpaired chemo analysis), Wilcoxon matched-pairs signed rank test (paired CD39 analysis), * denotes $p<0.05$.

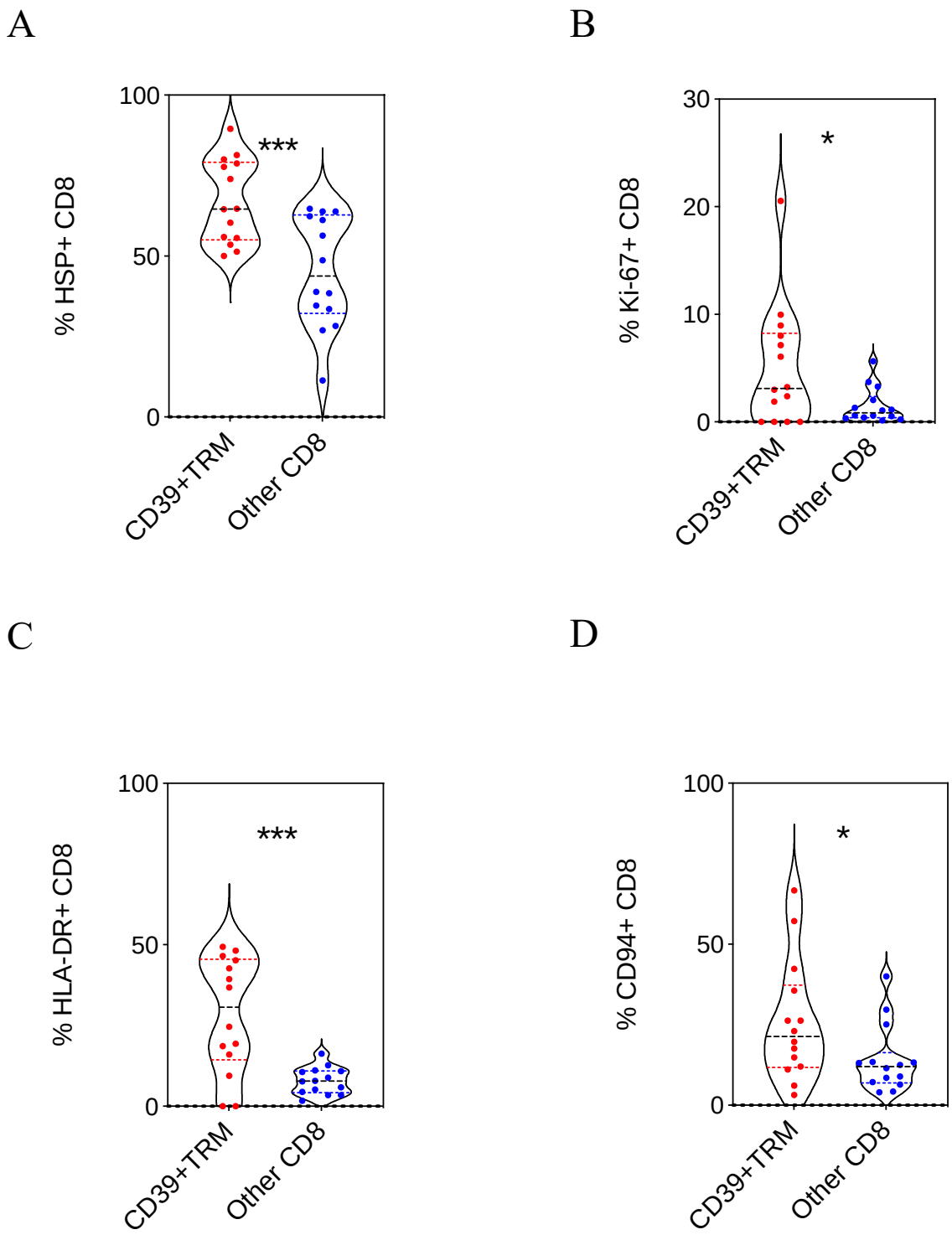

Figure 106. Phenotypic profile of CD8+ TRM in relation to expression of CD39
Expression of heat shock protein (A), Ki-67 (B), HLA-DR (C) and CD94 (D) in CD39+ TRM CD8 TIL as compared to all other CD8 T cell TILs (n=14). Each symbol represents an individual patient. Dashed horizontal lines indicate the median and dotted lines indicate the interquartile range. Data analysed by Wilcoxon matched-pairs signed rank test, *denotes $p<0.05$, *** denotes $p<0.001$.

Granzyme expression within CD4+ T cells in the tumour microenvironment

I next went on to undertake comparable analyses in relation to the CD4+ population within the OAC tumour microenvironment.

Initial comparative assessment of matched PBMC and TIL demonstrated no differences in expression of Granzyme A, B or K (Figure 108). Overall expression of granzyme was low within these populations and is in line with modest cytotoxic activity within this T cell lineage. However, analysis of matched CD4+ TRM and non-TRM TIL populations showed that Granzyme A and B were substantially increased in TRM from 4.6% to 15% and 3.9% to 12% respectively (p=0.0006, p=0.04), while Granzyme K expression was comparable.

I also went on to assess granzyme expression in relation to memory T cell subset between blood and TIL populations.

Expression of all granzyme proteins was low and comparable within the naïve CD4+ T cell pool (p=0.59 p=0.54, p=0.94). This pattern was also seen in central memory CD4+ TIL (p=0.95, p=0.58, p=0.66, Figure 109). Expression levels were somewhat higher in effector memory CD4+ TIL but were again equivalent between blood and tumour (p=0.50, p=0.67, p=0.63). The only difference observed overall was an increased expression of granzyme K within the TEMRA CD4+ TIL population. In particular, this T cell subset increased from 4.3% within blood to 13% within tumour (p=0.005, Figure 110).

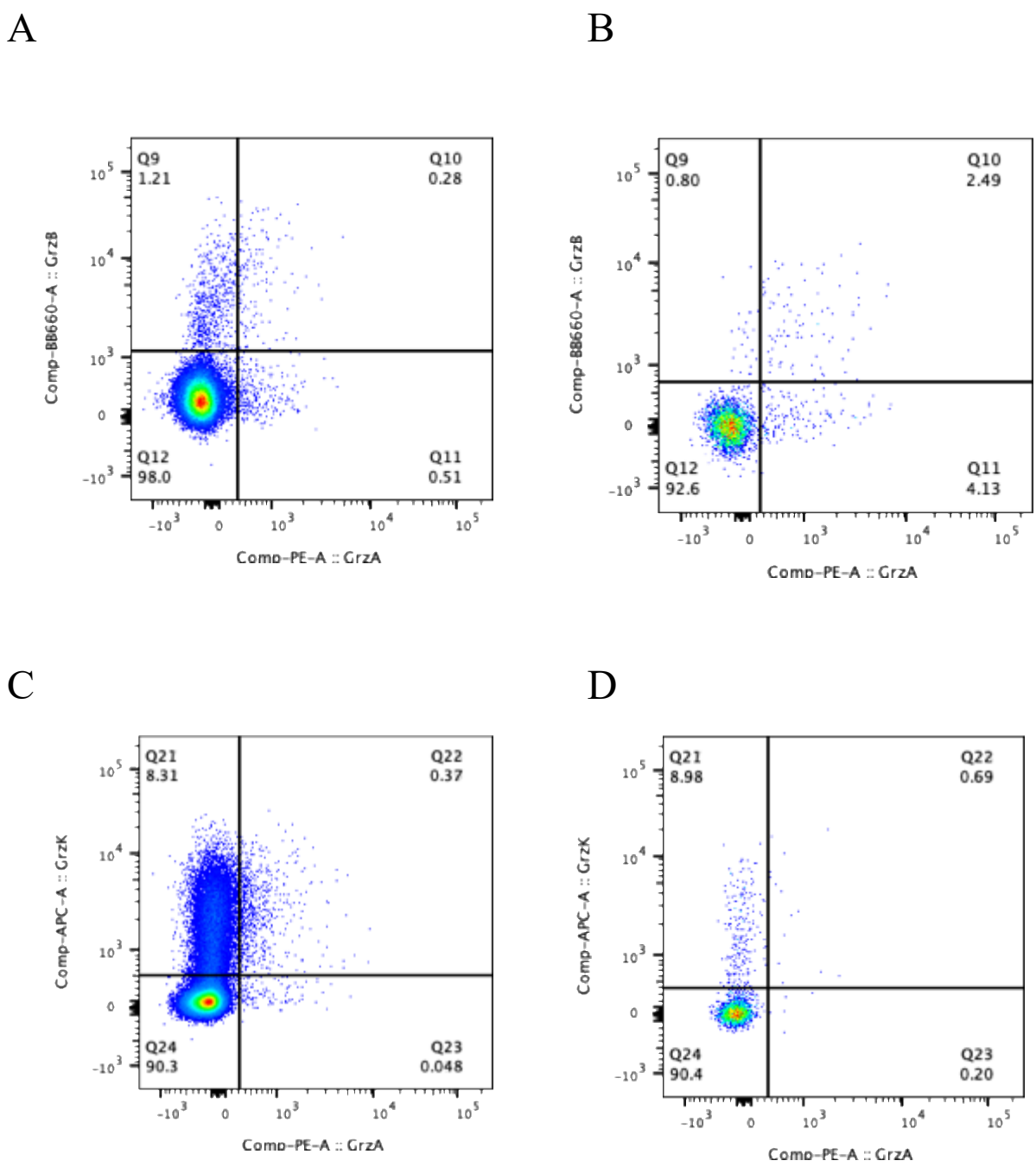

Figure 107. Representative flow plot of granzyme expression on CD4+ TIL
Granzyme expression was assessed in matched PBMC and TIL CD4+ T cells. Expression of Gzm A and Gzm B is shown in a representative sample on PBMC (A) and TIL (B). Expression of Gzm A and Gzm K is shown in a representative sample on PBMC (C) and TIL (D).

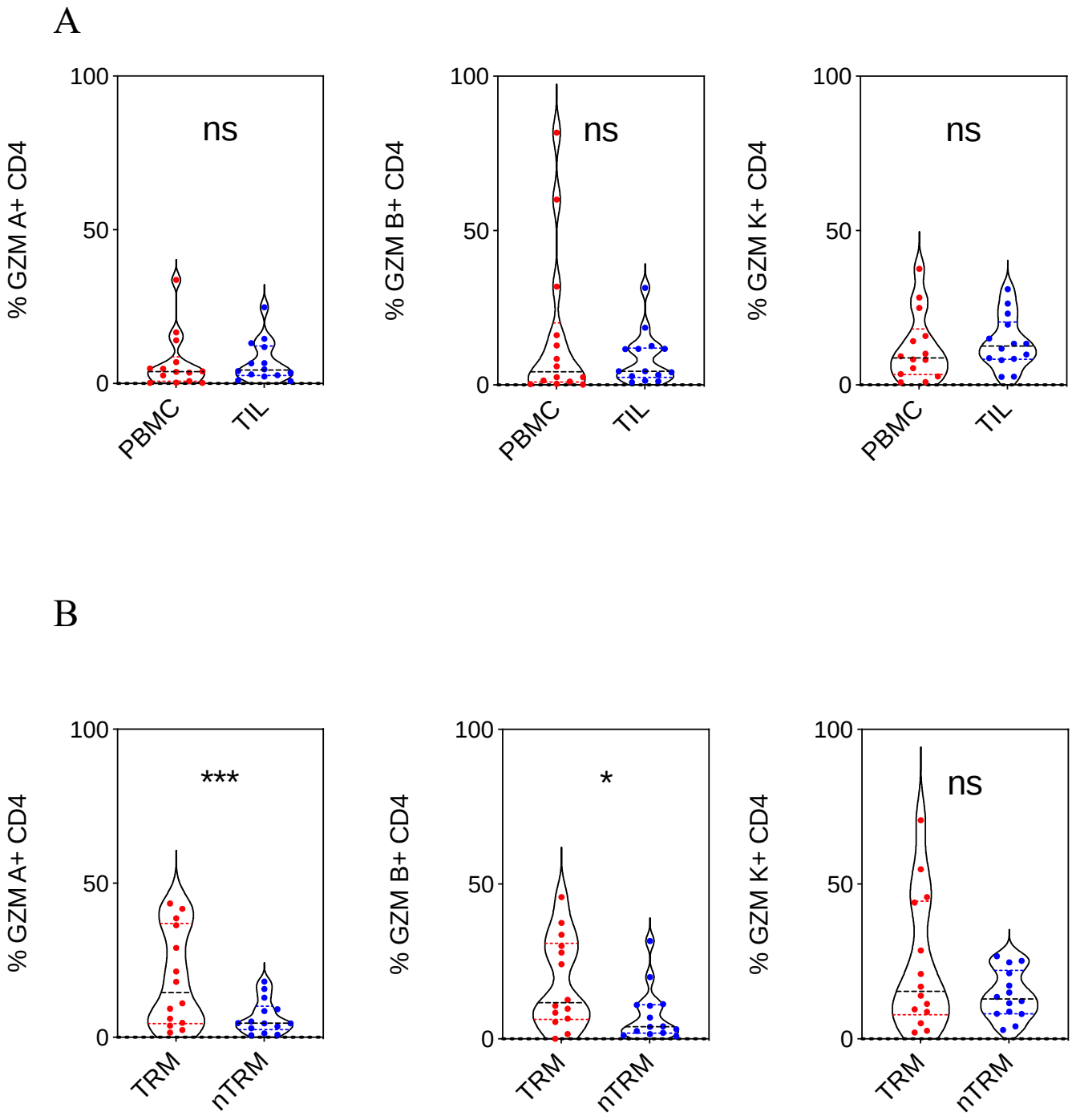

Figure 108. Profile of granzyme expression in PBMC, TIL and TRM CD4+ populations in OAC. Granzyme expression (Gzm A, B and K) in matched PBMC and TIL CD4 T cells (n=14, A). Granzyme expression (Gzm A, B and K) is also examined in tissue resident memory and non-TRM CD4+ T cells (n=14, B). Each symbol represents an individual patient. Dashed horizontal lines indicate the median and dotted lines indicate the interquartile range. Data analysed by Wilcoxon matched-pairs signed rank test, * denotes $p<0.05$ and *** 0.001.

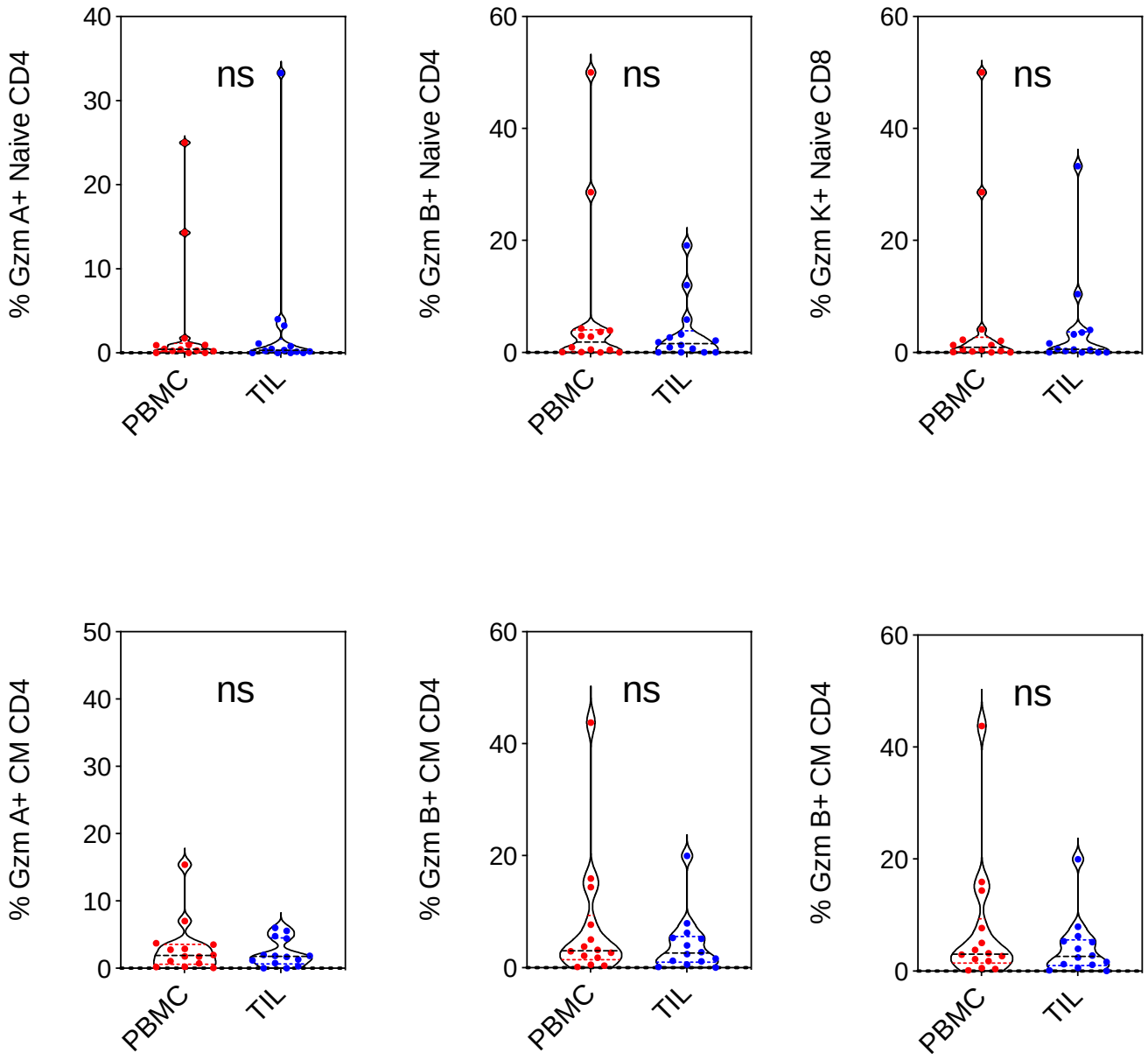

Figure 109. Profile of granzyme expression in matched PBMC and TIL naïve and central memory phenotype CD4+ T cells.
Granzyme expression (Gzm A, B and K) in matched PBMC and TIL naïve (n=14, A) and central memory CD4 T cells (n=14, B). Each symbol represents an individual patient. Dashed horizontal lines indicate the median and dotted lines indicate the interquartile range. Data analysed by Wilcoxon matched-pairs signed rank test.

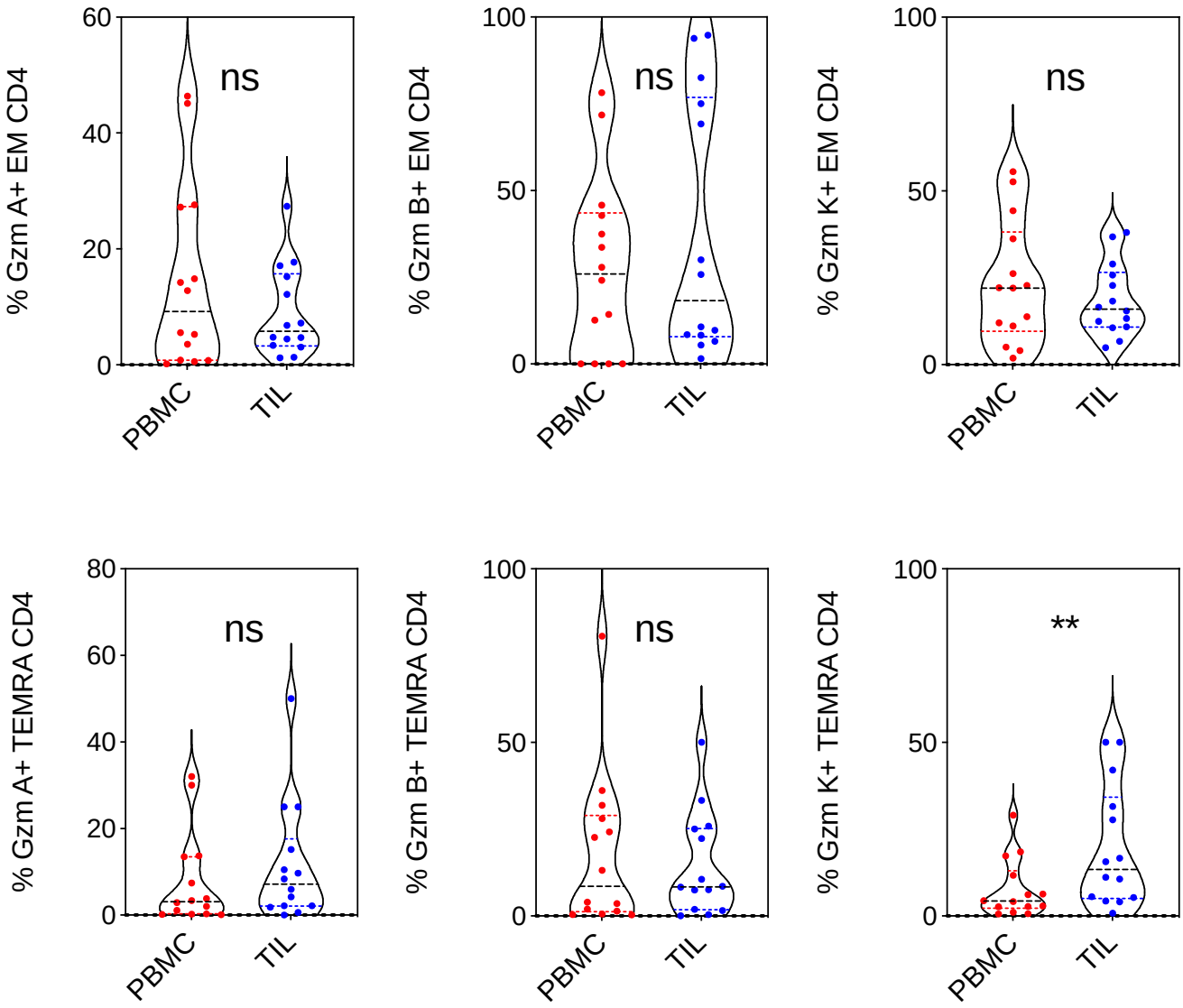

Figure 110. Profile of granzyme expression in matched effector and TEMRA CD4+ T cells in PBMC and TIL

Granzyme expression (Gzm A, B and K) in matched PBMC and TIL central memory (n=14, A) and TEMRA CD8 T cells (n=14, B). Each symbol represents an individual patient. Dashed horizontal lines indicate the median and dotted lines indicate the interquartile range. Data analysed by Wilcoxon matched-pairs signed rank test.

Expression of activating and inhibitory proteins on CD4+ T cells within TIL

I next went on to assess expression of the activating and regulatory proteins, that I had used previously to interrogate CD8+ populations, on the CD4+ pool in order to allow a comparative profile of their expression on the two major T cell lineages.

Of note, CD39+ was strongly expressed on CD4+ TRM and was observed on 10% of cells compared to 1.3% of the non-TRM pool (p=0.001). GITR expression was also increased modestly from 0.3% to 2.6% (p=0.0006, Figure 111).

Comparative assessment of PBMC and TIL CD4+ T cells demonstrated upregulation of Ki-67 and HLA-DR within the tumour whereas there was no change in HSP70 or CD94 (p=0.002, p=0.0002, p=0.06, p=0.71, Figure 112). As such, CD4+ T cells within tumour appear to be undergoing higher levels of activation and proliferation.

Next, I examined expression of these proteins within TRM and non-TRM subsets. Higher expression of HSP70, Ki-67 and HLA-DR was observed on TRM whilst CD94 levels were comparable (p=0.002; p=0.02; p=0.0001; p=0.58, Figure 113). The relative increase in proliferation and activation was particularly marked within the TRM pool.

A

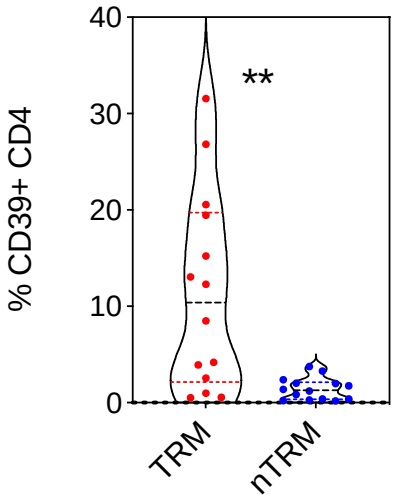

B

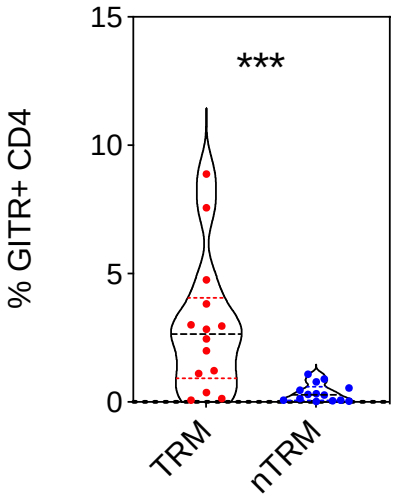

Figure 111. CD39 and GITR expression on CD4+ T cells in relation to tissue residency status in OAC. Expression of CD39 on TRM and non-TRM CD4 TIL(A) and GITR expression on TRM and non-TRM CD4 TIL(B) (n=14, TRM-CD69+CD103+, nonTRM- CD69-CD103-, CD69+CD103-, CD69-CD103+). Each symbol represents an individual patient. Dashed horizontal lines indicate the median and dotted lines indicate the interquartile range. Data analysed by Wilcoxon matched-pairs signed rank test, ** denotes $p<0.01$, *** denotes $p<0.001$.

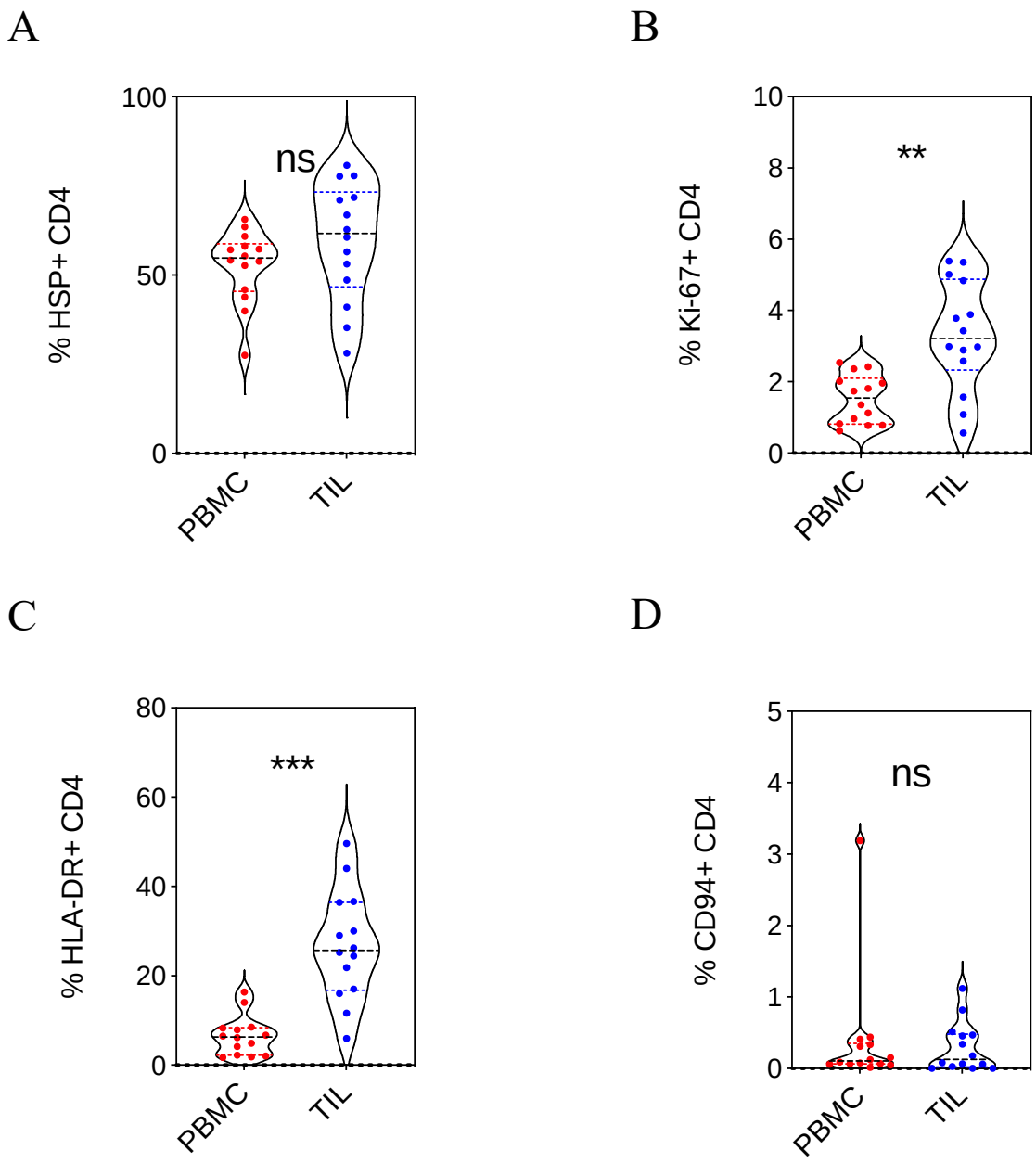

Figure 112. Phenotypic profile of CD4+ cells in PBMC and TIL of patients with OAC
Expression of heat shock protein (A), Ki-67 (B), HLA-DR (C) and CD94 (D) was assessed in matched PBMC and TIL CD4+ T cells (n=14). Each symbol represents an individual patient. Dashed horizontal lines indicate the median and dotted lines indicate the interquartile range. Data analysed by Wilcoxon matched-pairs signed rank test.

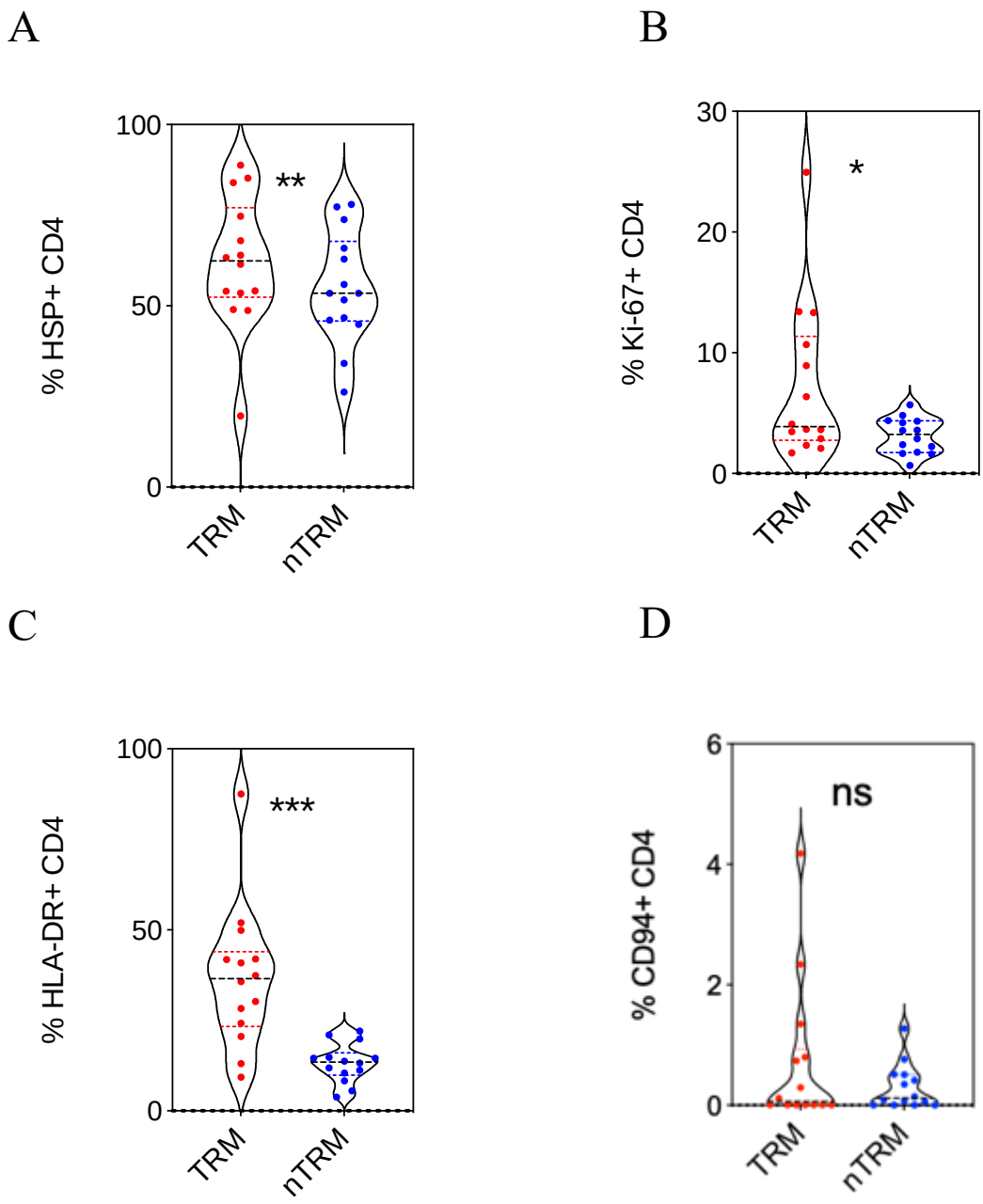

Figure 113. Phenotypic variation of CD4 T cells in relation to tissue residency
Expression of heat shock protein (A), Ki-67 (B), HLA-DR (C) and CD94 (D) in matched PBMC and TIL CD4 T cells (n=14, TRM-CD69+CD103+, nonTRM- CD69-CD103-, CD69+CD103-, CD69-CD103+). Each symbol represents an individual patient. Dashed horizontal lines indicate the median and dotted lines indicate the interquartile range. Data analysed by Wilcoxon matched-pairs signed rank test, ** denotes $p<0.01$ and *** $p<0.001$.

Comparative analysis of CD4+ memory subsets in blood and tumour of patients with OAC

My subsequent analysis determined the level of protein expression on CD4+ memory T cell subsets in tumour and blood.

On the naïve CD4+ pool, HSP70, Ki-67 and CD94 expression was comparable between PBMC and TIL. However, higher levels of HLA-DR were seen on within the TIL (3.7% vs 0.7% (p=0.02)). Central memory CD4+ TIL upregulated Ki-67 from 1.2% to 3.7% and HLA-DR from 2.5% to 13.7%, whereas HSP70 and CD94 were unaltered (p=0.006, p=0.0001, p=0.30, p=0.22, Figure 114). Effector memory CD4 TIL significantly upregulated HLA-DR from 5.6% to 16.5% whereas there was no change in Ki-67, HSP70 or CD94 (p=0.0002, p=0.058, p=0.27, p=0.86, Figure 115). TEMRA CD4 TIL significantly upregulated HLA-DR from 5.4% to 12.5% whereas there was no change in Ki-67, HSP70 or CD94 (p=0.03, p=0.14, p=0.14, p=0.33, Figure 116).

As such, the predominant proliferative pool within OAC is the central memory pool whilst the activation marker HLA-DR is expressed widely across all effector populations. HSP70 and CD94 show no differences between blood and tumour.

Administration of neoadjuvant chemotherapy did not have any impact of the expression of HSP70, Ki-67, HLA-DR or CD94 on CD4+ TIL although there was a trend towards an increase in HLA-DR expression after treatment (Figure 118). Chemotherapy also did not alter granzyme expression within T cell subsets (Figure 119).

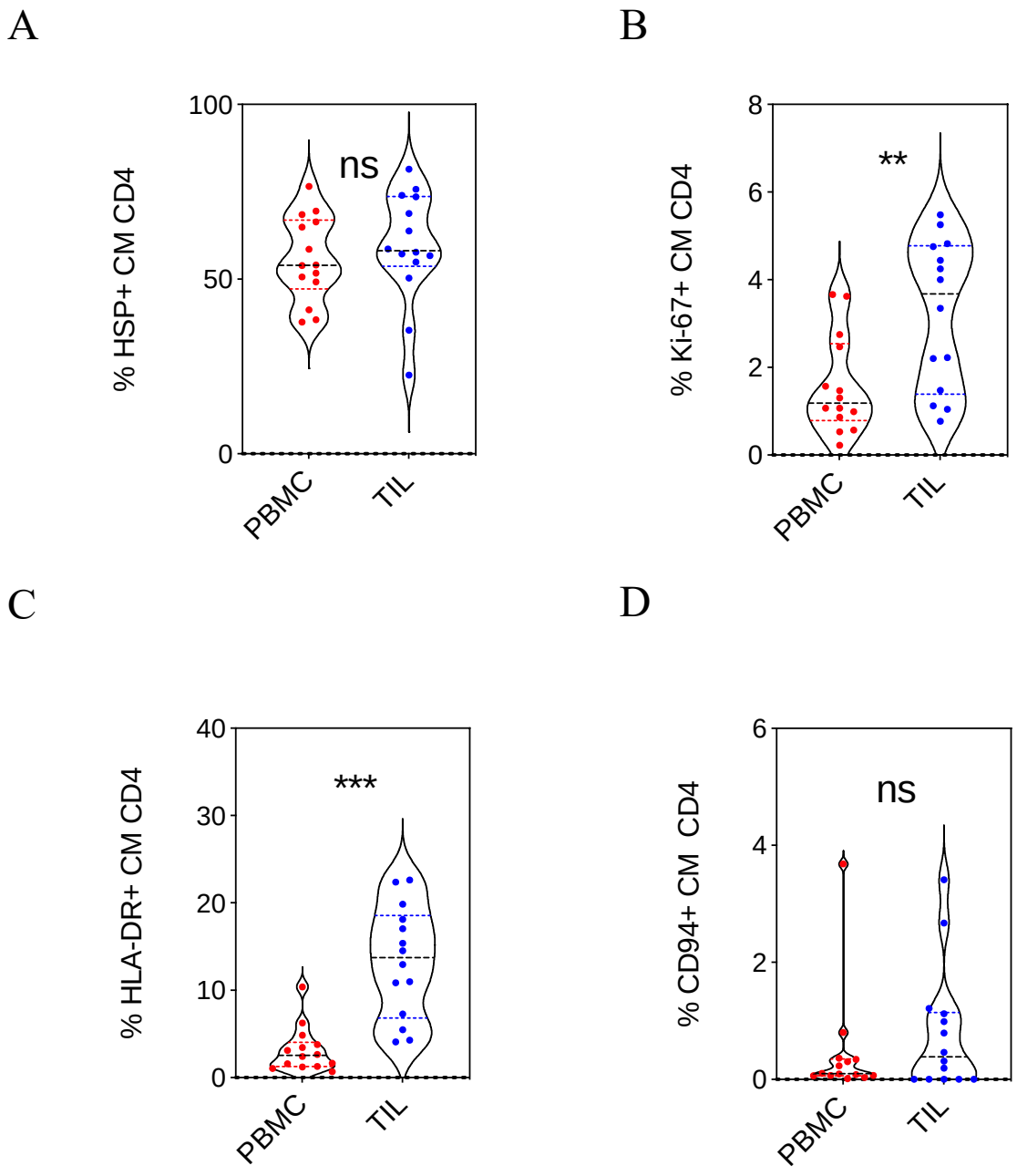

Figure 114. Phenotypic profile of matched PBMC and TIL Central Memory CD4+ T cells.
Expression of heat shock protein (A), Ki-67 (B), HLA-DR (C) and CD94 (D) in matched PBMC and TIL CM CD4 T cells (n=14, CM: CCR7+CD45RA-). Each symbol represents an individual patient. Dashed horizontal lines indicate the median and dotted lines indicate the interquartile range. Data analysed by Wilcoxon matched-pairs signed rank test.

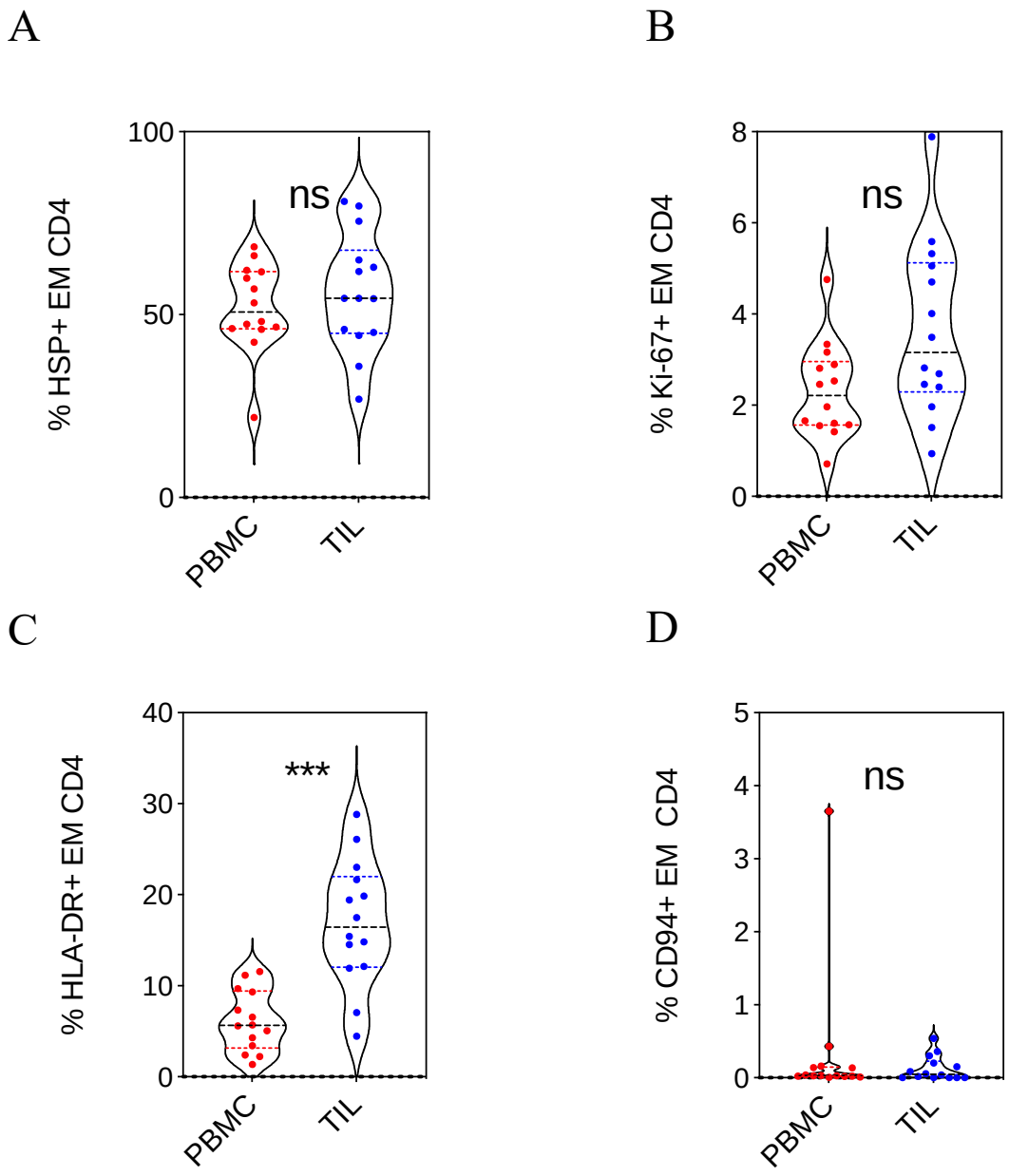

Figure 115. Phenotypic profile of matched PBMC and TIL effector memory (EM) CD4+ T cells. Expression of heat shock protein (A), Ki-67 (B), HLA-DR (C) and CD94 (D) was determined in matched PBMC and TIL EM CD4+ T cells (n=14, CCR7-CD45RA-). Each symbol represents an individual patient. Dashed horizontal lines indicate the median and dotted lines indicate the interquartile range. Data analysed by Wilcoxon matched-pairs signed rank test.

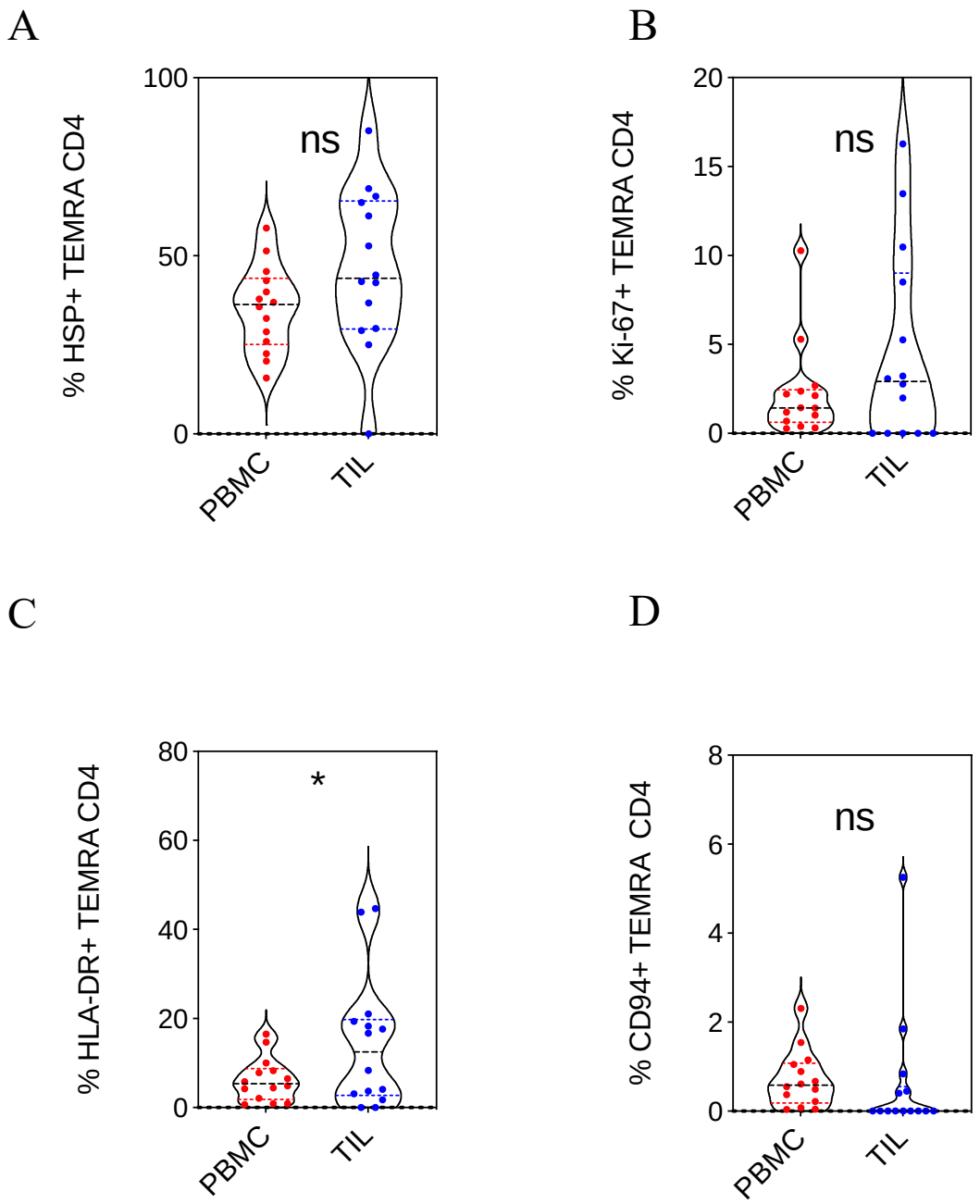

Figure 116. Phenotypic profile of matched PBMC and TIL TEMRA CD4+ T cells.
Expression of heat shock protein (A), Ki-67 (B), HLA-DR (C) and CD94 (D) in matched PBMC and TIL EM CD4 T cells (n=14, CCR7-CD45RA+). Each symbol represents an individual patient. Dashed horizontal lines indicate the median and dotted lines indicate the interquartile range. Data analysed by Wilcoxon matched-pairs signed rank test,.

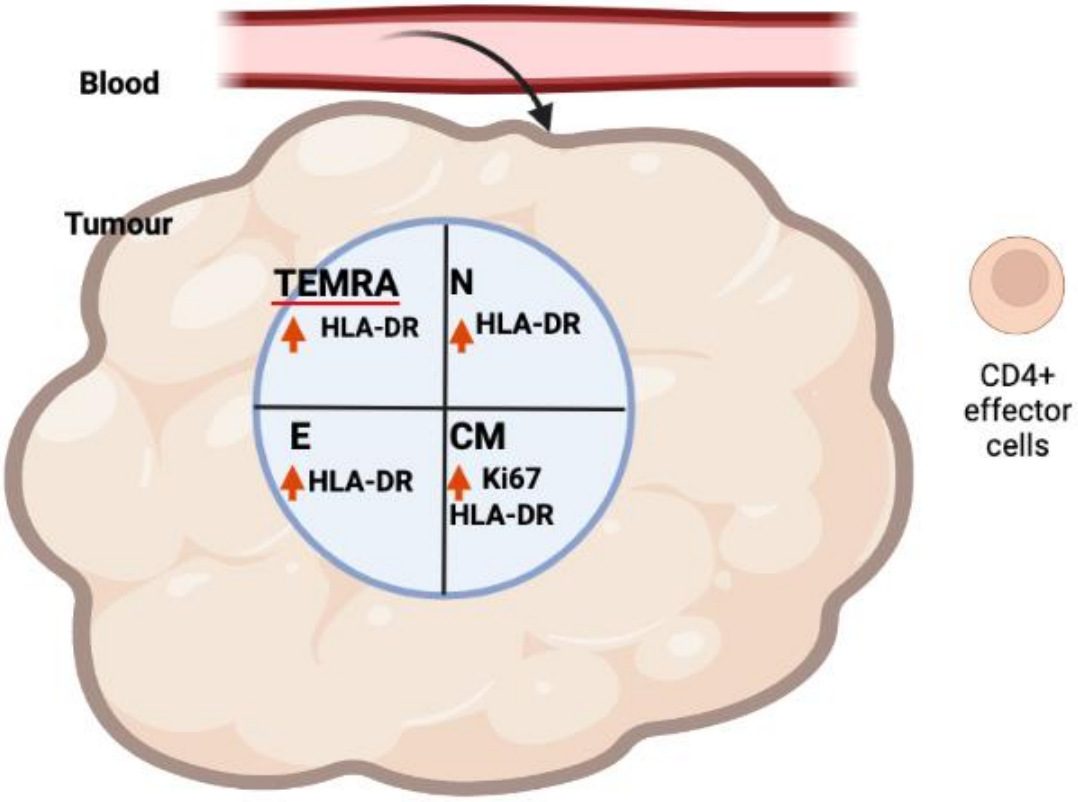

Figure 117. Graphical representation of relative phenotype of CD4+ effector memory subsets within PAC tumour compared to blood
Increased expression of HLA-DR is observed on all memory subsets whilst proliferation is increased only within the central memory pool.
N=naive, CM=central memory, E=effector, TEMRA=CD45RA+ effector memory.

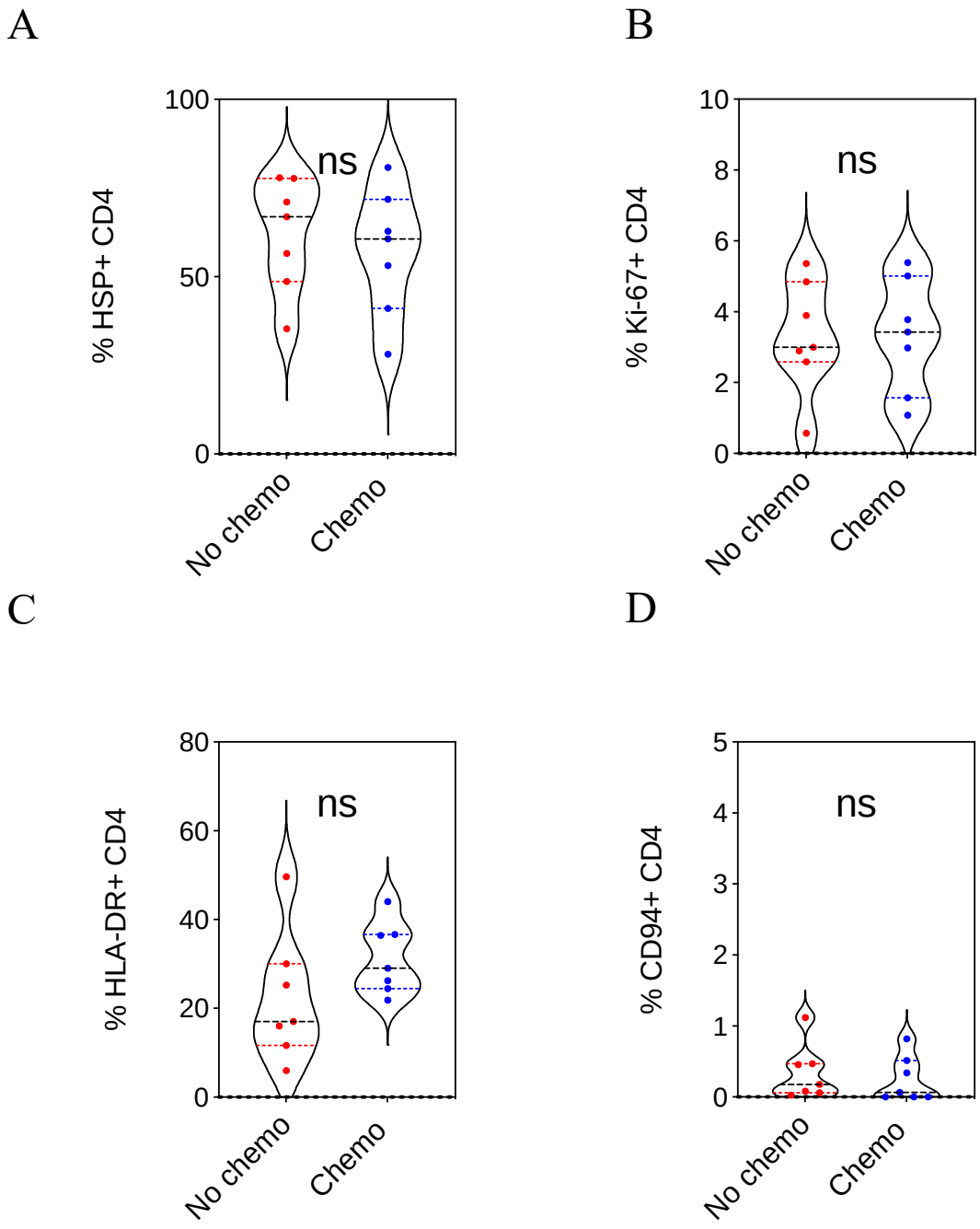

Figure 118. Phenotypic profile of CD4+ T cells in tumour in relation to neoadjuvant chemotherapy usage
Expression of heat shock protein (A), Ki-67 (B), HLA-DR (C) and CD94 (D) on CD4+ TIL within patients who have and have not received neoadjuvant chemotherapy (No chemo n=7, chemo n=7). Each symbol represents an individual patient. Dashed horizontal lines indicate the median and dotted lines indicate the interquartile range. Data analysed by Mann Whitney Test.

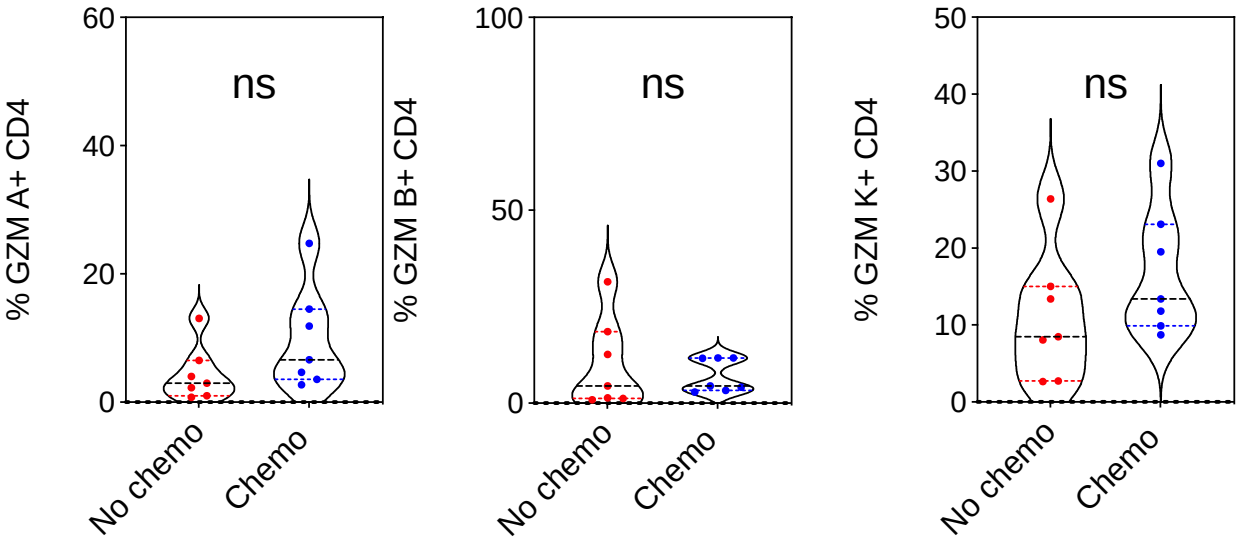

Figure 119. Profile of granzyme expression on CD4+ TIL in relation to chemotherapy administration
Granzyme expression (Gzm A, B and K) in CD4+ TIL for patients who have and have not received neoadjuvant chemotherapy (No chemo n=7, chemo n=7, A). Each symbol represents an individual patient. Dashed horizontal lines indicate the median and dotted lines indicate the interquartile range. Data analysed by Mann Whitney Test (unpaired chemo analysis), Wilcoxon matched-pairs signed rank test (paired CD39 analysis), * denotes $p<0.05$.

Phenotypic expression of CD39+ CD4+ T cells within OAC

Next, I assessed the expression of HSP70, Ki-67, HLA-DR and CD94 of conventional CD4+ T cells in relation to the expression of CD39, given its potential significance as a marker of tumour specificity within the CD8+ T cell compartment.

Here it was noteworthy that expression of Granzyme A was doubled in CD39+ TRM compared to CD39- CD4+ T cells, at 9.0% compared to 4.5% respectively (p=0.01). In contrast, expression of Granzyme B and K was comparable between these two subsets (Figure 120).

Expression of HSP70, Ki-67 and HLA-DR were significantly increased on CD39+ TRM compared to all other CD4 T cells (p=0.0001, p=0.0001, p=0.0001). In particular, HSP70 expression increased from 55% to 64%, Ki-67 from 3.4% to 6.8% and HLA-DR from 16% to 32%. Expression of CD94 in CD39+ TRM was unaltered (Figure 121).

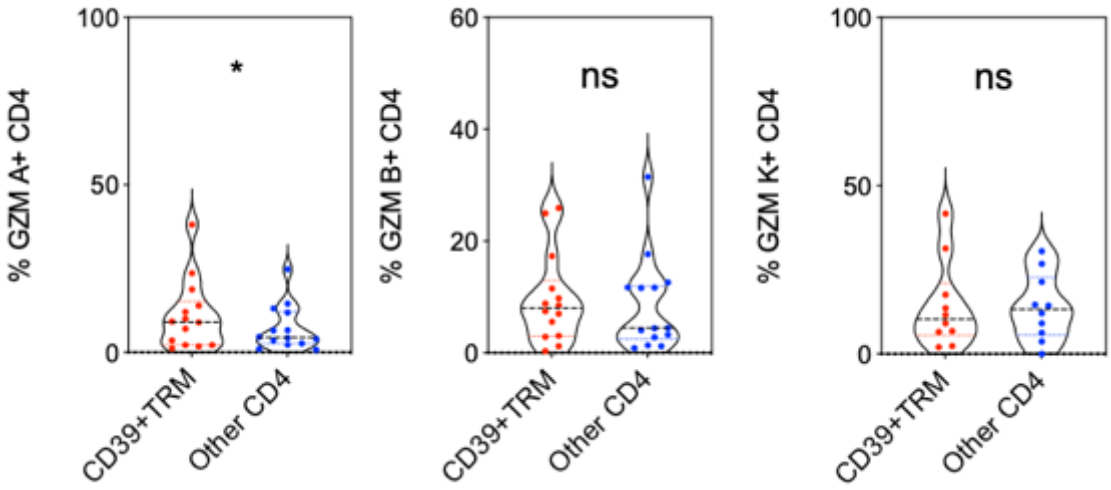

Figure 120. Profile of granzyme expression on CD4+ TIL in relation to expression of CD39
Granzyme expression (Gzm A, B and K) was assessed on CD4+ T cells in relation to CD39 expression on TRM (n=14). Each symbol represents an individual patient. Dashed horizontal lines indicate the median and dotted lines indicate the interquartile range. Data analysed by Mann Whitney Test (unpaired chemo analysis), Wilcoxon matched-pairs signed rank test (paired CD39 analysis), * denotes $p<0.05$.

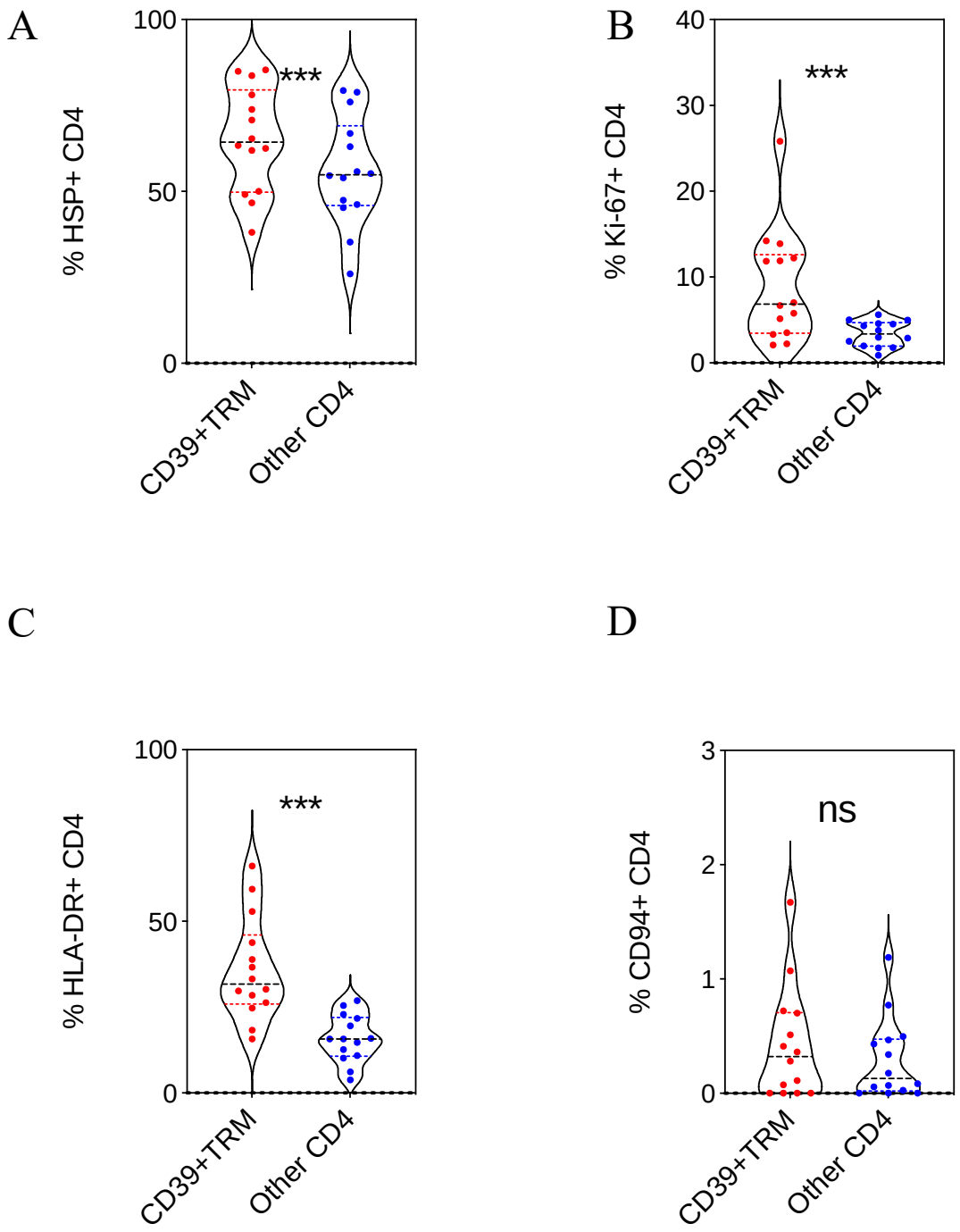

Figure 121. Phenotypic profile of CD4+ TRM within TIL in relation to expression of CD39+
Expression of heat shock protein (A), Ki-67 (B), HLA-DR (C) and CD94 (D) on CD39+ TRM CD4 TIL compared to CD39- subsets (n=14). Each symbol represents an individual patient. Dashed horizontal lines indicate the median and dotted lines indicate the interquartile range. Data analysed by Wilcoxon matched-pairs signed rank test, *denotes $p<0.05$, **** denotes $p<0.0001$.

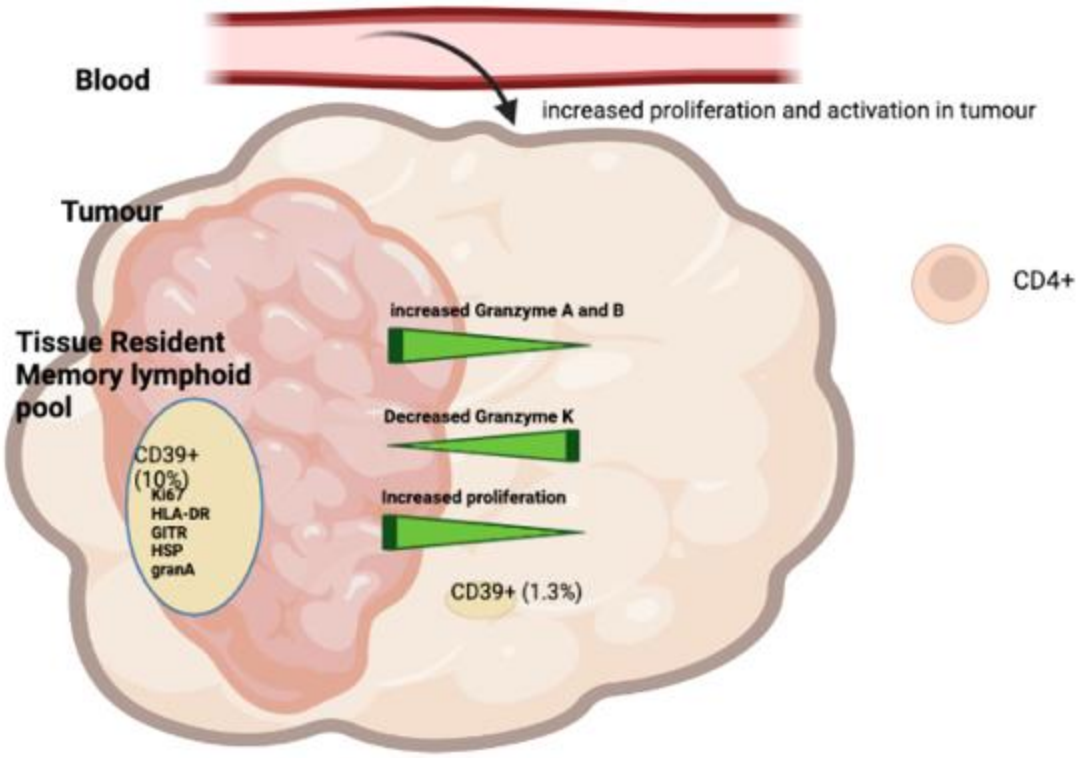

Figure 122. Graphical representation of phenotype of effector CD4+ T cells within the OAC microenvironment
CD4+ cells within the TRM pool show increased proliferation and granzyme expression whilst this is further enhanced in the CD39+ subset within TRM.

Phenotypic analysis of T regulatory cells within OAC

Finally, I was also interested to determine the extended phenotype of CD4+ T regulatory cells in OAC. These were defined as cells with a CD4+CD25+CD127- phenotype.

Initial studies looked at the expression of granzyme proteins which are typically expressed at low levels within the CD4+ population. Comparative assessment in PBMC and TIL showed no significant difference in Granzyme A, B or K expression on Treg between blood and tumour ($p=0.08$, $p=0.86$ $p=43$, Figure 124).

I next went on to assess TRM subpopulations of T reg cells. Here I found that expression of Granzyme B was markedly increased in TRM from 1.1% to 7.0% ($p=0.04$). This suggests that Treg with a cytotoxic phenotype may be present within the TRM pool. In contrast, there was no difference in Granzyme A and K expression between TRM and non-TRM populations ($p=0.13$, $p=0.06$).

Comparative assessment of granzyme expression in different memory subsets of Treg cells within PBMC and TIL was also undertaken. Granzyme levels were very low in the naïve population but increased somewhat in the effector pools. However, there were no differences observed between values in blood or tumour (Figures 125,126).

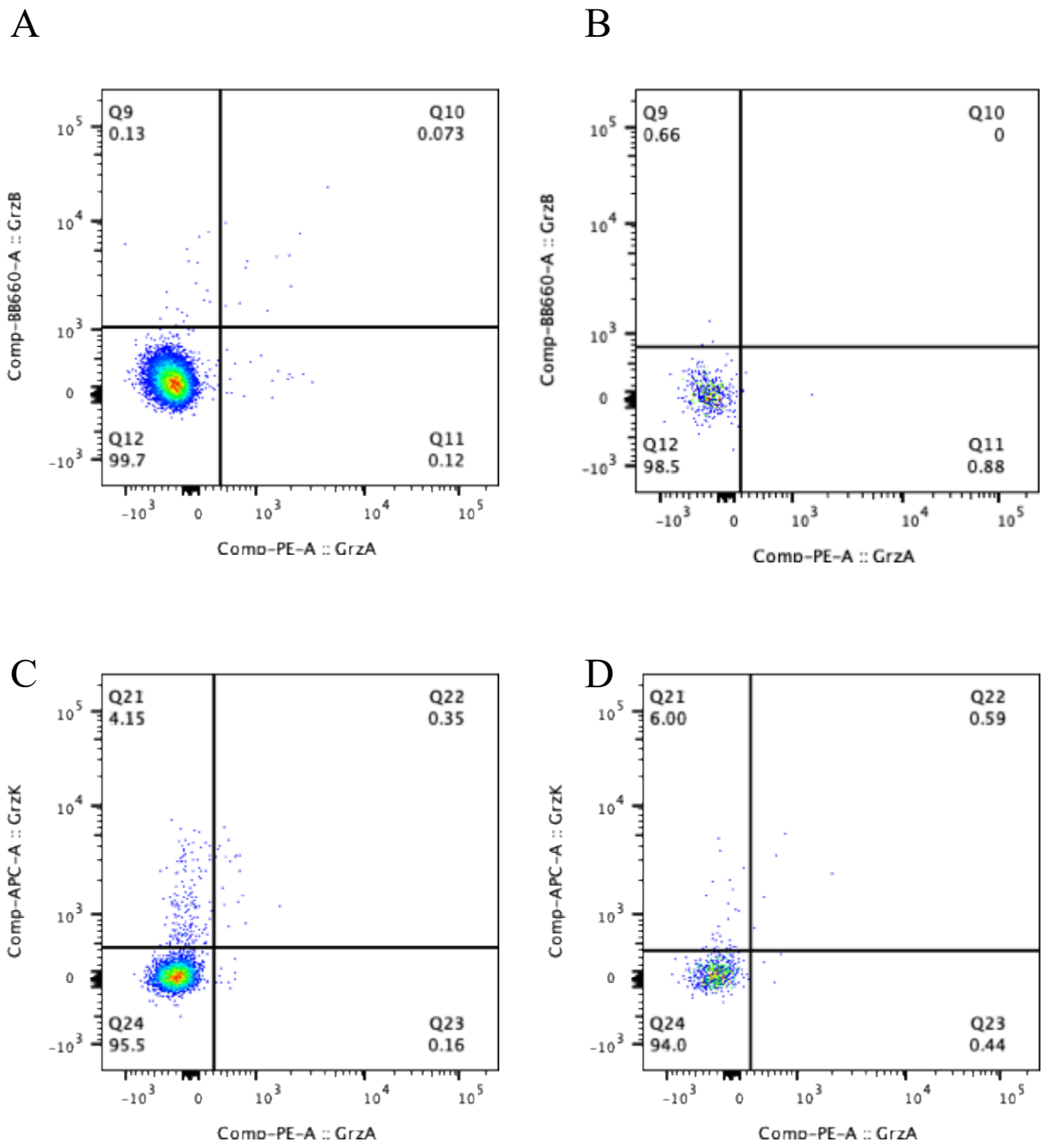

Figure 123. Representative flow plot of granzyme expression on Treg TIL
Granzyme expression was assessed in matched PBMC and TIL T regulatory cells. Expression of Gzm A and Gzm B is shown in a representative sample on PBMC (A) and TIL (B). Expression of Gzm A and Gzm K is shown in a representative sample on PBMC (C) and TIL (D).

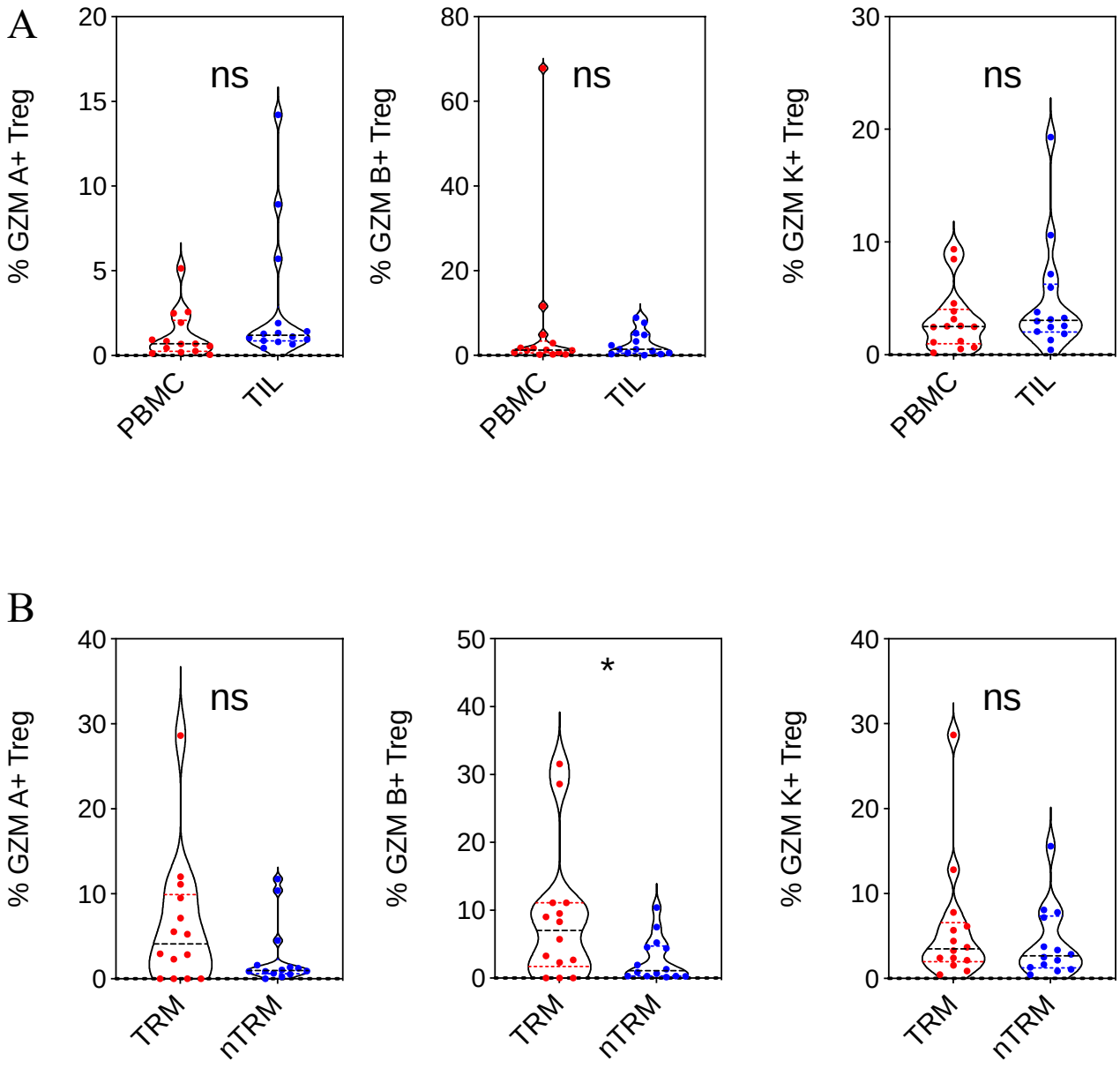

Figure 124. Profile of granzyme expression in Treg cells within PBMC/TIL or TRM subsets
Granzyme expression (Gzm A, B and K) was determined in matched PBMC and TIL T reg (n=14, A) and also in tissue resident memory (TRM) or non-TRM T reg cells (n=14, B). Each symbol represents an individual patient. Dashed horizontal lines indicate median value whilst dotted lines indicate the interquartile range. Data analysed by Wilcoxon matched-pairs signed rank test, * denotes $p<0.05$ and *** 0.001.

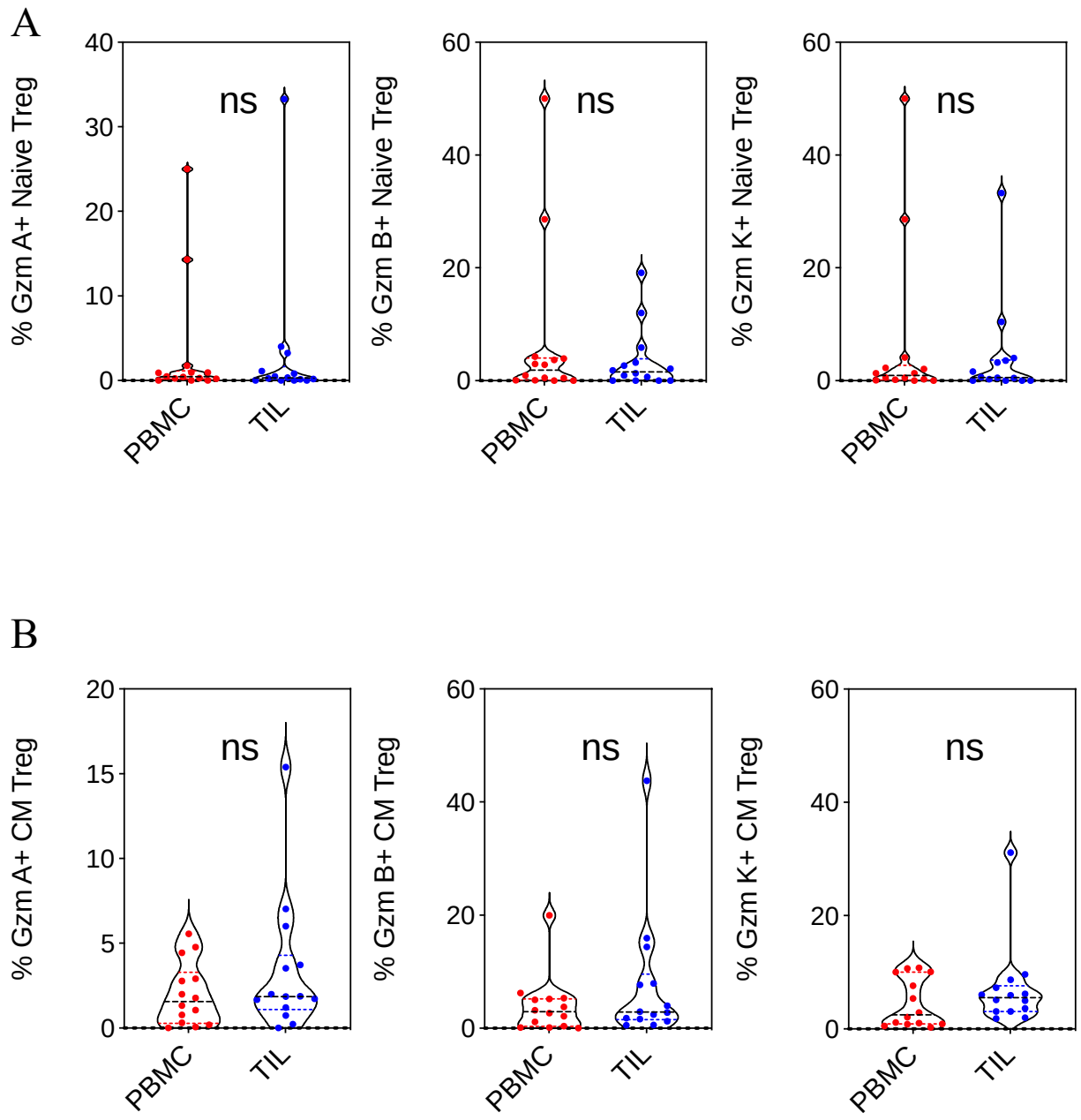

Figure 125. Profile of granzyme expression in PBMC and TIL Treg memory subsets
Granzyme expression (Gzm A, B and K) was determined in matched PBMC and TIL naïve (n=14, A) and central memory Treg (n=14, B). Each symbol represents an individual patient. Dashed horizontal lines indicate the median and dotted lines indicate the interquartile range. Data analysed by Wilcoxon matched-pairs signed rank test, * denotes $p<0.05$.

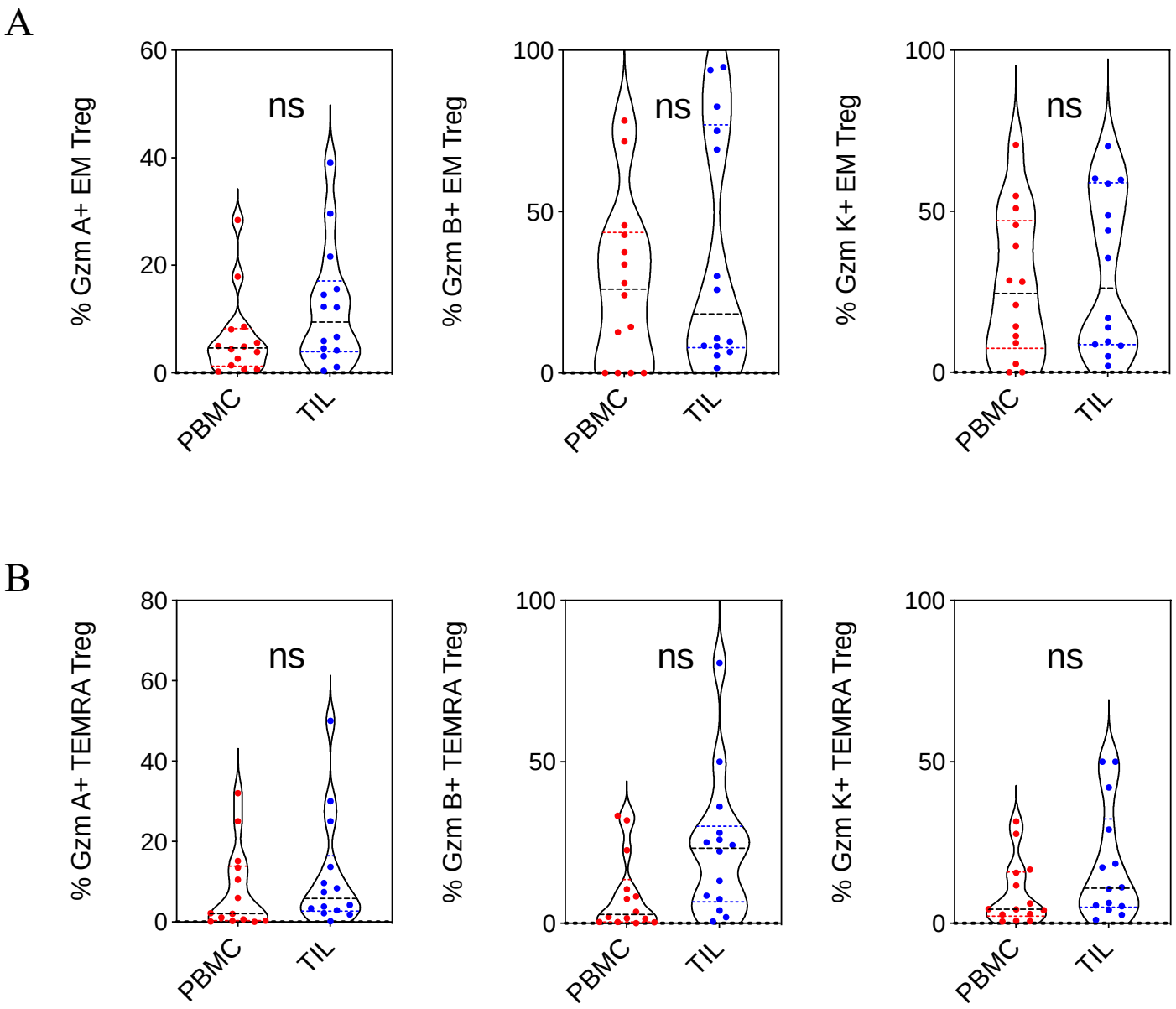

Figure 126. Profile of granzyme expression in PBMC and TIL Treg memory subsets
Granzyme expression (Gzm A, B and K) was determined in matched PBMC and TIL effector memory (n=14, A) and CD45RA effector memory T reg (n=14, B). Each symbol represents an individual patient. Dashed horizontal lines indicate the median and dotted lines indicate the interquartile range.
Data analysed by Wilcoxon matched-pairs signed rank test, ** denotes $p<0.01$, ***denotes $p<0.001$.

Expression of proliferation, activation and inhibitory proteins on Treg cells in OAC

Comparative assessment of Treg populations within PBMC and TIL demonstrated strong upregulation of Ki-67 and HLA-DR expression within the tumour, indicating proliferation and activation of Treg cells within that environment (p=0.02, p=0.02). Ki6-7 was observed within 12% of Treg within tumour compared to 5% within blood. The comparable increase for HLA-DR was from 7.5% to 18%. In contrast there were no major differences in HSP70 or CD94 expression (Figure 127).

Comparison of TRM and non-TRM TIL Treg demonstrated marginal downregulation of HSP70 in TRM (64% vs 61%; p=0.049) but otherwise no differences in Ki-67, HLA-DR or CD94 expression (Figure 128). In addition, comparison of these markers within different memory subsets of Tregs demonstrated no differences (Figures 129-132).

Finally, in order to complete my analysis of T cell phenotypes I determined the Treg phenotype in relation to neo-adjuvant chemotherapy. Administration of neoadjuvant chemotherapy did not significantly alter HSP70, Ki-67, HLA-DR or CD94 expression in Treg TIL (Figure 133). In contrast, usage of chemotherapy acted to increase expression of granzymes in Treg cells. Granzyme A expression increased from 0.9% to 1.4% and that of granzyme K from 2.5% to 6% compared to patients who did not receive neoadjuvant chemotherapy (p=0.02, p=0.03, Figure 134).

These findings suggest that the small cytotoxic subset of regulatory T cells undergoes a relative increase following neo-adjuvant chemotherapy.

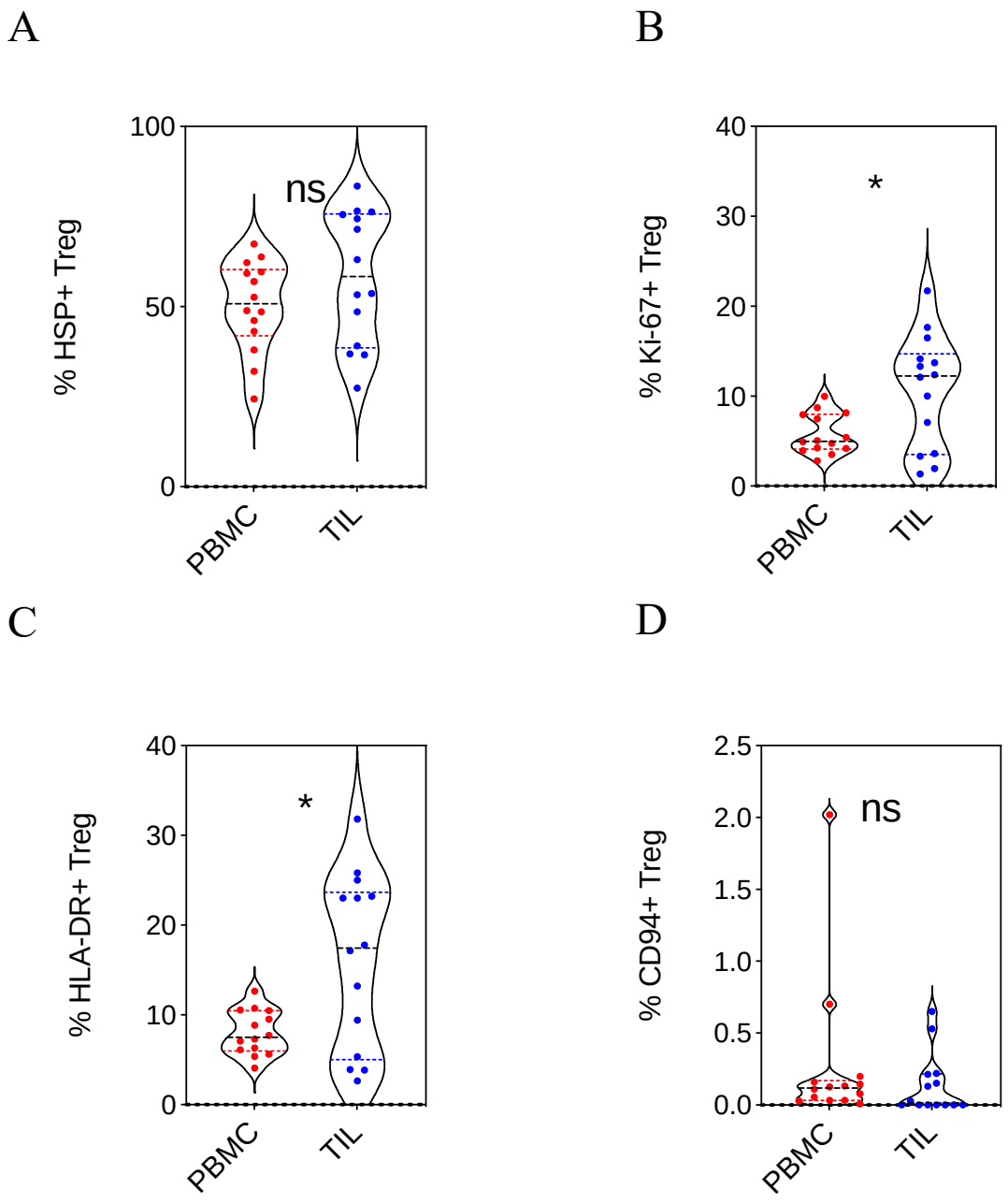

Figure 127. Phenotypic analysis of T reg cells in PBMC and tumour.
Expression of heat shock protein (A), Ki-67 (B), HLA-DR (C) and CD94 (D) was determined in matched PBMC and TIL Treg cells (n=14). Each symbol represents an individual patient. Dashed horizontal lines indicate the median and dotted lines indicate the interquartile range. Data analysed by Wilcoxon matched-pairs signed rank test, * denotes $p<0.05$ and ** $p<0.01$.

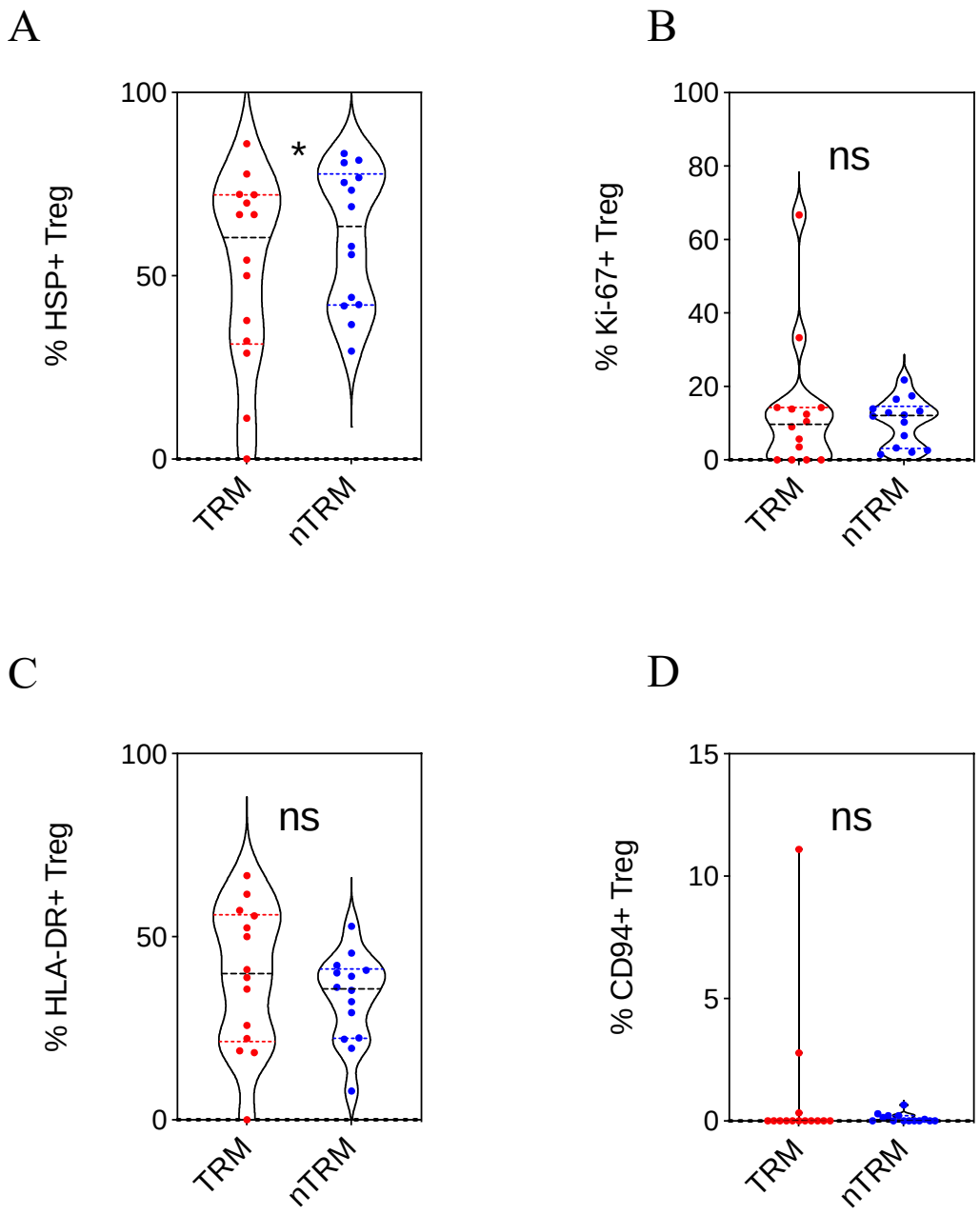

Figure 128. Phenotypic profile of T regulatory cells in relation to TRM status.
Expression of heat shock protein (A), Ki-67 (B), HLA-DR (C) and CD94 (D) on Treg in matched PBMC and TIL samples according to TRM or non-TRM status (n=14). Each symbol represents an individual patient. Dashed horizontal lines indicate the median and dotted lines indicate the interquartile range. Data analysed by Wilcoxon matched-pairs signed rank test, ** denotes $p<0.01$ and *** $p<0.001$.

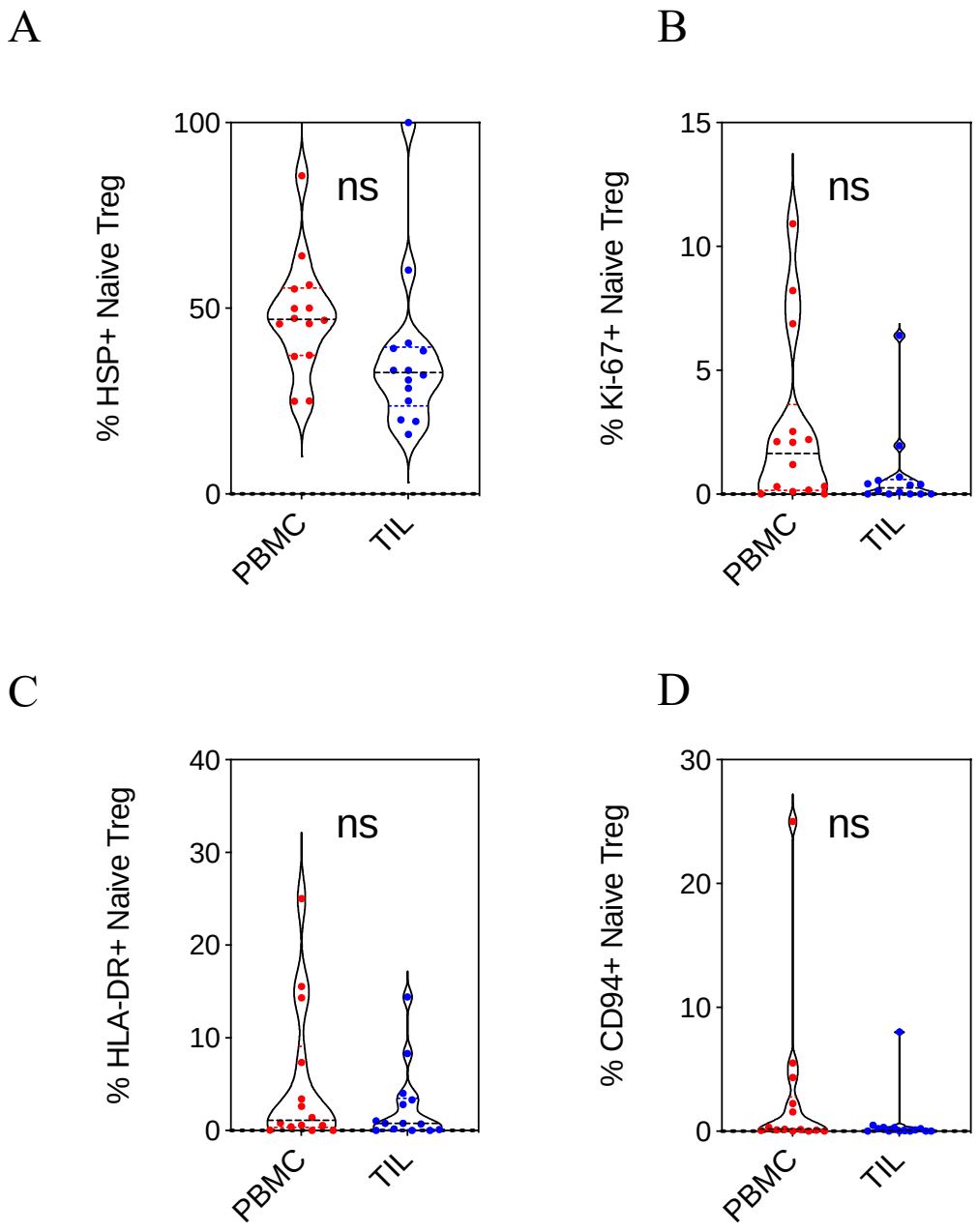

Figure 129. Phenotypic profile of naïve Treg in blood and tumour of patients with OAC
Expression of heat shock protein (A), Ki-67 (B), HLA-DR (C) and CD94 (D) in matched PBMC and TIL naive Treg cells (n=14). Each symbol represents an individual patient. Dashed horizontal lines indicate the median and dotted lines indicate the interquartile range. Data analysed by Wilcoxon matched-pairs signed rank test.

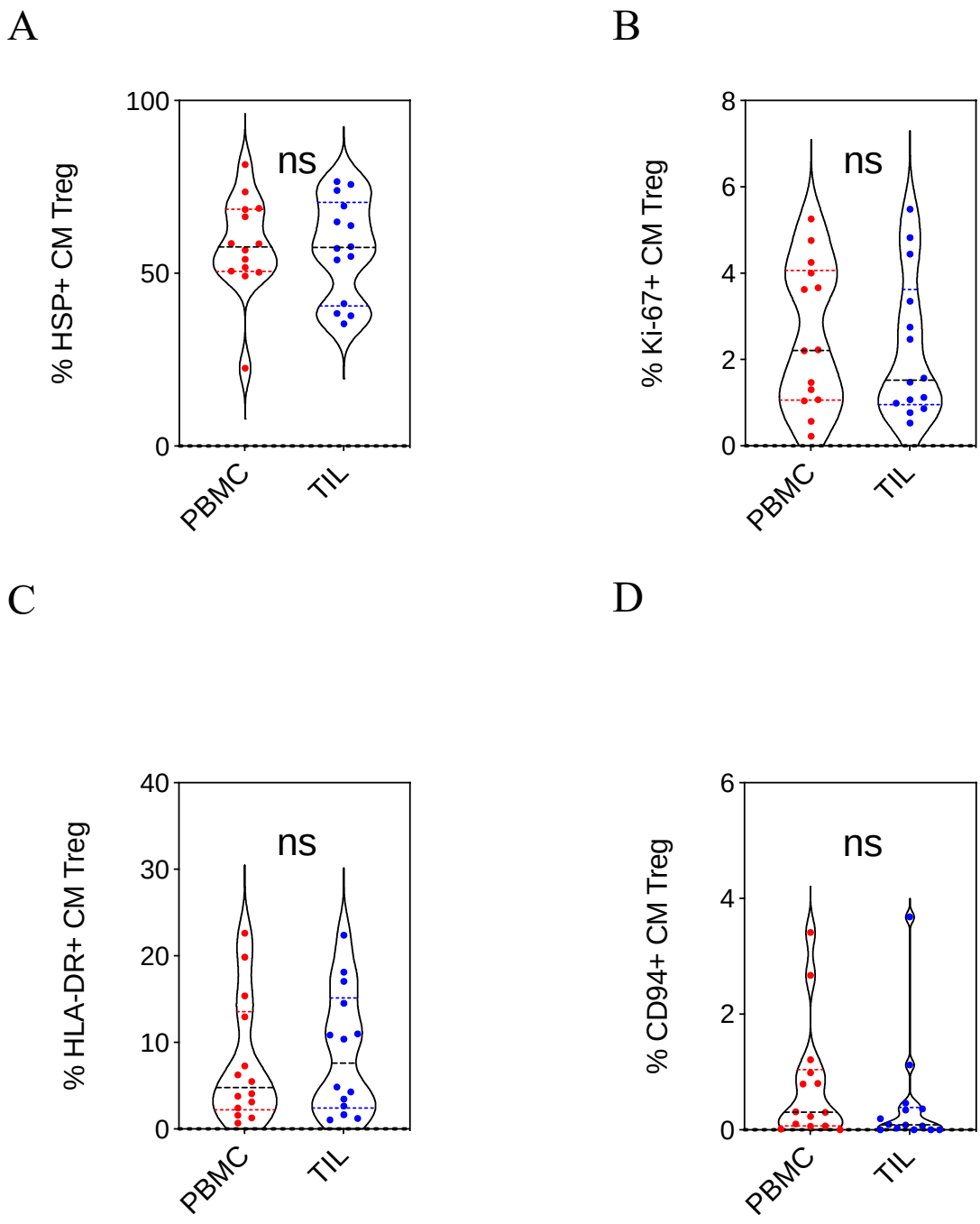

Figure 130. Phenotypic profile of central memory Treg in blood and tumour of patients with OAC
Expression of heat shock protein (A), Ki-67 (B), HLA-DR (C) and CD94 (D) in matched PBMC and TIL CM Treg (n=14). Each symbol represents an individual patient. Dashed horizontal lines indicate the median and dotted lines indicate the interquartile range. Data analysed by Wilcoxon matched-pairs signed rank test.

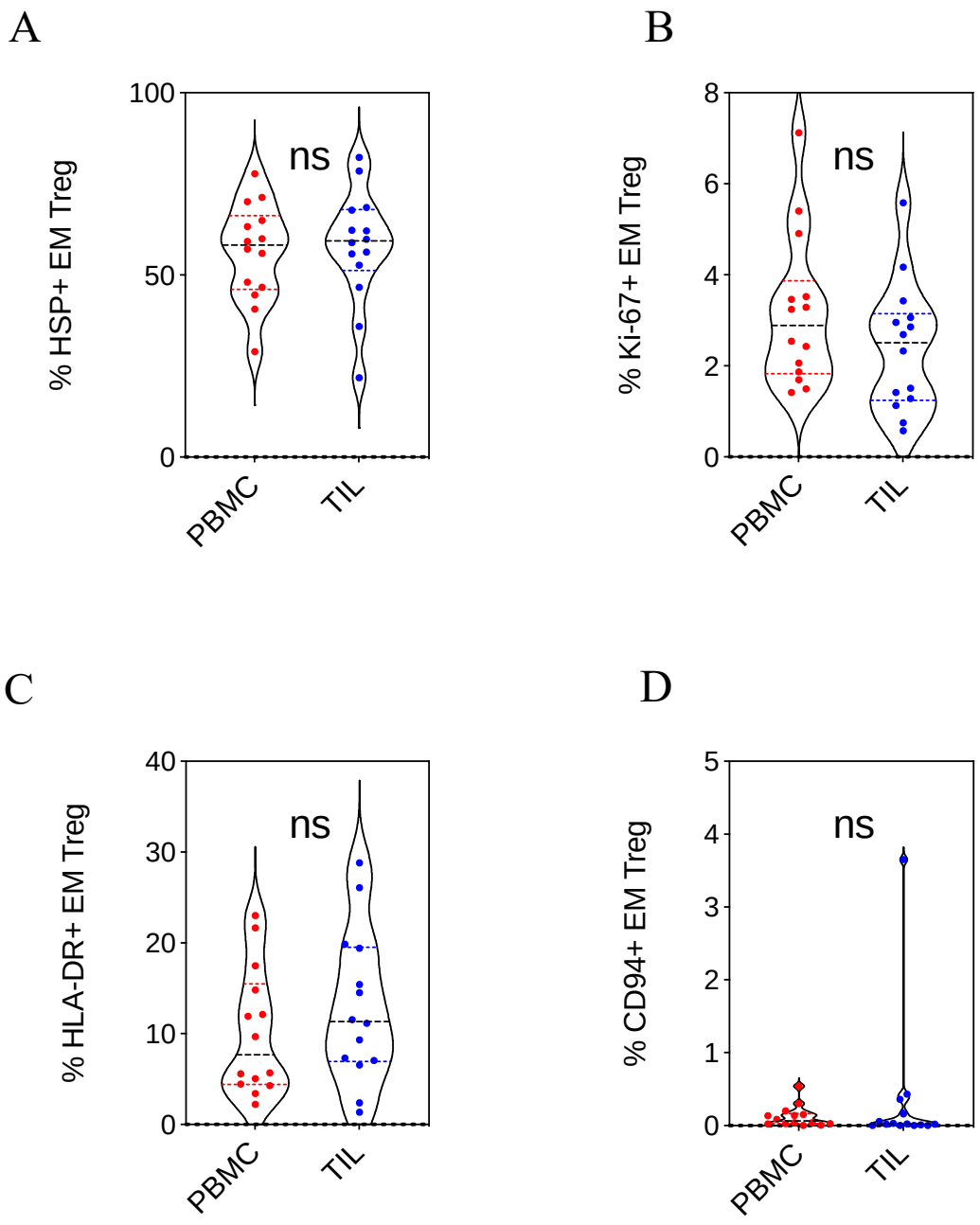

Figure 131. Phenotypic profile of effector memory Treg in blood and tumour of patients with OAC

Expression of heat shock protein (A), Ki-67 (B), HLA-DR (C) and CD94 (D) in matched PBMC and TIL EM CD4 T cells (n=14). Each symbol represents an individual patient. Dashed horizontal lines indicate the median and dotted lines indicate the interquartile range. Data analysed by Wilcoxon matched-pairs signed rank test.

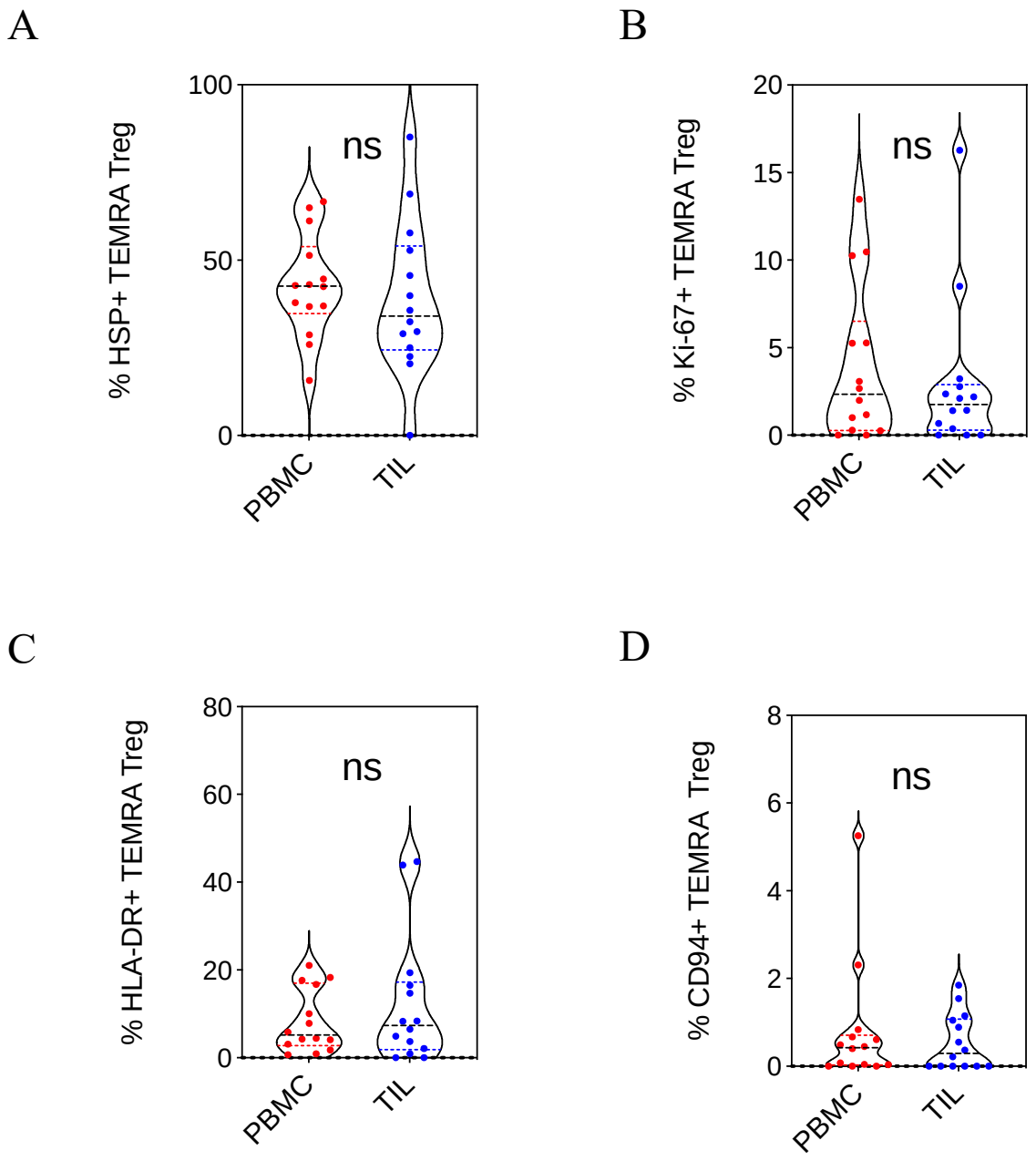

Figure 132. Profile of CD45RA+ effector Treg in blood and tumour of patients with OAC
Expression of heat shock protein (A), Ki-67 (B), HLA-DR (C) and CD94 (D) in matched PBMC and TIL of CD45RA+ EM Treg (n=14). Each symbol represents an individual patient. Dashed horizontal lines indicate the median and dotted lines indicate the interquartile range. Data analysed by Wilcoxon matched-pairs signed rank test.

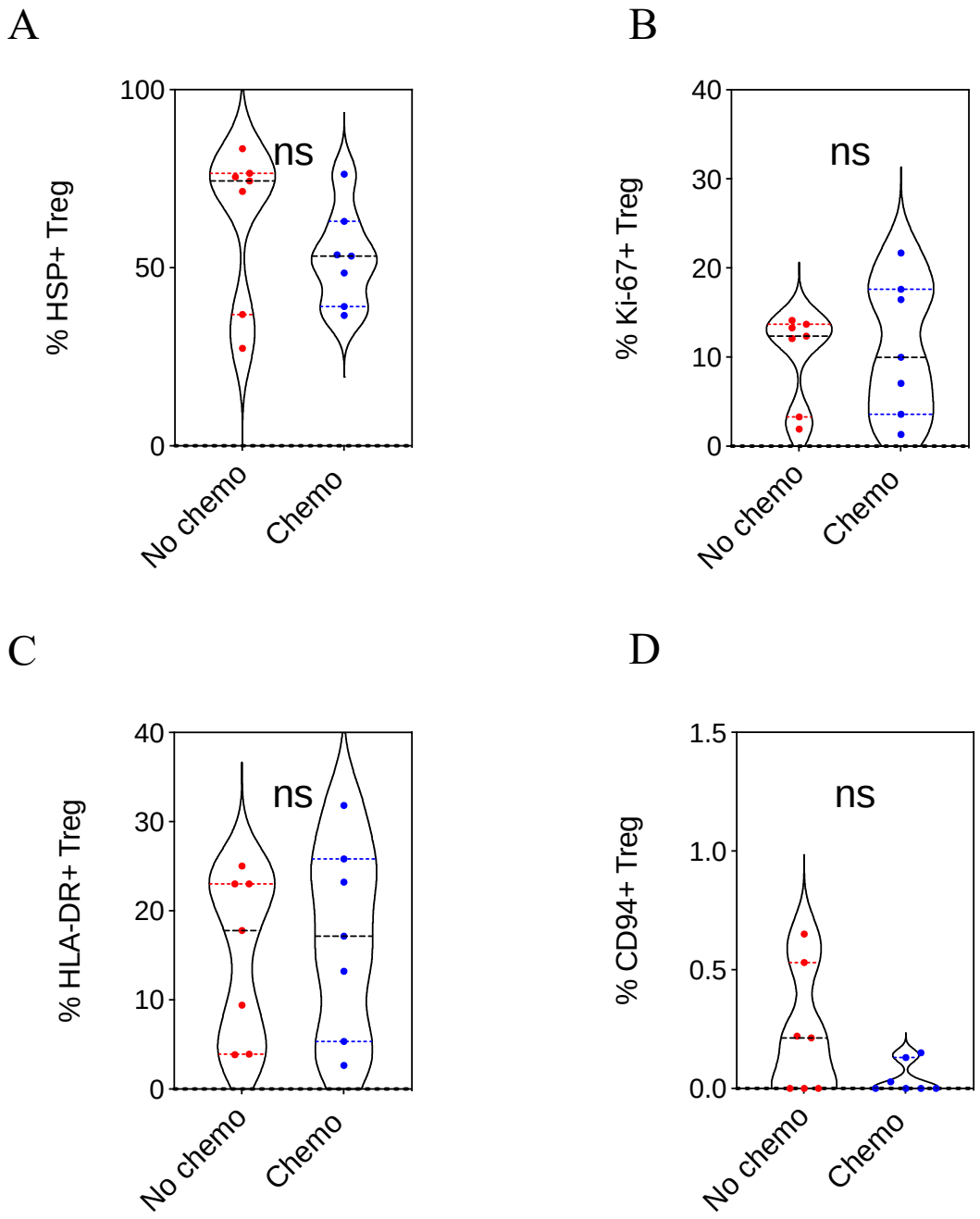

Figure 133. Phenotype of T regulatory cells within TIL in relation to prior usage of neoadjuvant chemotherapy.
Expression of heat shock protein (A), Ki-67 (B), HLA-DR (C) and CD94 (D) on T reg in TIL for patients who have and have not received neoadjuvant chemotherapy (No chemo n=7, chemo n=7). Each symbol represents an individual patient. Dashed horizontal lines indicate the median and dotted lines indicate the interquartile range. Data analysed by Mann Whitney Test.

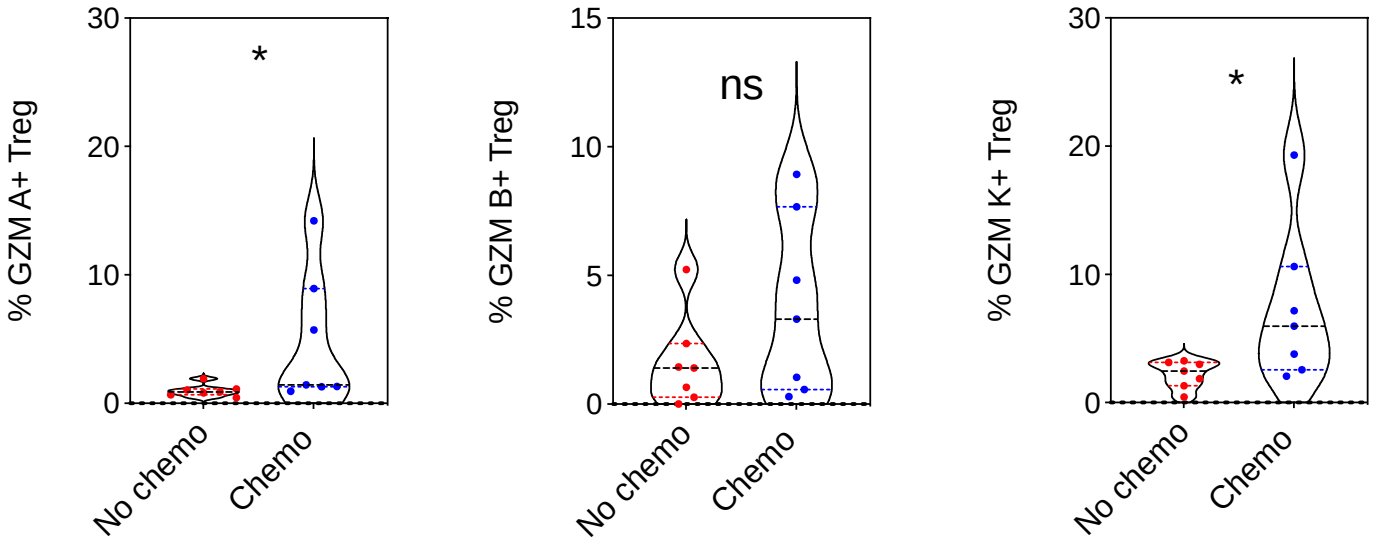

Figure 134. Profile of granzyme expression in Treg within TIL in relation to prior usage of neo-adjuvant chemotherapy

Granzyme expression (Gzm A, B and K) was determined in T regulatory TIL for patients who have and have not received neoadjuvant chemotherapy (No chemo n=7, chemo n=7). Each symbol represents an individual patient. Dashed horizontal lines indicate the median and dotted lines indicate the interquartile range. Data analysed by Mann Whitney Test, * denotes $p<0.05$.

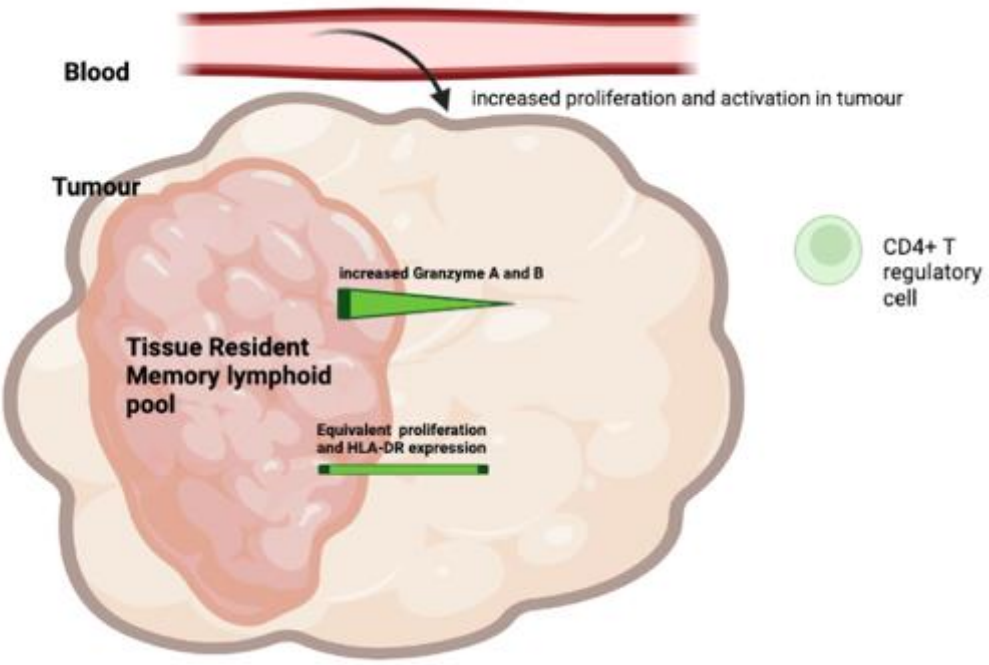

Figure 135. Graphical representation of phenotype of CD4+ T regulatory cells within the OAC microenvironment

T-reg within tumour show increased proliferation and HLA-DR expression but this is comparable across the TRM and non-TRM populations. Granzyme A and B are increased in the TRM compartment, suggesting an increased cytotoxic component.

NK Profiles in Oesophageal Adenocarcinoma

Phenotypic analysis of 30 patients in cohort 1 had identified a range of interesting features regarding NK phenotype within the OAC microenvironment. As such, I assessed this further using the extended flow cytometric panel. NK populations were identified as previously outlined in chapter 3.

Initial results confirmed substantial differences in the phenotype of NK cell profiles when comparing match PBMC and TIL (n=14). There was a pronounced increase in CD16- NK within TIL compared to PBMC where these comprised 13% of NK within PBMC compared to 56% in TIL (p=0002). A reciprocal change was seen in CD16+ NK cell pool (p=0002, Figure 136).

I next assessed granzyme expression in relation to CD16 expression on NK cells in blood and tumour. Expression of the major cytotoxic granzymes, granzyme A and granzyme B, was markedly downregulated in NK cells within the tumour. This pattern was observed for both the CD16- (Gzm A p=0.002, Gzm B p=0.0001) and CD16+ subsets TIL (Gzm A p=0.0006, Gzm B p=0.0006), although granzyme levels were overall somewhat higher in the CD16+ population. Granzyme K expression was also lower in CD16- NK cells within TIL (p=0.01) although the opposite profile was observed within the CD16+ pool (p=0.041).

Evaluation of granzyme expression in the CD16- NK pool demonstrated the levels of granzyme A were reduced from 70% to 43%, Granzyme B from 68% to 28% and Granzyme K reduced from 28% to 15%. Within CD16+ NK cells granzyme A was reduced from 89% in blood to 67% in tumour whilst corresponding values for Granzyme B were 95% and 77% respectively and Granzyme K increased from 4% to 8%.

I next assessed other phenotypic markers on NK cell subsets. Assessment of the CD16- NK pool showed that the proliferative marker Ki-67 was reduced within tumour whilst increased expression of HSP70 and HLA-DR was seen on TIL (p=0.02, p=0.005, Figure 137). In

particular, expression of HSP70 increased from 24% to 49% and that of HLA-DR from 3.5% to 9.5%. Ki-67 levels were reduced from 4.8% in blood to 1.9% in tumour (p=0.005). A similar profile was seen for CD16+ NK with increased expression of HLA-DR within TIL (2.0% vs 5.6%; p=0.049) (Figure 138) despite lower levels of proliferation. Ki-67 reduced from 2.3% to 1.7% whilst a small reduction in CD94, from 74% to 70.0%, was also seen (p=0.02, p=0.04).

Within TIL populations expression of granzymes A and B was markedly increased in the CD16+ NK pool compared to CD16- subsets (Gzm A p=0.0001, Gzm B p=0.0001; Figure 139) whilst granzyme K was comparable. Granzyme A was expressed in 43% of CD16- and 67% of CD16+ NK whilst Granzyme B was expressed in 28% and 77% respectively. No phenotypic changes between CD16- and CD16+ were seen in HSP70, Ki-67, HLA-DR or CD94 expression (p=0.15, p=0.36, p=0.68, p=0.07).

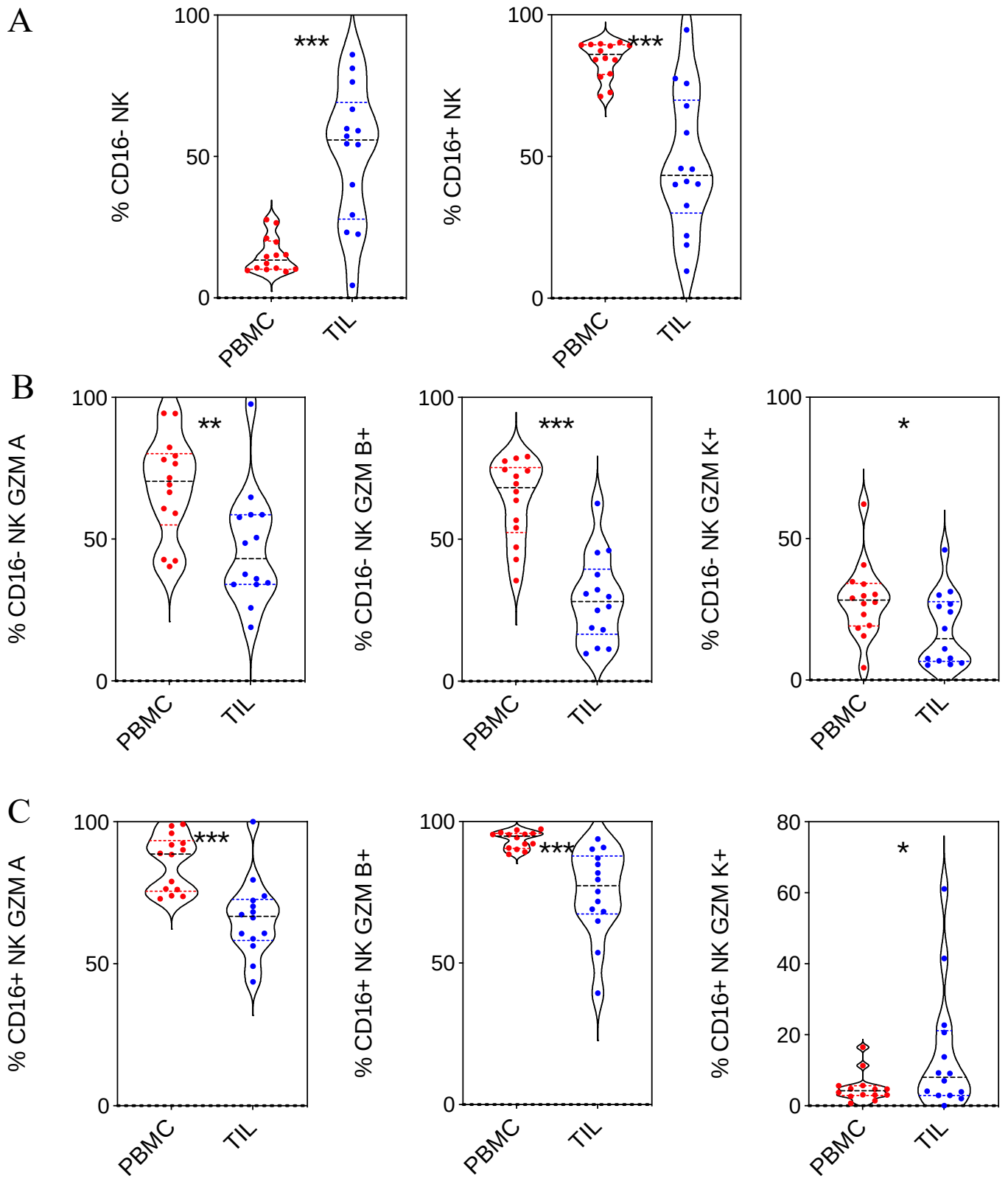

Figure 136. Expression of CD16 and granzyme in NK cells of patients with OAC
Proportion of CD16- and CD16+ NK in matched PBMC and TIL (n=14, A). Relative granzyme expression (Gzm A, B and K) in CD16- (n=14, B) and CD16+ NK subsets (n=14, C). Each symbol represents an individual patient. Dashed horizontal lines indicate the median and dotted lines indicate the interquartile range. Data analysed by Mann Whitney Test, * denotes $p<0.05$, ** denotes $p<0.01$, *** denotes $p<0.001$.

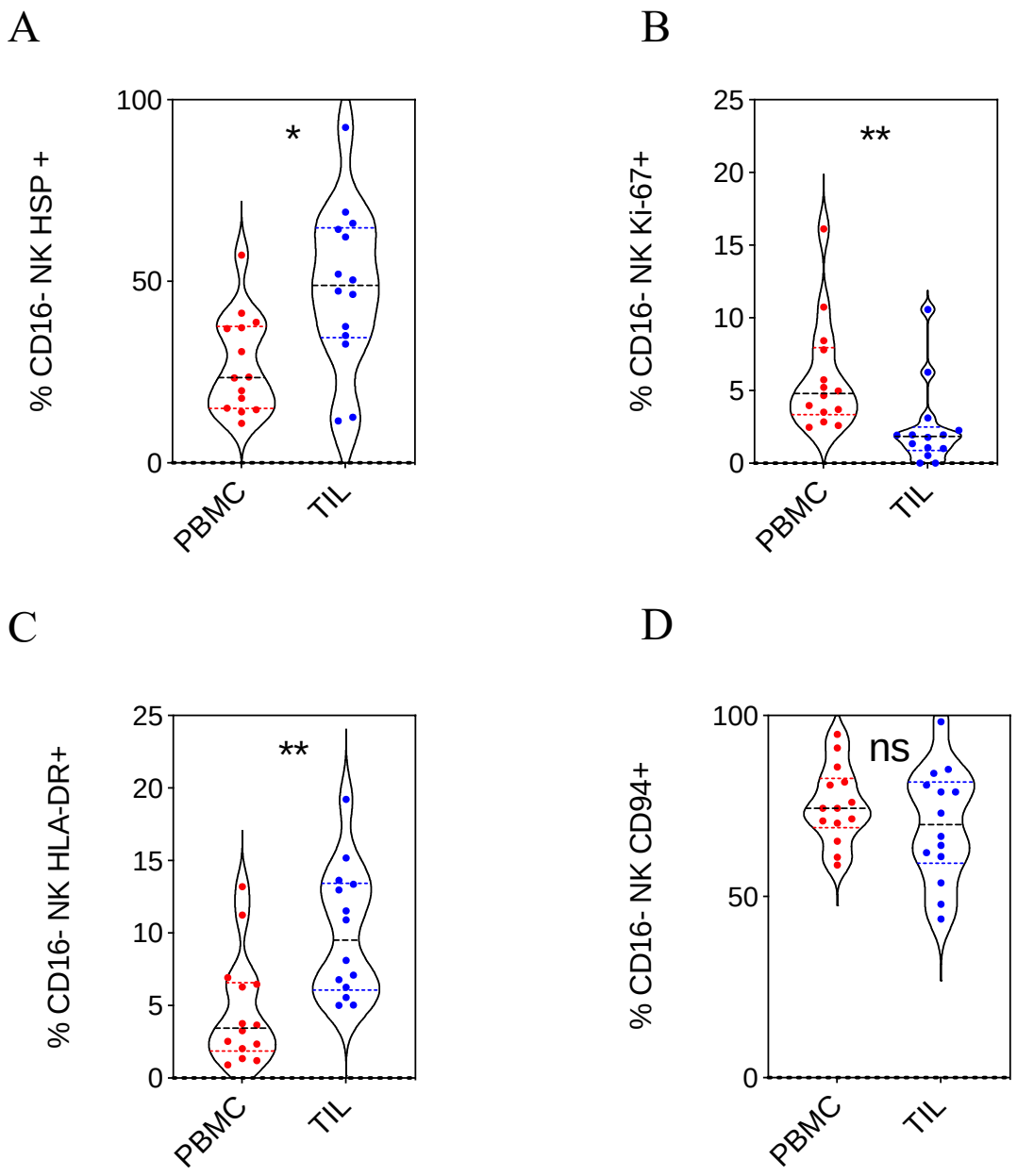

Figure 137. Phenotypic variation of CD16- NK cells in matched PBMC and TIL.
Expression of heat shock protein (A), Ki-67 (B), HLA-DR (C) and CD94 (D) in matched PBMC and TIL CD16-NK cells (n=14). Each symbol represents an individual patient. Dashed horizontal lines indicate the median and dotted lines indicate the interquartile range. Data analysed by Wilcoxon matched-pairs signed rank test, * denotes $p<0.05$ and ** $p<0.01$.

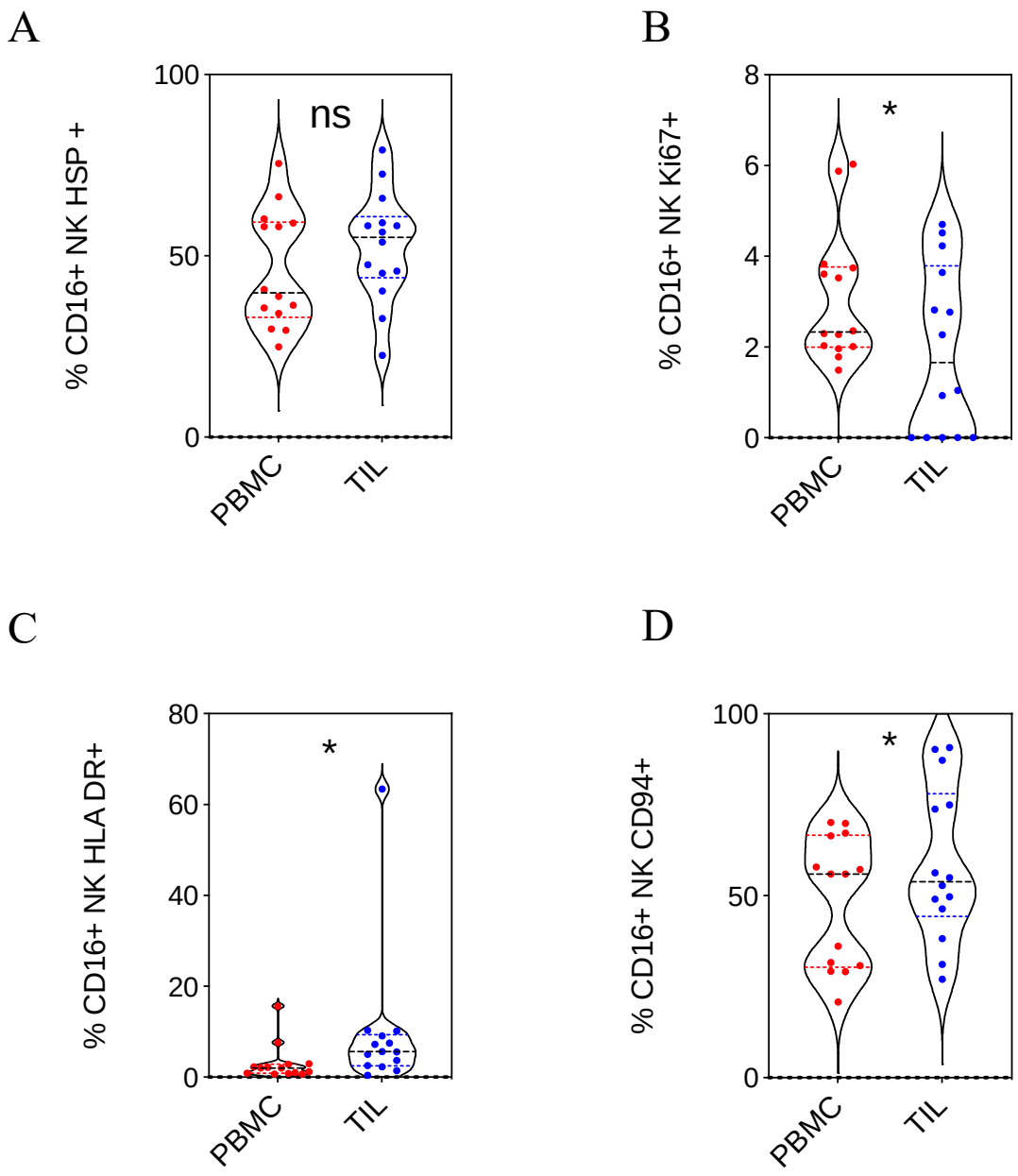

Figure 138. Phenotypic variation of CD16+ NK cells in matched PBMC and TIL.
Expression of heat shock protein (A), Ki-67 (B), HLA-DR (C) and CD94 (D) in matched PBMC and TIL CD16+ NK cells (n=14). Each symbol represents an individual patient. Dashed horizontal lines indicate the median and dotted lines indicate the interquartile range. Data analysed by Wilcoxon matched-pairs signed rank test, * denotes $p<0.05$.

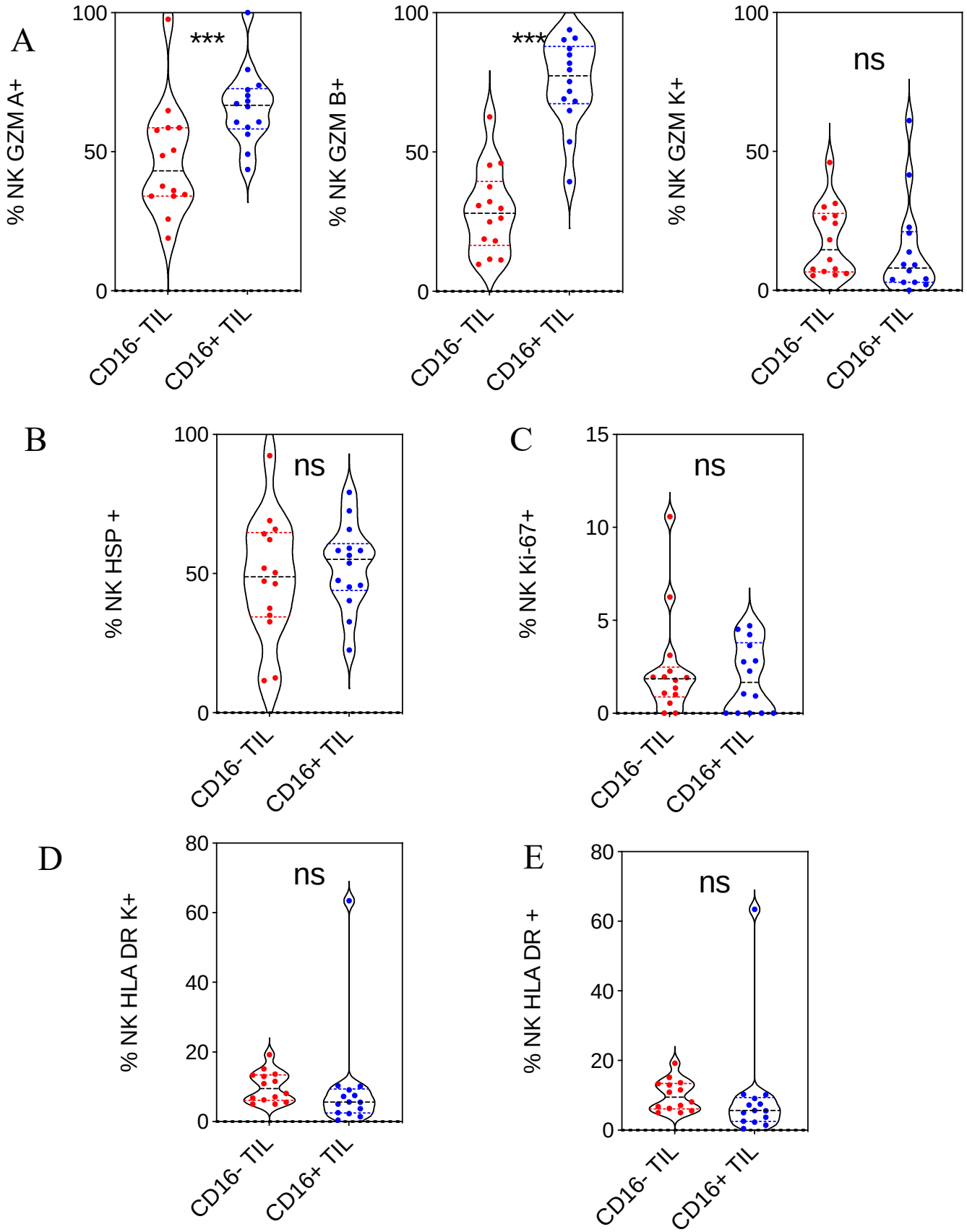

Figure 139. Phenotypic analysis of matched CD16- and CD16+ NK within TIL
Granzyme expression in CD16- and CD16+ NK TIL (n=14, A). Expression of heat shock protein (B), Ki-67 (C), HLA-DR (D) and CD94 (E) in matched CD16- and CD16+ NK TIL (n=14). Each symbol represents an individual patient. Dashed horizontal lines indicate the median and dotted lines indicate the interquartile range. Data analysed by Wilcoxon matched-pairs signed rank test, * denotes $p<0.05$, *** denotes $p<0.001$.

Tissue Resident Memory NK TIL

Finally, the phenotypic profile of tissue resident memory NK cells was assessed. The proportion of TRM NK was evaluated in both CD16- and CD16+ TIL. TRM NK (CD69+CD103+) are significantly reduced as compared to non-TRM profiles in both CD16- and CD16+ TIL (p=0.02, p=0.0001, Figure 140). Features of tissue residency are significantly higher on CD16- NK as compared to CD16+ TIL (p=0.0001). TRM NK accounts for 33% of CD16- NK TIL (IQR 30.9-52.6) whereas TRM only accounts for 9% of CD16+ TIL (IQR 3.7-17.4).

Assessment of Granzyme expression in relation to TRM phenotype showed that granzyme B was strongly expressed in NK cells without a TRM phenotype. However, expression was low within cells with TRM phenotype and this pattern was seen irrespective of CD16 status (CD16-,p=0.0004; CD16+,p=0.007) (Figure 141). Granzyme B expression was seen in 9% of CD16- TRM (IQR 1.4-24.0) and 49% of CD16+ NK TRM (IQR 32.9-73.5).

These findings indicate that cytotoxic capacity, as determined by granzyme expression, is reduced in tumour compared to blood. Furthermore, this is particularly suppressed in the CD16- subset. Cytotoxic capacity also resides primarily within the non-tissue resident memory NK pool which may represent a population of NK cells that has recently entered the tumour microenvironment.

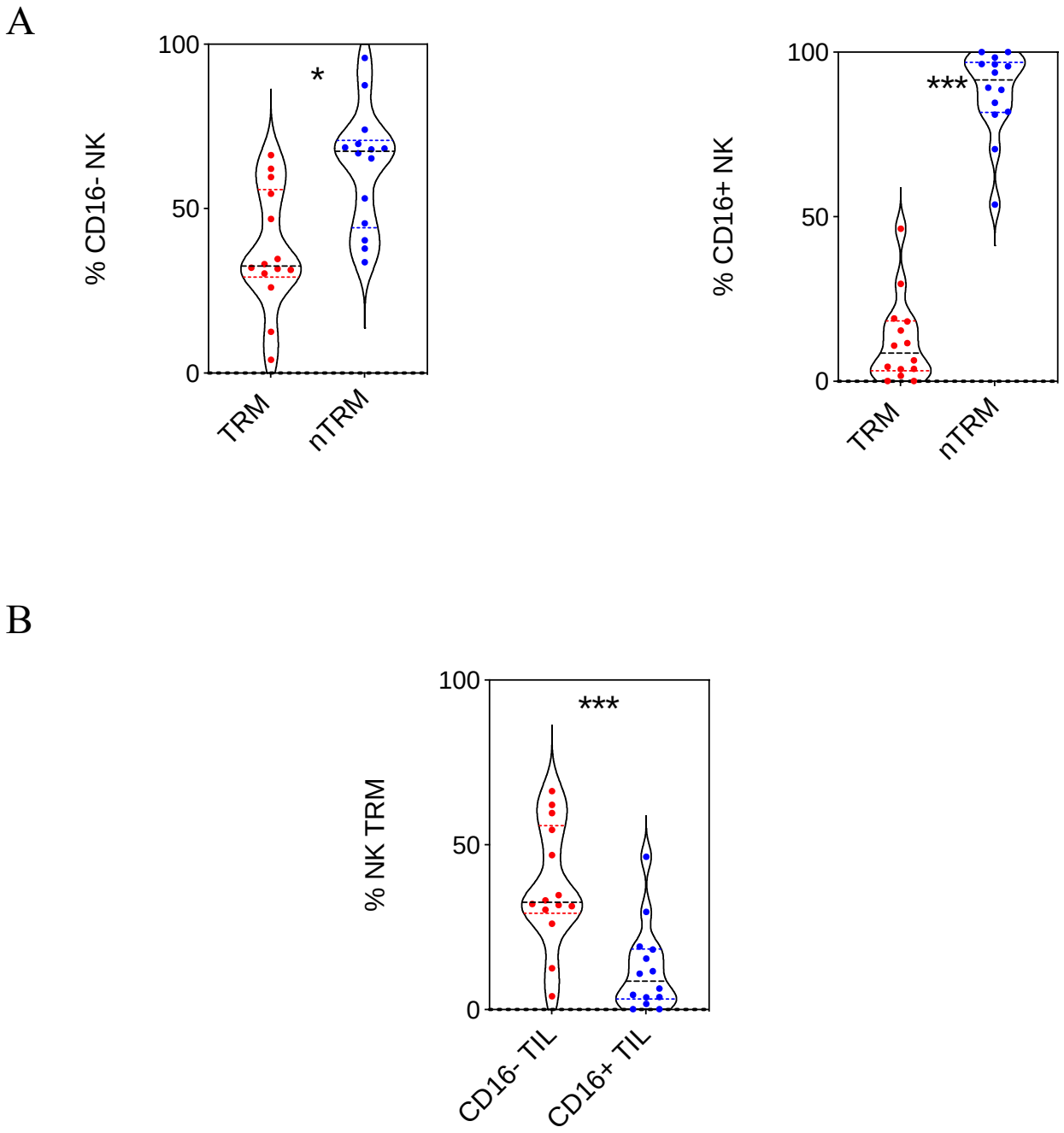

Figure 140. Phenotypic variation of matched TRM NK TIL.
Differential proportions of CD16- NK TIL in TRM and non-TRM phenotypes,(n=14, A). Comparative assessment of TRM phenotype in CD16- and CD16+ NK (n=14, B). Each symbol represents an individual patient. Dashed horizontal lines indicate the median and dotted lines indicate the interquartile range. Data analysed by Wilcoxon matched-pairs signed rank test, * denotes $p<0.05$, *** denotes $p<0.001$.

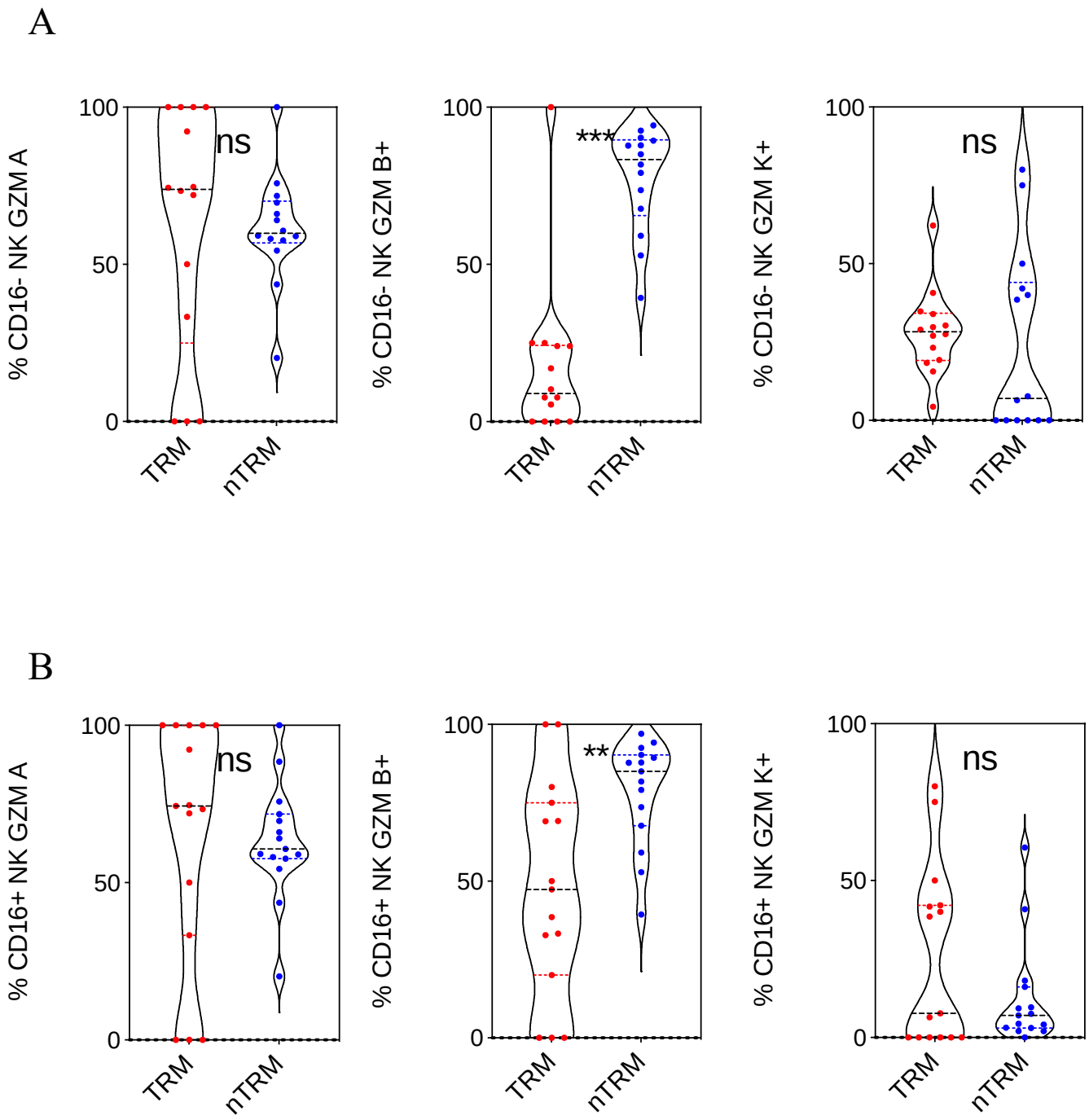

Figure 141. Phenotypic variation of matched TRM NK TIL.
Differential proportions of CD16- NK TIL in TRM and non-TRM phenotypes,(n=14, A). Comparative assessment of TRM phenotype in CD16- and CD16+ NK (n=14, B). Each symbol represents an individual patient. Dashed horizontal lines indicate the median and dotted lines indicate the interquartile range. Data analysed by Wilcoxon matched-pairs signed rank test, ** denotes p<0.01, *** denotes p<0.001.

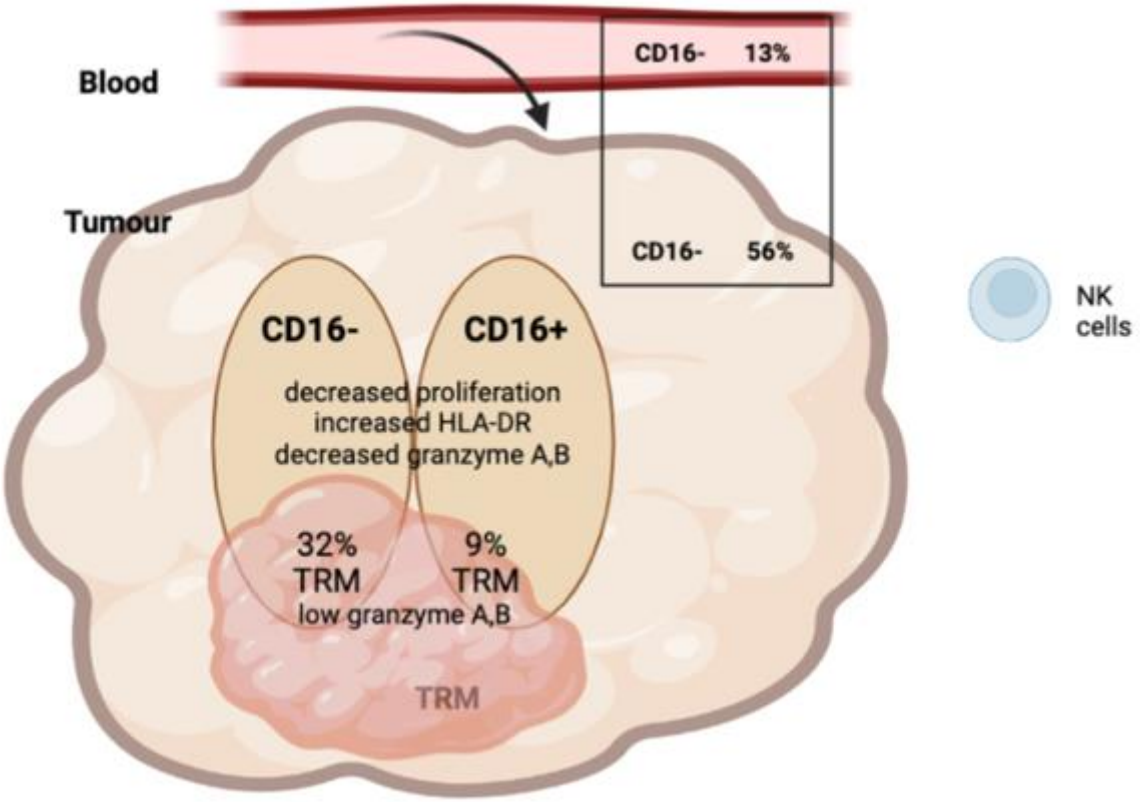

Figure 142. Graphical representation of the phenotypic profile of NK cells within the OAC microenvironment

CD16- cells are increased within tumour. All populations showed low levels of proliferation compared to blood but HLA-DR activation is increased. Granzyme A, B expression is reduced within tumour and this is particularly marked within the TRM subset

Discussion

In this chapter I was able to examine a range of novel features to further understand the biology of tissue resident memory cells within oesophageal adenocarcinoma.

Cytotoxic CD8 T cells have been identified as the major contributor to immune mediated tumour destruction and granzyme proteins are important mediators of target cell lysis. Currently five granzymes have been identified which enable cell destruction, A, B, H, K and M[219]. The relative importance of individual granzymes in OAC is currently unknown and we sought to identify the distribution of granzymes across differential cellular populations in the TME to determine the cytotoxic potential of the immune response within the TME.

Results from our preceding transcriptomic analysis had identified that T cell subsets with differential granzyme expression are observed within OAC. Granzyme A is the most abundant protease present in cytotoxic granules and is reported as a dominant mediator of toxicity[220]. It provides an alternative mechanism of apoptosis in cells that are resistant to granzyme B through overexpression of bcl-2 family anti-apoptotic proteins or granzyme B protease inhibitors[221]. Reduced efficacy of the perforin-granzyme system has been seen in OSCC and has been identified as a potential mechanism for resistance from trastuzumab mediated antibody dependent cellular cytotoxicity[222]. Granzyme A was seen to be reduced in CD8+ TIL in OAC, although increased in TRM subsets. Levels were also reduced in CD39+ cells which may have tumour specificity. Granzyme B shows a similar reduction in TIL. Murine models have suggested that transcriptional downregulation of granzyme A is associated with exhaustion but I did not assess functional activity in this chapter[223]. Immunohistochemical analysis of granzyme B expression in normal controls and OAC tumour biopsies has not shown significant differences[224]. The percentage of cells positive for granzyme B and perforin expression has been seen to be inversely correlated with the status of regional node metastasis in lung and

breast cancer although its potential importance in relation to metastasis in OAC is unknown[225]. Some attempts to increase granzyme delivery to tumours have been suggested but this has not yet found a clinical role [226].

Conversely, levels of granzyme K were elevated in OAC TIL and this was most apparent within the central memory and TEMRA populations. Granzyme K has both intracellular and extracellular function, enabling cytotoxicity and modulation of a pro-inflammatory immune cytokine response[227]. Evidence also suggests that expression of granzyme K may identify a pre-dysfunctional state that is associated with significant upregulation of checkpoint proteins[228]. Indeed, *GZMK*-expressing subsets of effector memory T cells and memory T cells may resemble the pre-dysfunctional states identified in melanoma, NSCLC and HCC[169,229–231]. The presence of a gradient of cell states rather than discrete populations is consistent with an intratumoural differentiation process, resulting in cells that reside along a continuum of dysfunction[162].

In addition to providing an understanding of the potential cytotoxicity of effector cells, analysis of granzyme expression may also enable assessment of treatment response. Fluorine-labelled peptide, [^{18}F]AlF-mNOTA-GZP, targeting granzyme B has been used to stratify checkpoint inhibitor response in two syngeneic models of colon cancer[232].Uptake of [^{18}F]AlF-*m*NOTA-GZP in PET imaging has been shown to correlates well with changes in CD8+ T cell populations and is able to stratify tumour response to a range of checkpoint inhibitors administered as monotherapies or in combination. Granzyme B expression in colorectal cancer has also been shown to have a significant prognostic impact and it is likely therefore that PET assessed granzyme expression may equally show prognostic relevance in OAC[233].

Granzyme expression is also seen in a subset of CD4+ T cells which are likely to display cytotoxic activity although they may have a regulatory role. Granzyme B-deficient $CD4^+$ T cells show increased IL-17 production and can impact on the outcome of murine models of autoimmune disease[234]. I found granzyme A,B and K expression in small subsets of CD4+ cells, although as expected this was substantially less than seen in CD8+ populations[235]. Granzyme K was also increased in CD4+ TIL and it was also notable that granzyme expression was higher in the TRM subsets. The significance of this in relation to potential tumour specificity is unclear although granzyme expression in CD4+ T cells has been linked to TCR-driven transendothelial migration, potentially suggesting a relationship with antigen recognition within the tumour[236].

CD39+ is an ectoenzyme which converts ATP or ADP to adenosine monophosphate (AMP) and acts in concert with CD73 to generate adenosine which acts in an immunosuppressive role. It has been suggested that CD39 expression is a marker of tumour-specificity within the tumour microenvironment and as such it is the subject of considerable investigation.

My work shows that CD39 is expressed on a considerable minority of the T cell population within OAC TIL and as these express granzyme express they may prove a potential option for future immunotherapy. However, harnessing the beneficial effects of granzymes remains challenging in an immunosuppressed TME.

I was also able to study the relative expression of the heat shock protein HSP70 on lymphoid subsets. Heat shock proteins have differential function dependent on location. Intracellular HSP70 respond to oxidative stress and act as molecular chaperones to limit cellular damage and apoptosis. In contrast extracellular HSPs have immunomodulatory functions and can cross present peptides for stimulation of innate[237,238] or adaptive immune response[239]. HSPs are often upregulated on tumour cells and typically associated with therapeutic resistance, metastasis, and poor clinical outcome[240]. No difference in HSP70 expression was observed on CD4+,

CD8+ or NK cells within PBMC and TIL. However, levels were increased on TRM subsets and further elevated on the CD39+ subset. Strategies to target HSPs have focused on extracellular tumour bound HSP where is may regulate radiosensitivity[241]. I found that HSP70 levels were not altered after neoadjuvant chemotherapy but as the only current immunotherapy licenced in potentially curable OAC is neoadjuvant chemoradiation, HSP should not be ignored as an area of interest in optimising outcomes in OAC.

Ki-67 assesses cell cycle status and provides a reliable mechanism to determine T cell proliferation[242]. In addition to looking at markers to detect cell cycle phase, minichromosomal maintenance (MCM) proteins may represent more accurate markers of proliferation. Indeed, MCM4 and 7 are significantly correlated with Ki-67 in OAC and values >70% are associated with lymph node metastasis[243]. Ki-67 levels have also been shown to correlate with TGF-B3 which together are a poor prognostic indication in OSCC[244]. I found that CD4+ and CD8+ cells upregulated Ki-67 in TIL and, although levels were comparable in TRM and non-TMR subsets, higher levels were seen in CD39+ cells. As such, these potentially tumour-specific cells retain the capability to proliferate despite many features of exhaustion and this indicates a degree of anti-tumour resilience.

My analysis of NK cells showed high levels of HLA-DR expression within the tumour. HLA-DR^+ NK cells are highly functional may be involved in presentation of antigen to $CD4^+$ and $CD8^+$ T cells[245,246]. Increased levels of HLA-DR were also observed on T cells and is of note as this is a sensitive and potentially predictive factor of response to neoadjuvant chemotherapy in some cancer subsets[247]. However, I did not find HLA-DR to be associated with neoadjuvant response on any lymphoid subsets in OAC.

Another marker that I assessed was CD94 which was elevated on NK TIL and on CD4+ and CD8+ TRM. CD94 was initially described as an inhibitory receptor which acted to limit autoimmunity, and inhibition of the CD94/NKG2A immune checkpoint has shown

encouraging improvement in natural killer cell and T cell effector function in preclinical cancer models[248,249].

As previously described multicolour flow cytometry pushes the boundaries of what can be achieved with the available technology. This work has identified key and novel populations within OAC however despite accurate information reflecting exhaustion and activation, flow cytometry does not provide a functional assessment of cellular populations cytotoxic capacity. In addition to location of cells within the microenvironment as could be assessed in Vectra, functional analyses would provide an additional layer of understanding to the complexity of TIL in OAC.

Conclusion

Transcriptomic identification of TIL subsets in OAC had identified a range of genes of interest on lymphoid subsets and I was able to examine protein expression from these genes in this chapter. T and NK cells showed variation in granzyme expression but it was notable that both TRM and the potential 'tumour specific' CD39+ populations maintained high cytotoxic potential. CD39+ populations also upregulated features of activation and proliferation. I had previously demonstrated high levels of inhibitory checkpoints on immune infiltrates of OAC but this work shows that these populations retain a number of functional properties, such as proliferation and activation, and as such supports further investigation into approaches to activate autologous tumour-specific TIL in patients with OAC.

Thesis Summary

Oesophageal adenocarcinoma is one of the great challenges within oncology at the current time and is listed by Cancer Research UK as a 'tumour of unmet need'. As such, research which helps to direct the introduction of new treatments is urgently needed. Despite its poor clinical outcome, there are encouraging signs that OAC is an immunogenic tumour and that immunotherapeutic treatments have the potential to improve patient survival. In particular this is being noted in the early results from checkpoint blockade clinical trials using reagents that disrupt the PD-1 and PD-L1 interaction. If appropriate targeted therapies can be introduced it will be imperative that they are based on a detailed knowledge of the oesophageal tumour microenvironment. This was the aim of my thesis.

My work used a combination of flow cytometric analysis and transcriptional studies. These are complementary technologies which offer a range of different advantages and limitations. Flow cytometry has been used in immunology for over 30 years and offers the potential to assess the expression of proteins on immune cell subsets. Protein expression is very dynamic, such that the number of molecules of an individual protein can vary by many orders of magnitude and this can be assessed using antibody detection. However, flow cytometry is limited by the number of antibodies that can be used simultaneously. In contrast, transcriptional analysis allows assessment of all RNAs produced within cells and, when using a single cell analysis as included in my thesis, this offers a tremendous opportunity to discover new transcriptional pathways with potential therapeutic insight. However, the magnitude of RNA expression does not correlate exactly with the level of protein expression from each RNA transcript and, as such, both approaches are used widely in contemporary analysis of the tumour microenvironment.

In chapter 3, my first results chapter, I used a flow cytometry panel comprising 10 antibodies to study the broad profile of immune cells within the blood and tumour of 30 patients with OAC. I saw equivalent ratios of CD4+ and CD8+ T cells within blood and tumour although subsequent chapters showed that T cells were highly activated within the tumour microenvironment. I chose to focus on three subpopulations of T cells, gamma-delta, MAIT and CD161+ cells, as these have unique roles in lymphoid immune defence. T cells with a gamma-delta TCR were actually reduced within tumour which is of note given interest in their potential use for immunotherapy. In contrast, MAIT and CD161+ cells were both increased three fold within tumour although none of these ratios were influenced by chemotherapy. This indicates that future work to study T cell responses to bacterial and non-peptide targets may be interest in OAC. Unsurprisingly, T regulatory cells were increased within tumour and represent an important target for human immunotherapy. An important finding was that checkpoint proteins PD-1, TIGIT and Tim-3 were all increased on CD8+ and CD4+ T cells within tumour. Indeed, similar profile was even seen on the regulatory CD4+ T cells and there was an increase in the TIGIT expression following chemotherapy. This chapter also made the initial identification of the substantial reduction in NK cells within tumour and the marked distortion of NK memory subsets with an expansion of the $CD56^{dim}CD16^{negative}$ population that has been identified in several cancer microenvironments. Finally, I observed equivalent levels of B cells within the tumour although an increase in the memory pool.

This chapter was able to incorporate patients who had received neoadjuvant chemotherapy and I was able to assess these patterns in relation to prior treatment. Overall, little difference was noted in the immune microenvironment following chemotherapy although the proportion of CD8+ cells in the blood was decreased. This modest impact of NACT on immune repertoire was also seen in my later work and is discussed further below.

In chapter 4, I supported and contributed to an analysis of the single cell transcriptomic profile of immune cells within OAC. As discussed in the chapter, single cell transcriptomic analysis is transforming cancer research but had not yet been applied to OAC. One feature of scRNA-Seq analysis is that, due to complexity and financial cost, only limited numbers of patients can be studied. Here I studied four patients before chemotherapy and four following NACT treatment but this allowed full transcriptomic analysis of 52,387 cells.

Many of the findings concurred with my flow cytometric analysis. However, there were differences such as decreased transcriptional expression of checkpoint proteins following NACT treatment which I did not subsequently observe in chapters using flow cytometry. This may represent a discrepancy between transcriptional activity and protein expression. There was also decrease in T regulatory populations which again was not observed with flow cytometry. The discovery potential of single cell sequencing was reflected in the observation that CXCL13 and CCL4 were both expressed highly on T cells and associated with poor prognosis. These should now be a target for study of protein expression in future work. Finally, one of the most exciting discoveries within the transcriptional analysis was the observation that the most proliferative cells had a tissue resident memory phenotype, with high level RNA expression from the genes for CD103 and CD69, and also expressed RNA encoding the putative tumour-specific marker CD39. As such, this work provided a basis for my future flow cytometric analysis.

In chapter 5 I built on these transcriptional studies to seek to identify tissue resident memory cells within OAC using flow cytometry. As such, I used antibodies against CD103 and CD69, co-expression of which defines TRM phenotype. This work was able to identify clear and significant populations of TRM cells within OAC. Indeed, these comprised 35% of the CD8+ pool within this small subset of 10 patients. Similar populations were seen to comprise around

15% of the CD4+ lymphoid pool within the tumour. I also identified TRM cells with an NK phenotype which is an emerging area of immunology. This chapter was also the first in the thesis to use CD39 and GITR expression on lymphoid cells. I chose CD39 as its expression is correlated with tumour specificity whilst GITR is an inhibitory receptor expressed on many T cells within tumours.

This chapter was the first to identify TRM T cell populations in OAC and building on from this I then went on to develop two broader flow cytometry panels to dissect the phenotype of TRM cells in more detail.

In chapter 6 I first started to use the BD FACSymphony flow cytometer. This instrument was brought into our research laboratory during my research tenure and allows assessment of up to 24 different proteins using a range of fluorochromes. I was interested to combine markers of TRM phenotype with assessment of memory subset expression, an extended profile of checkpoint proteins, and markers of late differentiation.

Assessment of memory subsets showed that effector T cells were the dominant population within the tumour microenvironment. This is thought likely to represent local antigen recognition but it is also conceivable that activation may result from cytokine activation. My use of CD57 and KLRG1 to define terminal differentiation showed an interesting differential pattern where CD57+ cells were more common within tumour whilst KLRG1 was relatively downregulated. Both proteins are associated with regulation of immune responses and initial evidence suggests they may correlate with tumour outcome. As such, they are important targets for future investigation. Extension of checkpoint expression profile revealed a range of interesting findings, notable of which was the increased expression of LAG3 on T cells within TRM, and antibody blockade of LAG3 is emerging as a potential treatment in oncology. My work suggests this could be transferred to OAC. DNAM expression was differentially observed

on T cells and NK cells and, as an important activating receptor, points towards the potential targeting of checkpoint blockade directed against cell subtypes. I also found ICOS and CD96 to be increased on TRM and this increases their potential as therapeutic targets in OAC. Overall, this chapter identified a pattern of high checkpoint expression profile of effector cells within the TRM pool and implies that combinatorial blockade may be a therapeutic opportunity.

My final chapter utilised a different flow cytometry panel in which I was able to assess the expression of different granzyme proteins within TRM subsets. I also was interested to focus on the proliferation of these cells using Ki-67 whilst activation was assessed through HLA-DR and additional markers. This chapter was fascinating as it showed that T cell proliferation was expanded within the tumour microenvironment and increased within some TRM subsets. This again supports their potential importance in recognition of tumour proteins. Expression of granzyme protein showed high levels of the cytotoxic-associated granzyme A and B proteins within tumour although granzyme K was rather excluded from the TRM pool. Expression of granzymes was seen within small subsets of the CD4+ pool indicating a potential importance of cytotoxic CD4+ and T regulatory cells in tumour control. HLA-DR was widely expressed within tumour and, notably, was expressed on all memory CD4+ subsets. The importance of HLA class II expression in relation to clinical outcome of tumours is a topic of intense interest. Analysis of NK cells confirmed marked downregulation of CD16 within tumour, and, as an important immunoglobulin Fc receptor, this indicates that any local tumour-specific antibody production would be limited in terms of ability to activate antibody dependent cell cytotoxicity (ADCC).

Reflections and Future area for Investigation

My thesis has shown a range of interesting findings within the OAC microenvironment. It is encouraging that clinical trials are showing that OAC tumours are not refractory to checkpoint inhibition and my work points to approaches that may help to improve responses further.

I focused on tissue resident memory cells was able to show that these were highly activated, express cytotoxic granzymes and operative. They also expressed CD39, indicating potential tumour specificity. However, their activity is likely to be regulated by widespread and high-level expression of checkpoint proteins. The targeting of these may represent a new dimension for OAC immunotherapy.

Assessment of other immune subsets reinforces the importance of reducing or suppressing T regulatory cell activity. NK cells appear somewhat downregulated within OAC although it is of interest that this may reflect the requirement for extreme immune evasion from this immune subset.

My work leads to a number of potential areas for future investigation.

- A priority will be to assess the specificity of T cells within the tissue resident memory pool. It is possible these are responsive to tumour-specific peptides such as those arising from neoantigens due to somatic mutations within the tumour. Recognition of tumour-associated differentiation proteins or ‘cancer testis antigen’ proteins are also possibilities. This work would require complex laboratory analysis, such as cloning T cells from the TRM environment and assessing their specificity against peptide pools. This will be further complicated by HLA restriction.

- It will be interesting to assess whether there is expansion of T cell clonality within the TRM pool compared to T cells outside this site. Indeed, this approach is now feasible with transcriptomic analysis but does not define peptide specificity.
- A powerful new technology that would be excellent to apply to OAC is CITE-Seq analysis which combines surface antibody labelling with individual cell transcriptional sequencing. The research team in which I work has applied this to pancreatic cancer but its great expense has, so far, limited its applications within oesophageal cancer. The opportunities that this allows, in terms of defining biochemical pathways of immune exhaustion within defined phenotypic immune subsets, is remarkable.
- Future work should also try to culture or expand individual immune cell subsets from the OAC microenvironment based on surface of expressions of markers such as CD96, ICOS and LAG3. This could help to define how these markers correlate with functional capacities such as proliferation, cytokine production or cytotoxicity.

Ultimately, this work aims to improve clinical outcomes of patients. The future immunotherapy of OAC is encouraging. A range of approaches might be adopted including the use of extended checkpoint therapy targeted against proteins identified in my thesis, or its combination with other therapies. These could include chemotherapy or reagents that seek to reduce the immune suppression within the tumour microenvironment, such as blockade of TGF-beta. Finally, chimeric antigen receptor T cells (CAR-T) are being developed for solid tumours and their potential utility in OAC, directed against tumour-associated proteins, could represent a future option. My personal feeling, having completed this thesis, is that the future utility of immunotherapy in OAC is encouraging and that patients with this challenging disease will have a range of therapeutic options available within the medium term.

References

1. Delves, P. J. & Roitt, I. M. The immune system. First of two parts. *N. Engl. J. Med.* (2000). doi:10.1056/NEJM200007063430107
2. Parkin, J. & Cohen, B. An overview of the immune system. *Lancet* (2001). doi:10.1016/S0140-6736(00)04904-7
3. Kumar, H., Kawai, T. & Akira, S. Pathogen recognition by the innate immune system. *Int. Rev. Immunol.* (2011). doi:10.3109/08830185.2010.529976
4. Kurosaki, T., Kometani, K. & Ise, W. Memory B cells. *Nat. Rev. Immunol.* (2015). doi:10.1038/nri3802
5. Takaba, H. & Takayanagi, H. The Mechanisms of T Cell Selection in the Thymus. *Trends in Immunology* (2017). doi:10.1016/j.it.2017.07.010
6. Davis, M. M. *et al.* Ligand recognition by αβ T cell receptors. *Annual Review of Immunology* (1998). doi:10.1146/annurev.immunol.16.1.523
7. Takada, K. & Takahama, Y. Positive-selection-inducing self-peptides displayed by cortical thymic epithelial cells. in *Advances in Immunology* (2015). doi:10.1016/bs.ai.2014.09.003
8. Clevers, H., Alarcon, B., Wileman, T. & Terhorst, C. THE T CELL RECEPTORjCD3 COMPLEX: A DYNAMIC PROTEIN ENSEMBLE T CELL RECEPTORS DO NOT ACT ALONE. *Ann. Rev. Immunol* (1988).
9. Muñoz-Ruiz, M., Sumaria, N., Pennington, D. J. & Silva-Santos, B. Thymic Determinants of γδ T Cell Differentiation. *Trends in Immunology* (2017). doi:10.1016/j.it.2017.01.007
10. Taghon, T., Yui, M. A., Pant, R., Diamond, R. A. & Rothenberg, E. V. Developmental and molecular characterization of emerging β- and γδ-selected pre-T cells in the adult mouse thymus. *Immunity* (2006). doi:10.1016/j.immuni.2005.11.012

11. Wieczorek, M. *et al.* Major histocompatibility complex (MHC) class I and MHC class II proteins: Conformational plasticity in antigen presentation. *Frontiers in Immunology* (2017). doi:10.3389/fimmu.2017.00292

12. Chen, L. & Flies, D. B. Molecular mechanisms of T cell co-stimulation and co-inhibition. *Nature Reviews Immunology* (2013). doi:10.1038/nri3405

13. Chattopadhyay, K. *et al.* Sequence, structure, function, immunity: Structural genomics of costimulation. *Immunological Reviews* (2009). doi:10.1111/j.1600-065X.2009.00778.x

14. Jameson, S. C. & Masopust, D. Understanding Subset Diversity in T Cell Memory. *Immunity* (2018). doi:10.1016/j.immuni.2018.02.010

15. Martin, M. D. & Badovinac, V. P. Defining memory CD8 T cell. *Frontiers in Immunology* (2018). doi:10.3389/fimmu.2018.02692

16. Verma, K. *et al.* Human CD8+ CD57- TEMRA cells: Too young to be called 'old'. *PLoS One* (2017). doi:10.1371/journal.pone.0177405

17. Kim, H. P., Imbert, J. & Leonard, W. J. Both integrated and differential regulation of components of the IL-2/IL-2 receptor system. *Cytokine and Growth Factor Reviews* (2006). doi:10.1016/j.cytogfr.2006.07.003

18. Steinke, J. W. & Borish, L. Th2 cytokines and asthma. Interleukin-4: Its role in the pathogenesis of asthma, and targeting it for asthma treatment with interleukin-4 receptor antagonists. *Respiratory Research* (2001). doi:10.1186/rr40

19. Kimura, A. & Kishimoto, T. IL-6: Regulator of Treg/Th17 balance. *European Journal of Immunology* (2010). doi:10.1002/eji.201040391

20. Whiteside, T. L. What are regulatory T cells (Treg) regulating in cancer and why? *Seminars in Cancer Biology* (2012). doi:10.1016/j.semcancer.2012.03.004

21. Weber, J. P. *et al.* ICOS maintains the T follicular helper cell phenotype by down-

regulating krüppel-like factor 2. *J. Exp. Med.* (2015). doi:10.1084/jem.20141432

22. Reina-Campos, M., Scharping, N. E. & Goldrath, A. W. CD8+ T cell metabolism in infection and cancer. *Nature Reviews Immunology* (2021). doi:10.1038/s41577-021-00537-8

23. Moretta, A. *et al.* Early liaisons between cells of the innate immune system in inflamed peripheral tissues. *Trends in Immunology* (2005). doi:10.1016/j.it.2005.09.008

24. Smyth, M. J. *et al.* Activation of NK cell cytotoxicity. *Molecular Immunology* (2005). doi:10.1016/j.molimm.2004.07.034

25. Pradeu, T., Jaeger, S. & Vivier, E. The speed of change: Towards a discontinuity theory of immunity? *Nature Reviews Immunology* (2013). doi:10.1038/nri3521

26. Wang, W., Erbe, A. K., Hank, J. A., Morris, Z. S. & Sondel, P. M. NK cell-mediated antibody-dependent cellular cytotoxicity in cancer immunotherapy. *Frontiers in Immunology* (2015). doi:10.3389/fimmu.2015.00368

27. Stabile, H., Fionda, C., Gismondi, A. & Santoni, A. Role of distinct natural killer cell subsets in anticancer response. *Frontiers in Immunology* (2017). doi:10.3389/fimmu.2017.00293

28. Ohaegbulam, K. C., Assal, A., Lazar-Molnar, E., Yao, Y. & Zang, X. Human cancer immunotherapy with antibodies to the PD-1 and PD-L1 pathway. *Trends in Molecular Medicine* (2015). doi:10.1016/j.molmed.2014.10.009

29. Dong, P., Xiong, Y., Yue, J., Hanley, S. J. B. & Watari, H. Tumor-intrinsic PD-L1 signaling in cancer initiation, development and treatment: Beyond immune evasion. *Frontiers in Oncology* (2018). doi:10.3389/fonc.2018.00386

30. Limagne, E. *et al.* Tim-3/galectin-9 pathway and mMDSC control primary and secondary resistances to PD-1 blockade in lung cancer patients. *Oncoimmunology* (2019). doi:10.1080/2162402X.2018.1564505

31. Postow, M. A. *et al.* Nivolumab and Ipilimumab versus Ipilimumab in Untreated Melanoma. *N. Engl. J. Med.* (2015). doi:10.1056/nejmoa1414428

32. Robert, C. *et al.* Nivolumab in Previously Untreated Melanoma without BRAF Mutation . *N. Engl. J. Med.* (2015). doi:10.1056/nejmoa1412082

33. Kang, Y. K. *et al.* Nivolumab in patients with advanced gastric or gastro-oesophageal junction cancer refractory to, or intolerant of, at least two previous chemotherapy regimens (ONO-4538-12, ATTRACTION-2): a randomised, double-blind, placebo-controlled, phase 3 trial. *Lancet* (2017). doi:10.1016/S0140-6736(17)31827-5

34. Reck, M. *et al.* Pembrolizumab versus Chemotherapy for PD-L1–Positive Non–Small-Cell Lung Cancer. *N. Engl. J. Med.* (2016). doi:10.1056/nejmoa1606774

35. Kudo, T. *et al.* Nivolumab treatment for oesophageal squamous-cell carcinoma: an open-label, multicentre, phase 2 trial. *Lancet Oncol.* (2017). doi:10.1016/S1470-2045(17)30181-X

36. Lupo, K. B., Matosevic, S. & Matosevic, S. CD155 immunoregulation as a target for natural killer cell immunotherapy in glioblastoma. *Journal of Hematology and Oncology* (2020). doi:10.1186/s13045-020-00913-2

37. Song, Y. *et al.* T-cell Immunoglobulin and ITIM Domain Contributes to CD8 + T-cell Immunosenescence. *Aging Cell* (2018). doi:10.1111/acel.12716

38. Josefsson, S. E. *et al.* TIGIT and PD-1 Mark Intratumoral T Cells with Reduced Effector Function in B-cell Non-Hodgkin Lymphoma. *Cancer Immunol. Res.* (2019). doi:10.1158/2326-6066.CIR-18-0351

39. Bray, F. *et al.* Global cancer statistics 2018: GLOBOCAN estimates of incidence and mortality worldwide for 36 cancers in 185 countries. *CA. Cancer J. Clin.* (2018). doi:10.3322/caac.21492

40. Kamangar, F. *et al.* The global, regional, and national burden of oesophageal cancer

and its attributable risk factors in 195 countries and territories, 1990–2017: a systematic analysis for the Global Burden of Disease Study 2017. *Lancet Gastroenterol. Hepatol.* (2020). doi:10.1016/S2468-1253(20)30007-8

41. Arnold, M., Ferlay, J., Van Berge Henegouwen, M. I. & Soerjomataram, I. Global burden of oesophageal and gastric cancer by histology and subsite in 2018. *Gut* (2020). doi:10.1136/gutjnl-2020-321600

42. Pandeya, N., Olsen, C. M. & Whiteman, D. C. Sex differences in the proportion of esophageal squamous cell carcinoma cases attributable to tobacco smoking and alcohol consumption. *Cancer Epidemiol.* (2013). doi:10.1016/j.canep.2013.05.011

43. Uhlenhopp, D. J., Then, E. O., Sunkara, T. & Gaduputi, V. Epidemiology of esophageal cancer: update in global trends, etiology and risk factors. *Clinical Journal of Gastroenterology* (2020). doi:10.1007/s12328-020-01237-x

44. Lin, Y. *et al.* Epidemiology of Esophageal Cancer in Japan and China. *J. Epidemiol.* **23**, 233–242 (2013).

45. Liu, J., Wang, J., Leng, Y. & Lv, C. Intake of fruit and vegetables and risk of esophageal squamous cell carcinoma: A meta-analysis of observational studies. *Int. J. Cancer* (2013). doi:10.1002/ijc.28024

46. Clinton, S. K., Giovannucci, E. L. & Hursting, S. D. The World Cancer Research Fund/American Institute for Cancer Research Third Expert Report on Diet, Nutrition, Physical Activity, and Cancer: Impact and Future Directions. *Journal of Nutrition* (2020). doi:10.1093/jn/nxz268

47. Zgaga, L. *et al.* Markers of Vitamin D exposure and esophageal cancer risk: A systematic review and meta-analysis. *Cancer Epidemiology Biomarkers and Prevention* (2016). doi:10.1158/1055-9965.EPI-15-1162

48. Smyth, E. C. *et al.* Oesophageal cancer. *Nat. Rev. Dis. Prim.* (2017).

doi:10.1038/nrdp.2017.48

49. Aguiar Pastrez, P. R. *et al.* The relation of HPV infection and expression of p53 and p16 proteins in esophageal squamous cells carcinoma. *J. Cancer* (2017). doi:10.7150/jca.17080

50. Liyanage, S. S. *et al.* The Aetiological Role of Human Papillomavirus in Oesophageal Squamous Cell Carcinoma: A Meta-Analysis. *PLoS One* (2013). doi:10.1371/journal.pone.0069238

51. Petrick, J. L. *et al.* Prevalence of human papillomavirus among oesophageal squamous cell carcinoma cases: Systematic review and meta-analysis. *Br. J. Cancer* (2014). doi:10.1038/bjc.2014.96

52. Song, Y. *et al.* Identification of genomic alterations in oesophageal squamous cell cancer. *Nature* (2014). doi:10.1038/nature13176

53. Lin, D. C. *et al.* Genomic and molecular characterization of esophageal squamous cell carcinoma. *Nat. Genet.* (2014). doi:10.1038/ng.2935

54. Gao, Y. B. *et al.* Genetic landscape of esophageal squamous cell carcinoma. *Nat. Genet.* (2014). doi:10.1038/ng.3076

55. Ahrens, T. D., Werner, M. & Lassmann, S. Epigenetics in esophageal cancers. *Cell and Tissue Research* (2014). doi:10.1007/s00441-014-1876-y

56. Avgerinos, K. I., Spyrou, N., Mantzoros, C. S. & Dalamaga, M. Obesity and cancer risk: Emerging biological mechanisms and perspectives. *Metabolism: Clinical and Experimental* (2019). doi:10.1016/j.metabol.2018.11.001

57. Dirac, M. A. *et al.* The global, regional, and national burden of gastro-oesophageal reflux disease in 195 countries and territories, 1990–2017: a systematic analysis for the Global Burden of Disease Study 2017. *Lancet Gastroenterol. Hepatol.* (2020). doi:10.1016/S2468-1253(19)30408-X

58. Maret-Ouda, J. *et al.* Esophageal Adenocarcinoma After Antireflux Surgery in a Cohort Study From the 5 Nordic Countries. *Ann. Surg.* (2019). doi:10.1097/sla.0000000000003709

59. Markar, S. R. *et al.* The influence of antireflux surgery on esophageal cancer risk in England: National Population-based Cohort Study. in *Annals of Surgery* (2018). doi:10.1097/SLA.0000000000002890

60. Hu, Q. *et al.* Proton pump inhibitors do not reduce the risk of esophageal adenocarcinoma in patients with Barrett's esophagus: A systematic review and meta-analysis. *PLoS One* (2017). doi:10.1371/journal.pone.0169691

61. Coleman, H. G., Xie, S. H. & Lagergren, J. The Epidemiology of Esophageal Adenocarcinoma. *Gastroenterology* (2018). doi:10.1053/j.gastro.2017.07.046

62. Liao, L. M. *et al.* Nonsteroidal anti-inflammatory drug use reduces risk of adenocarcinomas of the esophagus and esophagogastric junction in a pooled analysis. *Gastroenterology* (2012). doi:10.1053/j.gastro.2011.11.019

63. Coyle, C. *et al.* ADD-ASPIRIN: A phase III, double-blind, placebo controlled, randomised trial assessing the effects of aspirin on disease recurrence and survival after primary therapy in common non-metastatic solid tumours. *Contemp. Clin. Trials* (2016). doi:10.1016/j.cct.2016.10.004

64. Singh, S., Singh, A. G., Singh, P. P., Murad, M. H. & Iyer, P. G. Statins are associated with reduced risk of esophageal cancer, particularly in patients with barrett's esophagus: A systematic review and meta-analysis. *Clinical Gastroenterology and Hepatology* (2013). doi:10.1016/j.cgh.2012.12.036

65. Su, Z. *et al.* Common variants at the MHC locus and at chromosome 16q24.1 predispose to Barrett's esophagus. *Nat. Genet.* (2012). doi:10.1038/ng.2408

66. De Jonge, P. J. F., Van Blankenstein, M., Grady, W. M. & Kuipers, E. J. Barrett's

oesophagus: Epidemiology, cancer risk and implications for management. *Gut* **63**, 191–202 (2014).

67. White, N. *et al.* Barrett's esophagus and cardiac intestinal metaplasia: Two conditions within the same spectrum. *Can. J. Gastroenterol.* (2008). doi:10.1155/2008/243254

68. Quante, M. *et al.* Bile acid and inflammation activate gastric cardia stem cells in a mouse model of barrett-like metaplasia. *Cancer Cell* (2012). doi:10.1016/j.ccr.2011.12.004

69. Owen, R. P. *et al.* Single cell RNA-seq reveals profound transcriptional similarity between Barrett's oesophagus and oesophageal submucosal glands. *Nat. Commun.* (2018). doi:10.1038/s41467-018-06796-9

70. Kim, J. *et al.* Integrated genomic characterization of oesophageal carcinoma. *Nature* **541**, 169–174 (2017).

71. Secrier, M. *et al.* Mutational signatures in esophageal adenocarcinoma define etiologically distinct subgroups with therapeutic relevance. *Nat. Genet.* **48**, 1131–1141 (2016).

72. Frankell, A. M. *et al.* The landscape of selection in 551 Esophageal Adenocarcinomas defines genomic biomarkers for the clinic. *bioRxiv* 310029 (2018). doi:10.1101/310029

73. von Loga, K. *et al.* Extreme intratumour heterogeneity and driver evolution in mismatch repair deficient gastro-oesophageal cancer. *Nat. Commun.* (2020). doi:10.1038/s41467-019-13915-7

74. Noorani, A. *et al.* Genomic evidence supports a clonal diaspora model for metastases of esophageal adenocarcinoma. *Nat. Genet.* (2020). doi:10.1038/s41588-019-0551-3

75. Codipilly, D. C. *et al.* The Effect of Endoscopic Surveillance in Patients With Barrett's Esophagus: A Systematic Review and Meta-analysis. *Gastroenterology* (2018).

doi:10.1053/j.gastro.2018.02.022

76. Rice, T. W., Ishwaran, H., Ferguson, M. K., Blackstone, E. H. & Goldstraw, P. Cancer of the Esophagus and Esophagogastric Junction: An Eighth Edition Staging Primer. *J. Thorac. Oncol.* **12**, 36–42 (2017).

77. Girling, D. J. *et al.* Surgical resection with or without preoperative chemotherapy in oesophageal cancer: A randomised controlled trial. *Lancet* (2002). doi:10.1016/S0140-6736(02)08651-8

78. Al-Batran, S.-E. *et al.* Perioperative chemotherapy with fluorouracil plus leucovorin, oxaliplatin, and docetaxel versus fluorouracil or capecitabine plus cisplatin and epirubicin for locally advanced, resectable gastric or gastro-oesophageal junction adenocarcinoma (FLOT4): a ra. *Lancet* (2019). doi:10.1016/S0140-6736(18)32557-1

79. Kelly, R. J. *et al.* Adjuvant Nivolumab in Resected Esophageal or Gastroesophageal Junction Cancer. *N. Engl. J. Med.* (2021). doi:10.1056/nejmoa2032125

80. Kohei Shitara. Neoadjuvant and adjuvant pembrolizumab plus chemotherapy in locally advanced gastric or gastro-oesophageal cancer (KEYNOTE-585): an interim analysis of the multicentre, double-blind, randomised phase 3 study. *Lancet Oncol.* (2023).

81. Janjigian, Y. Y. *et al.* MATTERHORN: phase III study of durvalumab plus FLOT chemotherapy in resectable gastric/gastroesophageal junction cancer. *Futur. Oncol.* **18**, (2022).

82. Van Den Ende, T. *et al.* Neoadjuvant chemoradiotherapy combined with atezolizumab for resectable esophageal adenocarcinoma: A single-arm phase ii feasibility trial (PERFECT). *Clin. Cancer Res.* (2021). doi:10.1158/1078-0432.CCR-20-4443

83. Janjigian, Y. Y. *et al.* The KEYNOTE-811 trial of dual PD-1 and HER2 blockade in HER2-positive gastric cancer. *Nature* **600**, (2021).

84. Kelly, R. J. *et al.* Neoadjuvant nivolumab plus concurrent chemoradiation in stage

II/III esophageal/gastroesophageal junction cancer. *J. Clin. Oncol.* (2019). doi:10.1200/jco.2019.37.4_suppl.142

85. Fuchs, C. S. *et al.* Safety and efficacy of pembrolizumab monotherapy in patients with previously treated advanced gastric and gastroesophageal junction cancer: Phase 2 clinical KEYNOTE-059 trial. *JAMA Oncol.* (2018). doi:10.1001/jamaoncol.2018.0013

86. Moehler, M. H. *et al.* CheckMate 649: A randomized, multicenter, open-label, phase III study of nivolumab (NIVO) + ipilimumab (IPI) or nivo + chemotherapy (CTX) versus CTX alone in patients with previously untreated advanced (Adv) gastric (G) or gastroesophageal junction (GEJ) . *J. Clin. Oncol.* (2018). doi:10.1200/jco.2018.36.4_suppl.tps192

87. Cunningham, D. *et al.* Peri-operative chemotherapy with or without bevacizumab in operable oesophagogastric adenocarcinoma (UK Medical Research Council ST03): primary analysis results of a multicentre, open-label, randomised phase 2–3 trial. *Lancet Oncol.* **18**, 357–370 (2017).

88. Al-Batran, S. E. *et al.* Perioperative chemotherapy with fluorouracil plus leucovorin, oxaliplatin, and docetaxel versus fluorouracil or capecitabine plus cisplatin and epirubicin for locally advanced, resectable gastric or gastro-oesophageal junction adenocarcinoma (FLOT4): a ra. *Lancet* (2019). doi:10.1016/S0140-6736(18)32557-1

89. McCormick Matthews, L. H. *et al.* Systematic review and meta-analysis of immunohistochemical prognostic biomarkers in resected oesophageal adenocarcinoma. *Br. J. Cancer* (2015). doi:10.1038/bjc.2015.179

90. Sudo, T. *et al.* Clinical Impact of Tumor-Infiltrating Lymphocytes in Esophageal Squamous Cell Carcinoma. *Ann. Surg. Oncol.* (2017). doi:10.1245/s10434-017-5796-4

91. Okadome, K. *et al.* Prognostic Nutritional Index, Tumor-infiltrating Lymphocytes, and Prognosis in Patients with Esophageal Cancer. *Ann. Surg.* (2020).

doi:10.1097/SLA.0000000000002985

92. Boon, T., Cerottini, J. C., Van Den Eynde, B., Van Der Bruggen, P. & Van Pel, A. Tumor antigens recognized by T lymphocytes. *Annual Review of Immunology* (1994). doi:10.1146/annurev.iy.12.040194.002005

93. Mukai, S., Kjærgaard, J., Shu, S. & Plautz, G. E. Infiltration of tumors by systemically transferred tumor-reactive T lymphocytes is required for antitumor efficacy. *Cancer Res.* (1999).

94. Tan, Q. *et al.* Isolation of T cell receptor specifically reactive with autologous tumour cells from tumour-infiltrating lymphocytes and construction of T cell receptor engineered T cells for esophageal squamous cell carcinoma. *J. Immunother. Cancer* (2019). doi:10.1186/s40425-019-0709-7

95. Nozoe, T., Maehara, Y. & Sugimachi, K. Preoperative sorting of circulating T lymphocytes in patients with esophageal squamous cell carcinoma: Its prognostic significance. *World J. Gastroenterol.* (2005). doi:10.3748/wjg.v11.i42.6689

96. Liu, Q., Hao, C., Su, P. & Shi, J. Down-regulation of HLA class i antigen-processing machinery components in esophageal squamous cell carcinomas: Association with disease progression. *Scand. J. Gastroenterol.* (2009). doi:10.1080/00365520902998679

97. Barkal, A. A. *et al.* Engagement of MHC class i by the inhibitory receptor LILRB1 suppresses macrophages and is a target of cancer immunotherapy article. *Nat. Immunol.* (2018). doi:10.1038/s41590-017-0004-z

98. Wagener-Ryczek, S. *et al.* Immune profile and immunosurveillance in treatment-naive and neoadjuvantly treated esophageal adenocarcinoma. *Cancer Immunol. Immunother.* (2020). doi:10.1007/s00262-019-02475-w

99. Mari, L. *et al.* microRNA 125a Regulates MHC-I Expression on Esophageal

Adenocarcinoma Cells, Associated With Suppression of Antitumor Immune Response and Poor Outcomes of Patients. *Gastroenterology* (2018). doi:10.1053/j.gastro.2018.06.030

100. Beatty, G. L. & Gladney, W. L. Immune escape mechanisms as a guide for cancer immunotherapy. *Clinical Cancer Research* (2015). doi:10.1158/1078-0432.CCR-14-1860

101. Yagi, T. *et al.* PD-L1 Expression, Tumor-infiltrating Lymphocytes, and Clinical Outcome in Patients with Surgically Resected Esophageal Cancer. *Ann. Surg.* (2019). doi:10.1097/SLA.0000000000002616

102. McCormick Matthews, L. H. *et al.* Systematic review and meta-analysis of immunohistochemical prognostic biomarkers in resected oesophageal adenocarcinoma. *Br. J. Cancer* (2015). doi:10.1038/bjc.2015.179

103. Gao, Y. *et al.* Prognostic value of tumor-infiltrating lymphocytes in esophageal cancer: an updated meta-analysis of 30 studies with 5,122 patients. *Ann. Transl. Med.* (2020). doi:10.21037/atm-20-151

104. Kiyozumi, Y. *et al.* IDO1 Expression Is Associated With Immune Tolerance and Poor Prognosis in Patients With Surgically Resected Esophageal Cancer. *Ann. Surg.* (2019). doi:10.1097/SLA.0000000000002754

105. Schumacher, K., Haensch, W., Röefzaad, C. & Schlag, P. M. Prognostic significance of activated CD8+ T cell infiltrations within esophageal carcinomas. *Cancer Res.* (2001).

106. Zingg, U. *et al.* Tumour-infiltrating lymphocytes and survival in patients with adenocarcinoma of the oesophagus. *Eur. J. Surg. Oncol.* (2010). doi:10.1016/j.ejso.2010.05.012

107. Thomas, M. L., Samant, U. C., Deshpande, R. K. & Chiplunkar, S. V. γδ T cells lyse

autologous and allogenic oesophageal tumours: Involvement of heat-shock proteins in the tumour cell lysis. *Cancer Immunol. Immunother.* (2000). doi:10.1007/s002620050014

108. Sato, Y. *et al.* Adoptive γδT-cell transfer alone or combined with chemotherapy for the treatment of advanced esophageal cancer. *Cytotherapy* (2021). doi:10.1016/j.jcyt.2021.02.002

109. Melo, A. M. *et al.* Mucosal-associated invariant T cells display diminished effector capacity in oesophageal adenocarcinoma. *Front. Immunol.* (2019). doi:10.3389/fimmu.2019.01580

110. Li, Z., Wu, Y., Wang, C. & Zhang, M. Mouse CD8+NKT-like cells exert dual cytotoxicity against mouse tumor cells and myeloid-derived suppressor cells. *Cancer Immunol. Immunother.* (2019). doi:10.1007/s00262-019-02363-3

111. Konduri, V. *et al.* CD8+CD161+ T-Cells: Cytotoxic Memory Cells With High Therapeutic Potential. *Frontiers in Immunology* (2021). doi:10.3389/fimmu.2020.613204

112. Yoshioka, T. *et al.* Infiltrating regulatory T cell numbers is not a factor to predict patient's survival in oesophageal squamous cell carcinoma. *Br. J. Cancer* (2008). doi:10.1038/sj.bjc.6604294

113. Noble, F. *et al.* Tumour infiltrating lymphocytes correlate with improved survival in patients with oesophageal adenocarcinoma. *Cancer Immunol. Immunother.* (2016). doi:10.1007/s00262-016-1826-5

114. Zheng, X. *et al.* Prognostic role of tumor-infiltrating lymphocytes in esophagus cancer: A meta-analysis. *Cell. Physiol. Biochem.* (2018). doi:10.1159/000487164

115. Stein, A. V. *et al.* High intratumoural but not peritumoural inflammatory host response is associated with better prognosis in primary resected oesophageal adenocarcinomas.

Pathology (2017). doi:10.1016/j.pathol.2016.10.005

116. Zhu, Y. *et al.* CD8+/FOXP3+ ratio and PD-L1 expression associated with survival in pT3N0M0 stage esophageal squamous cell cancer. *Oncotarget* (2016). doi:10.18632/oncotarget.12213

117. Nabeki, B. *et al.* Interleukin-32 expression and Treg infiltration in esophageal squamous cell carcinoma. *Anticancer Res.* (2015).

118. Yue, Y. *et al.* Interleukin-33-nuclear factor-κB-CCL2 signaling pathway promotes progression of esophageal squamous cell carcinoma by directing regulatory T cells. *Cancer Sci.* (2020). doi:10.1111/cas.14293

119. Liu, J. Y. *et al.* CTL- vs Treg lymphocyte-attracting chemokines, CCL4 and CCL20, are strong reciprocal predictive markers for survival of patients with oesophageal squamous cell carcinoma. *Br. J. Cancer* (2015). doi:10.1038/bjc.2015.290

120. Hefetz-Sela, S. *et al.* Acquisition of an immunosuppressive protumorigenic macrophage phenotype depending on c-Jun phosphorylation. *Proc. Natl. Acad. Sci. U. S. A.* (2014). doi:10.1073/pnas.1409700111

121. Lian, J. *et al.* Eomes promotes esophageal carcinoma progression by recruiting Treg cells through the CCL20-CCR6 pathway. *Cancer Sci.* (2021). doi:10.1111/cas.14712

122. Sharpe, A. H., Wherry, E. J., Ahmed, R. & Freeman, G. J. The function of programmed cell death 1 and its ligands in regulating autoimmunity and infection. *Nature Immunology* (2007). doi:10.1038/ni1443

123. Leng, C. *et al.* Relationship between expression of PD-L1 and PD-L2 on esophageal squamous cell carcinoma and the antitumor effects of CD8+ T cells. *Oncol. Rep.* (2016). doi:10.3892/or.2015.4435

124. Khunger, M. *et al.* Programmed Cell Death 1 (PD-1) Ligand (PD-L1) Expression in Solid Tumors As a Predictive Biomarker of Benefit From PD-1/PD-L1 Axis

Inhibitors: A Systematic Review and Meta-Analysis. *JCO Precis. Oncol.* (2017). doi:10.1200/po.16.00030

125. Ohigashi, Y. *et al.* Clinical significance of programmed death-1 ligand-1 and programmed death-1 ligand-2 expression in human esophageal cancer. *Clin. Cancer Res.* (2005). doi:10.1158/1078-0432.CCR-04-1469

126. Zhao, J. J. *et al.* Orchestration of immune checkpoints in tumor immune contexture and their prognostic significance in esophageal squamous cell carcinoma. *Cancer Manag. Res.* (2018). doi:10.2147/CMAR.S181949

127. Svensson, M. C. *et al.* Expression of PD-L1 and PD-1 in chemoradiotherapy-Naïve esophageal and gastric adenocarcinoma: Relationship with mismatch repair status and survival. *Front. Oncol.* (2019). doi:10.3389/fonc.2019.00136

128. Feng, M. Z. C. C. N. R. F. C. H. T. M. M. A. S. B. F. F. S. E. B. Y. K. S. M. H. H. C. P. C. T. S. Y. *et al.* Pembrolizumab in Combination with Neoadjuvant Chemoradiotherapy for Patients with Resectable Adenocarcinoma of the Gastroesophageal Junction. *Clin. Cancer Res.* (2022).

129. O'Donnell, J. S., Madore, J., Li, X. Y. & Smyth, M. J. Tumor intrinsic and extrinsic immune functions of CD155. *Seminars in Cancer Biology* (2020). doi:10.1016/j.semcancer.2019.11.013

130. Kurtulus, S. *et al.* TIGIT predominantly regulates the immune response via regulatory T cells. *J. Clin. Invest.* (2015). doi:10.1172/JCI81187

131. Chauvin, J. M. *et al.* TIGIT and PD-1 impair tumor antigen-specific CD8+ T cells in melanoma patients. *J. Clin. Invest.* (2015). doi:10.1172/JCI80445

132. Joller, N. *et al.* Cutting Edge: TIGIT Has T Cell-Intrinsic Inhibitory Functions. *J. Immunol.* (2011). doi:10.4049/jimmunol.1003081

133. Lozano, E., Dominguez-Villar, M., Kuchroo, V. & Hafler, D. A. The TIGIT/CD226

Axis Regulates Human T Cell Function. *J. Immunol.* (2012). doi:10.4049/jimmunol.1103627

134. Jinhua, X. *et al.* Expression of immune checkpoints in T cells of esophageal cancer patients. *Oncotarget* (2016). doi:10.18632/oncotarget.11611

135. Zhao, K. *et al.* CD155 Overexpression Correlates With Poor Prognosis in Primary Small Cell Carcinoma of the Esophagus. *Front. Mol. Biosci.* (2021). doi:10.3389/fmolb.2020.608404

136. Blake, S. J. *et al.* Suppression of metastases using a new lymphocyte checkpoint target for cancer immunotherapy. *Cancer Discov.* (2016). doi:10.1158/2159-8290.CD-15-0944

137. Dougall, W. C., Kurtulus, S., Smyth, M. J. & Anderson, A. C. TIGIT and CD96: new checkpoint receptor targets for cancer immunotherapy. *Immunological Reviews* (2017). doi:10.1111/imr.12518

138. Wainberg, Z. *et al.* LBA-5 Phase Ib study of the anti-TIGIT antibody tiragolumab in combination with atezolizumab in patients with metastatic esophageal cancer. *Ann. Oncol.* (2021). doi:10.1016/j.annonc.2021.06.012

139. Goodman, K. A. *et al.* SKYSCRAPER-07: A phase III, randomized, double-blind, placebo-controlled study of atezolizumab with or without tiragolumab in patients with unresectable ESCC who have not progressed following definitive concurrent chemoradiotherapy. *J. Clin. Oncol.* (2022). doi:10.1200/jco.2022.40.4_suppl.tps374

140. Johnston, R. J. *et al.* The Immunoreceptor TIGIT Regulates Antitumor and Antiviral CD8+ T Cell Effector Function. *Cancer Cell* (2014). doi:10.1016/j.ccell.2014.10.018

141. Hong, M. H. *et al.* High CD3 and ICOS and low TIM-3 expression predict favourable survival in resected oesophageal squamous cell carcinoma. *Sci. Rep.* (2019). doi:10.1038/s41598-019-56828-7

142. Zheng, Y. *et al.* TNF-α-induced Tim-3 expression marks the dysfunction of infiltrating natural killer cells in human esophageal cancer. *J. Transl. Med.* (2019). doi:10.1186/s12967-019-1917-0

143. Guillerey, C., Huntington, N. D. & Smyth, M. J. Targeting natural killer cells in cancer immunotherapy. *Nature Immunology* (2016). doi:10.1038/ni.3518

144. Lim, K. S., Mimura, K., Kua, L. F., Shiraishi, K. & Kono, K. Implication of Highly Cytotoxic Natural Killer Cells for Esophageal Squamous Cell Carcinoma Treatment. *J. Immunother.* (2018). doi:10.1097/CJI.0000000000000227

145. He, E., Pan, F., Li, G. & Li, J. Fractionated ionizing radiation promotes epithelial-mesenchymal transition in human esophageal cancer cells through PTEN deficiency-mediated Akt activation. *PLoS One* (2015). doi:10.1371/journal.pone.0126149

146. Svensson, M. C. *et al.* The integrative clinical impact of tumor-infiltrating T lymphocytes and NK cells in relation to B lymphocyte and plasma cell density in esophageal and gastric adenocarcinoma. *Oncotarget* (2017). doi:10.18632/oncotarget.19437

147. Liu, Y. *et al.* Increased expression of programmed cell death protein 1 on NK cells inhibits NK-cell-mediated anti-tumor function and indicates poor prognosis in digestive cancers. *Oncogene* (2017). doi:10.1038/onc.2017.209

148. Petrovas, C. *et al.* PD-1 is a regulator of virus-specific CD8+ T cell survival in HIV infection. *J. Exp. Med.* (2006). doi:10.1084/jem.20061496

149. Christina Svensson, M. *et al.* T cells, B cells, and PD-L1 expression in esophageal and gastric adenocarcinoma before and after neoadjuvant chemotherapy: relationship with histopathological response and survival. *Oncoimmunology* (2021). doi:10.1080/2162402X.2021.1921443

150. Sung, H. *et al.* Global Cancer Statistics 2020: GLOBOCAN Estimates of Incidence

and Mortality Worldwide for 36 Cancers in 185 Countries. *CA. Cancer J. Clin.* (2021). doi:10.3322/caac.21660

151. Van Hagen, P. *et al.* Preoperative chemoradiotherapy for esophageal or junctional cancer. *N. Engl. J. Med.* (2012). doi:10.1056/NEJMoa1112088

152. Shah, M. A., Hofstetter, W. L. & Kennedy, E. B. Immunotherapy in patients with locally advanced esophageal carcinoma: ASCO treatment of locally advanced esophageal carcinoma guideline rapid recommendation update. *J. Clin. Oncol.* (2021). doi:10.1200/JCO.21.01831

153. Wang, Z. X. *et al.* Toripalimab plus chemotherapy in treatment-naïve, advanced esophageal squamous cell carcinoma (JUPITER-06): A multi-center phase 3 trial. *Cancer Cell* (2022). doi:10.1016/j.ccell.2022.02.007

154. Sun, J. M. *et al.* Pembrolizumab plus chemotherapy versus chemotherapy alone for first-line treatment of advanced oesophageal cancer (KEYNOTE-590): a randomised, placebo-controlled, phase 3 study. *Lancet* (2021). doi:10.1016/S0140-6736(21)01234-4

155. Zhang, X. *et al.* Dissecting esophageal squamous-cell carcinoma ecosystem by single-cell transcriptomic analysis. *Nat. Commun.* (2021). doi:10.1038/s41467-021-25539-x

156. Chen, Z. *et al.* Dissecting the single-cell transcriptome network in patients with esophageal squamous cell carcinoma receiving operative paclitaxel plus platinum chemotherapy. *Oncogenesis* (2021). doi:10.1038/s41389-021-00359-2

157. Wu, H. *et al.* Single-cell RNA sequencing reveals diverse intratumoral heterogeneities and gene signatures of two types of esophageal cancers. *Cancer Lett.* (2018). doi:10.1016/j.canlet.2018.09.017

158. Kumar, D. *et al.* Integrating transcriptome and proteome profiling: Strategies and applications. *Proteomics* (2016). doi:10.1002/pmic.201600140

159. Croft W, Evans R, Pearce H, Elshafie M, Griffiths EA, M. P. The single cell transcriptional landscape of esophageal adenocarcinoma and its modulation by neoadjuvant chemotherapy. *Mol. Cancer* **21.1**, 1–17 (2022).

160. Thommen, D. S. *et al.* A transcriptionally and functionally distinct pd-1+ cd8+ t cell pool with predictive potential in non-small-cell lung cancer treated with pd-1 blockade. *Nat. Med.* (2018). doi:10.1038/s41591-018-0057-z

161. Donlon, N. E. *et al.* Linking circulating serum proteins with clinical outcomes in esophageal adenocarcinoma—an emerging role for chemokines. *Cancers (Basel).* (2020). doi:10.3390/cancers12113356

162. van der Leun, A. M., Thommen, D. S. & Schumacher, T. N. CD8+ T cell states in human cancer: insights from single-cell analysis. *Nature Reviews Cancer* (2020). doi:10.1038/s41568-019-0235-4

163. Puiffe, M. L. *et al.* IL4I1 Accelerates the Expansion of Effector CD8+ T Cells at the Expense of Memory Precursors by Increasing the Threshold of T-Cell Activation. *Front. Immunol.* (2020). doi:10.3389/fimmu.2020.600012

164. Peng, H. & Tian, Z. Diversity of tissue-resident NK cells. *Seminars in Immunology* (2017). doi:10.1016/j.smim.2017.07.006

165. Szabo, P. A., Miron, M. & Farber, D. L. Location, location, location: Tissue resident memory T cells in mice and humans. *Science Immunology* (2019). doi:10.1126/sciimmunol.aas9673

166. Park, S. L., Gebhardt, T. & Mackay, L. K. Tissue-Resident Memory T Cells in Cancer Immunosurveillance. *Trends in Immunology* (2019). doi:10.1016/j.it.2019.06.002

167. Mueller, S. N. & Mackay, L. K. Tissue-resident memory T cells: Local specialists in immune defence. *Nature Reviews Immunology* (2016). doi:10.1038/nri.2015.3

168. Gebhardt, T., Mueller, S. N., Heath, W. R. & Carbone, F. R. Peripheral tissue

surveillance and residency by memory T cells. *Trends in Immunology* (2013). doi:10.1016/j.it.2012.08.008

169. Guo, X. *et al.* Global characterization of T cells in non-small-cell lung cancer by single-cell sequencing. *Nat. Med.* (2018). doi:10.1038/s41591-018-0045-3

170. Workel, H. H. *et al.* CD103 defines intraepithelial CD8+ PD1+ tumour-infiltrating lymphocytes of prognostic significance in endometrial adenocarcinoma. *Eur. J. Cancer* (2016). doi:10.1016/j.ejca.2016.02.026

171. Savas, P. *et al.* Single-cell profiling of breast cancer T cells reveals a tissue-resident memory subset associated with improved prognosis. *Nat. Med.* (2018). doi:10.1038/s41591-018-0078-7

172. Bösmüller, H. C. *et al.* Combined immunoscore of CD103 and CD3 identifies long-term survivors in high-grade serous ovarian cancer. *Int. J. Gynecol. Cancer* (2016). doi:10.1097/IGC.0000000000000672

173. Edwards, J. *et al.* CD103+ tumor-resident CD8+ T cells are associated with improved survival in immunotherapy-naïve melanoma patients and expand significantly during anti-PD-1 treatment. *Clin. Cancer Res.* (2018). doi:10.1158/1078-0432.CCR-17-2257

174. Duhen, T. *et al.* Co-expression of CD39 and CD103 identifies tumor-reactive CD8 T cells in human solid tumors. *Nat. Commun.* (2018). doi:10.1038/s41467-018-05072-0

175. Canale, F. P. *et al.* CD39 expression defines cell exhaustion in tumor-infiltrating CD8+ T cells. *Cancer Res.* (2018). doi:10.1158/0008-5472.CAN-16-2684

176. Von Rahden, B. H. A. *et al.* Glucocorticoid-induced TNFR family-related receptor (GITR)-expression in tumor infiltrating leucocytes (TILs) is associated with the pathogenesis of esophageal adenocarcinomas with and without Barrett's mucosa. *Cancer Biomarkers* (2010). doi:10.3233/CBM-2010-0192

177. Chu, K. L., Batista, N. V., Wang, K. C., Zhou, A. C. & Watts, T. H. GITRL on

inflammatory antigen presenting cells in the lung parenchyma provides signal 4 for T-cell accumulation and tissue-resident memory T-cell formation. *Mucosal Immunol.* (2019). doi:10.1038/s41385-018-0105-5

178. Chu, K. L., Batista, N. V., Girard, M., Law, J. C. & Watts, T. H. GITR differentially affects lung effector T cell subpopulations during influenza virus infection. *J. Leukoc. Biol.* (2020). doi:10.1002/JLB.4AB1219-254R

179. Han, L. *et al.* Characterization of CD103+ CD8+ tissue-resident T cells in esophageal squamous cell carcinoma: may be tumor reactive and resurrected by anti-PD-1 blockade. *Cancer Immunol. Immunother.* (2020). doi:10.1007/s00262-020-02562-3

180. Chu, Y. *et al.* CD103+ tumor-infiltrating lymphocytes predict favorable prognosis in patients with esophageal squamous cell carcinoma. *J. Cancer* (2019). doi:10.7150/jca.30354

181. Nose, Yohei, Takuro Saito, Kei Yamamoto, Kotaro Yamashita, Koji Tanaka, Kazuyoshi Yamamoto, T. M. et al. The Tissue-Resident Marker CD103 on Peripheral Blood T Cells Predicts Responses to Anti-PD-1 Therapy in Gastric Cancer. *Researchsquare* (2022). doi:https://doi.org/10.21203/rs.3.rs-1415877/v1

182. Zheng, Y. *et al.* IL-6-induced CD39 expression on tumor-infiltrating NK cells predicts poor prognosis in esophageal squamous cell carcinoma. *Cancer Immunol. Immunother.* (2020). doi:10.1007/s00262-020-02629-1

183. Simoni, Y. *et al.* Bystander CD8+ T cells are abundant and phenotypically distinct in human tumour infiltrates. *Nature* (2018). doi:10.1038/s41586-018-0130-2

184. Kared, H., Martelli, S., Ng, T. P., Pender, S. L. F. & Larbi, A. CD57 in human natural killer cells and T-lymphocytes. *Cancer Immunol. Immunother.* (2016). doi:10.1007/s00262-016-1803-z

185. Henson, S. M. & Akbar, A. N. KLRG1-more than a marker for T cell senescence. *Age*

(2009). doi:10.1007/s11357-009-9100-9

186. Pan, C. *et al.* Phenotypic profiling and prognostic significance of immune infiltrates in esophageal squamous cell carcinoma. *Oncoimmunology* (2021). doi:10.1080/2162402X.2021.1883890

187. Rauser, S. *et al.* High number of CD45RO+ tumor infiltrating lymphocytes is an independent prognostic factor in non-metastasized (stage I-IIA) esophageal adenocarcinoma. *BMC Cancer* (2010). doi:10.1186/1471-2407-10-608

188. Enomoto, K. *et al.* Prognostic importance of tumour-infiltrating memory T cells in oesophageal squamous cell carcinoma. *Clin. Exp. Immunol.* (2012). doi:10.1111/j.1365-2249.2012.04565.x

189. Salem, A., Alotaibi, M., Mroueh, R., Basheer, H. A. & Afarinkia, K. CCR7 as a therapeutic target in Cancer. *Biochimica et Biophysica Acta - Reviews on Cancer* (2021). doi:10.1016/j.bbcan.2020.188499

190. Donlon, N. *et al.* P09.04 Impact of major oncologic surgery on immune responses in the immediate post-operative setting in oesophageal adenocarcinoma patients; a guide to harnessing the double-edged sword of cancer surgery. in (2021). doi:10.1136/jitc-2021-itoc8.54

191. Ouyang, Q. *et al.* Dysfunctional CMV-specific CD8+ T cells accumulate in the elderly. in *Experimental Gerontology* (2004). doi:10.1016/j.exger.2003.11.016

192. Nunes, C. *et al.* Expansion of a CD8 +PD-1 + replicative senescence phenotype in early stage CLL patients is associated with inverted CD4:CD8 ratios and disease progression. *Clin. Cancer Res.* (2012). doi:10.1158/1078-0432.CCR-11-2630

193. Campisi, J. Aging, cellular senescence, and cancer. *Annual Review of Physiology* (2013). doi:10.1146/annurev-physiol-030212-183653

194. Effros, R. B. Telomere/telomerase dynamics within the human immune system: Effect

of chronic infection and stress. *Experimental Gerontology* (2011). doi:10.1016/j.exger.2010.08.027

195. Hu, G. & Wang, S. Prognostic role of tumor-infiltrating CD57-positive lymphocytes in solid tumors: A meta-analysis. *Oncotarget* (2018). doi:10.18632/oncotarget.23621

196. Attig, S. *et al.* Simultaneous infiltration of polyfunctional effector and suppressor T cells into renal cell carcinomas. *Cancer Res.* (2009). doi:10.1158/0008-5472.CAN-09-0852

197. Greenberg, S. A., Kong, S. W., Thompson, E. & Gulla, S. V. Co-inhibitory T cell receptor KLRG1: Human cancer expression and efficacy of neutralization in murine cancer models. *Oncotarget* (2019). doi:10.18632/oncotarget.26659

198. Tata, A. *et al.* Combination blockade of KLRG1 and PD-1 promotes immune control of local and disseminated cancers. *Oncoimmunology* (2021). doi:10.1080/2162402X.2021.1933808

199. Maurice, N. J., McElrath, M. J., Andersen-Nissen, E., Frahm, N. & Prlic, M. CXCR3 enables recruitment and site-specific bystander activation of memory CD8+ T cells. *Nat. Commun.* (2019). doi:10.1038/s41467-019-12980-2

200. Schietinger, A. *et al.* Tumor-Specific T Cell Dysfunction Is a Dynamic Antigen-Driven Differentiation Program Initiated Early during Tumorigenesis. *Immunity* (2016). doi:10.1016/j.immuni.2016.07.011

201. Wang, X. *et al.* MHC class I-independent activation of virtual memory CD8 T cells induced by chemotherapeutic agent-treated cancer cells. *Cell. Mol. Immunol.* (2020). doi:10.1038/s41423-020-0463-2

202. Guerra, N. *et al.* NKG2D-Deficient Mice Are Defective in Tumor Surveillance in Models of Spontaneous Malignancy. *Immunity* (2008). doi:10.1016/j.immuni.2008.02.016

203. O'Sullivan, T. *et al.* Cancer immunoediting by the innate immune system in the absence of adaptive immunity. *J. Exp. Med.* (2012). doi:10.1084/jem.20112738

204. Freeman, B. E., Meyer, C. & Slifka, M. K. Anti-Inflammatory Cytokines Directly Inhibit Innate but Not Adaptive CD8+ T Cell Functions. *J. Virol.* (2014). doi:10.1128/jvi.00658-14

205. Kinter, A. L. *et al.* The Common γ-Chain Cytokines IL-2, IL-7, IL-15, and IL-21 Induce the Expression of Programmed Death-1 and Its Ligands. *J. Immunol.* (2008). doi:10.4049/jimmunol.181.10.6738

206. Chen, L. *et al.* CD38-mediated immunosuppression as a mechanism of tumor cell escape from PD-1/PD-l1 blockade. *Cancer Discov.* (2018). doi:10.1158/2159-8290.CD-17-1033

207. Kim, K. H. *et al.* PD-1 blockade-unresponsive human tumor-infiltrating CD8+ T cells are marked by loss of CD28 expression and rescued by IL-15. *Cell. Mol. Immunol.* (2021). doi:10.1038/s41423-020-0427-6

208. Starzer, A. M. & Berghoff, A. S. New emerging targets in cancer immunotherapy: CD27 (TNFRSF7). *ESMO Open* (2020). doi:10.1136/esmoopen-2019-000629

209. Paulsen, M. & Janssen, O. Pro- and anti-apoptotic CD95 signaling in T cells. *Cell Commun. Signal.* (2011). doi:10.1186/1478-811X-9-7

210. Davern, M. *et al.* 776 A role for immune checkpoint blockade to enhance T cell-mediated responses in combination with chemotherapy in oesophageal adenocarcinoma. *J. Immunother. Cancer* (2020). doi:10.1136/jitc-2020-sitc2020.0776

211. Wang, W. *et al.* PD1 blockade reverses the suppression of melanoma antigen-specific CTL by CD4+CD25Hi regulatory T cells. *Int. Immunol.* (2009). doi:10.1093/intimm/dxp072

212. Chen, X. *et al.* PD-1 regulates extrathymic regulatory T-cell differentiation. *Eur. J.*

Immunol. (2014). doi:10.1002/eji.201344423

213. Wang, C. *et al.* In vitro characterization of the anti-PD-1 antibody nivolumab, BMS-936558, and in vivo toxicology in non-human primates. *Cancer Immunol. Res.* (2014). doi:10.1158/2326-6066.CIR-14-0040

214. Lucca, L. E. *et al.* TIGIT signaling restores suppressor function of Th1 Tregs. *JCI Insight* (2019). doi:10.1172/jci.insight.124427

215. Fourcade, J. *et al.* CD226 opposes TIGIT to disrupt Tregs in melanoma. *JCI insight* (2018). doi:10.1172/jci.insight.121157

216. Maeda, Y. *et al.* Depletion of central memory CD8+ T cells might impede the antitumor therapeutic effect of Mogamulizumab. *Nat. Commun.* (2021). doi:10.1038/s41467-021-27574-0

217. Weulersse, M. *et al.* Eomes-Dependent Loss of the Co-activating Receptor CD226 Restrains CD8+ T Cell Anti-tumor Functions and Limits the Efficacy of Cancer Immunotherapy. *Immunity* (2020). doi:10.1016/j.immuni.2020.09.006

218. Oliviero, B. *et al.* Defective DNAM-1 mediated cytotoxicity in NK cells infiltrating hepatocellular carcinoma. *J. Hepatol.* (2018). doi:10.1016/s0168-8278(18)31590-3

219. Bots, M. & Medema, J. P. Granzymes at a glance. *J. Cell Sci.* (2006). doi:10.1242/jcs.03239

220. Froelich, C. J., Pardo, J. & Simon, M. M. Granule-associated serine proteases: granzymes might not just be killer proteases. *Trends Immunol.* (2009). doi:10.1016/j.it.2009.01.002

221. Lieberman, J. Granzyme A activates another way to die. *Immunological Reviews* (2010). doi:10.1111/j.0105-2896.2010.00902.x

222. Kawaguchi, Y., Kono, K., Mizukami, Y., Mimura, K. & Fujii, H. Mechanisms of escape from trastuzumab-mediated ADCC in esophageal squamous cell carcinoma:

Relation to susceptibility to perforin-granzyme. *Anticancer Res.* (2009).

223. Zachary LeeZer Hay, Dale Kim, A. L. S. and J. E. S. The impact of the tumor microenvironment on granzyme production by CD8 T cells. *J. Immunol.* **204**, (2020).

224. Milano, F. *et al.* Expression pattern of immune suppressive cytokines and growth factors in oesophageal adenocarcinoma reveal a tumour immune escape-promoting microenvironment. *Scand. J. Immunol.* (2008). doi:10.1111/j.1365-3083.2008.02183.x

225. Kontani, K. *et al.* Involvement of granzyme B and perforin in suppressing nodal metastasis of cancer cells in breast and lung cancers. *Eur. J. Surg. Oncol.* (2001). doi:10.1053/ejso.2000.1060

226. Kurschus, F. C. & Jenne, D. E. Delivery and therapeutic potential of human granzyme B. *Immunological Reviews* (2010). doi:10.1111/j.0105-2896.2010.00894.x

227. Bouwman, A. C., van Daalen, K. R., Crnko, S., ten Broeke, T. & Bovenschen, N. Intracellular and Extracellular Roles of Granzyme K. *Frontiers in Immunology* (2021). doi:10.3389/fimmu.2021.677707

228. Li, H. *et al.* Dysfunctional CD8 T Cells Form a Proliferative, Dynamically Regulated Compartment within Human Melanoma. *Cell* (2019). doi:10.1016/j.cell.2018.11.043

229. Zheng, C. *et al.* Landscape of Infiltrating T Cells in Liver Cancer Revealed by Single-Cell Sequencing. *Cell* (2017). doi:10.1016/j.cell.2017.05.035

230. Azizi, E. *et al.* Single-Cell Map of Diverse Immune Phenotypes in the Breast Tumor Microenvironment. *Cell* (2018). doi:10.1016/j.cell.2018.05.060

231. Zhang, L. *et al.* Lineage tracking reveals dynamic relationships of T cells in colorectal cancer. *Nature* (2018). doi:10.1038/s41586-018-0694-x

232. Goggi, J. L. *et al.* Granzyme B PET Imaging of Immune Checkpoint Inhibitor Combinations in Colon Cancer Phenotypes. *Mol. Imaging Biol.* (2020). doi:10.1007/s11307-020-01519-3

233. Daemen, A. *et al.* Transcriptomic profiling of adjuvant colorectal cancer identifies three key prognostic biological processes and a disease specific role for granzyme B. *PLoS One* (2021). doi:10.1371/journal.pone.0262198

234. Hoek, K. L. *et al.* Granzyme B prevents aberrant IL-17 production and intestinal pathogenicity in CD4+ T cells. *Mucosal Immunol.* (2021). doi:10.1038/s41385-021-00427-1

235. Lin, L. *et al.* Granzyme B secretion by human memory CD4 T cells is less strictly regulated compared to memory CD8 T cells. *BMC Immunol.* (2014). doi:10.1186/s12865-014-0036-1

236. Manes, T. D. & Pober, J. S. Polarized Granzyme Release Is Required for Antigen-Driven Transendothelial Migration of Human Effector Memory CD4 T Cells. *J. Immunol.* (2014). doi:10.4049/jimmunol.1401665

237. Multhoff, G., Pockley, A. G., Schmid, T. E. & Schilling, D. The role of heat shock protein 70 (Hsp70) in radiation-induced immunomodulation. *Cancer Letters* (2015). doi:10.1016/j.canlet.2015.02.013

238. Multhoff, G., Pockley, A. G., Streffer, C. & Gaipl, U. S. Dual Role of Heat Shock Proteins (HSPs) in Anti-Tumor Immunity. *Curr. Mol. Med.* (2012). doi:10.2174/156652412803306666

239. Srivastava, P. K. Immunotherapy for human cancer using heat shock protein-peptide complexes. *Current Oncology Reports* (2005). doi:10.1007/s11912-005-0035-8

240. Radons, J. The human HSP70 family of chaperones: where do we stand? *Cell Stress and Chaperones* (2016). doi:10.1007/s12192-016-0676-6

241. Murakami, N. *et al.* Role of membrane Hsp70 in radiation sensitivity of tumor cells. *Radiat. Oncol.* (2015). doi:10.1186/s13014-015-0461-1

242. Di Rosa, F., Cossarizza, A. & Hayday, A. C. To Ki or Not to Ki: Re-Evaluating the

Use and Potentials of Ki-67 for T Cell Analysis. *Front. Immunol.* (2021). doi:10.3389/fimmu.2021.653974

243. Choy, B., LaLonde, A., Que, J., Wu, T. & Zhou, Z. MCM4 and MCM7, potential novel proliferation markers, significantly correlated with Ki-67, Bmi1, and cyclin E expression in esophageal adenocarcinoma, squamous cell carcinoma, and precancerous lesions. *Hum. Pathol.* (2016). doi:10.1016/j.humpath.2016.07.013

244. Zhang, X., Chen, Y., Li, Z., Han, X. & Liang, Y. TGFBR3 is an independent unfavourable prognostic marker in oesophageal squamous cell cancer and is positively correlated with Ki-67. *Int. J. Exp. Pathol.* (2020). doi:10.1111/iep.12380

245. Erokhina, S. A. *et al.* HLA-DR-expressing NK cells: Effective killers suspected for antigen presentation. *Journal of Leukocyte Biology* (2021). doi:10.1002/JLB.3RU0420-668RR

246. Revenfeld, A. L. S. *et al.* Presence of HLA-DR Molecules and HLA-DRB1 mRNA in Circulating CD4+ T Cells. *Scand. J. Immunol.* (2016). doi:10.1111/sji.12462

247. Saraiva, D. P., Jacinto, A., Borralho, P., Braga, S. & Cabral, M. G. HLA-DR in cytotoxic T lymphocytes predicts breast cancer patients' response to neoadjuvant chemotherapy. *Front. Immunol.* (2018). doi:10.3389/fimmu.2018.02605

248. Creelan, B. C. & Antonia, S. J. The NKG2A immune checkpoint — a new direction in cancer immunotherapy. *Nature Reviews Clinical Oncology* (2019). doi:10.1038/s41571-019-0182-8

249. Eugène, J. *et al.* The inhibitory receptor CD94/NKG2A on CD8+ tumor-infiltrating lymphocytes in colorectal cancer: a promising new druggable immune checkpoint in the context of HLAE/β2m overexpression. *Mod. Pathol.* (2020). doi:10.1038/s41379-019-0322-9